

2015

## Quantification of the Effect of Tool Geometric Features on Aspects of Friction Stir Welding

Md. Reza-E-Rabby  
*University of South Carolina*

Follow this and additional works at: <https://scholarcommons.sc.edu/etd>



Part of the [Mechanical Engineering Commons](#)

---

### Recommended Citation

Reza-E-Rabby, M.(2015). *Quantification of the Effect of Tool Geometric Features on Aspects of Friction Stir Welding*. (Doctoral dissertation). Retrieved from <https://scholarcommons.sc.edu/etd/3594>

This Open Access Dissertation is brought to you by Scholar Commons. It has been accepted for inclusion in Theses and Dissertations by an authorized administrator of Scholar Commons. For more information, please contact [digres@mailbox.sc.edu](mailto:digres@mailbox.sc.edu).

QUANTIFICATION OF THE EFFECT OF TOOL GEOMETRIC FEATURES ON ASPECTS  
OF FRICTION STIR WELDING

By

Md. Reza-E-Rabby

Bachelor of Science

Bangladesh University of Engineering and Technology, 2006

Master of Science

Tuskegee University, 2010

---

Submitted in Partial Fulfillment of the Requirements

For the Degree of Doctor of Philosophy in

Mechanical Engineering

College of Engineering and Computing

University of South Carolina

2015

Accepted by:

Anthony P. Reynolds, Major Professor

Stephen McNeill, Committee Member

Guiren Wang, Committee Member

Jasim Imran, Committee Member

Lacy Ford, Vice Provost and Dean of Graduate Studies

© Copyright by Md. Reza-E-Rabby, 2015  
All Rights Reserved

## DEDICATION

To my parents

## ACKNOWLEDGEMENTS

The author would like to express his earnest and profound gratitude to his advisor, Professor Anthony P. Reynolds, for his continuous guidance, support, encouragement and invaluable advices throughout his Ph.D. study. It has been a great privilege and honor for the author to work with him. Thank you Dr. Reynolds also for recommending several opportunities, including internships and conferences that fostered author's professional development as well as comprehensive understanding the science of friction stir welding. The author gratefully acknowledge the financial support from the Center for Friction Stir Processing (CFSP) which is a National Science Foundation-Industry/ University Cooperative Research Centers (NSF-I/UCRC) supported by Grant no. EEC- 0437341.

The author is also indebted to his Ph.D. committee members, Prof. Stephen McNeill, Prof. Guiren Wang and Prof. Jasim Imran, for their comments, suggestions, time and effort while going through the research proposal and dissertation.

The author would like to thank Dr. Wei Tang and Associate Engineer Daniel Wilhelm. Dr. Tang assisted in designing experimental procedure and laboratory testing. Without Dan, the duration of the Ph.D. research would be doubled than that is now. Thank you Dan for your time in manufacturing all the tool pins as well as preparing the weld joints for this study. The author appreciates the support from Mr. Juergen Silvanus at Airbus Group, Ottobrun, Germany during the summer internship there. Thank you Mr. Silvanus for providing wonderful accommodation as well as facilitating industrial

visits/training that also aided the research interests towards the structural analysis of the tool pins.

I would like to specially acknowledge administrative personnel of the Department of Mechanical Engineering, USC: Professor Jamil Khan (Chair), Mr. Glenn Severt (IT Manager), Ms. Renee Jenkins (Admin. Assist.), Ms. Misty O'Donnell (Admin. Assist.), Ms. Lalitha Ravi (Admin. Assist.) for their supports in many occasions of academic affairs. Special thanks to past and present colleagues of FSW Lab at USC: Dr. Venkateswaran Perumal, Dr. Piyush Upadhyay, Mr. Clinton Canaday, Mr. Joel Chrisfield, Mr. Huseyin Sahiner, Mr. Maxime Barra, Ms. Xiaomin Huang, Mr. Xiao Li, Mr. Hejun Yu, Mr. Ryan Widejko and Mr. Dawei Li for their support, suggestions and contribution in my Ph.D.

I would like to thank my friends, Drs. A.K.M. Monjur Morshed, Hossen Asiful Mustafa, Jahid Ferdous and Titan Paul for their support that make my life as a Ph.D. student much enjoyable. My sincere thanks go to contemporary members of Bangladesh Student Association at USC who helped me in many aspects during the graduate life to feel this city, Columbia like: 'home away from home'.

I reserve my thanks for my parents and family members for their encouragements, unconditional love and moral support in every moment of my research. Finally, I acknowledge Israt Jahan Disha, my wife for her incredible support and sacrifice of many weekends and evening hours in order for me to accomplish the research.

## ABSTRACT

In the friction stir welding (FSW) process, tool stirring and synchronized movement of the weld materials along a pre-existing seam line causes thermal gradients and severe plastic deformation resulting in the bonding of the adjacent materials. For a given set of welding parameters, tool pin geometries (dimensions, shape) and vertical/helical features that dictate the material motion also have significant effects on process response variables during FSW. Among the primary process controlling parameters in FSW, tool pin geometry and feature vary multifariously in terms of shape, dimensions, feature insertion technique depending on the weld material and application of joint. The current state-of-the-art of FSW tool design is evolved with instinctive perceptions which are typically based on empirical knowledge. It is important to understand the behavior of FSW process response variables such as, in-plane reaction forces, torque, weld power, stir zone temperature and material transport phenomena with the variation of pin features and geometries in order for the process to flourish over a range of manufacturing applications. This dissertation seeks to systematically quantify and establish the relationships among the tool geometric parameters, welding parameters and FSW process response variables to a reasonable extent.

In this work, the friction stir weldability of different aluminum alloys in similar/dissimilar joints as well as other aspects of the process including: condition of defect free welds, material flow, process temperature, forces, etc. are examined. The feasibility of using different pin features (thread forms/flats/flutes) coupled with a

conventional scrolled shoulder configuration was investigated. Results revealed that joint quality, tool reaction forces, temperature and weld power are highly affected by complex geometric features of the pin. Thread form was found to be an essential component in pin design criteria for effective downward material movement during welding. Completely defect free welds as well as lower in-plane forces were produced in both similar and dissimilar butt joint arrangement while using a mildly tapered conical coarse threaded pin having three shallow flats. The placement of the stronger alloy on the advancing side during bi-material welds also resulted in an effective material flow to produce defect free welds as well as involved with less in-plane forces. In order to prevent premature failure of the pin during the welding process, the stress condition and stress concentration of the pin were also estimated using finite element method (FEM). Moreover, the structural analysis using FEM also provided an optimum dimension of pin features. Finally, welding was performed using a stationary shoulder configuration to demonstrate the effectiveness of a coarse threaded conical pin with three flats in producing defect free welds. Taken together, the studies encompassed in this dissertation provided the basis for a systematic evaluation of tool design criteria as well as the basis to optimize processing window as FSW technology continues to evolve.

## TABLE OF CONTENTS

DEDICATION .....	iii
ACKNOWLEDGEMENTS .....	iv
ABSTRACT .....	vi
LIST OF TABLES .....	x
LIST OF FIGURES .....	xi
CHAPTER 1 INTRODUCTION .....	1
1.1. Friction Stir Welding Process .....	1
1.2. Research Motivation and Objectives .....	2
1.3. Dissertation Layout .....	5
CHAPTER 2 LITERATURE REVIEW .....	7
2.1 General Background .....	7
2.2 Tool parameters Effect on Response Variables in FSW.....	9
2.3 Tool Parameters Effect on Weld.....	14
2.4 Effect of Tool Parameters on Material Motion during FSW .....	18
2.5 State of the Art in Designing FSW Tool Pin .....	26
CHAPTER 3 MATERIALS AND EXPERIMENTAL PROCEDURES .....	38
3.1 Materials .....	38
3.2 Experimental Facilities .....	43
3.3 Systematic Design Approach of FSW Tools .....	44
3.4 Details of Welding .....	47

CHAPTER 4 RESULTS AND DISCUSSIONS.....	52
4.1 Effect of Tool Pin Thread Pitch on Friction Stir Weldability of Different Aluminum alloys.....	52
4.2 Effect of Thread Interruption by Machining Flats in Pin .....	65
4.3 Effect of Complex Geometric Features of Pin on Friction Stir Weldability of AA6061 Aluminum Alloy .....	81
4.4 Effect of Tool Pin Features on Process Response Variables during FSW of Dissimilar Aluminum Alloys.....	99
4.5 Understanding the effect of tool eccentricity and placement of alloy in dissimilar material friction stir welding.....	115
4.6 Tool Features Effect on Material Flow during FSW of Lap Joints .....	130
4.7 Effects of Pin Flat Depth on Process Responses Variables during FSW of Different Aluminum Alloys.....	137
4.8 Analyses of FSW Pin Stresses due to In-plane Reactions using Finite Element Method (FEM) .....	149
4.9 Comparing Response Variables between Stationary Shoulder and Conventional Shoulder FSW.....	159
CHAPTER 5 CONCLUSIONS AND FUTURE WORK.....	165
5.1 Concluding Remarks.....	165
5.2 Future Works .....	169
REFERENCES .....	171
APPENDIX A DETAILING OF FSW TOOL .....	184
APPENDIX B LIST OF ALL WELDING PROCESS CONTROL PARAMETERS ...	186
APPENDIX C DESIGN OF EXERIMENT-STATGRAPHICS RESULTS.....	194

## LIST OF TABLES

Table 3.1 Nominal composition (% weight) of aluminum alloys used .....	38
Table 3.2 Relevant property data for the considered aluminum alloys .....	42
Table 3.3 Pin designations and dimensions of different thread forms.....	46
Table 3.4 Summary of the variation in pin geometric features and welding parameters in FSW .....	49
Table 3.5 Weld Parameters for different aluminum alloys for bead on plate welds on AA7050 and AA6061 .....	50
Table 3.6 Process control parameters for dissimilar material for different combination of aluminum alloys: (a) AA2050-AA6061 and (b) AA6061-AA7050.....	50
Table 4.1 Spread of the orientation (angles are in degree) of resultant reaction with respect to the axis of zero X force .....	72
Table 4.2 Information about defective welds (with defect location codes*) or defect free (with '√' mark) weld for friction stir welding of AA6061 for different welding parameters using various pin features .....	86
Table 4.3 Spread of the orientation (angles are in degree) of resultant reaction with respect to the axis of zero X force .....	91
Table 4.4 Defect content and position in welds.....	101
Table 4.5 Material properties of H13 steel with consistent unit for ABAQUS environment.....	151

## LIST OF FIGURES

Figure 2.1 Schematic diagram of the typical FSW in the butt weld configuration with corresponding terminologies .....	8
Figure 2.2 Conventional force co-ordinate system in FSW process.....	10
Figure 2.3 Process control parameters affecting the response variables .....	11
Figure 2.4 Interactions among welding and response variables with their physical effects.....	12
Figure 2.5 A typical weld transverse section with three distinct weld zones for aluminum alloys.....	15
Figure 2.6 Qualitative hardness profile along the weld transverse section for different aluminum alloys .....	17
Figure 2.7 Hardness distribution along weld cross sections for welding on AA7075-T351 .....	18
Figure 2.8 Two dimensional flow model and tracer material position .....	19
Figure 2.9 Two dimensional flow prediction with different pin geometric features and validation with tracer material experimentation .....	20
Figure 2.10 Commonly used geometric shape and features in Friction Stir Welding community .....	26
Figure 2.11 Model of the first tool used in friction stir welding.....	28
Figure 2.12 (a) Possible force distribution, (b) pin pressure in area model and (c) Extrusion area due to pin pressure in extrusion model.....	34
Figure 2.13 Load distribution on a cylindrical tool pin (left) with a cross sectional view of pin (right).....	34
Figure 2.14 Bearing and torsional loading on tool pin for predicting stress distribution.....	37
Figure 3.1 FSW tool shoulders and pin geometry .....	45

Figure 3.2 Pin models illustrating different thread forms with corresponding designation.....	46
Figure 3.3 Threaded conical pins ( $8^{\circ}$ taper) with different features.....	47
Figure 4.1 Transverse macro-sections of weld nugget for bead on plate weld on (a) AA7050 and (b) AA6061.....	53
Figure 4.2 Volume of the threaded channel cut for different pitches.....	54
Figure 4.3 Main effect plot of area of defect for different alloys obtained from design of experiment results.....	56
Figure 4.4 Contour of estimated surface plot for different welding speed.....	57
Figure 4.5 In plane forces (a-b), torque (c) and pin peak temperature (d) as a function of tool rotation for bead on plate weld on AA7050.....	59
Figure 4.6 Reaction forces, torque and pin peak temperature as a function of tool rotation for bead on plate weld on AA6061.....	60
Figure 4.7 Polar plot of In-plane reactions on pin for welding on AA7050 and AA6061.....	62
Figure 4.8 Peak temperature as a function of weld power for welding speed 102 mm/min.....	64
Figure 4.9 Transverse macro cross sections of weld nugget zone for weld with pins having various thread form and flat numbers.....	67
Figure 4.10 Defect contents area as a function of welding parameters having different flat numbers of unthreaded pin.....	68
Figure 4.11 Microscopic defects near weld crown.....	68
Figure 4.12 Unthreaded pin (left) and threaded pin (right) showing material adhering to flats (or not).....	69
Figure 4.13 Applied Forge force during FSW process on the basis of maintaining similar contact condition between weld materials and tool shoulder due to variation of pin features.....	70
Figure 4.14 Polar plots of average in-plane Reaction forces for tool having different flat numbers.....	72
Figure 4.15 Tool torque as a function of rotational speed for different flat numbers.....	73

Figure 4.16 Pin peak temperature as a function of rotational speed for different flat numbers .....	74
Figure 4.17 Percent of volume cut from a cylindrical smooth pin to machine flats and threads.....	76
Figure 4.18 ‘Force Footprint’ of in-plane forces for one complete cycle for threaded pins with various flat numbers at 240 RPM and 102 mm/min.....	78
Figure 4.19 Overlapping nugget geometries for FSW with threaded pins having various flat numbers at 240 RPM and 102 mm/min .....	79
Figure 4.20 Peak to peak amplitude as a function of flat number for different welding conditions.....	80
Figure 4.21 Weld macro cross section for FSW made with different pin thread forms with various geometric features.....	83
Figure 4.22 Microstructural defects in the nugget zone for different tool features and different welding conditions .....	84
Figure 4.23 Geometric shape (depth) of the nugget zones as a function of weld energy for FSW with various pin features at different welding parameters .....	87
Figure 4.24 Required forge force for different tool pin features under different welding parameters.....	89
Figure 4.25 In-plane reaction force (avg. X-Y forces) in Polar plot for different pin features, weld parameters with the arrow marks showing conventional force co-ordinate system in FSW process.....	90
Figure 4.26 FSW torque as a function of tool rotational speed and forge force for various pin features .....	92
Figure 4.27 Average torque as a function of average required forge force for different welding parameters.....	93
Figure 4.28 Pin peak temperature as a function of weld power.....	95
Figure 4.29 Macro Cross sections of bi-material FSW of AA2050 and AA6061 using different pin features and weld parameters with alloy placement .....	100
Figure 4.30 Microscopic defects in weld cross sections at the advancing side of nugget zone during friction stir welding with pin having thread+3 counter-flow flutes for different welding parameters .....	102

Figure 4.31 Normalized interface length between 6061 and 2050 depending on pin type .....	103
Figure 4.32 Average In-plane reaction force in Polar plot for different pin features, weld parameters and alloy placement with the arrow marks showing conventional force co-ordinate system in FSW process.....	106
Figure 4.33 Torque as a function of Forge force for different tool and weld parameter .....	108
Figure 4.34 Pin Peak Temperature as a function of weld power for different tools and weld parameters .....	109
Figure 4.35 Grain structure of center of nugget for friction stir welding with pins: a) threaded only, b) thread+3 flats, c) thread+ 3 co-flow flutes & d) thread+ 3 counter-flow flutes under welding parameters: 300 RPM & 406 mm/min with 2050 on advancing side .....	111
Figure 4.36 Average grain size a function of peak temperature for different pin features and welds parameters: (a) AA2050, (b) AA6061, (c) AA2050 excluding defected welds & (d) AA6061 excluding defected welds.....	113
Figure 4.37 Misaligned friction stir welding set up .....	116
Figure 4.38 Weld transverse macrostructures of misaligned welds .....	118
Figure 4.39 Polar plot of in-plane reaction forces while pin eccentricity move from advancing side material to retreating side material as indicated by the arrow mark .....	118
Figure 4.40 Response variables as a function of tool pin eccentricity.....	119
Figure 4.41 Weld transverse macrostructures of AA7050 to AA6061 centered welds .....	124
Figure 4.42 Weld transverse macrostructures of AA7050 and AA6061 welds with different tool eccentricity.....	124
Figure 4.43 Polar plot of in-plane reaction forces while pin eccentricity move from advancing side material to retreating side material as indicated by the arrow mark .....	125
Figure 4.44 Response variables as a function of tool pin eccentricity.....	129
Figure 4.45 Macro cross sections of lap joint FSW of AA6056 with various pin.....	131

Figure 4.46 Microscopic defect at advancing side in the nugget zone for welding with counter-flow fluted pin at 240 RPM rotational speed .....	132
Figure 4.47 Tracing of interfacial movement in lap joint arrangement and method of measuring maximum interfacial displacement .....	133
Figure 4.48 Maximum vertical displacement of interfaces for friction stir welding with different pin features.....	134
Figure 4.49 Process variables as a function of tool rotation rate: (a) Forge force, (b) Avg. X force, (c) Avg. Y force, (d) Torque, (e) Power & (f) Temperature vs. Rotational Speed .....	135
Figure 4.50 Weld Transverse macro structural images for welding of different aluminum alloys with variation of pin flat depth (corresponding rows) and tool rotational speed (corresponding column).....	139
Figure 4.51 Microstructural defects in the nugget zone for welding different aluminum alloys at different welding conditions with various pin flat depths.....	140
Figure 4.52 Required forge force as a function of tool rotational speed for friction stir welding of different aluminum alloys with pin having various flat depths.....	141
Figure 4.53 Average X and Y –axes forces as a function of tool rotational speed for friction stir welding of different aluminum alloys with pin having various flat depths.....	143
Figure 4.54 In-plane resultant forces as a function of tool rotational speed for friction stir welding of different aluminum alloys with pin having various flat depths.....	144
Figure 4.55 Polar plot of force footprints on three different pins for welding aluminum alloys.....	145
Figure 4.56 Torque as a function of rotational speed for FSW different aluminum alloys using threaded pin having different depth .....	146
Figure 4.57 Weld power as a function of rotational speed for FSW different aluminum alloys using threaded pin having different depth.....	147
Figure 4.58 Temperature as a function of rotational speed for FSW different aluminum alloys using threaded pin having different depth.....	148
Figure 4.59 Schematically showing loading and boundary conditions for structural analysis of pin.....	150

Figure 4.60 Snap shot of meshed geometry inside ABAQUS with manual re-meshing rule applied near stress concentration area .....	152
Figure 4.61 Mesh convergence study: von Mises maximum stress vs. relative mesh density.....	153
Figure 4.62 Orientation of forces and corresponding maximum stress (von Mises).....	154
Figure 4.63 Orientation of first flat cut in models with respect to thread termination ...	155
Figure 4.64 Maximum stresses on FSW tool pin having different flat cut orientation under different orientation of loading.....	155
Figure 4.65 Proposed flat cut orientations to minimize maximum stress on tool pin, flat trailing edge is defined as the edge which lag behind the tool rotational direction and flat leading edge is the front of flat.....	156
Figure 4.66 Stress distributions with stress concentration on pin due to corresponding In-plane resultant reactions .....	158
Figure 4.67 Weld surface comparison between conventional shoulder (CS) and stationary shoulder (SS) FSW .....	160
Figure 4.68 Weld transverse macro sections for conventional and stationary shoulder FSW for different welding parameters .....	161
Figure 4.69 Superposition of deformation zone using CSFSW and SSFSW .....	162
Figure 4.70 Comparison of process response variables for CSFSW and SSFSW.....	163
Figure A.1 FSW tool design with shank, shoulder and pin with corresponding dimensions for cylindrical pin.....	185

# CHAPTER 1

## INTRODUCTION

### **1.1. Friction Stir Welding Process**

The Corporate Average Fuel Economy (CAFE) standard for cars and light-duty trucks by the Model Year 2025 was set to the equivalent of 54.5 miles per gallon (mpg).<sup>1</sup> This CAFE target requires the automotive industries' trend towards energy efficient vehicles to continue with advanced technologies. There are several possible ways of meeting the CAFE target for the automotive manufacturers, such as: (a) introduction of hybrid (electric) vehicles, (b) incorporation of the high efficiency engine with alternative bio-fuels, (c) modify aerodynamic design to minimize drag or, (d) weight reduction of vehicles by using lightweight materials. There is always a pursuit of materials with high specific strength in transportation industries such as, aerospace, shipbuilding and automotive manufacturing companies in order to reduce the fuel consumptions. The fuel efficiency can be enhanced by introducing energy efficient materials and/or advancing appropriate manufacturing processes of new or existing materials. In order to achieve this goal, new research expeditions have taken investigators through designing new lightweight materials or developing new manufacturing process for the existing materials. Nevertheless, joining of different materials is the part and parcel of manufacturing applications because implementation of formability or machinability is often restricted for specific structural components and closures in automotive and aerospace industries. Over the years, efforts have been made by many researchers to produce high quality

joints between two components with the consideration for structural rigidity, manufacturing rapidity as well as cost effectiveness. Among the endeavors, introduction of Friction Stir Welding (FSW) <sup>2</sup> by The Welding Institute (TWI) is the innovative breakthrough of the state-of-the-art manufacturing process for joining aluminum, magnesium, copper, steel, nickel and titanium alloys. This process functions with both similar and dissimilar alloy joints. The FSW process offers a potential advantage in manufacturing industries to eliminate mechanical fastening such as riveted or bolted joints. <sup>3, 4</sup> Incorporation of light aluminum alloy coupled with steel by the FSW process as sub-frame component in auto industries also yields a milestone in the weight reduction capability of this process. <sup>5</sup> There is no melting involved in FSW process, hence this solid state joining technique offers some specific advantages over fusion weld by preserving material properties in the joint closest to that of base materials. The potential and some recent applications of FSW in the aerospace industries (airframe, fuel tanks), shipbuilding industries (hulls, freezer panel, deck and storage vassals), automotive industries (sheet bodyworks, support frame), railway industries (wagon, bulk carrier tanks, trucks) and electronic industries (joining the front and back piece of the iMac) are the evidence of the increasing importance and robustness of the FSW process. <sup>5-13</sup>

## **1.2. Research Motivation and Objectives**

Numerous studies have been devoted to understanding FSW of aluminum alloys in the areas of heat generation, flow behavior, microstructural characterizations and properties of weld material due to the effect of welding parameters and tool geometries. Depending on the weld material and their dimensions as well as variation in applications of FSW joints, tools are introduced with multifaceted requirements by means of shape,

dimension, feature of the shoulder and the pin. However, the present practice in FSW process as well as selection of tool design criteria of FSW tools is based on intuitive knowledge which is pragmatically implemented for a given set of welding parameters.<sup>14</sup>

In a conventional FSW tool configuration with shoulder and pin, shoulders are designed to prevent expulsion of material as well as producing frictional heat. A large body of knowledge has accumulated over the years to standardize the shoulder geometries.<sup>15</sup> Because of recent advancement in tool design, including scrolled shoulder<sup>16-20</sup> or sophisticated stationary shoulder<sup>21-23</sup>, it is imperative that the comparative effectiveness in material transportation for producing good quality welds by FSW depends on pin only while using unvarying shoulder configurations, thermal boundary conditions and welding parameters. Since the application of FSW is increasing, it will be important to understand the behavior of process variables like in-plane reaction forces, torque, power and stir zone temperature with the change in pin features in order for the process to thrive. Numerous efforts have been devoted to understanding the relationship between tool parameters (including geometric shape, dimensions and thread features) and mechanical-microstructural properties of different alloys within a wide range of welding conditions.<sup>24-28</sup> In all experimental studies, it is determined that pin features (thread forms/flats/flutes) explicitly affect material movement to produce defect free welds by FSW. However, there is a scarcity of systematic studies on tool profile, specifically pin geometric shape/features coupled with variation of other process parameters to investigate weldability of different aluminum alloys. Experimentation using systematic variation in thread forms with different process control parameters may provide useful insight into the problem. Therefore, the objectives of this dissertation are to provide

quantitative information regarding the effects of various tool pin features on (a) material motion in friction stir welding, (b) process response variables and (c) welding parameter envelopes. In addition, attempts are also being made to elucidate effects of material properties on weldability of different alloys and provide guidance for dissimilar material welding. Another objective of this research is to predict stress on the pin in order to avoid premature failure of the pin during welding. It is expected to have a longer pin life in terms of total weld length when the pin encounters lesser stress and temperature due to interaction with the workpiece during FSW.

The general approach is to systematically vary the tool pin profile (pin geometric shape and features) and measure/quantify response variables. The defect content and material flow in the weld are also needed to be verified in order to substantiate proper consolidation by the pin features. Series of welds are made with various pin geometric features for a range of process windows with an unvarying shoulder configuration and constant thermal boundary conditions. Both similar and dissimilar materials joints were produced by FSW with different aluminum alloys using various pin features with widely varying process controlling parameters (welding and rotational speed). The experiments conducted in this dissertation with respect to pin feature variations are divided into several groups: (a) pin thread form effects on FSW of different aluminum alloys, (b) thread interruption with the flats on the selected thread form of cylindrical pin, (c) conical pins with different features (threads/flats/flutes) effect on similar and dissimilar material butt welds and lap weld. Finite element method (FEM) was employed to estimate the stress distribution on the pin. Tool design is modified by introducing different thread interruptions (flats/flutes), which are also expected to lessen the maximum load on the

pin, eventually minimizing stress concentration. However, this modification in tool design is developed based on the ability to produce high quality welds by pins as well as induce the minimization of in-plane reaction forces on the pin as to obtain from experimental feedback.

### **1.3. Dissertation Layout**

This dissertation is divided into five chapters.

**Chapter 1** presents a brief introduction to FSW as a manufacturing process with its anticipated cost effectiveness and some industrial applications. The motivation and objective of this dissertation are also elucidated.

**Chapter 2** provides general background for the FSW process with a critical review on relevant process control parameters and their influences on response variables. The state of the art of FSW tool design criteria is also presented with the advancement of the process since its invention. The emphasis is given to pins and their effectiveness on material flow and weld quality.

**Chapter 3** includes the relevant metallurgical background of several aluminum alloys employed in this research with their precipitation sequences and properties. The experimental facilities to fulfill the current research objectives are also presented in this chapter. Metallographic sample preparation and macro/micro-structural evaluation techniques are also discussed for post weld characterization.

**Chapter 4** includes the analyses of experimental results obtained from the systematic study of FSW pins with different features. Essentially, this chapter discusses the results by grouping those into several categories: (a) effect of tool pin thread pitch on friction stir weldability of different aluminum alloys, (b) effect of thread interruption by

machining flats in pin, (c) effect of complex geometric features of pin on friction stir weldability of AA6061 aluminum alloy, (d) effect of tool pin features on process response variables during friction stir welding of dissimilar aluminum alloys, (e) understanding the effect of tool eccentricity and placement of alloy in dissimilar material friction stir welding, (f) tool features effect on material flow during friction stir welding of lap joints, (g) the effects of FSW pin flat depth on process response variables during friction stir welding of different aluminum alloys, (h) analyses of FSW pin stresses due to in-plane reactions using finite element method (FEM) and (i) compare response variables between stationary shoulder and conventional shoulder FSW.

Finally, a summary of the research outcome is stipulated in **Chapter 5** with the concluding remarks and provision of future works for further research directions.

## CHAPTER 2

### LITERATURE REVIEW

#### 2.1 General Background

Friction stir welding (FSW) is a solid state thermo-mechanical joining process in which bonding between two parts occurs by severe plastic deformation of the adjacent interfaces under the conditions of hydrostatic pressure. A non-consumable rotating tool moves along the weld seam with a pin immersed in the work-piece. The conventional FSW tool is comprised of (a) shoulder and (b) pin, where the shoulder prevents the expulsion of material from the weld zone and also contributes to heat generation. The role of FSW tool pin is to provide sufficient plastic deformation to cause bonding across any pre-existing interfaces while transporting material to positions behind the tool. Figure 2.1 illustrates the typical friction stir welding process with corresponding terminology and it is expedient here to refer to a recent paper by Threadgill <sup>29</sup> which provides a clear description on general terminologies adopted by the friction stir welding community. The peak temperature during FSW may be well below the melting temperature of the welded material which might be beneficial for lessening typical undesirable effects of welding processes. FSW is an especially good choice for welding high strength aluminum alloys and the process has been adopted in some aerospace and automotive applications. Both heat treatable and non-heat treatable aluminum alloys exhibit a recrystallized nugget zone and a heat affected zone (HAZ) after FSW, which contribute to mechanical property changes compared to the base metal. However, better dimensional stability, preservation

of base material properties, resistance to hot cracking, etc. have made FSW superior to other joining techniques for aluminum alloys.<sup>11, 30, 31</sup>

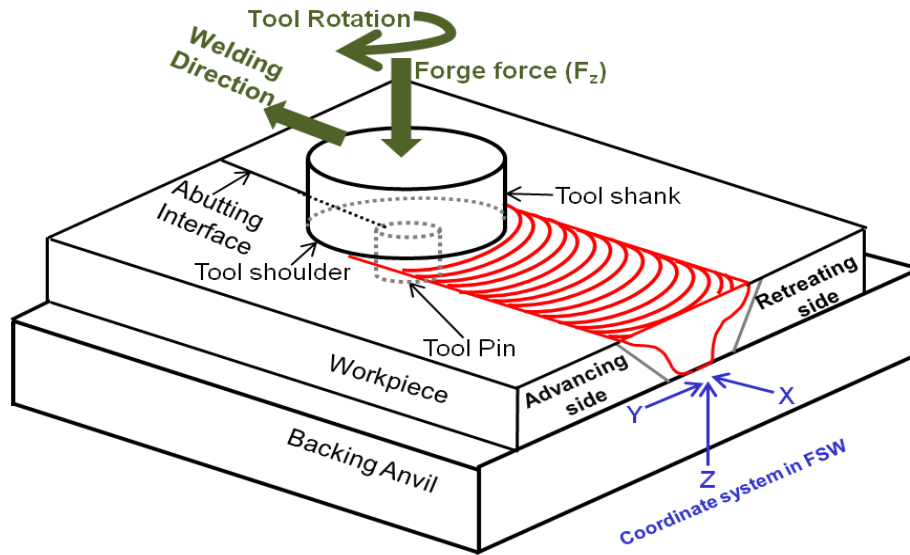


Figure 2.1 Schematic diagram of the typical FSW in the butt weld configuration with corresponding terminologies

The primary process control parameters in FSW include tool rotational and welding speed, forge force, and tool geometry. All of the controlling parameters have important roles to play in producing high quality welds and all control parameters have been included as critical variables in weldability studies. However, tool geometry studies are necessarily limited as the potential variation in geometry is essentially infinite. Moreover, it is required to consider the properties of workpiece material to be welded in order for obtaining mechanically and metallurgically excellent welded joints for a suitable set of welding and tool parameters. Detailed metallurgy with thermal and mechanical properties of the workpiece materials employed in this work will be described in Chapter 3. The thermal management is another aspect that has an important influence on weld properties in FSW.<sup>32, 33</sup> The effect of thermal boundary conditions is not considered for the work of this dissertation. Hence the invariant thermal boundary

conditions in each weld are obtained by using partial penetrating pins upon an unvarying anvil. The variations in pin geometries and features in friction stir welding are the focal point of this dissertation work. With regards to joining different aluminum alloys using various pin geometries and features, the process response variables, weldability ranges, flowability and microstructures of similar/dissimilar material FSW are of primary interest.

## **2.2 Tool parameters Effect on Response Variables in FSW**

The response variables during friction stir welding include, required torque (and hence the power of the weld), weld temperature and in plane reaction force (X-axis force and Y-axis force). Torque is a fundamental process response variable in friction stir welding that is significantly influenced by welding and tool parameters, forge force, etc. The power of a weld can be measured from tool torque directly according to the following equation:

$$Power = T\omega + F_x V \approx T\omega$$

where, T is the tool torque,  $\omega$  is the tool angular velocity,  $F_x$  is the X-axis force encountered by pin opposite to welding direction and V is the welding speed. It was evident that, in most normal cases, influence of tool translational force is insignificant while calculating weld power, therefore  $F_x V$  terms can be omitted. Weld specific energy (heat input per weld length or, power divided by welding speed) is another important parameter that can be directly related to the weld temperature and microstructural evolution in the weld zone. Temperature response in the stir zone is also crucial since it eventually dictates the properties of the welded part. Studies have shown that tool

rotational speed and welding speed significantly influences the process peak temperature.<sup>34, 35</sup>

The in-plane forces on the pin result from the resistance to material flow during FSW. Figure 2.2 schematically presents the conventional direction of positive X and Y axes forces (red arrows) during FSW. The force exerted by the work piece that impedes the motion of the tool is defined as the positive X axis force. The positive Y-axis force acts perpendicular to the X direction towards the advancing side from retreating side.

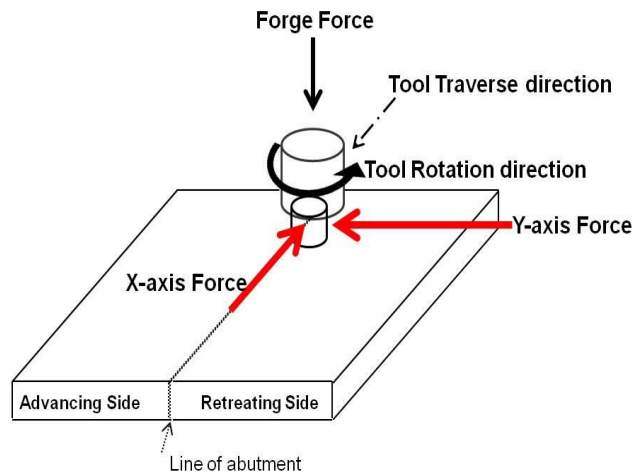


Figure 2.2 Conventional force co-ordinate system in FSW process

All the control parameters have an influential role on the response variables and on weld and its mechanical-microstructural properties like, grain size, micro hardness, tensile strength, residual stress, etc. The process control parameters are varied depending on work-piece dimensions for obtaining acceptable weld quality. For examples, Figure 2.3(a-c) illustrates the effect of several process control parameters on weld response variables: weld temperature, micro-hardness etc.

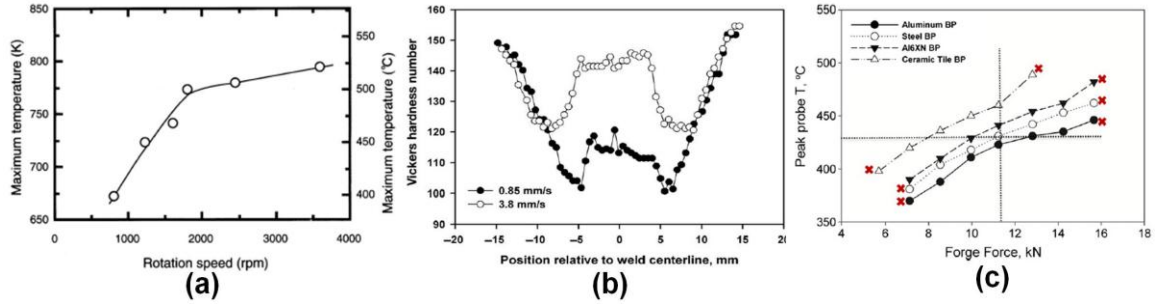


Figure 2.3 Process control parameters affecting the response variables: (a) peak process temperature increases with increasing tool rotational speed <sup>36</sup>, (b) Hardness profile in weld traverse are observed higher for faster welds than slower welds for welding at same advance per revolution (0.42mm/rev) <sup>35</sup> & (c) forge force (Z-axis force) and thermal boundary condition (backing plate thermal diffusivity) influencing weld peak temperature while keeping tool rotational and traverse speed constant <sup>33</sup>

Hence, for obtaining a desired weld quality using a suitable set of process parameters, it is important to understand the interrelationship among the process control parameters (welding and tool geometric parameters) and response variables. Nevertheless, the diversity in tool geometric parameters, welding parameters, properties of material to be welded etc. have made the process complicated for establishing a general correlation among the parameters and mechanical-microstructural properties of welded parts. A conceptual model has been proposed by Colligan and Mishra <sup>37</sup> with the plausible mechanism of heat generation as suggested from the interpretation of the interactions of process control and response variables. Flow chart in Figure 2.4 illustrates the complex interrelationship among the process control parameters and response variables with their physical effects. Moreover, the complication is amplified if one of the subsets of the influential factors in the conceptual model: tool geometric features are expanded to vary considerably. Nevertheless, tool parameters occasionally have considerable influence over usable control parameters as well as on process response variables. It was observed for a given set of welding and rotational speed that, the



aluminum alloy using pins with left and right hand threads having different pitches. They reported that, with decreasing pitch dimension (the distance between corresponding points on adjacent threads, measured parallel to the thread axis) more heat was being generated, therefore more homogenous grain size was observed in case of welding with pin having small pitch compared to a higher pitch. Numerical studies have also been made to predict the effect of tool profile on heat generation<sup>39, 40, 42</sup>; however, these studies are frequently coupled with material flow characteristics which will be discussed in Section 2.4.

The in-plane reaction forces might be correlated with quality of welds during FSW. Unfortunately, results and observations regarding tool parameters effect on process forces (in-plane reaction forces) are scarcely available in open literature. Colegrove and Shercliff<sup>43</sup> compared the transverse force on trivex and triflute pins where, trivex pin was found to reduce the downward force as well as traverse force (X-axis force) in both experimental and numerical analysis. However, use of isothermal material properties caused under-predicted traverse force in their computational analysis. Trimble et al.<sup>44</sup> experimentally and numerically investigated the force generation in FSW on smooth and threaded cylindrical pins. They reported that, the maximum vertical forces were evident during plunging stage and reduced significantly (35% reduction) during translational stage. Moreover, lower maximum vertical (Z-axis force) and translational (X-axis force) forces were also reported for threaded pin compared with smooth pins. Nevertheless, the process forces are generally governed by the welding parameters and heat input. It has also been reported that, decreasing heat input during FSW resulted in a increased forces which might decrease the heat affected zone.<sup>45</sup> This might also be attributed to the

resistance of materials flow during tool stirring. An excellent effort has also been made by Hattingh et al.<sup>46</sup> where they investigated the effect of tool geometries on welding force and mechanical properties of friction stir welds of AA5083 aluminum alloy to obtain an optimum friction stir welding tool. Systematic variation in number of flutes, flute depth and angles, pin diameter and taper angle, and thread pitch were reported with the reaction forces on the pin and correlated with the resulting tensile strength. A tapered pin with three flutes and pitch around 10% of pin diameter was suggested to be a successful tool design.<sup>46</sup> Of course, in this as in every case, only a local optimum can be claimed.

### **2.3 Tool Parameters Effect on Weld**

The efficiency of the welded part is determined by the mechanical and microstructural properties in and near the weld zone, which are governed by process parameters in FSW. Materials are being subjected to high temperature for a short period of time and an intense plastic deformation during the processing time alter mechanical and microstructural properties compared to that of the base material. Three distinct microstructural regions are observed in weld transverse sections after friction stir welding. Figure 2.5 shows a typical weld transverse section with different regions separated by dark lines. The nugget zone (Zone A in Fig 2.5) undergoes severe plastic deformation. Since the FSW process is performed below the melting temperature of the weld material the fine equiaxed grain is suggested to develop by continuous dynamic recrystallization<sup>47, 48</sup>, geometric dynamic recrystallization<sup>49</sup> or static recrystallization and grain growth<sup>50</sup>. The thermo-mechanically affected zone (TMAZ) (Zone B in Fig 2.5) that appears on both sides of the nugget zone, experiences significant deformation and

thermal cycle, however recrystallization of grain structures is not evident. The heat affected zone (HAZ) (Zone C in Fig 2.5) endures significant thermal cycle, however, no deformational changes are observed in grain structures. For friction stir welding of precipitation hardening aluminum alloys, the HAZ is normally the critical zone as the mechanical properties in these zones are degraded due to over-aging. The size and shape of the nugget zone and a portion of the adjacent TMAZ zone are strongly dependent on the tool pin geometry. However, the HAZ zone size is determined from the localized hardness response which is mostly depends on the thermal cycle at this zone, thermal conductivity-diffusivity of work piece materials, the thermal boundary conditions applied to the FSW process and welding speed.

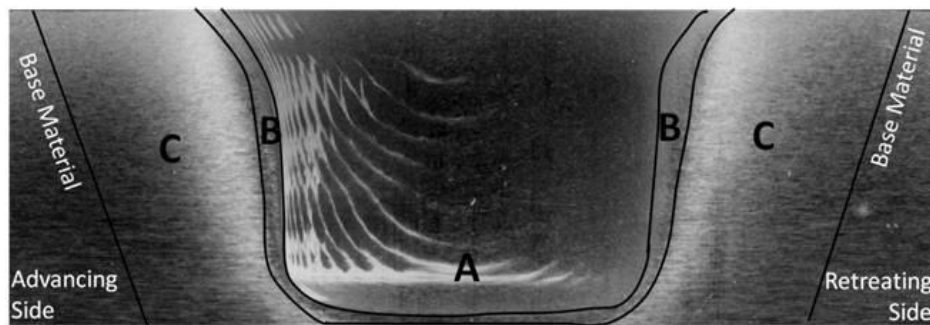


Figure 2.5 A typical weld transverse section with three distinct weld zones for aluminum alloys

Early studies have shown that microstructure and micro-hardness of the friction stir welded part are strongly influenced by the process peak temperature<sup>36, 50, 51</sup>, which in turn is governed by the weld power and welding speed<sup>35, 50</sup>. Therefore, the functional relationship among tool pin geometric features, microstructural and mechanical properties are expected to be present if there is a dependence of temperature on pin profile. Several experimental investigations have been made to evaluate the correlation of pin geometries and weld properties.<sup>24, 26, 27, 41, 52, 53</sup> However, very few researchers have

reported on temperature dependant microstructural characteristics under various tool studies.<sup>26, 41</sup> Fujii et al.<sup>26</sup> observed almost the similar grain size near the weld center while welding with different tool pins, however, grain size were significantly smaller in the weld root in the case of triangular shaped pin compared to smooth cylindrical or threaded cylindrical pin due to lower peak temperature for triangular pin.

The tensile properties of friction stir welded specimen are mostly affected by welding parameters and defect formations irrespective of the tool pin profile as reported in many investigations.<sup>24, 26, 27, 41, 53</sup> Hardness measurement quantitatively provides important information about the microstructural changes during the friction stir welding process. Numerous studied have been devoted to understanding the microstructural development and corresponding hardness evolution.<sup>18, 34, 36, 48, 50, 52, 54-57</sup> Unfortunately a very few reported on the effect of tool features on hardness distribution of aluminum alloys.<sup>52, 58</sup> A minute peak temperature difference might result in similar hardness distribution along weld cross-section.<sup>52</sup> Qualitative mid plane hardness distribution along weld cross sections for heat treatable and non-heat treatable aluminum alloys are presented in Figure 2.6. Deviation of hardness distribution from base metal hardness obviously indicates the property changes due to friction stir welding process. Weld properties of precipitation hardened aluminum alloys can be improved by minimizing the thermal effect on the HAZ zone. It was evident that, HAZ hardness is increased with higher welding speed.<sup>35</sup> This phenomenon has been evident for a precipitation hardened Al alloy (AA7050-T7451) and explained from metallurgical point of view: presumably because of the maximum rate of formation of eta ( $\eta$ ) phase at a temperature of 350°C with adequate time of exposure at high welding speed.<sup>35</sup>

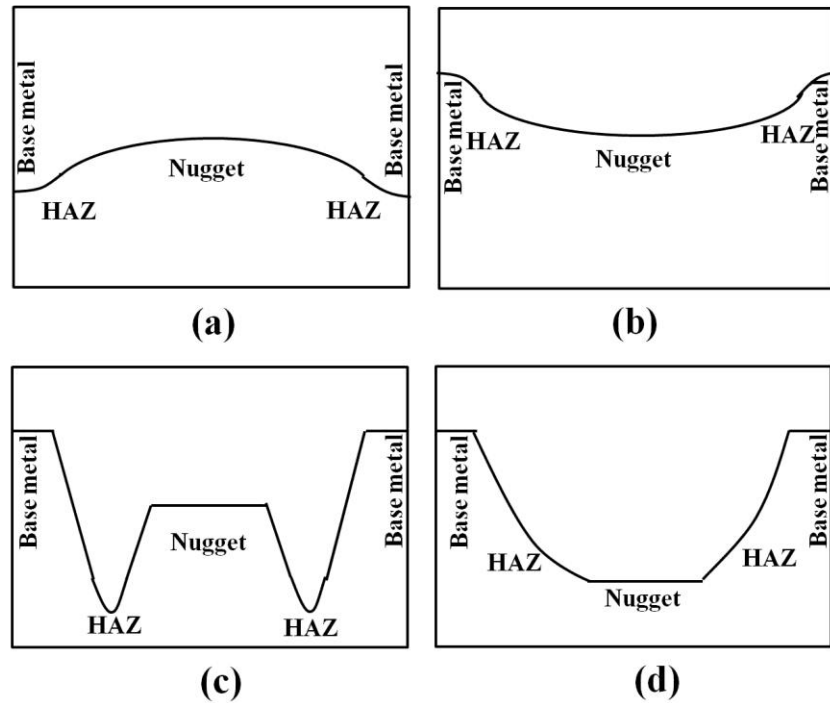


Figure 2.6 Qualitative hardness profile along the weld transverse section for different aluminum alloys: (a) Annealed-O tempered 1xxx & 5xxx series Al alloys, (b) Work hardened H-tempered 1xxx & 5xxx series Al alloys, (c) Precipitation hardened 2xxx, 6xxx and 7xxx series Al alloys with peak temperature approaching solution heat treatment temperature and (d) Precipitation hardened 2xxx, 6xxx and 7xxx series Al alloy with peak temperature around 350°C. Adapted from the references<sup>18, 34-36, 48, 50, 52, 54-58</sup>

Threadgill et al.<sup>58</sup> reported a combined effect of tool geometry and thermal management on narrowing the HAZ. Figure 2.7 illustrates the transverse hardness data for welding on 6 mm thick AA7075-T7351 plate with contemporary welding process within a five years period using: (1) conventional threaded tool pin in the year 1995, (2) conventional threaded tool pin with high conductivity back anvil in the year 1997 and (3) advanced tri-fluted in the year 2000. As evident from figure 2.7, hardness properties were obviously improved by using advanced tool used in the year 2000. Unfortunately the details of welding procedure (welding / rotational speed, nature of aging, etc.) for these hardness distributions were not reported. The faster welding speed along with high conductivity anvil may also be the critical issue for narrowing region between HAZ

minimum hardness along with increasing the hardness number. It was anticipated that decreasing heat input leads to increased minimum HAZ hardness eventually reducing the overall width of the HAZ.

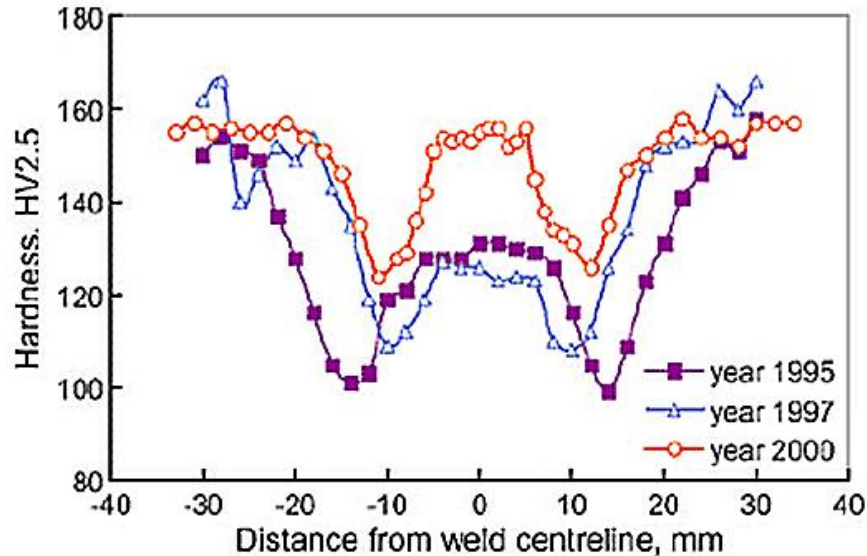
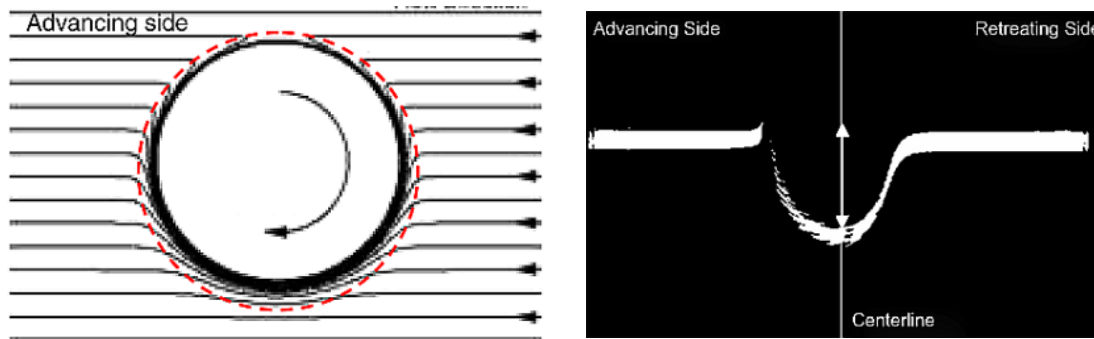


Figure 2.7 Hardness distribution along weld cross sections for welding on AA7075-T351: (a) traditional threaded pin tool in the year 1995, (b) traditional threaded pin with high heat extraction from the bottom of pin in the year 1997 and (c) tri-fluted pin in the year 2000<sup>58</sup>

## 2.4 Effect of Tool Parameters on Material Motion during FSW

Effective material flow and apposite consolidation behind the tool are the keys to a successful friction stir welding process. The complex mechanism of material flow in friction stir welding is predominated by tool pin, necessarily influenced by the properties of the material to be welded and process parameters as well. Over the years, investigations have been made by many researchers to evaluate the material motion during the FSW process using both experimental methods<sup>59-67</sup> and computational approach<sup>43, 68-73</sup>. To monitor and quantify the flow behavior in friction stir welding, experimental studies have been conducted using marker insertion technique<sup>59, 62-67</sup> and/or stop action technique<sup>59, 61, 74</sup>.

A generic two dimensional flow path with a cylindrical tool pin as predicted from computational fluid dynamics is shown in Figure 2.8(a)<sup>75</sup> where the tool is being rotated in the clockwise direction (viewed from top) and weld material is passed from right to left while sticking boundary condition were assumed between work piece and pin. The materials in the streamlines intersecting the path of pin are supposed to be transported behind the pin by a distance equal to the chord of the probe circle at which intersection occurs. This flow model was supported by the marker study where, the maximum rearward material movement was approximately one diameter as seen in Figure 2.8-b.<sup>75</sup> It was also noted here that convergence of the marker area on advancing side in figure 2.8-b is due to vertical material movement during FSW.



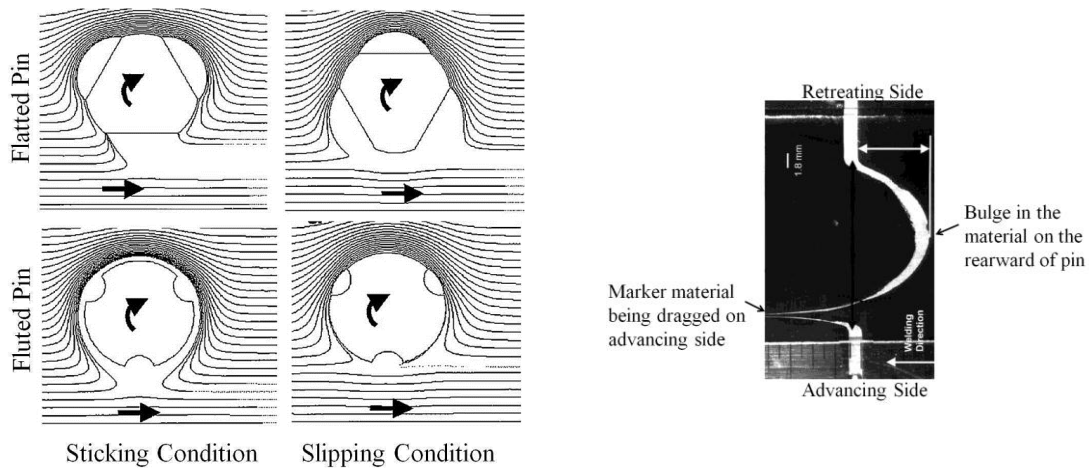
(a) 2-D material flow path simulated with streamlines following pin rotational flow field within shear zone (red dashed circle)

(b) final marker position after friction stir welding

Figure 2.8 Two dimensional flow model and tracer material position<sup>75</sup>

Using a 2D material flow model, the interaction of different tool features was also predicted by Colegrove and Shercliff<sup>43</sup> with slipping condition governing the interface between pin and work piece. The streamlines of the flow model are being swept round the retreating side with the insertion of flats or flutes in pin indicating greater deformation region in retreating side of the pin as seen in figure 2.9 (a). This phenomenon in material

flow was also evident from marker study conducted by London et al.<sup>76</sup> A bulge in the wake of the tool was also anticipated in the streamline of the material flow model which was previously visualized in the experiments with tracer material as seen in Figure 2.9-(b).<sup>62, 64</sup> Furthermore, in a three dimensional isothermal model by Colegrove and Shercliff<sup>43</sup>, slipping conditions were predicted to be dominated for trivex pin. With convex surface, it was anticipated that sticking to the material is being avoided by trivex pin, which eventually reduces shear forces as well as transverse forces on this pin compared to trifluted pin.



(a) Predicted flow field in streamlines with the effect of pin features (each row for corresponding pin features) and interfacial boundary condition effect (each column for corresponding BC of sticking and slipping)<sup>43</sup>

(b) Flow visualization using marker insertion illustrating the bulge in material behind tool and deformation pattern<sup>62, 64</sup>

Figure 2.9 Two dimensional flow prediction with different pin geometric features and validation with tracer material experimentation

Fratini et al.<sup>77</sup> experimentally and numerically investigated the flow behavior of AA7075-T6 under the influence of weld pitch (welding speed/rotational speed) and tool pin shape (cylindrical smooth and conical smooth pin with different taper angles). In experimental approach, copper marker was introduced in the directions both parallel and

perpendicular to the weld centerline. An effective material movement with minimum defect formation was evident for welding with the conical shape pin. On the other hand, irregular flow pattern was observed from the final position of copper particle in the weld cross section with cylindrical tool pin indicate that formation of defect is most likely to take place with such flowing pattern. Moreover qualitative information about material flow was highlighted in the numerical analysis based on the final position of nodes in FEM analysis. These nodes, originally placed on the welding line, coincided with experimental observation of copper marker final position.<sup>77</sup> However, it has been observed that, the effect of vertical components of pin that is, pin features such as threads/flutes were not captured in most of the three dimensional flow models. The prevailing complication while predicting material flow with featured pin is not only because of the geometric shape of pin but also because of the inherent sensitivity of contact condition (sticking<sup>73</sup> / slipping<sup>43</sup>) between the work piece and pin which is still the subject of debate. Moreover, temperature and strain rate dependent material flow stress that is also needed to be considered in predicting material flow during friction stir welding is missing in most of the investigations. A relevant study has been performed by Zhao et al.<sup>67</sup> in which they experimentally investigated the effect of pin geometries and features on material flow in friction stir welding using marker insertion technique. It was evident that, the vertical motion of material was not developed for cylindrical or taper pin without threads; therefore material flow results in wormhole defects on the advancing side. On the contrary, more obvious vertical material movement with taper threaded pin was observed as evident from final position of marker material in the 3D reconstructed images of the successive slices. In essence, it should be noted here that, marker studies in

FSW are only limited to the post weld visualization that identifies final morphology of welds rather than the flow path. Moreover, there might be a chance of changing flow pattern due to difference in flow stress behavior of foreign marker material and work piece material that might influence actual flow behavior. <sup>67</sup>

Interrupting pin thread with flats/flutes was also found to be beneficial in FSW by many researchers for effective material flow around tool as evidentiary supported by experimental investigations. <sup>17, 20, 46, 52, 78, 79</sup> Microstructural observations of weld material in the front vicinity of pin suggest the trapping of the materials in the thread and subsequent release near flat after experiencing one or more rotation along with the pin as revealed from ultrafine grains with texture and their orientation from an experimentation of sudden freezing FSW process. <sup>74</sup> Evident of additional two weaker rings or smaller peaks within the major microstructural band or strong intensity peak of texture component also suggested the disrupted material flow by flat in every third of APR while friction stir welding with a threaded and three flatted pin. <sup>60, 74</sup> However, eccentricity of an off-centered tool occasionally causes reversal shear orientation in texture possibly due to oscillation of response force component. <sup>60</sup>

#### *Material flow in dissimilar aluminum alloys FSW*

Dissimilar material friction stir welding (FSW) has received increasing interest, since aerospace and automotive industries adopted this process for some applications in order to eliminate mechanical fastening such as rivets or bolted joints. <sup>3, 4</sup> The eventual purpose is to improve fuel efficiency by reducing weight of specific components. Many combinations of dissimilar aluminum alloys (precipitate hardened and/or solution hardened) are successfully joined using FSW. <sup>80-96</sup> It is noted that, the difference in

material properties at the abutting interface is a critical issue in dissimilar material welds. Therefore, the choice of suitable welding parameters, tool parameters and alloy placement in advancing/retreating side have significant influence on obtaining the best possible properties in bi-material friction stir welded parts.

Numerous studies have been devoted to understanding the material flow in the dissimilar material FSW in butt weld arrangement by using different tool geometries.<sup>19, 80, 84, 85, 90</sup> The geometries of the shoulder were investigated by Leal et al.<sup>19</sup> to study material flow during bi-material FSW of thin (1 mm) sheet AA5182 and AA6016 with AA5182 on the advancing side. Conical cavity (10 mm diameter) and scrolled (14 mm diameter) shoulder were compared. A shoulder driven intense material flow was evident from macroscopic and X-ray images while using scrolled shoulder since the ratio of shoulder diameter to plate thickness is high. Pin driven flow was reported to be predominant in the case of the conical cavity shoulder. However, completely different welding conditions were employed for the different shoulders in their study. Jamshidi Aval et al.<sup>86</sup> studied the tool geometric effect on the mechanical and microstructural properties for dissimilar friction stir butt welding of AA5086-O and AA6061-T6 with 5086 on the advancing side. They reported that a tool with concave conical shoulder and tapered unthreaded/smooth pin with three grooves generated higher heat (as observed from measured peak temperature at 10 mm from weld centerline both in advancing and retreating sides) relative to a tool with a cylindrical smooth or threaded pin with grooves. At higher rotational speed and/or lower welding speed, they observed substantial material movement as evidenced from complex features in macro cross sections and magnesium distribution in the nugget zone from EDX analysis. Park et al.<sup>94</sup> also examined the effect

of placing AA6061 and AA5052 on both advancing and retreating sides and reported the comparison of mixing state of materials in the nugget zone and correlated with weld properties. When AA5052 was placed on the advancing side more uniform distribution of magnesium in the weld nugget zone was observed. This was evident from their electron probe microanalysis. Da Silva et al.<sup>84</sup> studied the material flow in the friction stir butt welding of dissimilar alloy AA2024-T3 and AA7075-T6 with 7075 on the advancing side using a threaded pin. They observed an unstable rotational flow around the threaded pin with a formation of the cavity behind the pin. This instability in material flow was evident from the micrographs of longitudinal sections of weld embedded with a pin as captured after immediately stopping the process. Full contact of the pin thread with the material was observed on leading edge, whereas, a gap in the interface of tool thread and weld material observed on the trailing edge resulted in cavity formation on the advancing side. With higher rotational speed onion ring structures were also evident in their observation. Dissimilar friction stir welding was also investigated by Peel et al.<sup>95</sup> with exchanging the AA5083 and AA6082 in the advancing and the retreating sides successively. A higher interfacial disruption was evident from macrographs at a higher rotational speed when AA5083 were placed on the advancing side. Formation of voids was also reported when 6082 was placed on the advancing side at low rotational speed. In some occasion, effects of positional dependence of the FSW tool with respect to weld centerline, in other word tool eccentricity dictates the material flows as well as strength of joints in dissimilar material friction stir welding. A study of misaligned FSW by Kumar and Kailas<sup>97</sup> revealed that defect free welds can be produced when tool eccentricity on the advancing side was 0.5 mm from the weld centerline. However, tool

geometric configurations, such as, conical angle (frustum shape) and round/flat bottom of a pin have dramatic effects on intermixing of bi-materials in the stir zone to eliminate wormhole defects or joint line remnant (kissing bond defect).

In summary, there is a common theme observed while reviewing the literature: with high heat input resulting from high rotational speed, the effect of the placement of alloy (advancing or retreating side) in bi-material FSW might be minimized. However, delaminations or cracks at the weld surface were also reported at higher rotational speed bi-material welding presumably caused by incipient local melting.<sup>80</sup> So, the high heat input solution is not always feasible. On the other hand, controversies exist regarding which alloy of a dissimilar metal pair should be placed on the advancing (or retreating) side. Some works on dissimilar material FSW have reported that quality of welds can be improved by placing the alloy with lower strength on the advancing side<sup>83, 89, 90, 98</sup>, while other studies indicated that weld properties were significantly improved by placing of the stronger material on the advancing side<sup>81, 85, 94-96</sup>. Moreover, there is a complex interaction of material flow with tool geometries and features for a given set of process parameters. Some references can be found in the literatures which acknowledge that the weldability and flowability of material results from the combination of the effects of alloy placement on advancing/retreating side, friction stir welding parameters, and pin features. A very recent study was made by Izadi et al.<sup>85</sup> They observed the effect of pin features on bi-material friction stir welding of AA2024 and AA6061 in both lap and butt weld arrangement with different pin features. In the case of lap welding with a grooved pin, the horizontal interface of the lapping surface was not disrupted after welding which they deemed to result from poor vertical intermixing. On the other hand, promotion of

vertical intermixing was reported when a flatted pin was employed in lap welds as evident from micrographs and EDX mapping of Cu. Moreover, at very low welding speed (33 mm/min) a threaded only pin resulted in fine scale intermixed lamella in the nugget zone regardless of the position of either alloy on advancing/ retreating side.<sup>85</sup>

## 2.5 State of the Art in Designing FSW Tool Pin

It is required to consider several primary factors for an effective FSW tool design: geometric shape and features of the pin, load to be encountered by pin and corresponding stress distribution. Of course, these primary features mostly depend on the dimensions and physical properties of the work piece material, process control parameters, thermal boundary conditions, etc. This section will explicitly describe the state of art of friction stir welding tool pin with the consideration of these governing factors.

### 2.5.1 FSW tool pin geometries and features

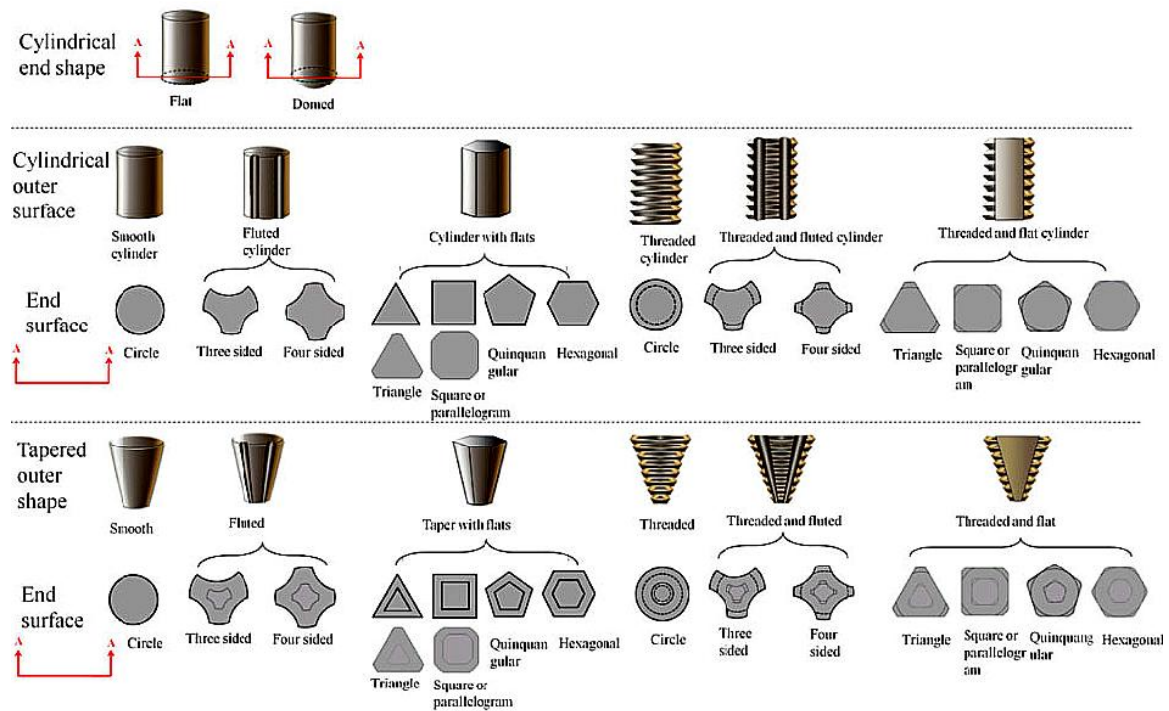


Figure 2.10 Commonly used geometric shape and features in Friction Stir Welding community<sup>99</sup>

Right after the invention of friction stir welding by TWI in 1991, efforts have been made towards designing FSW tool pins.<sup>2, 17, 20, 79, 100-104</sup> Figure 2.10 provides a first glimpse about the possible variables in pin geometric shape and features that are generally used in the friction stir welding community.<sup>99</sup> These variations in pin profile, shapes and their dimensions distinctly affect the process control parameters as well as response variables in turn affect joint efficiency.

The primitive tool for friction stir welding consisted of a threaded pin with round bottom and a concave shoulder as shown in Figure 2.11.<sup>2</sup> This tool was expected to produce quality welds with minimum forge force and eliminate stress concentration at pin root at optimum dome radius (75% of the pin diameter).<sup>100</sup> The concavity of shoulder requires the tool to be tilted about 1°- 4° against the welding direction with respect to the normal to the work piece in order for producing a compressive forging force in the trailing edge of tool for effective consolidation of materials.<sup>15</sup> While analytically calculating the bottom surface velocity of the tilted tool pin, it was predicted that material deformation by round bottom (dome shaped) pin near the root is lower than that of flat bottom pin. The premise of arguments on the issue of changing pin design from round bottom to flat bottom can be found in the reference.<sup>15</sup> With the advancement of tool design using scrolled shoulder<sup>16-20</sup> or the latest addition of the stationary shoulder<sup>21</sup> concept, reasonable endeavors have been made on modifying pin only since the effectiveness of material flow is strongly reliant on pin geometric features in such unvarying shoulder configurations.

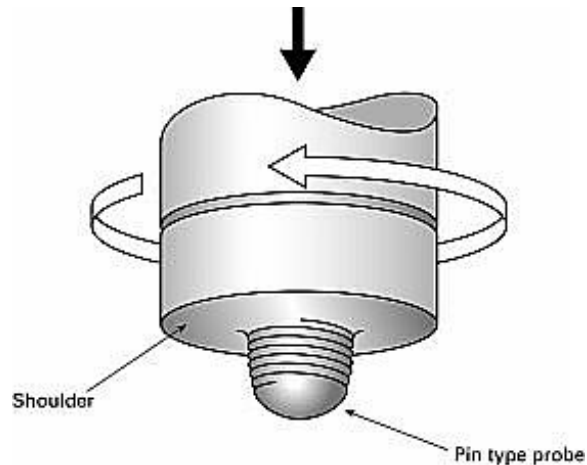


Figure 2.11 Model of the first tool used in friction stir welding<sup>2, 100</sup>

Friction stir welding tool pins are often featured with threads for effective material transportation near the weld root. The material transport phenomenon around the tool pin is not fully understood until now. However, vertical movements of material during FSW are presumed to be predominated by helical features in pin.<sup>25, 59, 105</sup> Welding with unthreaded or smooth pins have shown insufficient material movement near root causing voids or wormhole defects on the advancing side of weld nugget.<sup>25, 27, 28, 106, 107</sup> Nevertheless, these formations of defects also depend on alloy properties and flowability as well as welding parameters. Fujii et al.<sup>26</sup> investigated the effect of tool pin geometric shape on weldability of three different aluminum alloys under different welding conditions. They observed that a columnar pin without threads produced good quality welds for low deformation resistance aluminum alloys (e.g. AA1050-H24). It was also evident from their study that, pin shape and thread form (over the range examined) have no significant effect on weld quality and mechanical-microstructural properties of 6061-T6 welds. However, for the relatively high hot-strength aluminum alloy, 5083-O, a columnar pin with threads produced better quality welds at lower rotational speed (RPM) and a triangular prismatic pin performed better at higher RPM.

Orientation of thread forms in tool pin also plays an important role during friction stir welding. Having established that material flow is driven by threads of tool pin<sup>25, 41, 59, 105, 108</sup>, it is imperative to introduce apposite orientation of threads during FSW for producing good quality welds. Apparently, a right hand threaded pin rotating in a counter-clock wise direction (when viewed from above) will cause the material to move downward. On the contrary, the reverse orientation of the thread or opposite direction of tool rotation leads to upward material movements that produce flash on the surface of friction stir welds. The quality of the weld surface may be affected by the orientation of threads (right/left hand thread).<sup>41</sup> Chowdhury et al.<sup>108</sup> also observed the effect of thread orientation on weld quality during friction stir welding of magnesium alloy (AZ31B-H24). A qualitative analysis of pressure and traction force on the threaded part of pin was also established to understand the material flow mechanism by right and left hand threaded pin in their study. Unfortunately, these force analyses didn't capture the actual mechanism of material flow in association with the in-plane force encountered by tool pin.

Geometric shape of pin is one of the important parameters that need to be explored in design consideration. As mentioned earlier that the cylindrical threaded tool pins were commonly used during friction stir welding of aluminum plate thickness up to 12 mm.<sup>15</sup> The shape of the pins was changed from cylindrical to frustum or conical shape while performing welds in thick plate (more than 12 mm).<sup>18, 103</sup> This change in shape provided significant benefits compared to cylindrical pin by reducing in-plane reactions on the tool, presumably by reducing the displaced volume of the pin.<sup>14, 104</sup> Thomas et al.<sup>102</sup> introduced a complex conical shaped pin with flutes termed the MX

Triflute<sup>TM</sup> which is a further modification of the Whorl<sup>TM</sup> pin developed by TWI. They reported on welding force reduction on these types of pins by reducing the displaced volume of the pin (60-70% decrease) as well as enhancing material flow to produce good quality welds.

Interrupting pin thread with flats/flutes was also found to be beneficial in FSW by many researchers from their experimental investigations.<sup>20, 46, 52, 78, 102</sup> Researchers also paid attention to randomly chosen pin geometric shapes, for example square/triangular/hexagonal/octagonal prismatic, taper square/octagonal were also studied in order to identify the effectiveness of these pin geometries for successful friction stir welds.<sup>26, 27, 93, 106</sup> In consequence, there are claims for local optimum tool geometric configurations under a range of examined welding parameters. Elangovan et al.<sup>27</sup> studied the effectiveness of tool pin geometric shape and threads on joint efficiency and the FSP zone formation in AA2219 aluminum alloy with constant shoulder geometry. A square cross sectional pin was sometimes reported to produce better quality welds compared with cylindrical threaded, triangular, or smooth tapered pins.<sup>27, 106</sup> It can be noted here that, square or triangular prismatic tool pins are special cases where flats (3 and 4 sides are for the triangular and square cross sections respectively) are cut into a cylindrical pin forming the corresponding cross section (square or triangle) inscribed in the cylinder.

Efforts have also been made in computational modeling to numerically design FSW tool.<sup>39, 40</sup> Buffa et al.<sup>39</sup> developed a numerical model to optimally design FSW tool pin shape using a commercial FEA software DEFORM-3DTM. With an unthreaded pin they predicted that with increasing pin taper angle, temperature increases uniformly

through the thickness of the material. Additionally, the downward plastic flow of the material was predicted using an intermediate taper angle pin (30°). Moreover, vertical force and advancing force (X-axis force) were expected to increase with increasing pin taper angle, however an X-force plateau is reached at a certain value of pin taper angle (20° angle). The numerical results obtained in this study were based on a continuum-3D-Lagrangian-thermomechanical- coupled rigid-viscoplastic model.<sup>109</sup> This transient model captures the heat generation phenomenon in the deformation zone by assuming constant interfacial shear stress between tool and workpiece with constant coefficient of friction. Colegrove and Shercliff<sup>40</sup> also compared experimentally and numerically the effect of tool geometries on material flow. In a two dimensional asymmetric flow model they predicted the greatest pressure difference with tri-flat tool followed by tri-flute and trivex tool pin.<sup>40</sup> Moreover, from experimental feedback, it was evident that tri-flatted tool pin performed better than trifle and trivex pin in terms of producing sound welds. In this model, the contact condition between workpiece and tool pin was assumed to be complete sticking. However, the model did not capture the phenomena of producing wormhole defects by trivex pin even though reasonable trends of traverse force for different pin features were predicted.

### 2.5.2 In-plane Forces on FSW Tool

Another important aspect in designing pin is the in-plane reaction forces (X-axis & Y-axis force) that pin experiences during FSW. As the increasing interest of the FSW process widens the field of application, it is necessary to maximize joint efficiency. One of the ways of improving joint efficiency as well as manufacturing rapidity is by using faster welding speeds that result in reduced heat input. However, reaction force on pin

increases drastically with increasing welding speed. Eventually the pin becomes susceptible to failure due to fatigue or overload. Therefore, it is necessary to develop advanced tools that minimize in-plane reaction forces as well as to prevent tool damage without compromising the weld quality. The shape and features of tool pin play important roles in this regard as discussed previously.

The in plane reaction forces might also have a role in material flow as well. Several studies have been dedicated to exploring the feedback forces and material flow pattern.<sup>110-114</sup> Boldsaikhan et al.<sup>112</sup> developed a 2D model of material flow using a ‘pseudo shear stress concept’ by characterizing the oscillation of the feedback forces to investigate the dynamics of the material flow in FSW. Furthermore, an algorithm has also been developed using the force signals for detecting defects in welds as a non-destructive evaluation technique which is a work in progress.<sup>111</sup> Long et al.<sup>114</sup> observed a minimum value of reaction force in conventional X axis direction at an intermediate tool rotation speed for a given welding speed. In another investigation, a similar phenomenon was predicted in a 2D fluid dynamic simulation with the assumption of a viscosity law which included a rapidly declining flow stress near the work piece melting point.<sup>113</sup> Balasubramanian et al.<sup>110</sup> attempted to understand the material flow phenomena using the tool feedback forces. The orientations of resultant forces (polar plot of in-plane reaction for single cycle) were observed to be shifted towards the retreating side and trailing edge for welds with wormhole defects as reported by Balasubramanian et al.

Pins encounter severe stresses at elevated temperature due to interaction with the workpiece during FSW. The viewpoint of the stress analysis of the tool is to estimate the tool life or determine ways of extending tool life. It is essential to understand and

characterize the forces acting on pin in order to analyze the stress on the pin. However, only a few researchers concentrated on the analysis of force on the tool pin during FSW.<sup>115-118</sup> Two conceptual force models were proposed by Sorensen and Stahl<sup>117</sup> to characterize the force on the tool pins. In the area model, the net pressure on the tool pin was assumed to apply to the projected area of pin as the tool travels through the work piece, whereas in the extrusion model, the force was assumed to be exerted by the extruded material within the channel bounded by the tool shoulder-pin contact surface and un-deformed material. Figure 2.12 illustrates the possible force distribution and schematic representation of proposed area and extrusion model of pressure distribution in tool pin.

The area model combines the diametric pressure distribution along the pin radius with respect to pin axis neglecting the variations of forces on pin caused by asymmetric material flow in advancing side and retreating side. The area model breaks down when the area force model equation is applied to the experimental fitted equation which was evident from the constant negative diametral force distribution along the pin length. Moreover, the extrusion model didn't capture the influence of area for same pin shape, having different geometric features that might affect the volume of material to be extruded. On the other hand, the experimentally measured data provide some useful correlation with feedback force and pin geometry such as, decreasing pin length lead to decreased longitudinal force and reaches an asymptote as the pin length approaches zero, where the shoulder predominantly encounter the longitudinal forces. However, the effect of variation of the pin diameter on the longitudinal force was not significant over the range of weld parameter and tool parameters examined by Sorensen and Stahl.<sup>117</sup>

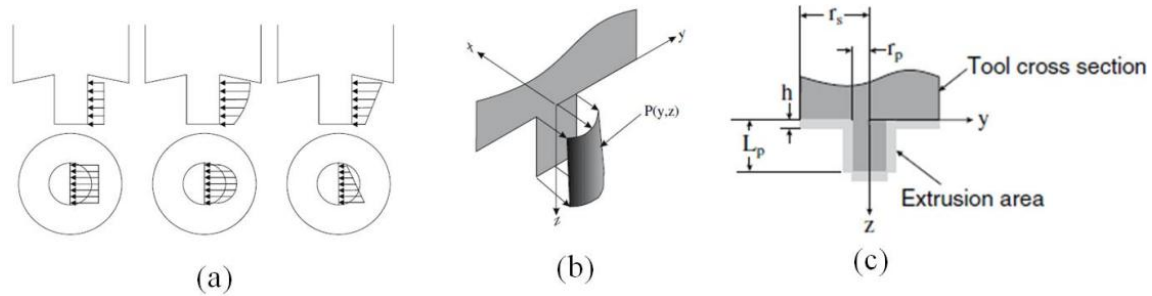


Figure 2.12 (a) Possible force distribution, (b) pin pressure in area model and (c) Extrusion area due to pin pressure in extrusion model<sup>117</sup>

Arora et al.<sup>115</sup> proposed a methodology to compute the traverse force and torque numerically using 3D heat transfer and viscoplastic material flow model with the consideration of temperature and strain rate dependent flow stress of weld material. Figure 2.13 shows proposed load distribution on tool pin with pin cross sectional view showing the maximum bending and shear stress along the circumference of the pin. The 2D load distributions that increase with pin height might arise from the temperature difference of weld crown and the root in which, material flow stress near root is higher because of low temperature near the root.

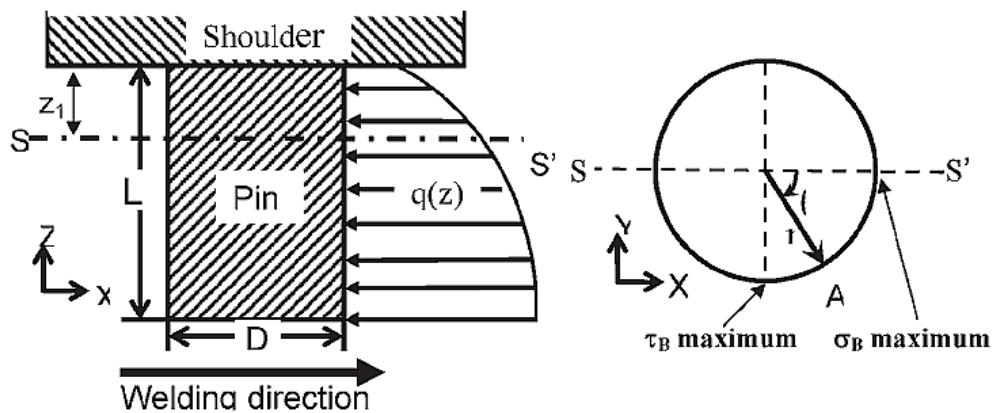


Figure 2.13 Load distribution on a cylindrical tool pin (left) with a cross sectional view of pin (right)<sup>115</sup>

The maximum bending normal stress ( $\sigma_B$ ), bending shear stress ( $\tau_B$ ) and shear stress ( $\tau_T$ ) due to torque at pin height  $Z_1$  from tool shoulder were expressed as:

$$\sigma_B = \frac{4 \cos \theta}{\pi r^3} \int_{Z_1}^L z q(z) dz \quad \dots\dots\dots (2.1)$$

$$\tau_B = \frac{4 \sin \theta}{3\pi r^3} \int_{Z_1}^L q(z) dz \quad \dots\dots\dots (2.2)$$

$$\tau_T = \frac{2}{\pi r^3} \oint \tau(1 - \delta) r_A dA \quad \dots\dots\dots (2.3)$$

where  $q(z)$  designate traverse force distribution on too pin,  $r$  is local pin radius and  $L$  is pin length,  $\delta$  is the spatial fractional slip. Therefore, the maximum possible shear stress at any point on tool pin of section S-S' in figure 2.13 was also expressed as:

$$\tau_{max} = \left[ \left( \frac{\sigma_B}{2} \right)^2 + (\tau_B + \tau_T \sin \theta)^2 + (\tau_T \cos \theta)^2 \right]^{1/2} \quad \dots\dots\dots (2.4)$$

Equation 2.1-2.4<sup>115</sup> also predicted the dynamic behavior of the pin forces where the highest and the lowest value of  $\tau_{max}$  were experienced by pin during one complete revolution. The maximum possible bending stress on pin can also be predicted near shoulder from these analytical equations. Conical shaped pin was found to be more capable of withstanding high stress on the tool pin compared to cylindrical pin since taper pin encounters lesser in-plane force than cylindrical pin.

### 2.5.3 Stress State on pins during FSW

While in-plane reaction forces and torque on the FSW pin can be measured experimentally, it is difficult to obtain the stresses on the pin from experiment. Finite element method (FEM) analysis can be considered a useful contrivance for numerically simulating the stress state of the physical FSW tool model. Studies have been devoted to determining stress on the pin under various loading conditions and compare various tools to obtain the most favorable pin design on the basis of stress distribution.<sup>102, 116, 118</sup> Von Mises yield criteria (equation 2.5) are often considered to be a comprehensive way of comparing the strength of tool pins.<sup>116, 118</sup>

$$\sigma_0 = \frac{1}{\sqrt{2}} \left[ (\sigma_x - \sigma_y)^2 + (\sigma_y - \sigma_z)^2 + (\sigma_z - \sigma_x)^2 + 6(\tau_{xy}^2 + \tau_{yz}^2 + \tau_{zx}^2) \right]^{1/2} \dots\dots (2.5)$$

Lin and co-workers<sup>116</sup> compared the stress distribution on two types of pins under same bearing and torsional load condition using a commercially available structural analysis tool: ANSYS. The load distributions on pin have been subjected to a lot of debate since actual loading distribution on the friction stir welding tool is unknown. It was conceived that the acting force on pin are similar to hydrostatic pressure. However, this hydrostatic pressure from real normal loads to the pin surface were replaced by the pressure distribution of an open-end journal bearing by replacing the actual pressure load with a half circle pattern along one half portion of pin circumference, where peak value would just be the yield stress  $\sigma_0$ . On the other hand, torsional load was applied that results from tangential component caused by shearing action according to Tresca Criterion of maximum shear stress ( $\tau_{max} = \sigma_0/2$ ). Figure 2.14 illustrates the loading distribution of Lin and co-worker's<sup>116</sup> tool models under the bearing and torsional forces.

Based on von Mises maximum stress, they concluded that one piece tool were stronger than two piece tool. Moreover, tool geometries were also modified with fillet radius for one piece tool and observed that, both torsional and bending strength were increased with increasing fillet radius. For two piece tool, with a decreasing ring thickness both bending and torsional strength increases, however the minimum thickness of the ring is required to avoid functioning as a shoulder. Similar FEM analyses have also been conducted by Gupta et al.<sup>118</sup> on cylindrical, frustum and conical shape pin. Cylindrical tool pin was found to encounter lesser maximum stress as well as lesser displacement vector sum under same loading condition. However, the distribution of load was not mentioned in this study. Moreover, experimentally, cylindrical tool pin is likely

to encounter higher reaction forces than conical or frustum shape pin and that was not considered in their study.

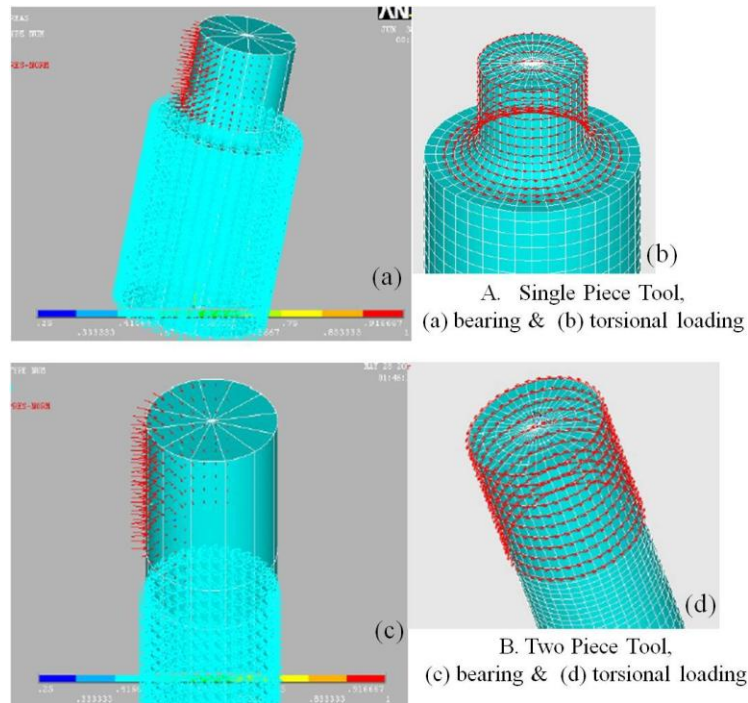


Figure 2.14 Bearing and torsional loading on tool pin for predicting stress distribution<sup>116</sup>

In all experimental and numerical studies of friction stir welding tool design, it was determined that pin shape and features (thread forms/flats/flutes) explicitly affect material movement to produce defect free welds by FSW. However, the effects of the tool features in FSW are poorly understood and in most case tool design criteria are pragmatically determined by trial and error method. A systematic study is required in order for obtaining quantitative information that enables the understanding of the effect of various tool features on (1) weldability of different alloys, (2) material flow and (3) process response variables and provide guidelines for designing more radical tool design in friction stir welding. This dissertation aims to at least partially achieve these goals.

## CHAPTER 3

### MATERIALS AND EXPERIMENTAL PROCEDURES

#### 3.1 Materials

A wide spectrum of investigations pertaining to variations in tool pin geometric features has been conducted in friction stir welding of different precipitation hardening aluminum alloys: AA2050-T3, AA6056-T451, AA6061-T651, AA7050-T7451 and AA7099-T7651. The alloying elements along with the nominal compositions of the alloys considered in this dissertation are shown in Table 3.1.<sup>119-122</sup>

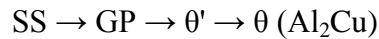
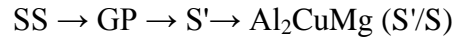
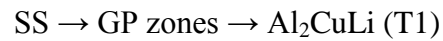
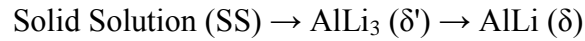
Table 3.1 Nominal composition (% weight) of aluminum alloys used

Alloy	Cu	Mg	Zn	Mn	Cr	Fe	Zr	Li	Si	Ti	Ag
AA2050	3.2-3.9	0.2-0.6	0.25	0.2-0.5	0.05	0.1	0.06-0.14	0.7-1.3	0.08	0.1	0.2-0.7
AA6056	0.8	0.9	0.4	0.7	0.25	≤0.5	≤0.2	-	1	≤0.2	-
AA6061	0.4	1.2	0.25	0.15	0.35	≤0.7	-	-	0.5	0.15	-
AA7050	2.3	2.2	6	0.1	0.04	≤0.15	0.1	-	≤0.12	≤0.06	-
AA7099	1.4-2.1	2.3	7.4-8.4	0.04	0.04	0.15	0.05-0.15	-	0.12	0.06	-

##### 3.1.1 Metallurgy of AA2050

Among the precipitation hardening alloys, AA2050 has some outstanding properties, such as high specific strength, fairly easy weldability using FSW, comparable mechanical strength of welded parts as of high strength 7xxx series aluminum alloys and weight benefit in terms of fuel efficiency of aircraft.<sup>121</sup> AA2050 alloy was developed, qualified and produced by Constellium, formerly known as Alcan Aerospace.

Depending upon the chemical compositions of the alloying elements and thermo-mechanical treatments, four precipitation sequences have been proposed during aging of 2xxx (Al-Cu-Mg-Li) alloys<sup>121, 123, 124</sup>:



The amount of Li (maximum 1.3% by weight) that is incorporated into AA2050 allow to avoid formation of  $\delta'$  phase, is detrimental to thermal stability. The main hardening precipitate of AA2050 is T1 ( $\text{Al}_2\text{CuLi}$ ). Moreover, this hardening effect of T1 phase is promoted by the addition of Cu. Other alloying elements have different functionalities such as: (i) Mn and Zr prevent static recrystallization and (ii) Ag in presence of Mg enhances the speed of the aging kinetics of AA2050 and hardness of the alloy. Lesser amount of  $\theta'$  phase has also been reported to be present in a strengthening phase of AA2050.<sup>121</sup>

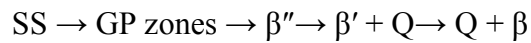
### 3.1.2 Metallurgy of AA6056 and AA6061

A medium strength aluminum alloy, AA6061 has a very good weldability, formability, machinability and corrosion resistance compared to many other aluminum alloys. On the other hand AA6056 is a relatively new alloy developed by Pechiney which as relatively higher yield strength compared to AA2024 and AA2524. Moreover, the better weldability range and resistance to intergranular corrosion of AA6056-T78 make the alloy a suitable replacement of 2XXX series aluminum alloys in aerospace

applications.<sup>125</sup> The general precipitation sequence for 6xxx ternary (Al-Mg-Si) system is reported as<sup>126, 127</sup>:



A more complex precipitation sequence is also proposed due to the presence of Cu in meta-stable condition under different designation of the quaternary Q phase ( $\text{Al}_5\text{Cu}_2\text{Mg}_8\text{Si}_6$ ).<sup>128-131</sup> Moreover, high temperature (above 400°) quaternary phase diagram also indicates coexistence of Al + Q +  $\beta$  phases in AA6056.<sup>128</sup> Therefore the proposed precipitation events for AA 6056 can also be sequenced as

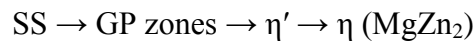


The metastable  $\beta''$  has been found to be present in a peak strength condition and was considered to be a precursor of both  $\beta'$  and Q phase of 6xxx aluminum alloys containing Cu.<sup>129, 131</sup>

### 3.1.3 Metallurgy of AA7050 and AA7099

The Al-Zn-Mg-Cu system alloys (7xxx family of alloy) are the highest strength aluminum alloys in which Zn and Mg are the principal alloying elements. Mg in Al-Zn alloy substantially increases the strength. Addition of Cu with very minuscule amount of Zr and Mn in Al-Zn-Mg alloy system increase strength by decreasing the quench sensitivity. Cu in the system reduces the resistance to general corrosion; however, it may increase the resistance to stress corrosion. Higher amount of Fe and Si may degrade fracture toughness. In addition, maximizing the amount of Mn and Cr in the 7xxx family alloy also offer increased quench sensitivity, unfortunately that decreases the overall strength of the alloy. It was reported that formation of  $\text{Al}_{15}(\text{FeMn})_3\text{Si}_2$  particle is being promoted by the addition of Mn that is hardly being dissolved during the heat treatment

process and retain in the final product.<sup>123</sup> Among the 7xxx alloys, AA7050 has been extensively employed in aerospace applications for its high toughness, stress-corrosion cracking resistance and exfoliation corrosion resistance. AA7099 is the alloy developed by Kaiser Aluminum which has been designed for an optimum combination of strength, stress corrosion cracking resistance and fracture toughness for the engineering applications in aerospace structures such as wing ribs, spars and skins as well as fuselage applications: frame and floor beam etc. The precipitation sequence of 7xxx series aluminum alloy are as follows:



The  $\eta'$  phase ( $\text{MgZn}_2$ ) is the major precipitates in AA7050-T7. In addition following five different types of phases may also exist at different temperature in 7xxx series alloys<sup>123</sup>:

1. T ( $\text{Al}_6\text{CuMg}_4$  &  $\text{Al}_2\text{Mg}_3\text{Zn}$ ): these phases exist in all system including ternary and quaternary.
2. M ( $\text{MgZn}_2$  &  $\text{AlCuMg}$ ): These phases exist in quaternary system more often in  $\eta$  phase.
3. Z ( $\text{Al}_5\text{Cu}_6\text{Mg}_2$  &  $\text{Mg}_2\text{Zn}_{11}$ )
4. S ( $\text{Al}_2\text{CuMg}$ ): S phase (46% Cu and 17% Mg)
5.  $\Theta$  ( $\text{Al}_2\text{Cu}$ )

It should also be noted here that, the solidification in 7XXX series alloy including AA7050 occurs with the formation of non-equilibrium eutectic at temperature 465°-469°C because the solubility of Zn and Mg decreases with decreasing temperature, which

has a considerable effect on precipitation hardening due to meta-stable modification of the phase  $\text{Al}_2\text{Mg}_3\text{Zn}$  ( $T'$ ) and  $\text{MgZn}_2$  ( $\eta'$ ).<sup>132</sup>

### 3.1.4 Comparison of physical and mechanical properties of aluminum alloys

It is clear from the above metallurgical evaluation of aluminum alloys that, properties of the alloy is predominated by the alloying elements (chemical compositions) and their complex interactions with microstructural characteristics during different heat treatment and deformation processing (temper). Therefore, typical tensile properties vary from 7-11 MPa for pure aluminum alloy to almost 700 MPa for a hard extruded product (AA7055-T77).<sup>124</sup> Among the heat treatable aluminum alloys, 6xxx series are relatively easy to deform compared to 2xxx and 7xxx series alloys. The ascending order of extrusion pressure for these alloys is also arranged as 6xxx, 2xxx and 7xxx.<sup>133</sup> As a consequence, the material flow and weldability range also depends on the physical and thermo-mechanical properties of these alloys along with the imposed process parameters. Typical strength properties including key temperature of the alloy considered are presented in table 3.2.<sup>119-122</sup>

Table 3.2 Relevant property data for the considered aluminum alloys

Alloy	Strength			Incipient Melting °C	SHT °C	Aging T °C (Temper)
	Yield (MPa)	UTS (MPa)	Hardness (Vickers)			
AA2050	520 (T8) 279 (T4)	556 (T8) 439 (T4)	120 (T4) 180(T8)	565	525	160 (T8)
AA6056	240(T4)	316(T4)	110(T4) 130(T6)	-	529	190 (T6)
AA6061	255(T6)	290(T6)	110(T6)	575	529	160 (T6)
AA7050	490(T6)	524(T7)	171(T6)	488	477	121 (T6)
AA7099	545(T7)	572(T7)	192 (T7)	480	-	121 (T6)

## **3.2 Experimental Facilities**

### **3.2.1 Friction Stir Welding**

A hydraulically powered MTS FSW process development system (PDS) was employed for performing all the experimental welds. The PDS is fully instrumented and semi-automatic controlled where all the process control parameters such as welding and rotational speed, forge force and tool displacement can be preprogrammed. The machine is capable of producing weld in both displacement controlled and force controlled mode. In displacement controlled process, the vertical position of the welding tool can be kept constant throughout the process, whereas in force controlled process the vertical force of the tool can be controlled and adjusted during the process. The tool is capable of applying a maximum vertical force of 135 kN, maximum traverse force in the X-axis direction of 66 kN, maximum torque of 475 N-m and a maximum weld traverse speed of 38mm/sec.

### **3.2.2 Data acquisition system for process response variables**

In-plane reaction force on FSW tool pins in conventional X direction is recorded from the signal produced from the piston pressure transducer on the X-axis hydraulic actuator. Y axis forces are obtained from the load cells in the spindle carriage. A data acquisition system for these forces signals can be adjusted up to a maximum frequency (sample rate) of 1000Hz. Tool torque can also be obtained from a torque transducer attached to the spindle. Weld power can be calculated from torque feedback and RPM. Temperature during welding will be monitored and recorded using a k-type thermocouple spot welded into the pin at mid depth in between the shoulder and pin tip along the axis of rotation. These tool temperature data during friction stir welding can be acquired using a HOBO data logger (Onset Computer Inc.).

### **3.3 Systematic Design Approach of FSW Tools**

#### **3.3.1 Materials selection for Friction Stir welding tools**

Materials use for manufacturing friction stir welding tool are commonly made from H13 tool steel, poly-crystalline boron nitride (PCBN), nickel and cobalt based alloys such as, nimonic 105 and MP159, tungsten-carbide (WC), densimet, tungsten-rhenium (W-Re), tungsten-lanthanum (W-La) etc. Among the materials, H13 is an appropriate candidate for friction stir welding of material with low melting temperatures such as aluminum, magnesium, lead and zinc while considering cost effectiveness, straightforwardness in machining for expected geometric shape and features. The other tool material have some limitations in welding Al alloys such as, PCBN and W-La are costly, coating is required on MP159 to avoid reaction with aluminum at high temperature, WC is more brittle than other materials, densimet is soft enough to machine features. The welding tools used in this study were made of H13 steel. The tool components were austenitized for 20 minutes at 980°C followed by quenching in oil to achieve hardness of 45-48 HRC. In a special case of stationary shoulder FSW, a three flatted pin was made from MP159.

#### **3.3.2 Design of FSW tool shoulder and pins**

In this study, tool shoulder geometry was kept constant while pin geometries and features were varied. This variation was facilitated by constructing the tools in two pieces with separate pins and shoulders. The shoulder dimensions were 25.4 mm diameter (1 inch), single scroll with a scroll pitch of 2.54 mm/revolution (0.1 inch/revolution). The dimensions of the cylindrical pins were 12.5 mm (0.5 inch) length and diameter of 15.9 mm (0.625 inch). Obviously, these are partial penetration welds and for the combination

of pin length and plate gages used in this study, no influence of the backing plate is anticipated. Figure 3.1(a-c) shows several views of a typical tool illustrating the manner in which the shoulder and pin are assembled. Note the presence of the hose clamp used to hold the thermocouple wire: a k-type thermocouple was embedded in the pin at the mid-height on the centerline. The standard detail of tool design with the shoulder and cylindrical pin are shown in appendix A.

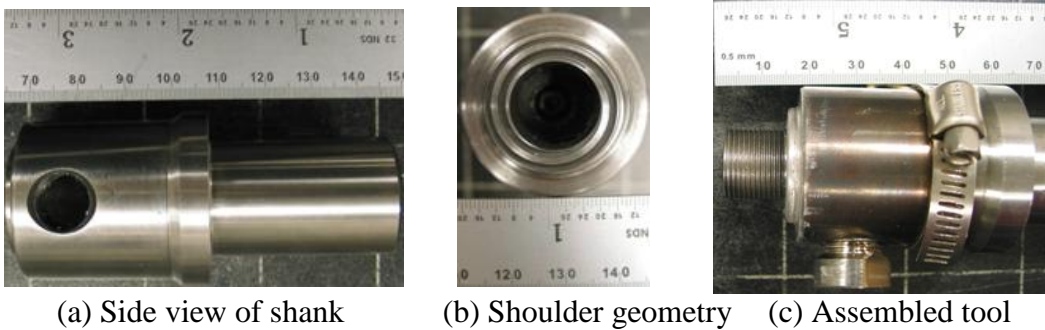


Figure 3.1 FSW tool shoulders and pin geometry

### 3.3.3 Variations in pin thread forms and thread interruptions

Four cylindrical pins were produced by machining right hand threads having different pitch dimensions as shown in Table 3.3. Figure 3.2 also illustrates the models associated with different thread forms. It should be noted here that threads on coarse threaded 2 pin (CT2) were only cut to the depth of the threads on coarse threaded 1 (CT1) pin as full depth would have resulted in a very small minor diameter. An unthreaded/smooth (U) cylindrical pin was also considered as a baseline to study and compare the effect of the thread form level during friction stir welding. Threads were interrupted by machining 1, 2, 3 & 4 flats on a CT1 pin. One, 2 and 4 flats were also cut in the smooth pin. Two, 3 and 4 flats were placed  $180^\circ$ ,  $120^\circ$  and  $90^\circ$  apart, respectively. Flats were cut to a depth of 1.35 mm, which is just beyond the depth of the thread root of CT1 pin since this thread form has highest root depth.

Table 3.3 Pin designations and dimensions of different thread forms

Pin Designation	Abbreviation in this study	Thread form detail (Pitch)	Volume of threaded channel, mm <sup>3</sup>	Helix angle, degree
Smooth/Unthreaded	U	None	0	0
Fine Threaded	FT	1.02 mm (25 Thread/inch)	268	3.6
Normal Threaded	NT	1.41 mm (18 Thread/inch)	331	5.1
Coarse Threaded 1	CT1	2.12 mm (12 Thread/inch)	480	7.6
Coarse Threaded 2	CT2	3.18 mm (8 Thread/inch)	323	11.3



Figure 3.2 Pin models illustrating different thread forms with corresponding designation

### 3.3.4 Change in pin shape and thread interruptions

The shape of the pin was subsequently changed to 8° taper for right handed normal threaded (NT) and coarse threaded1 (CT1) pins with additional features: 3 flats, 3 co-flow flutes and 3 counter-flow flutes. It is noted here that, when the orientation of pin thread and flute are in the same phase, the flute is considered as co-flow flutes and contrarily when the orientation of thread and flute are opposite the flute is termed as counter-flow flutes. The 3 flats and 3 flutes were positioned 120° from each other. Similar to cylindrical pins, flats and flutes were cut to a depth and width of 1.35 mm and 6.4 mm respectively. The pitch of flute is 76.2 mm (1 thread per 3 inches). The conical shape pins having different pin geometric features are shown in figure 3.3.

The study was also extended to investigate the optimum cutting depth of pin features and their effect on weldability and process response variables. The normal

cutting depth and width of flat were just mentioned in the earlier paragraph. Moreover, deeper flats were also cut to a depth of 2.70 mm (0.106 inch) in order to study the effect of flat depth during FSW. Hence, width of flat varies proportionally with the cutting depth.

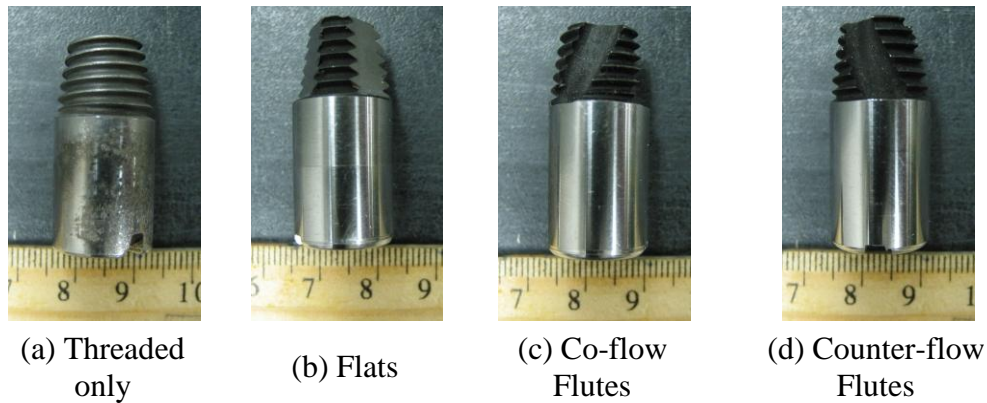


Figure 3.3 Threaded conical pins (8° taper) with different features

### 3.4 Details of Welding

#### 3.4.1 Control and Tool Parameter Setting, Weld Preparation

Bead on plate friction stir welding were performed on AA7050, AA6061, AA7099 using different sets of welding and tool parameters. Dissimilar material friction stir welding were produced in a butt joint arrangement with two different combinations of aluminum alloys using different pin features between: (i) AA2050 to AA6061 and (ii) AA7050 to AA6061. The effects of placement of alloys in advancing/retreating sides along with tool eccentricity were also considered during dissimilar material FSW. Lap welding of AA6056 was also performed with the variation in pin features and process parameters. The bead on plate friction stir welding was also performed with a stationary shoulder having identical pin (conical CT1 pin with three normal flat cut) and compared with conventional rotating shoulder FSW.

All the welds were performed using force control mode. For each weld parameter set, forge force (Z axis force) was adjusted to maintain similar depth of penetration based on observed contact conditions between the shoulder and top surface of the welded plate. Table 3.4 summarizes the welding performed with different pin geometric features and welding parameters for various welding arrangements of the considered aluminum alloys in this dissertation. The controlling parameters for corresponding welds are tabulated in Appendix B.

All the work pieces were cut to size using a radial saw and oxidation was removed from the top surface of each work piece using a hand grinder with a nylon bristle disk before performing bead on plate FSW. In the case of welding with cylindrical pin, pre-drilled holes (14.28 mm diameter and 12.2 mm depth) were made at the weld starting point to ease plunging. However, for welding with conical shape pins, these pre-drilled holes were made in two steps: (a) step 1: 12.7 mm diameter and 7.6 mm depth & (b) step 2:  $7^\circ$  taper drills with 9.5 mm tip diameter and 12.2 mm depth from the top surface of the weld material. Making pre-drilled holes ease the plunging process and avoid removal of extra materials from the weld zone.

In order to perform friction stir welding of dissimilar materials in butt joint arrangement, weld materials AA2050, AA6061 and AA7050 were cut to size using a radial saw and excess materials are removed by machining to obtain equal thickness plates. Plates were aligned and clamped by finger and side clamps on a steel back plate. All the welds were performed at a  $0^\circ$  spindle tilt angle. Misaligned welds in the butt joint arrangement were also performed in such a way that, at the starting point of pin plunge

into in advancing side material and at the end of weld pin retract from the retreating side material.

Table 3.4 Summary of the variation in pin geometric features and welding parameters in FSW

<b>Alloys &amp; Weld arrangement</b>	<b>Pin geometric variations</b>	<b>Welding Parameters</b>	<b>Discussed in Chapter 4</b>
AA7050 (32 mm thick) Bead on Pate	(a) Cylindrical pin having four different thread forms including smooth/unthreaded pin	Six sets of parameters (See Table 3.5 for 7050)	Section 4.1
	(b) Conical Coarse Threaded pin with variation in depth of flats	Three sets of parameters (Welding speed: 102 mm/min. & RPM: 240, 200, 160)	Section 4.7
AA6061 (25.4 mm thick) Bead on Plate	(a) Cylindrical pin having four different thread forms including smooth/unthreaded pin	Six sets of parameters (See Table 3.5 for 6061)	Section 4.1
	(b) Unthreaded and Coarse Threaded Cylindrical pins having different flat numbers (1, 2, 3, 4 flats)	Six sets of parameters (See Table 3.5 for 6061)	Section 4.2
	(c) Conical Normal and Coarse Threaded pin having different pin features (3 flats/ 3 co-flow flutes/ 3 counter-flow flutes)	Six sets of parameters (See Table 3.5 for 6061)	Sections 4.3, 4.9
	(d) Conical Coarse Threaded pin with variation in depth of flats	Six sets of parameters (See Table 3.5 for 6061)	Section 4.7
	(e) Coarse Threaded pin with 3 flat and Stationary Shoulder	Three sets of parameters (Welding speed: 102 mm/min. & RPM: 240, 200, 160)	Section 4.9
AA7099 (25.4 mm thick)	Conical Coarse Threaded pin with variation in depth of flats	Three sets of parameters (Welding speed: 102	Section 4.7

<b>Alloys &amp; Weld arrangement</b>	<b>Pin geometric variations</b>	<b>Welding Parameters</b>	<b>Discussed in Chapter 4</b>
Bead on plate		mm/min. & RPM: 240, 200, 160)	
AA6056 (4.2 mm thick) Lap	Conical Coarse Threaded pin having different pin features (3 flats/ 3 co-flow flutes/ 3 counter-flow flutes)	Three sets of parameters (Welding speed: 203 mm/min. & RPM: 400, 320, 240)	Section 4.6
AA2050 & AA6061 (Machined to 20 mm thick)	Conical Coarse Threaded pin having different pin features (threaded only/ 3 flats/ 3 co-flow flutes/ 3 counter-flow flutes)	Three sets of RPM and welding speed (See Table 3.6)	Section 4.4
AA 2050 & AA6061 Misaligned Butt	Conical Coarse Threaded pin having 3 flats	Table 3.6: Weld Series I	Section 4.5
AA6061 & AA7050 (Machined to 25.4 mm thick)	Conical Coarse Threaded pin with three flats	Two sets of RPM and welding speed (See Table 3.6: Weld Series I & II)	Section 4.5
AA 7050 & AA6061 Misaligned Butt	Conical Coarse Threaded pin having 3 flats	Table 3.6: Weld Series I	Section 4.5

Table 3.5 Weld Parameters for different aluminum alloys for bead on plate welds on AA7050 and AA6061

<b>Alloy</b>	<b>Tool Rotational Speed / Welding Speed (RPM &amp; mm/min)</b>					
AA 7050	120/51	150/51	180/51	<b>160/102</b>	<b>200/102</b>	<b>240/102</b>
AA 6061	<b>160/102</b>	<b>200/102</b>	<b>240/102</b>	240/203	320/203	400/203

Table 3.6 Process control parameters for dissimilar material for different combination of aluminum alloys: (a) AA2050-AA6061 and (b) AA6061-AA7050

<b>Weld Series</b>	<b>Rotational Speed (RPM)</b>	<b>Welding Speed (mm/min)</b>
I	150	102
II	300	203
III	300	406

### 3.4.3 Metallographic Sample Preparation

Metallographic specimens were cut using abrasive water jet at the location of 125 mm from the starting point of each weld for corresponding process control parameters. Grinding and polishing were performed using an automatic machine with 4 grinding steps having silicon carbide grit paper 240, 400, 600, 800 grades followed by 3 polishing steps with 5  $\mu\text{m}$  alumina, 3  $\mu\text{m}$  and finishing with colloidal silica ( $< 0.05 \mu\text{m}$ ). Specimens were chemically etched using Keller's reagent (2.5%  $\text{HNO}_3$ , 1.5%  $\text{HCl}$ , 1%  $\text{HF}$  and balance distilled water) for macro and micro structural observation. Etching time was adjusted for microstructural evaluation of different alloys depending upon the heat input during friction stir welding: relatively short time for AA2050, AA7050 and AA7099 (10-15 Sec) and long time for AA6061 (90-120 Sec). On the other hand other reagent (10%  $\text{H}_2\text{SO}_4$ , 5%  $\text{HF}$  and balance  $\text{H}_2\text{O}$ ) was used for etching AA6056.

### 3.4.4 Macro and microstructural evaluation

Weld transverse macrostructures were obtained using a scanner. All the micrographs were captured using an inverted metallurgical optical microscope: LECO Olympus PME3. Grain size at the center of weld nugget was measured using mean linear intercept (MLI) method.<sup>134</sup> These measurements were performed with 4-5 micrographs near center of nugget zone using four (4) random lines placement on each micrograph. ImageJ software was employed for processing all the images including area and length measurements.

## CHAPTER 4

### RESULTS AND DISCUSSIONS

#### **4.1 Effect of Tool Pin Thread Pitch on Friction Stir Weldability of Different Aluminum alloys**

The primary objective of current study is to investigate the parametric effects of the pin features (in current section: thread forms) on the response variables and friction stir weldability of two different aluminum alloys. A series of bead on plate friction stir welds were made with cylindrical tool pins having four thread pitches (fine thread- FT: 1.02 mm, normal thread-NT: 1.41 mm, coarse thread 1- CT1: 2.12 mm & coarse thread 2- CT2: 3.18 mm) including smooth/unthreaded pin assembled with an unvarying single scrolled shoulder. A range of process control parameters was examined in order to explore how the thread forms affect the process feedback forces and quality of the welds. It was observed that thread forms are obviously beneficial for improving tool performance and reducing in-plane reaction forces on the tool. Effective material transportation near the weld root was evident during FSW with threaded pins by eliminating/minimizing wormhole defects. Tool pins having intermediate thread pitches (1.41mm and 2.12 mm) perform better than either extreme over the range of attempted parameters. Welds were performed on aluminum alloys AA7050 and AA6061 plates and higher in plane reaction forces were observed for AA7050 in all otherwise comparable cases. Defects are far more prevalent in 7050 welds than in 6061. In order to evaluate the effect of three experimental factors (pin thread pitches, rotational speed and welding

speed) on defect contents and size of defects, a statistical tool: design of experiment (DoE) has also been employed.

#### 4.1.1 Macro-cross sectional investigation of AA7050 and AA6061 welds

Figure 4.1 illustrates the transverse macro sections of bead on plate nuggets, welded with pins having various thread pitches, where AA7050 FSWs are shown in Fig. 4.1(a) and AA6061 FSWs are shown in Fig. 4.1(b). In each image the advancing side is on the left. Each row of images shows the cross sections for a particular thread pitch (U, FT NT, CT1, and CT2) while each column is for a particular combination of rotation rate and welding speed.

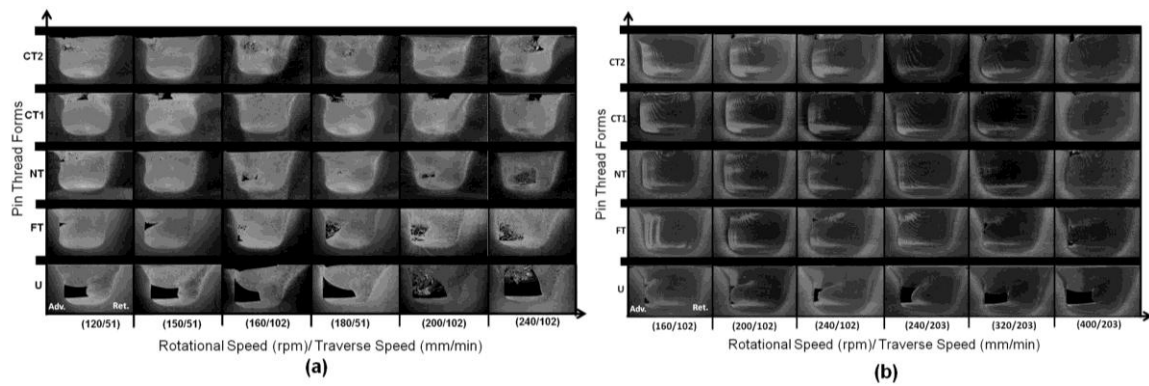


Figure 4.1 Transverse macro-sections of weld nugget for bead on plate weld on (a) AA7050 and (b) AA6061

The macrographs of 6061 indicate a much lower incidence of defects than in 7050 which is consistent with the general observation that 6061 is easy to weld relative to 7050. Defects are present in all of the 7050 welds with the largest defects associated with the unthreaded pin (U). Welding with threaded pins in both 7050 and 6061 can also lead to the formation of surface breaking defects under some welding conditions. The surface breaking defect formation may be due to the action of the threaded tool pushing material downward toward the weld root. This down thrust helps to eliminate near root wormhole

defects, but, if too much materials escape as flashes; a surface breaking defect may be created. Effective material flow was observed with intermediate thread forms (CT1) for both 7050 and 6061 welds within a subset of the attempted process parameters. Moreover, CT1 has the highest grip volume in the threaded channel compared to other thread form in this study as observed in Figure 4.2 (data are mentioned in Table 3.3). The ability of entrapping larger volume of materials along with the moderate helical angle (see Table 3.3) facilitates appropriate consolidation near the weld root by the pin having CT1 thread form.

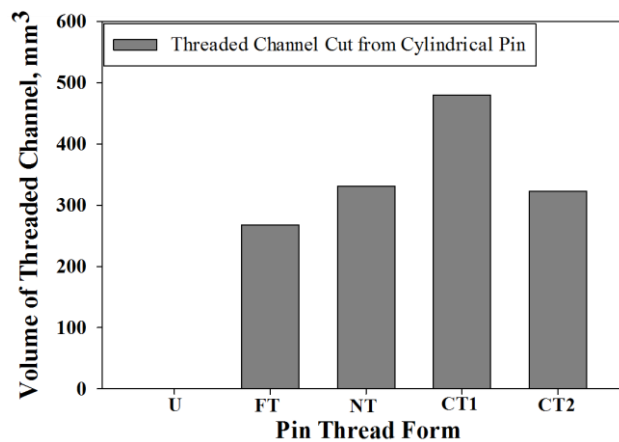


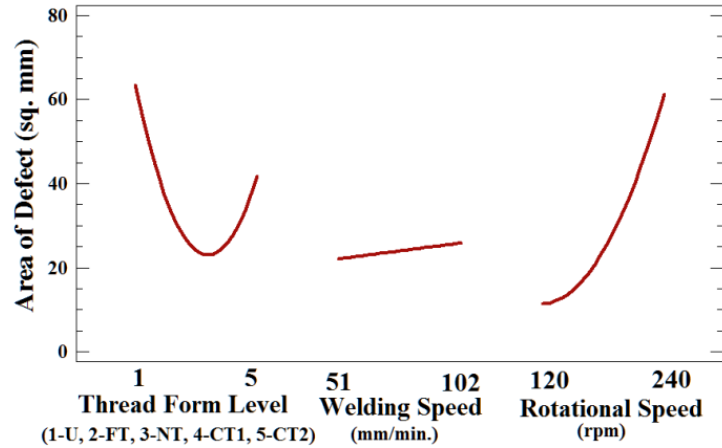
Figure 4.2 Volume of the threaded channel cut for different pitches

All tools produced the best results in 7050 with lower rotation speed. This is consistent with welding experience in thick plate 7XXX alloy and is sometimes claimed to be related to prevention of local melting.<sup>51</sup> This phenomenon is also evident in 6061 welds with the unthreaded pin. It is also observed that, defects are significantly reduced while welding at lower rotational and travel speed in both alloy welds. This is an interesting result in that it is not expected that local melting would be a problem in 6061 regardless of the applied rotation rate. There are several possible explanations for this phenomenon which do not require local melting. Compared with high tool rotation rate

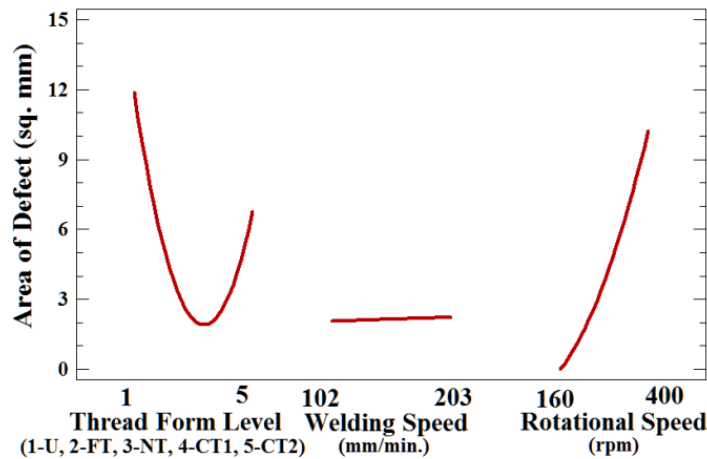
and welding speed, low rotational and welding speed during FSW most likely will result in a more gradual temperature gradient in the deformed material along the pin radius direction, gentler material flow/deformation as well as the less strain rate in the FSW. Besides, local melting is another major reason of defective nugget when low incipient melting point aluminum alloys, such as 7050 is joined with high rotational and welding speed parameters.

Figure 4.3 (a-b) shows the main effect plots for area of defect of weld vs. three experimental factors for AA7050 and AA6061 obtained from design of experiment (DoE) analysis. Commercially available software, Statgraphics Centurion version XV, was employed for operating response surface design of experiments. The quadratic effects were adopted in order to establish the correlation and dependence of the tool thread pitches and process control parameters with defect contents. Since all the welding was performed within a predetermined variable window (process control parameters), a user specified design was used to run the analysis in Statgraphics. The areas of defect in the weld macro cross sections were obtained using image processing software, ImageJ. The main effect plot estimates the variation in response (in this case: area of defects), when each of the affecting factors was changed from its low level to high level. It is evident from Figure 4.3 that, for both alloys, intermediate thread form level (pitch) of pin results in lower defect content. For both alloys the effect of rotational speed is significant. Increasing RPM increases defect content in both AA7050 and AA6061 welds. For both alloys, increasing welding speed correlates with larger defect content. This may be simply due to fact that higher welding speeds were used in 6061 and the effect is not

linear. ANOVA test results for corresponding analyses obtained from Statgraphics are reported in Appendix C.



(a) AA7050



(b) AA6061

Figure 4.3 Main effect plot of area of defect for different alloys obtained from design of experiment results

The progression of the defect formation trend with respect to thread forms and rotational speed effect under constant welding speed was also evaluated using response surface plot from DoE analyses. Figure 4.4 (a-d) presents the contour of the estimated surface plot for area of defects with different welding speed extracted from DoE analysis.

It appears in each welding speed that, the minimum defect formation converges to thread form level 3 and 4 (red region in Figure 4.4) which are NT and CT1 pins.

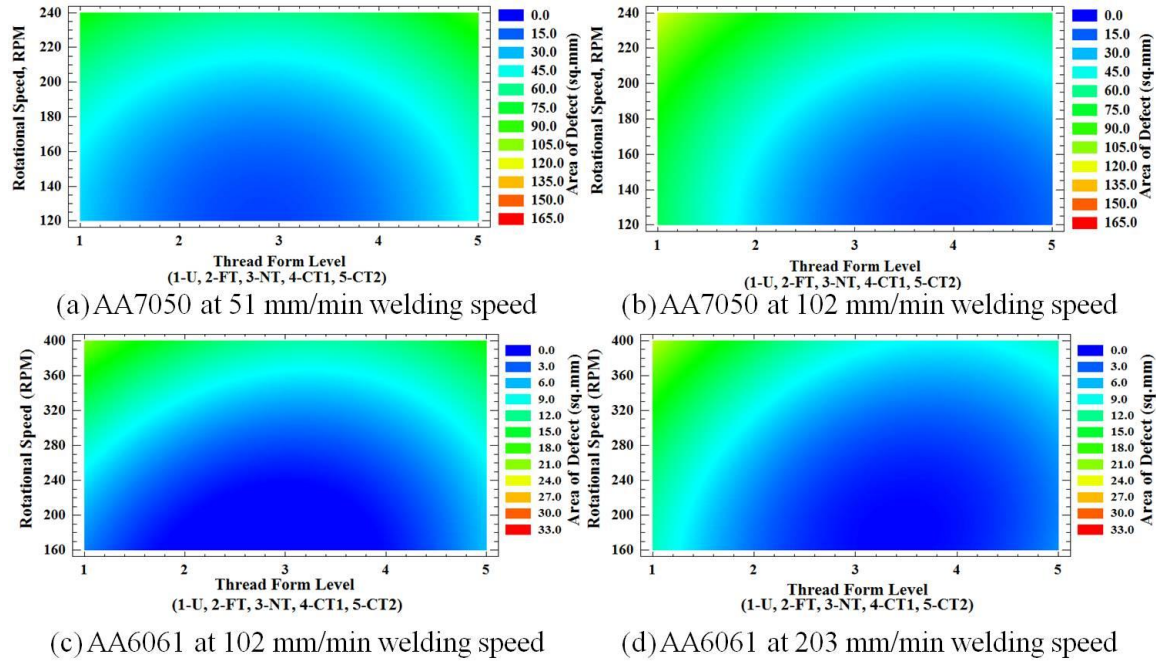


Figure 4.4 Contour of estimated surface plot for different welding speed

#### 4.1.2 Process Response variable for bead on Plate weld on AA7050

In plane reaction forces, torque and pin peak temperature as a function of tool rotational speed are shown in Figure 4.5 (a-d) for the 7050 welds. The filled symbols are for 51 mm/min. welding speed and the open symbols are corresponding to 102 mm/min. Each thread form has different symbol geometry. The average in-plane reaction forces were calculated over a weld length of 20 mm near the position where the specimens were cut for metallographic evaluation. The X-force plot (Figure 4.5-a) exhibits several salient features: (1) the U pin results in the highest X-force followed, generally, by the CT2, (2) in almost all cases, the X-force increases with increasing rotational speed and (3) increased welding speed leads to increased X-force. It should be noted that the threads on CT2 were only cut to the depth of the threads on CT1 as full depth; otherwise it would

have resulted in a very small minor diameter. So, the flat thread crest on the pin may contribute to the high X-force associated with the CT2 pin. The increase in X-force associated with the increase in RPM may in reality be an association with increased defect size. Y-axis force (see Figure 4.5-b) shows very little correlation with both RPM and welding speed, however, U pin has the highest forces followed by the FT in. The CT1 pin has the lowest forces, the magnitude of which is one third of U pin. The high force on the U pin is likely a result of unbalanced pressure on the pin related to defect formation. Mass conservation around the tool must be satisfied for producing defect free welds.<sup>75</sup> For the unthreaded pin, mass balance was not satisfied which is evident from the defect content in the welds (see Figure 4.1-a). Moreover, the approximately vertical edge of the wormhole defects on the advancing sides in weld cross sections for U pin (Figure 4.1-a) clearly suggest that materials those were extruded from advancing side by the cylindrical pin were not re-deposited behind the pin as tool move forward. Therefore, the resistance to material flow might produce additional pressure on the pin from the retreating side thus increases Y-force for U pins.

As might be expected, torque (Figure 4.5-c) is not a strong function of pin form. Torque declines with increasing rotational speed and is higher for the higher welding speed at a given rotation rate. In Figure 4.5-d it was observed that, temperature (measured in the pins) has an inverse relationship to the torque so increases with increasing rotational speed. The U pin exhibits the highest temperature and the CT1 demonstrates the lowest; however, it is somewhat risky to draw too strong a conclusion from this as small differences in thermocouple placement may have substantial effects on measured temperature. It is probably best to use probe T to judge the effects of changing control

parameters on the temperature for a single pin and not to compare between pins. Nevertheless, temperature measured at pin mid-depth along the axis of rotation reflects on the average process temperature during FSW. <sup>135</sup> One effect which is interesting is that the spread of temperature between the various pins is less for the higher welding speed than for the lower.

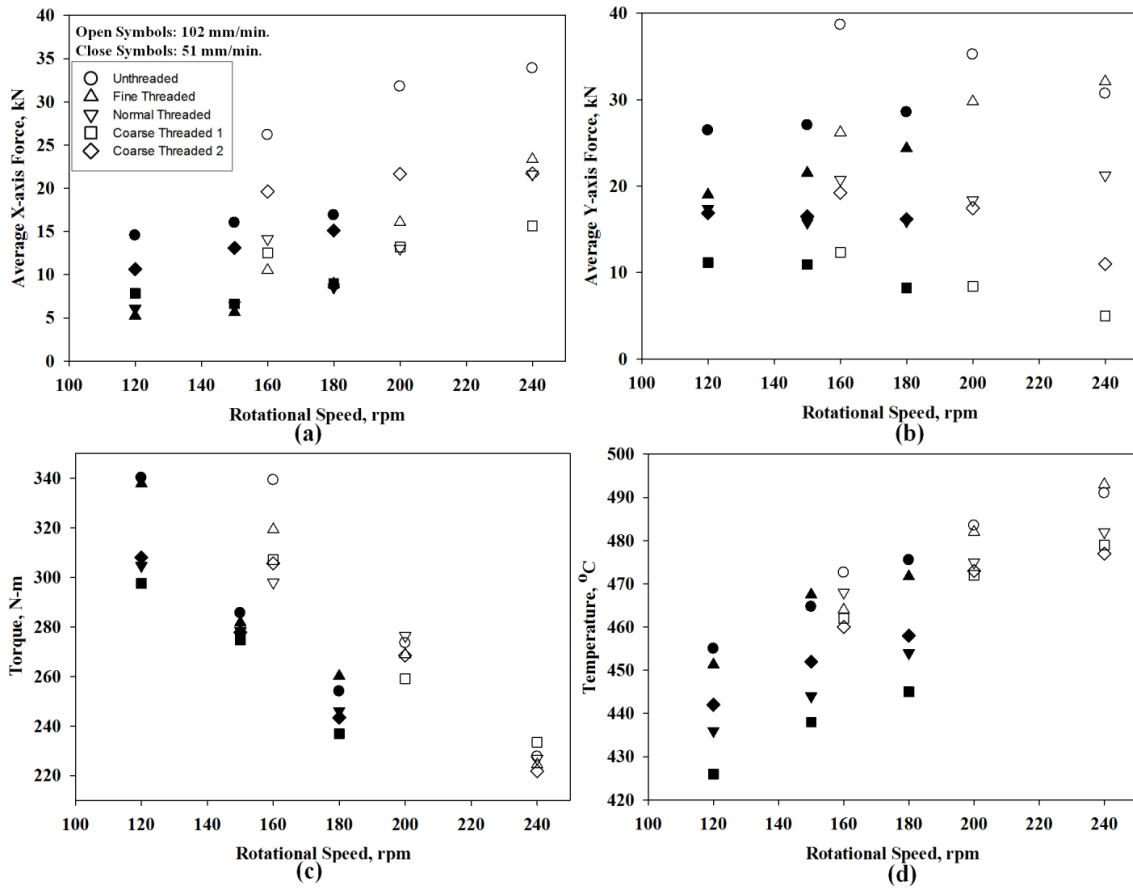


Figure 4.5 In plane forces (a-b), torque (c) and pin peak temperature (d) as a function of tool rotation for bead on plate weld on AA7050

#### 4.1.3 Process Response variable for bead on Plate weld on AA6061

Figure 4.6 is the process response variables (in-plane force, torque, temperature) as a function of tool rotation rate for the 6061 welds. The open symbols in Figure 4.6 are related to 102 mm/min. welding speed and the filled symbols are corresponding to 203 mm/min. A declining X-axis force with increasing rotational speed was observed in 6061

welds (Figure 4.6-a) which is the opposite of the trend seen in the 7050 welds (Figure 4.4-a).

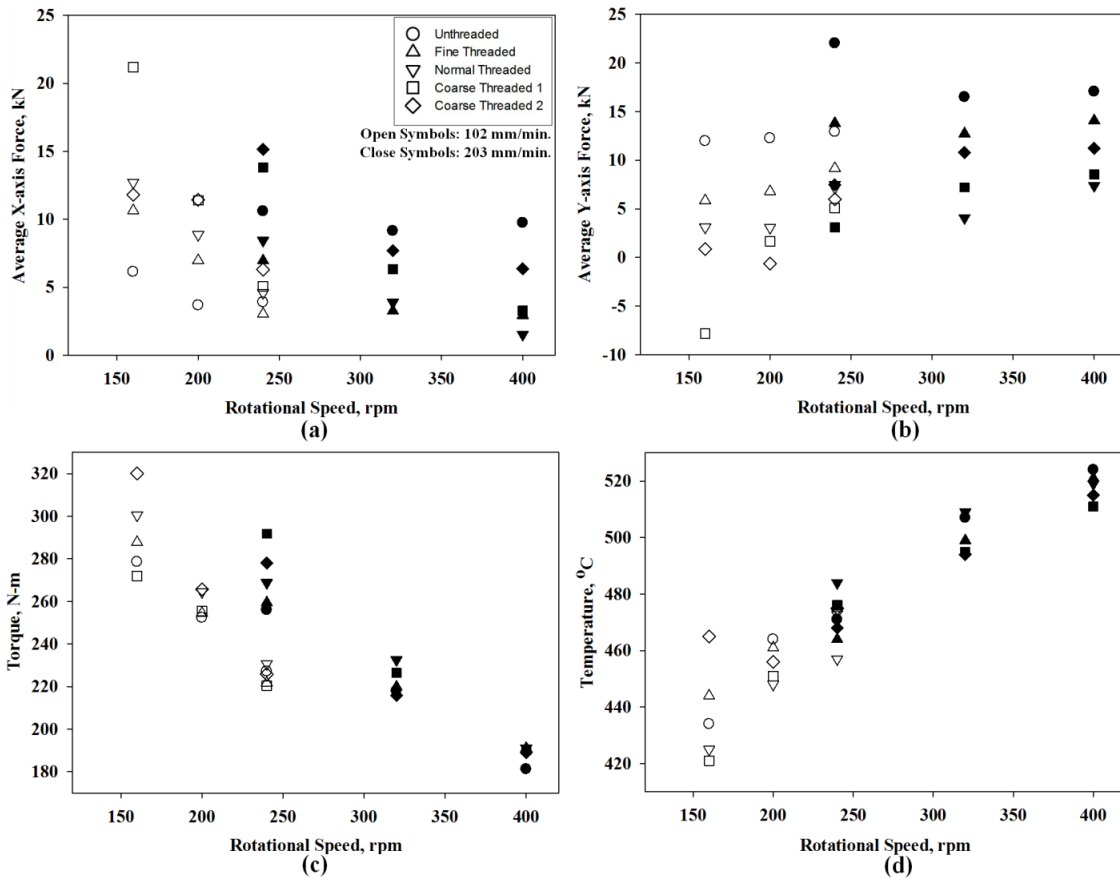


Figure 4.6 Reaction forces, torque and pin peak temperature as a function of tool rotation for bead on plate weld on AA6061

Significantly, the defect contents in 6061 welds are much lower than those of 7050 welds. However, if, as has been observed for many aluminum alloys, including 6061 and 7050, that an X-force minimum is associated with an intermediate RPM for a given welding speed,<sup>114</sup> it may be that the minimum is at higher RPM for 6061 than for 7050 and that this part of the weld parameter envelope has not been encountered in this study. Interestingly, there does not appear to be a strong relationship between pin thread forms and X-forces in these 6061 welds. Y-force exhibits a general, weak, trend to increase with increasing rotational speed. U and FT pins generally produce the highest

forces in 6061 welds. It is also interesting to note that, at lower rotational speed (CT1 at 160 RPM & CT2 at 200 RPM) Y-axis force acts on the pin in the opposite direction; from advancing to retreating side with surface defects on the advancing side (this is shown by the negative values for Y-force under those conditions). No explanation for this phenomenon is currently available. The torque and temperature relationships to rotational speed are “standard” and in-line with the 7050 although neither the temperature nor the torque exhibits an observable trend with pin form.

#### 4.1.4 Comparison of AA7050 & AA6061 welds for similar processing parameters

Overall, reaction forces on the pin for 7050 welds are significantly larger than those for 6061 welds. This is evident from a polar plot of these reaction forces shown in Figure 4.7 for a constant welding speed of 102 mm/min. This polar plot is set up with the convention that the force exerted by the work piece that impedes the motion of tool is defined as the positive X axis force. The positive Y-axis force acts perpendicular to X direction towards the advancing side from retreating side. In some subsequent analyses, references are made to the resultant force, which is the vector sum of average X and Y forces. However, these average X and Y forces are not necessarily in phase, therefore, at any moment the resultant force on the pin is not necessarily equal to the reported average resultant force. Clearly, pins encounter higher resultant reaction in 7050 than in 6061: 6061 and 7050 results are separated by the dotted ellipse in Figure 4.7. As mentioned earlier, the CT1 pin at 160 RPM exhibits negative Y force that corresponds to an anomalously high resultant reaction (22.6 kN) among 6061 welds. The range of the resultant reaction for 6061 is 7.2-22.6 kN, whereas for 7050, the range is 14.4-47.5 kN. Interestingly the resultant force on the CT1 pin was observed lowest for welding on 7050

in each welding parameter, the magnitudes of the forces are just above the upper bound of the U pin for 6061 welds. The orientations of the resultant reactions relative to pure x-force range between 15° and 60° for 7050 welds (total range is 45°). However, for 6061 welds, orientations of average in-plane resultant are more scattered, ranging between 330° (or -30°) and 90° (total range 120°).

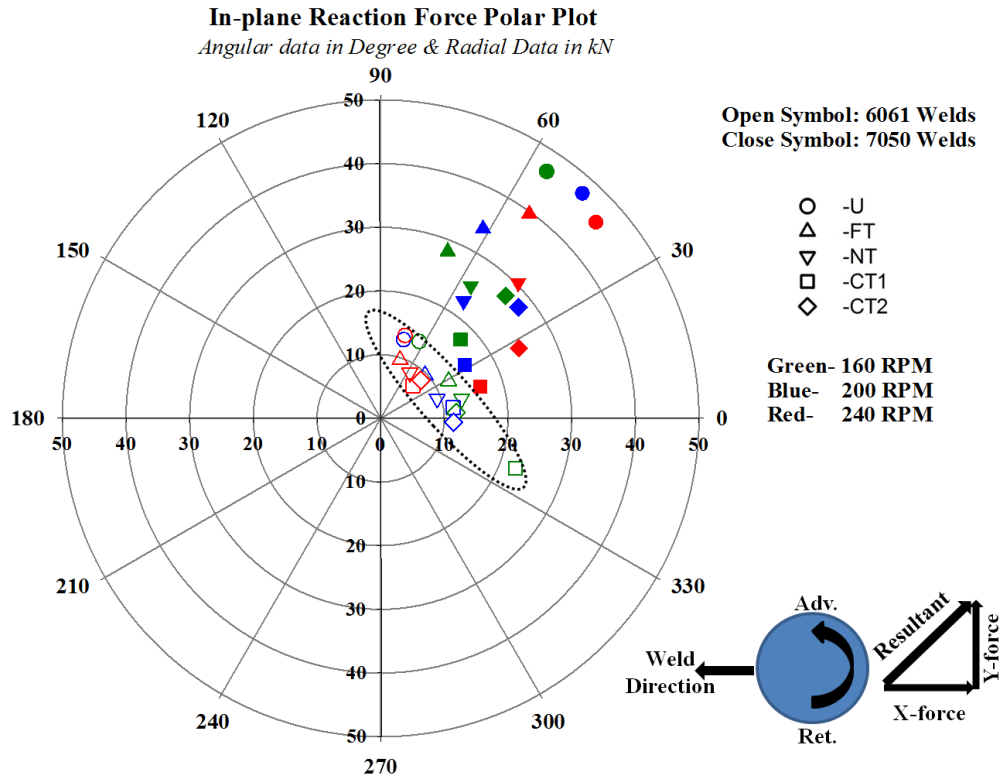


Figure 4.7 Polar plot of In-plane reactions on pin for welding on AA7050 and AA6061

It should be noted here that the periodic nature of the in-plane forces<sup>75, 110, 112</sup> that is, signals generated for X and Y forces has not been addressed at this point in the present analysis. However, these quantified magnitudes of average in-plane forces in this analysis provides an estimation of in-plane forces and the trends in the relationship among tool parameters, welding parameters and alloy properties. Moreover, the production of a fully consolidated, defect free weld may be associated with the pin shape and geometries,

features (thread forms and interruptions) and pressure on the pin which is in turn governed by process control parameters (RPM, welding speed and forge force).

Figure 4.8 presents the measured probe temperature as a function of weld power for a constant welding speed of 102 mm/min. for both AA7050 and AA6061 welds. Generally the peak temperature is directly proportional to power in friction stir welds and can reach a plateau with the increasing rotational speed at some welding speeds.<sup>35</sup> In Figure 4.8, the data were grouped by pin thread forms, that is, the same pin features have the same type of symbols. Weld power and temperature relationships shown in Figure 4.8 for AA6061 and AA7050 are typical when examined for constant tool geometry, that is, peak temperature increases with increasing weld power. Two linear least square fit lines have been drawn through the data for 7050 and 6061 separately exhibiting linear relationships between pin peak temperatures and weld power. However, the correlation coefficients for 7050 and 6061 are only 0.53 and 0.65. If three data points for U and FT pins in 7050 are omitted from the fit the correlation coefficient for 7050 can be improved to 0.83: the U and FT pin welds have large wormhole defects which may have anomalous effects on the supposed relationship. It has also been observed in previous work those small variations in thermocouple placement (and potentially, in pin geometry) may have an effect on measured temperature: this could affect the consistency of the power/temperature relationship as it is not certain that all thermocouple placements are equivalent. It is, however, interesting to note that in general, for a given weld power, the temperature in the 6061 weld is lower than the corresponding 7050 weld: this is consistent with the ranking of the thermal conductivities of the two alloys.

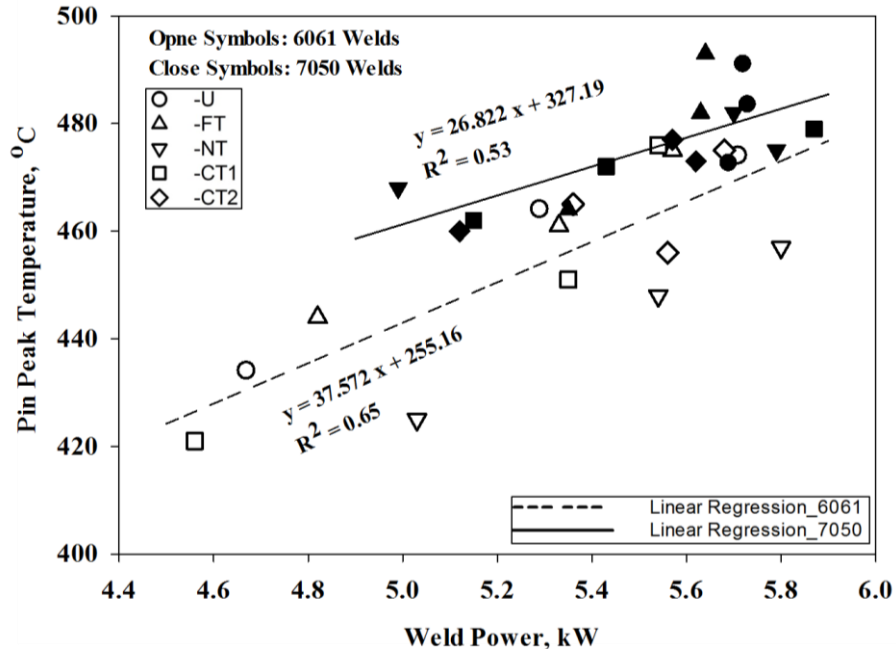


Figure 4.8 Peak temperature as a function of weld power for welding speed 102 mm/min

#### 4.1.5 Summary Observations on cylindrical pin study with different thread forms

The effect of tool pin thread forms and the process control parameters on the friction stir weldability of two different aluminum alloys along with some process response variables have been examined. The salient features extracted from the present study are as follows:

- Wormhole defects can be removed or minimized by machining helical features such as threads in tool pin during friction stir welding.
- Material flow around the tool pin is a complex function of thread form and process parameters. Intermediate threaded tool pins produced best quality welds with reduced defect production in both alloy systems.
- Defect contents are reduced when welding was performed at lower RPM.
- Alloys 7050 and 6061 have markedly different weldability.
  - In –plane forces are much higher in 7050 than in 6061.

- 7050 exhibit more defected welds than 6061.
- Over the range of examined rotational and welding speed, increasing RPM generally:
  - Decreases in-plane forces in 6061.
  - Increases in-plane forces in 7050.

While some of these observations may be general, this cannot with certainty be stated. Other process parameters ranges, alloys, gages, and tool designs may give different results. However, systematic information obtained in the present study was advantageous for subsequent tool development with more complex geometric features of pin.

#### **4.2 Effect of Thread Interruption by Machining Flats in Pin**

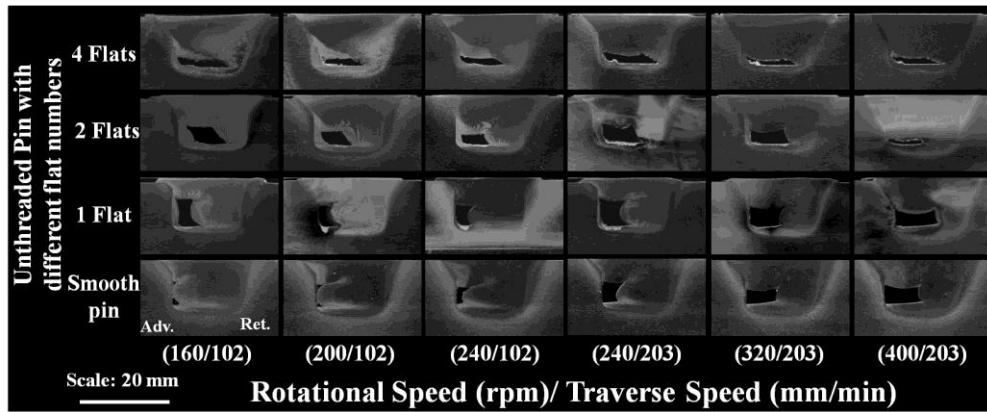
Having discussed the effect of pin thread form in the preceding section, the effect of thread interruption in friction stir welding is considered next. It has been established that the intermediate thread form level on a cylindrical pin has the greatest impact on minimizing defect formation. It is imperative to use appropriate thread pitch with the addition of vertical features in order for obtaining completely defect free welds. Since CT1 pin was found to produce better quality welds in terms of eliminating or minimizing defects compared to any of the U, FT NT or CT2 pins, therefore, this thread form, along with the U-pin (as a baseline) were considered for further modification with thread interruptions. Hence, the CT1 pin was termed as threaded pin in this section and was tested with different numbers of flats: 1, 2 (180° apart), 3 (120° apart), and 4 (90° apart) while the unthreaded pin (U-pin) was tested with 1, 2, and 4 flats. The weldability and process response variables were examined on AA6061 for a set of process control

parameters. It was observed that, threads with flats drastically improve weld quality by eliminating certain defects as well as minimize in-plane forces. Entrapment of weld materials in the threaded channel and subsequent release in the flat region near vicinity of three flatted rotating pins facilitates apposite consolidation near root to produce completely defect free welds under all welding conditions. Spectral analyses of in-plane reaction forces and weld cross sectional analysis were also investigated to establish correlation among pin flats, force dynamics and defect formation. The amplitudes of spectra of in-plane forces were consistently observed lowest for defect free welds.

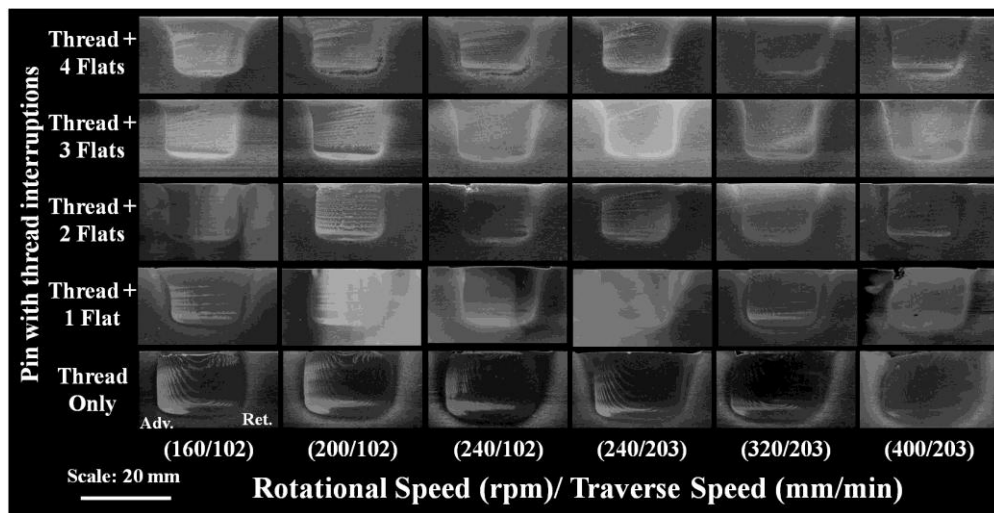
#### 4.2.1 Weld macro/microstructural evaluation of friction stir welded part

Figure 4.9 (a-b) shows the transverse macro sections of the welds with unthreaded pin (Figure 4.9-a) and threaded pin (Figure -b) having different flat numbers. It is interesting to note that the wormhole defects were not eliminated with the introduction of flats in the unthreaded pin as shown in Figure 4.9-a. Moreover, the size of the wormhole defects is most likely dependent on welding parameters as illustrated in Figure 4.10. In case of unthreaded pin without flat, defect area increases with increasing tool rotational speed (circular symbol in Figure 4.10). Contrarily, for the flatted pins, defect content decreases with increasing tool rotation rates for similar traverse speed (see Figure 4.10). Moreover, 2 and 1 flatted pins produce largest defects in the welds at welding speed of 102 mm/min. and 203 mm/min. respectively. Nevertheless, the defects are localized to the near root region on the advancing side as the number of flats is increased without altering much the volume of wormholes. This indicates the role of higher flat numbers in improving the material transport around the pin while also illustrating that helical features are necessary to produce downward flow in order to eliminate root defects. Therefore,

helical features such as threads or flutes are the only way of causing effective vertical flow of materials in case of cylindrical shape pins.



(a) Weld cross sections for unthreaded pin



(b) Weld cross sections for threaded pin

Figure 4.9 Transverse macro cross sections of weld nugget zone for weld with pins having various thread form and flat numbers

Moreover, macro and micro structural investigation revealed no wormhole defect, but surface breaking defects for many of the welds performed with threaded pins having different flat number (Figure 4.9-b). Figure 4.11 (a-b) shows two representative microscopic defects in the cross sections near weld crown. Interestingly, pin with 3 flats produced the best results based on the macro and microscopic examination.

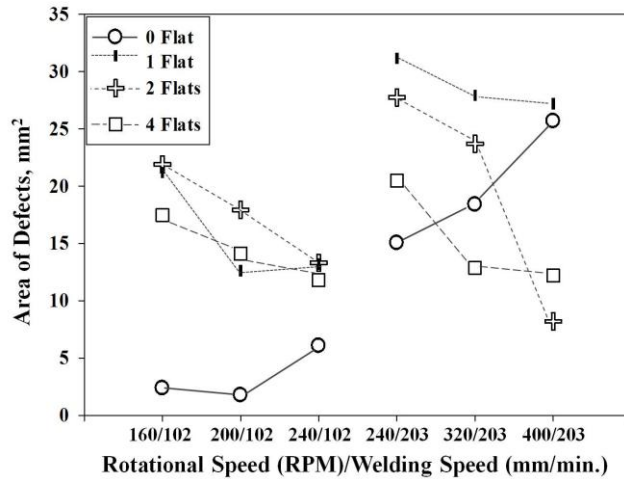


Figure 4.10 Defect contents area as a function of welding parameters having different flat numbers of unthreaded pin

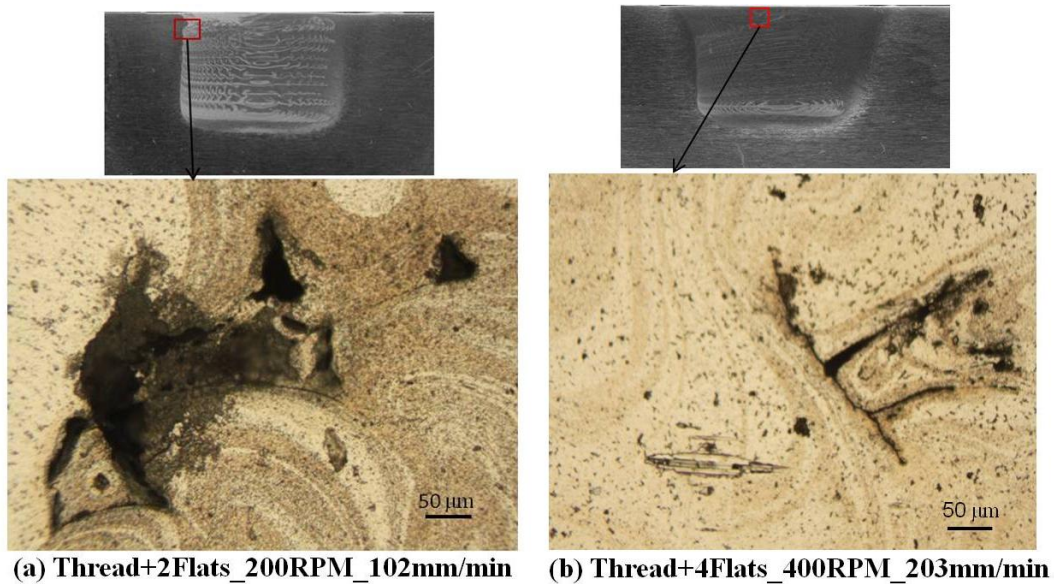


Figure 4.11 Microscopic defects near weld crown

It was observed that for many of the welding conditions, upon pin retraction, the unthreaded pins had some material adhering to the trailing side of the flat. On the other hand, the threaded pin with flats was found free from this adhesion. Examples are shown in Figure 4.12. This phenomenon of material adhesion might have an effect on tool reactions and can be explained by observing tool design criteria in manufacturing flats and threads in pin. More explanation of this will be discussed in Section 4.2.4 while

establishing the correlation among the process response variables, welding parameters and tool geometric variables.

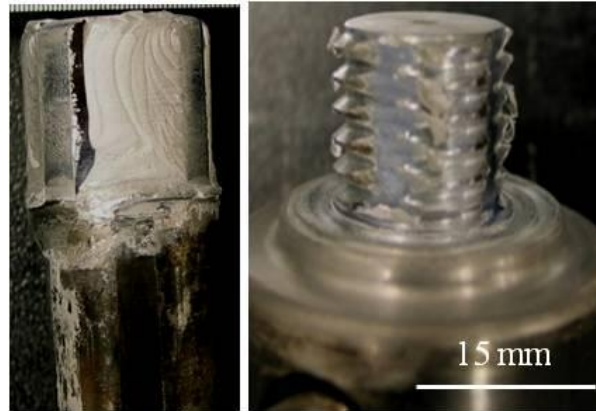


Figure 4.12 Unthreaded pin (left) and threaded pin (right) showing material adhering to flats (or not)

In a nutshell, it was observed from macro and micro structural evaluation that, completely defect free welds were produced with threaded pin having 3 flats. Hence, the performance of the cylindrical shape pin having a thread pitch of 2.12 mm and 3 flats was unique for the examined set of weld parameters in producing defect free welds on this particular weld material. It may be surmised that for the pin geometry used, the optimum balance of rotational transport and vertical transport of material is achieved for the threaded and three flats.

#### 4.2.2 Influence of flats on applied forge force and in-plane reaction forces

It was mentioned in the Chapter 3 that force control mode was used for studying friction stir welding in this dissertation. Since the forge force (Z force) was adjusted to obtain similar contact conditions between weld materials and tool shoulder, therefore Z-force was varied depending on the pin feature and welding parameters. The required forge forces as a function of welding parameters (rotational and welding speed) and flat numbers are shown in the form of a histogram in Figure 4.13: (i) unthreaded pins in

Figure 4.13-a and (ii) threaded pins in Figure 4.13-b. It is interesting to note from Figure 4.13-a that, required forge force is higher for higher flat numbers for similar welding condition in case of unthreaded pins for up to 240 RPM rotational speed and minute difference was observed at 320 and 400 RPM. However, threaded only pin (no flats) always require higher forge force compared to pin having different flat numbers for similar welding parameters. This is conceptually understandable since, materials in the threaded channel are to be transported in the downward direction continuously (no interruption in threaded only pin) resulting in an upward thrust on the tool for a right hand threaded pin rotating in counter-clock wise direction. Hence the additional forge force is required in this case.

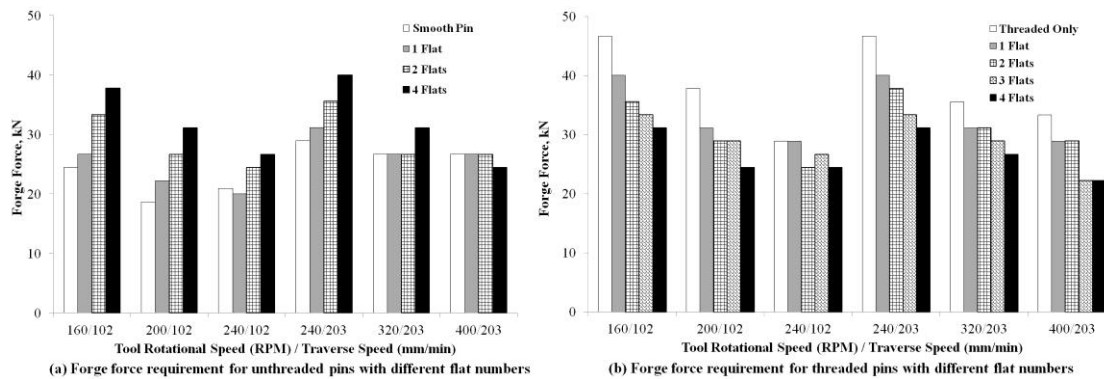


Figure 4.13 Applied Forge force during FSW process on the basis of maintaining similar contact condition between weld materials and tool shoulder due to variation of pin features

Tool feedback forces were analyzed to reveal the effect of flats on pin reaction forces during FSW. Figure 4.14 (a-e) shows the polar plots of average in-plane reaction forces for pins with different flat numbers. This polar plot is set up with the convention shown in Figure 4.14-f where, the force exerted by the work piece that impedes the motion of the tool in the welding direction is defined as the positive X axis force. The positive Y-axis force acts perpendicular to X direction towards the advancing side from

retreating side. It is observed in polar plots of Figure 4.14 that, the unthreaded pin produces the largest in plane forces (highest resultant magnitude) in all welding conditions and flat numbers compared to the threaded pin. It is also revealed from Figure 4.14 (a-e) that, the range of orientation ( $\theta$ ) of the in-plane resultant force does not vary much for unthreaded pins, however the average range of orientation decreased with increasing flat numbers.

On the contrary, the range of  $\theta$  is highest for no flats and decreases with increasing flat number for threaded pins (although, the spread for three and four flats are similar). Table 4.1 summarizes the spread of the orientation of resultants for different pin features (absence/presence of thread) and flat numbers. While considering similar welding parameters, it is worth to note that for unthreaded pin increasing flat number lead to orientation range of the resultant force to be decreased with respect to the axis of zero X-axis force. On the other hand, orientation range of the resultant increases with increasing flat number for threaded pin. The presence of three and four flats (Figure 4.14, d-e) continue the trend of narrowing  $\theta$  around a value near  $60^\circ$  without substantial variation in resultant magnitude. In general it can be said that the presence of flats does not greatly alter the magnitude of the resultant in-plane forces: this property seems to be dependent on thread form and weld parameters. However, the presence of flats does affect the direction of action of the resultant, narrowing the range of  $\theta$ .

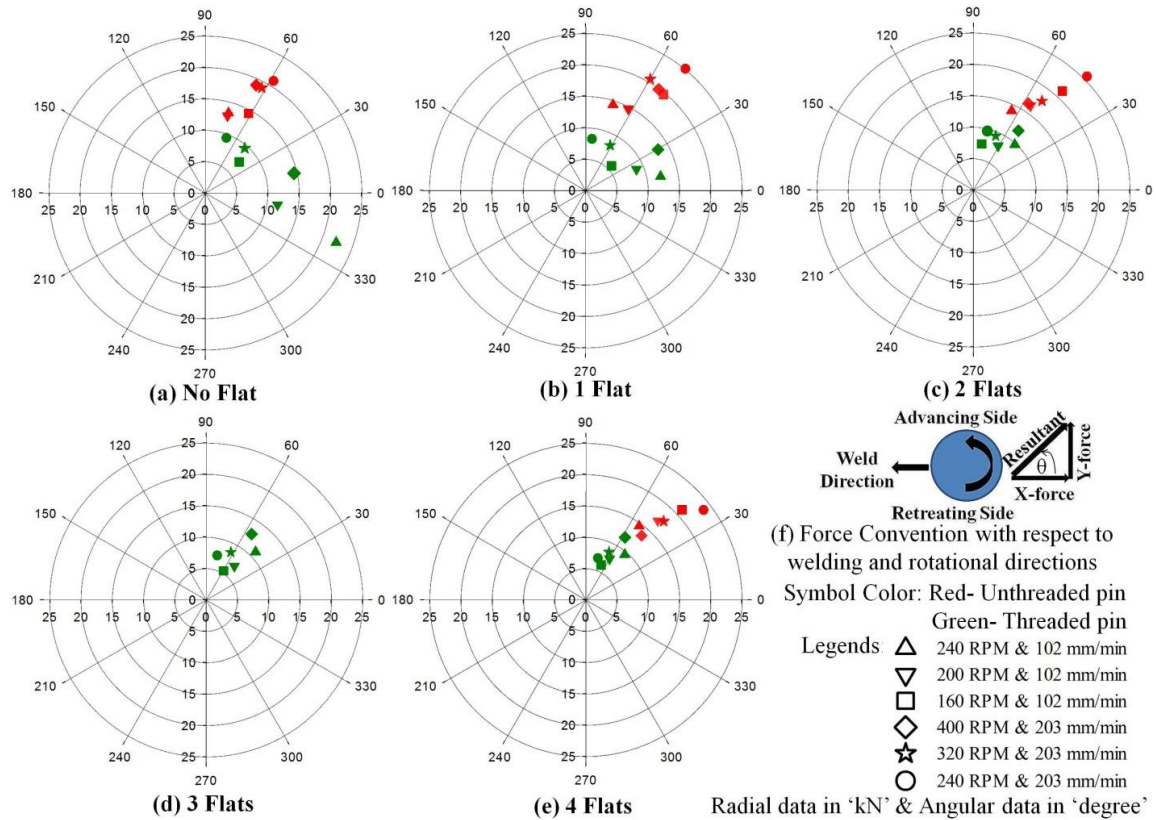


Figure 4.14 Polar plots of average in-plane Reaction forces for tool having different flat numbers

Table 4.1 Spread of the orientation (angles are in degree) of resultant reaction with respect to the axis of zero X force

Pin Flat Numbers	Average Orientation ( $\theta$ ) with range	
	Unthreaded	Threaded
No flat	$65.5^\circ \pm 8^\circ$	$23.5^\circ \pm 44^\circ$
1 Flat	$60^\circ \pm 11^\circ$	$41.5^\circ \pm 36^\circ$
2 Flats	$53.7^\circ \pm 10^\circ$	$64^\circ \pm 16^\circ$
3 Flats	-	$57.6^\circ \pm 15^\circ$
4 Flats	$46^\circ \pm 8^\circ$	$61.6^\circ \pm 12^\circ$

#### 4.2.3 Effect of pin flats on tool torque and temperature

Figure 4.15 (a-b) shows the measured torque as a function of tool rotational speed for unthreaded and threaded pins with various flat numbers. The measured torque monotonically decreases with increasing tool rotational speed for similar pin profile.

Considering the unthreaded pins (Figure 4.15-a), highest and lowest average torque was observed for 4 flatted and one flatted pin respectively while comparing similar welding condition, however difference in required torque for different pin features became insignificant 400 RPM rotational speed. Moreover, for threaded pins, no consistent trend in required torque was observed with respect to pin flat numbers while comparing similar welding parameter, yet also variation is insignificant at highest rotational speed (400 RPM). Overall the decrease in torque with increasing rotational speed is common phenomenon which is due to the lessening of resistance of plasticized material around tool. The basis of this phenomenon can be elucidated by examining the process temperature. Figure 4.16 shows the pin peak temperature versus weld power for unthreaded (Figure 4.16-a) and threaded (Figure 4.16-b) pins having different flat numbers. It should be noted here that, the temperature measured in pin can be considered as an average process temperature of weld material in contact with the pin that has been found to provide reasonable representation of nugget temperature with change in welding parameters.<sup>135</sup>

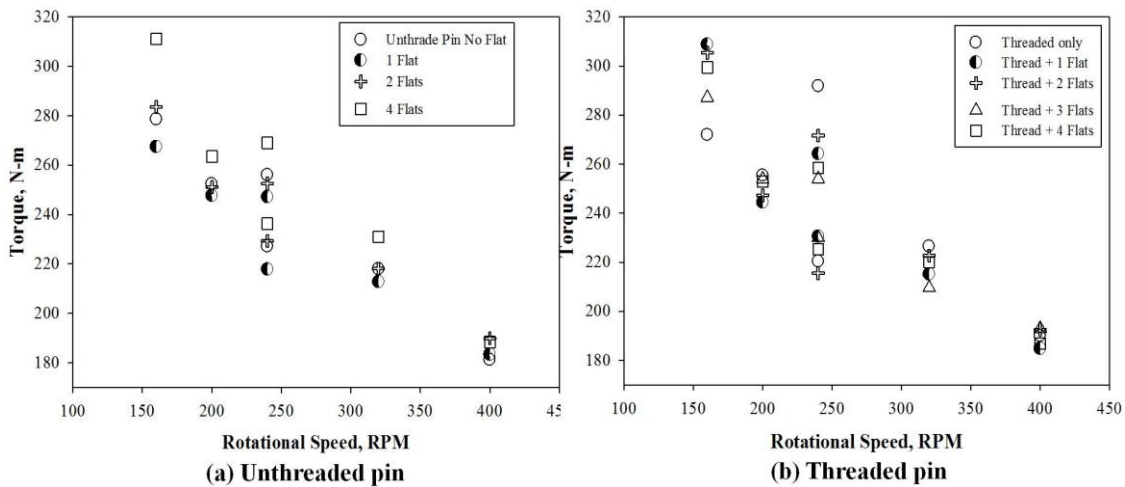


Figure 4.15 Tool torque as a function of rotational speed for different flat numbers

The pin peak temperature increases with increasing weld power or increasing tool rotational speed for constant welding speed in both unthreaded and threaded pins with various flat numbers. However, power increases significantly at high welding speed for rotation rate of 240 RPM while a minute decrease in pin peak temperature was observed. The decrease in peak temperature at high welding speed is might be due to short exposure of heat source which is directly associated with length of time for the weld material to stay above a certain temperature. A study by Reynolds et al.<sup>35</sup> has also shown that the temperature transient is governed by the welding speed. In general, variation of flat number for unthreaded pin does not greatly affect temperature; this is mostly dominated by welding parameters.

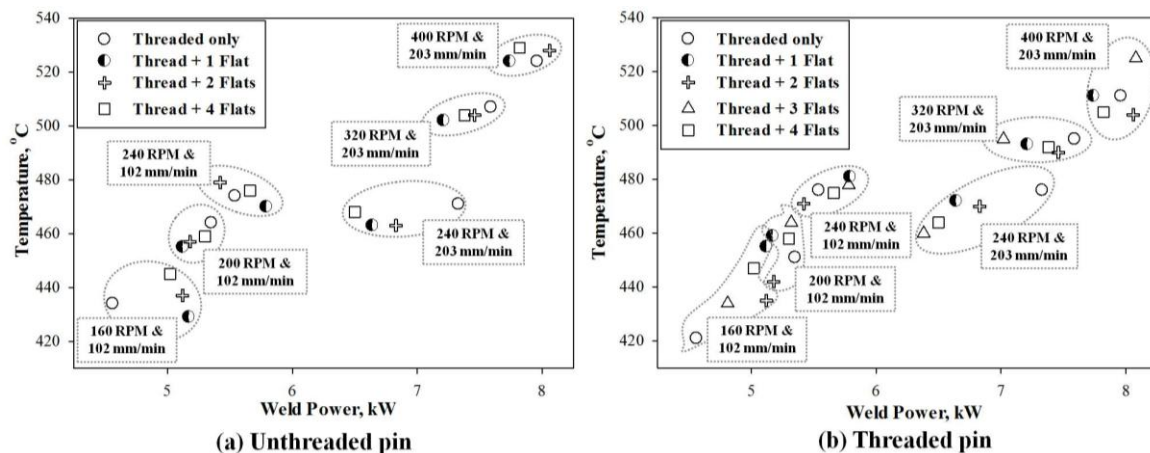


Figure 4.16 Pin peak temperature as a function of rotational speed for different flat numbers

On the other hand for threaded pin, while the relationship of temperature- power (Figure 4.16-b) reflects on the Torque-RPM plot in Figure 4.15-b, however is not consistent with regards to flat number. For example at 160 RPM rotational speed, pin with thread +1 Flat and threaded only pin have highest and lowest temperatures/power respectively. This difference is minimized with increasing rotational speed at a welding speed of 102 mm/min. Besides, threaded only and three flatted pin possess the highest

and the lowest temperature and power at 240 RPM & 203 mm/min respectively. Conversely highest weld power and temperature were evident for 3 flatted pin at a rotational speed of 400 RPM.

#### 4.2.4 Relationship among the pin features and response variables

The experimental investigation shown in the section 4.2.1 revealed that regardless of the welding parameters, the threaded pins with flats are capable of eliminating wormhole defects in the welds as compared to unthreaded pins. The variations in geometric features of unthreaded and threaded pins play a significant role in material movement during FSW. The behavior of extruded and stirred material adjacent to the pins can easily be understood taking into account the provision of cutting flats and threads in pin. It is obvious that mass conservation law must be satisfied to obtain defect free welds, in which volume of the stirring pin (always circular or small extend of elliptical in shape as observed in the plan view regardless of pin geometry) is to be replaced by extruded materials along the weld seam. Therefore, cutting of flats in a cylindrical pin doesn't alter the displaced or dynamic volume of the pin rather affect on the material transport phenomenon. Figure 4.17 illustrates the percent of materials were cut from a smooth cylindrical pin (pin geometric dimensions considered in this investigation are described in Chapter 3) due to machining flats on unthreaded pin and flats + threads in threaded pins. From Figure 4.17, it is comprehensible that volume of flat cut increases with increasing flat numbers in unthreaded pins that facilitate interaction of additional material (equal to the volume of flat cuts) during stirring action. It is interesting to note a similar trend of Figure 4.13 and Figure 4.17 (considering variations of flat number for the identical welding condition), where forge force

requirement and cutting volume of flats were increased with a higher flat number for unthreaded pin. Flats in unthreaded pin might facilitate additional material to interact during pin rotation. It is also worth to mention here by comparing Figure 4.14 for unthreaded pin that, the orientations of resultant reaction decrease and in-plane resultant forces increase with increasing flat numbers. These decreases in the orientations of resultant are consistent with increase in X component of the resultant in other word: X-axis force. Therefore, with the indication of material adhesion in flat trailing side (evident from Figure 4.12) it can reversibly be stated that, resistance of material flow increases with increasing flat numbers in unthreaded pin. This is also evident from the torque data where unthreaded pin with 4 flats always generate highest torque (see Figure 4.15-a).

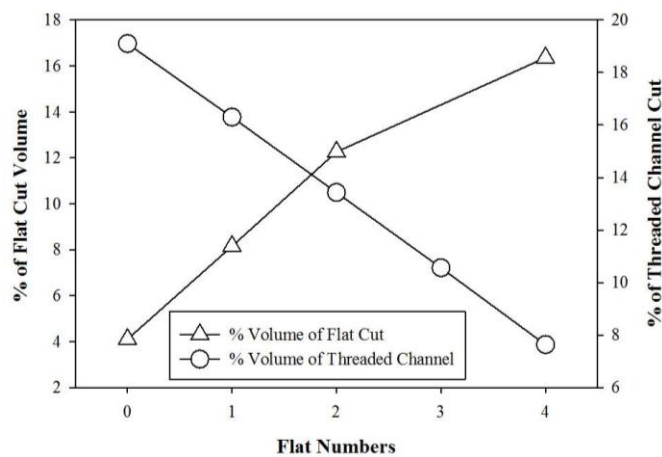


Figure 4.17 Percent of volume cut from a cylindrical smooth pin to machine flats and threads

Conversely, cutting of flats reduce the entrapped volume in the threaded channel as flat number increases (circular symbols in Figure 4.17) in case of threaded pins. Moreover, required forge force (see Figure 4.13-b) was also found to be decreased with increasing flat numbers for similar welding condition. The effectiveness of the pin thread on material transportation has been explained in Section 4.2.1. However, flats interrupt

the continuous downward movement of materials in the threaded channel. Therefore gripped materials in the threaded channel of the pin are being temporarily released near flat leading edge before the adjacent material are being entrapped in the threaded channel again near the trailing edge of the flat during pin rotation.<sup>74</sup> This was also evident from absence of material adhesion on the flat surface of threaded pins (Figure 4.12). Note that the orientations of resultant reaction increase and in-plane resultant forces decrease with increasing flat numbers. These increases in the orientations of resultant are also consistent with a decrease in X-axis force. Therefore, it can also be stated that increasing flat number eases the material flow around tool. These phenomena are also explained in the following paragraph with the consideration of the dynamic nature of in-plane forces.

Plasticized material movement was found to be highly periodic during FSW.<sup>59, 75,</sup>  
<sup>112</sup> Moreover, flats produce additional pulsating vibrations that may also influence the dynamic nature of feedback forces. Attempts have been made to correlate the defect occurrence with the force spectra.<sup>136, 137</sup> Figure 4.18 shows the polar plot of the “force footprints” for weld performed at 240 RPM and 102 mm/min with threaded pin having different flat numbers. A high frequency (1000 Hz) data acquisition system was used to investigate these X and Y force spectra. These polar plots illustrate the periodic nature of the X and Y forces spectra for one complete revolution of pins with different flat members. It was clearly observed from Figure 4.18 that, oscillation for 3 flatted pin is the lowest compared to pin with other flat numbers as evident from least enclosed area within the locus of in plane resultants designated by the green line. Moreover, the fluctuation of Y forces is more prominent than X force for all the pins. Increase in tool run-out during the FSW process might be attributed to such phenomenon.<sup>138</sup> Textural investigation of

the banded microstructure also suggested the occurrence of eccentric tool rotation.<sup>60</sup> Nevertheless, the macro-cross sectional evaluation in this study also discloses a comprehensive influence of tool shoulder and pin feature on nugget geometry.

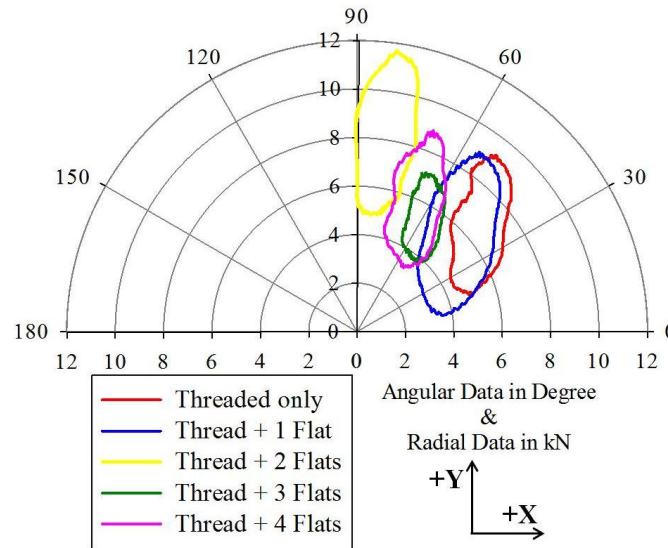


Figure 4.18 ‘Force Footprint’ of in-plane forces for one complete cycle for threaded pins with various flat numbers at 240 RPM and 102 mm/min

The overlapping transverse sections in Figure 4.19 illustrate the effect of thread interruption in pin on the thermo-mechanically affected zone (TMAZ) and nugget zone as outlined by different colors for corresponding flat numbers. For similar welding condition (240 RPM and 102 mm/min), an extended TMAZ on both advancing and retreating sides near weld crown was observed for three and four flatted pins, whereas vertical sharp edge on the advancing side along with extended TMAZ near retreating side was evident for zero, one and two flatted pins. Obviously the basin shape of nuggets are due to the shoulder induced deformation, which was observed relatively more symmetric for three and four flatted pin compared to other flat numbers including no flat. In friction stir welding Y-force generally tries to drive the tool to move towards the advancing side. Materials are being extruded continuously from the advancing side and higher Y force

might cause bending of tool and subsequent lack of shoulder contact near the advancing side. Therefore, the unstirred materials on the advancing side are being pushed by the cylindrical edge of pin thus resulted in a sharp edge on the advancing side that coincides with the vertical edge of cylindrical pin. This shear slippage constrict material movement in the advancing side also leads to a surface breaking defects near the weld crown on advancing side. <sup>139</sup> On the contrary, relatively low Y force with minute oscillatory amplitude facilitated by three and four flatted pin might cause uniform deformation of material beneath the shoulder ultimately leading to symmetric basin shape nugget.

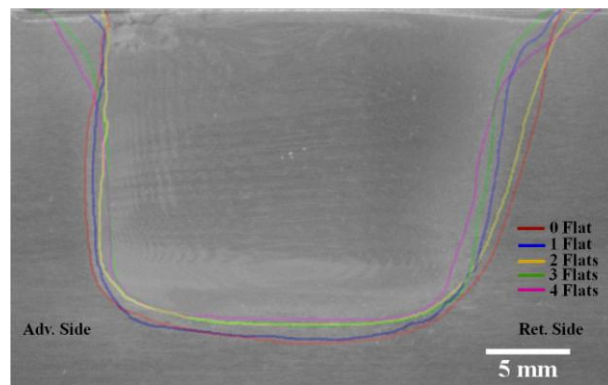


Figure 4.19 Overlapping nugget geometries for FSW with threaded pins having various flat numbers at 240 RPM and 102 mm/min

Based on the aforementioned discussion on the periodic nature of force spectra along with corresponding microstructural evaluation, an effort has also been made to analyze the peak to peak amplitudes of the X and Y forces for different frequency (in this case tool rotational speed) against the flat numbers. Figure 4.20 presents the X and Y force amplitude as a function of flat number under different welding parameters. Interestingly, in most of the welding conditions, it was observed that the peak to peak amplitudes of X and Y force spectra were lowest for pin with 3 flats. This result is more consistent in the case of Y force spectra. As discussed earlier Y force is related to the

pressure produced around pin due to material movement<sup>112</sup>, the fluctuation with high amplitude of the spectra might be associated with irregular material movement with different tool flat except that for 3 flats. Note that the threaded pin with 3 flats consistently possess lowest peak to peak amplitude in force spectra, as well as capable of producing complete defect free signals welds. Therefore, it might be appropriate to conceive here: defect in weld is most likely to occur when fluctuation of oscillation is higher, albeit X and Y forces are not necessarily in phase.

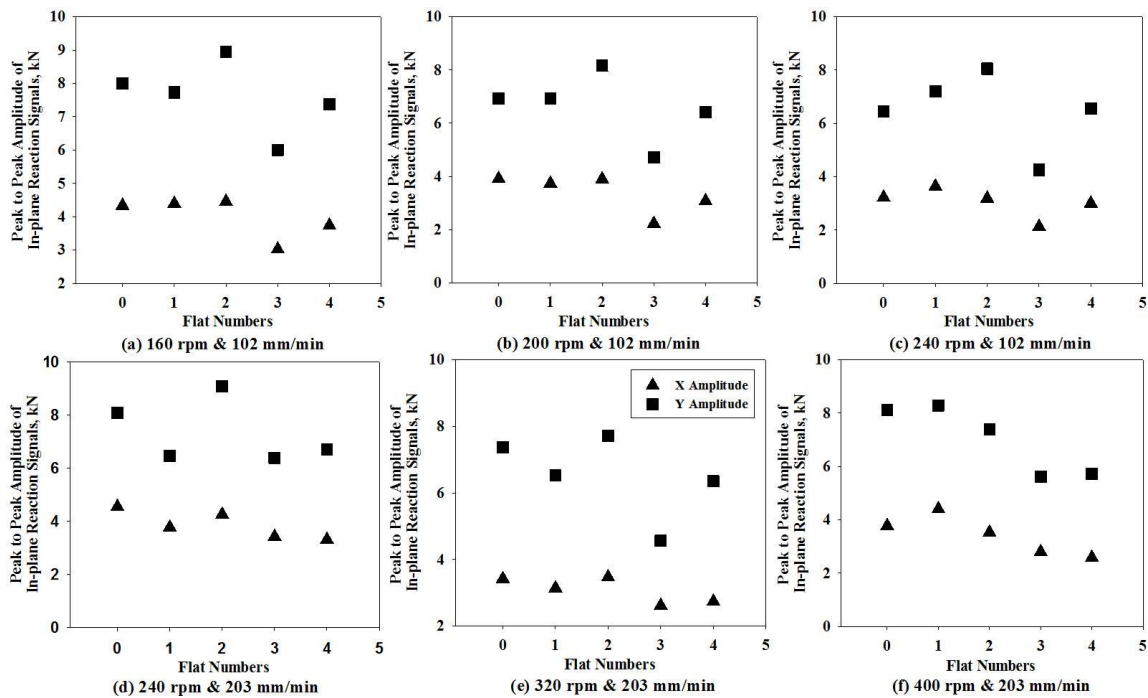


Figure 4.20 Peak to peak amplitude as a function of flat number for different welding conditions

#### 4.2.5 Summary Observations

The following observations can be drawn from the current study:

- Machining of flats on a cylindrical unthreaded pin does not improve the material flow to eliminate wormhole defects near the weld root regardless of the welding parameters for thick section welds.

- Threaded pins with different flat number significantly improve downward material movement as compared to unthreaded pins with flats. This may be due to entrapment of weld material in the threaded channel and releasing near flats continuously during tool rotation and traverse. Moreover, 3 flatted pin effectively eliminates both wormhole and surface breaking defects with the lowest in-plane reaction forces.
- The resistance to material flow/deformation was minimized by the introduction of threads and flats as evident from the reduced in-plane forces. Moreover, flats in pin reorder the distribution of the direction of in-plane resultant forces. While flat number increases, range of orientation of resultants decreases for threaded pin, however this range does not alter much for unthreaded pin.
- Peak to peak amplitude of the oscillation of feedback force signal is observed to be the smallest for the pin having 3 flats. This is associated with minor or even no defects in the welds. Moreover, significantly lower variation in force oscillation for three flatted pin perhaps leading to better fatigue life.

#### **4.3 Effect of Complex Geometric Features of Pin on Friction Stir Weldability of AA6061 Aluminum Alloy**

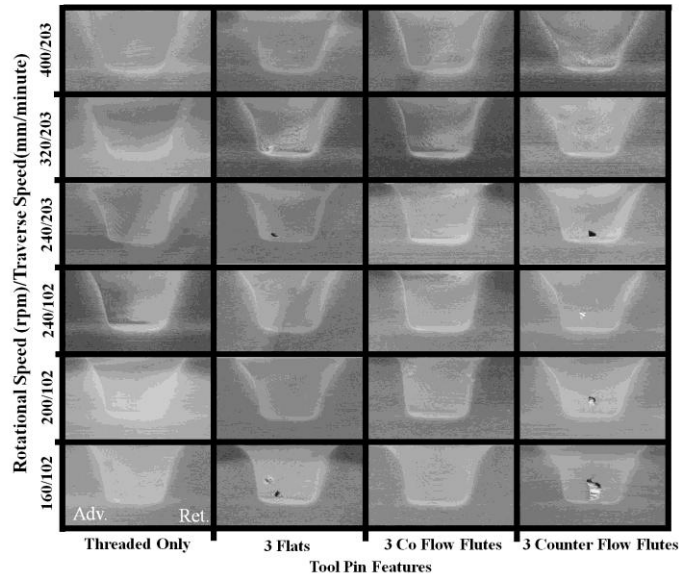
Earlier studies have shown that thread form and thread interruption with flats on the cylindrical pin have significant effect on friction stir welding (FSW). The results discussed in previous sections led the author to pursue studying further the effect of complex geometric features (thread/flat/flute) of pin on friction stir welding. Pin geometric variation such as conical shape of pin incorporation with threads, flutes, flats etc. dictates, to some extent, the material flow which in turn affects process forces,

temperature, heat input and joint quality. As reported in Section 4.1 that cylindrical pin having intermediate thread is capable of producing relatively good quality welds, therefore the concentration of this section is on normal thread (NT: 1.41 mm pitch) and coarse thread (CT: 2.12 mm pitch) forms on a mildly tapered ( $8^\circ$  angle) conical pin. The volumetric defect content and process response variables (in-plane forces, torque, power, temperature) as a function of pin thread forms and features (thread/flat/flute) were examined in AA6061-T6 welded parts for a range of applied welding parameters. It was observed that a pin with proper thread pitch performed better with different pin features for producing good quality welds compared to finer threaded pins with similar features. Forge force requirements can be minimized using a threaded pin with three counter-flow flutes. Variations of nugget geometry, torque, power, and temperature were also measured to provide information regarding their dependence on tool pin features under different welding conditions.

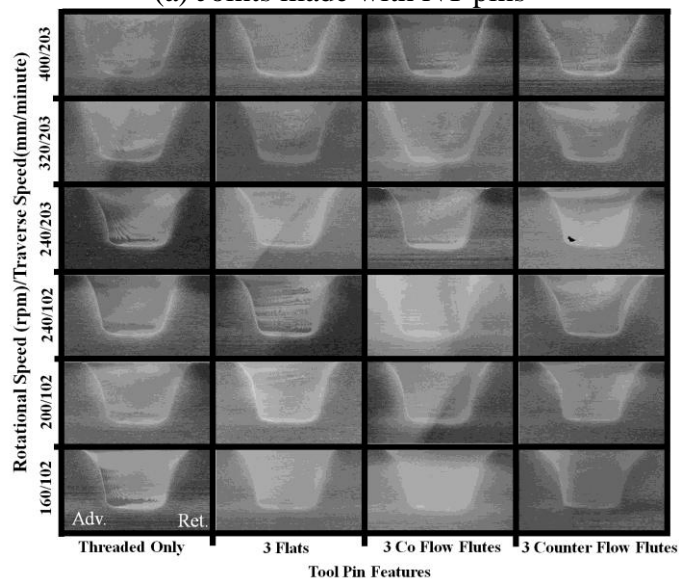
#### 4.3.1 Effect of tool features on weld defect and macrostructure

In order to investigate the effect of pin features on weld quality in terms of defect content during friction stir welding, metallographic cross sections were produced and defect locations were analyzed. Figure 4.21 (a-b) shows the transverse macro sections of weld nuggets for normal threaded (NT) and coarse threaded (CT) pins having different features for various weld parameters. In each cross section, the advancing side is on the left and the retreating side is on the right. The rotational and welding speeds are shown on the vertical edge of the image while each column of the images shows the cross sections for particular pin features (threaded only, thread+ 3 flats, thread+ 3 co-flow flutes and thread+ 3 counter-flow flutes). For some welding conditions and pin features

visible wormhole defects were observed in the macro cross sections, while other defects were only visible by viewing in the optical microscope: examples of the “micro defects” are shown in Figure 4.22 (a-f).



(a) Joints made with NT pins



(b) Joints made with CT pins

Figure 4.21 Weld macro cross section for FSW made with different pin thread forms with various geometric features

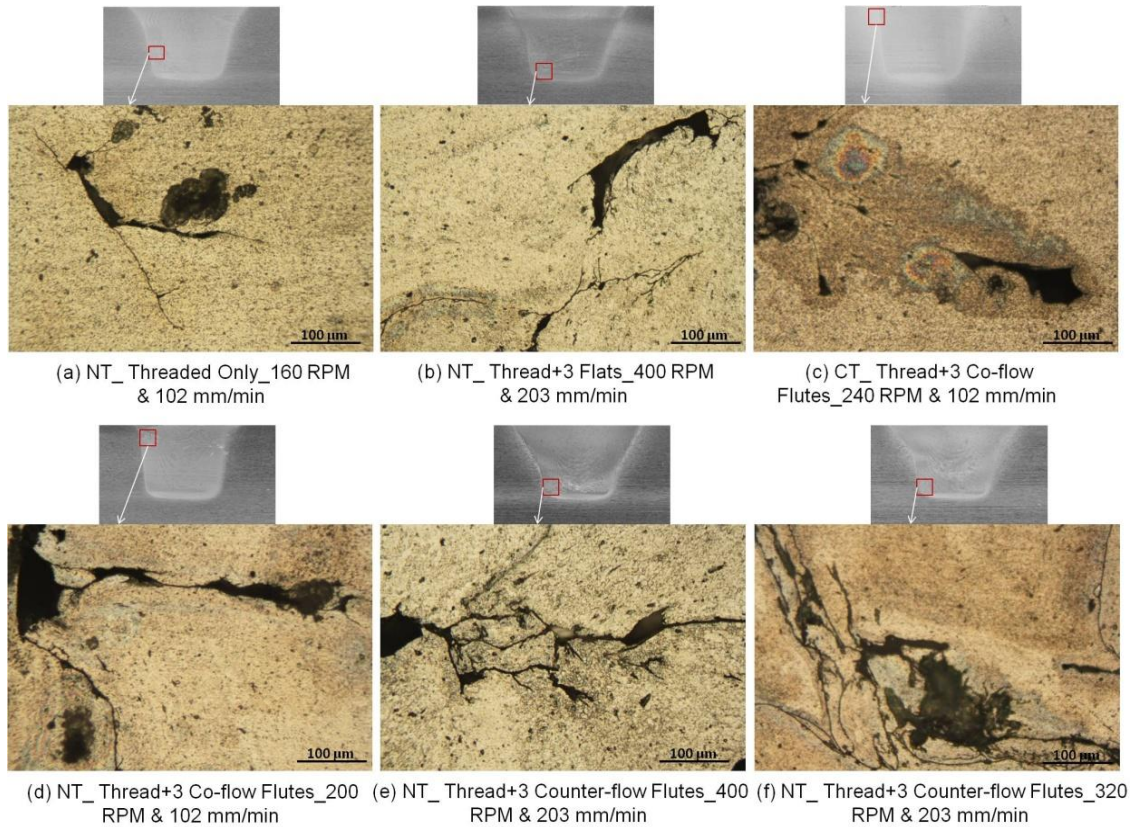


Figure 4.22 Microstructural defects in the nugget zone for different tool features and different welding conditions

Table 4.2 summarizes the information regarding quality of welds in terms of wormhole/micro defects (defect location codes) and defect free welds (‘√’ marks). In the left hand column, the tool rotation rate, welding speed, and tool advance per revolution, APR, are listed. Overall it was observed that a much greater proportion of the welding conditions resulted in defects when using the NT thread pins (50%) vs. the CT threads (8%). It was evident from macro and microstructural observation that the normal threaded (NT) pin without flat/flute produced defect free welds under most of the welding conditions except welding at 160 RPM and 102 mm/min, in which micro wormhole defect near weld mid depth on advancing side was observed (see Figure 4.22-a). Normal threaded + 3 flats pin produced defected welds under most of the welding

conditions except rotational speed of 200 RPM and 240 RPM with 102 mm/min welding speed. Normal thread + 3 co-flow fluted pin also produced defect free welds for most of the applied welding conditions; however, a surface breaking defect was evident from microscopic observation for a welding with 200 RPM and 102mm/min (Figure 4.22-d). Normal threaded pin with counter flow feature produced defective weld under all applied welding conditions as seen from macro and micrographs (Fig 4.21-a and 4.22-e-f). These defect formations may be due to the dominant action of counter-flow flutes over right hand thread during tool rotation in counter clock wise direction (as viewed from above). Therefore, excessive upward material movement due to the presence of counter flow flutes may lead to wormholes near the weld root when incorporated with the NT threads. Similarly insufficient downward movement of material with NT pin with 3 flats also may be the reason for wormhole defects for this pin with most of the welding conditions except two as mentioned earlier.

In case of the CT pin, except for two welds made using thread+3 counter-flow flutes (240 RPM and 203 mm/min) and thread +3 co-flow flutes (240 RPM and 102 mm/min), all the welds were defect free (see Figure 4.21-b & 4.22-c). For the two defective welds, the one made with thread+3 counter-flow flow flutes had a wormhole near root while the other made with thread+3 co-flow flutes had a surface breaking defect on the advancing side. Interestingly welding with both NT and CT pins having 3 co-flow flutes can lead to formation of surface breaking defects. The mechanism of surface breaking defect formation may be the opposite to the wormhole formation near root, since the right hand threaded tool with co-flow flutes rotating in the counter-clock wise direction (as viewed from above) thereby drive material down towards the weld root.

This downward thrust helps to eliminate near root wormhole defects, but if too much materials escape as flash, the surface breaking defect may be created. In a nut shell, it can be stated from the macro and microscopic investigations that defects in welds with normal threaded (finer pitch) pin are more prevalent than weld with coarse threaded pin for the tested conditions.

Table 4.2 Information about defective welds (with defect location codes\*) or defect free (with ‘√’ mark) weld for friction stir welding of AA6061 for different welding parameters using various pin features

Rotational Speed (RPM) / Welding Speed (mm/min) / APR (mm/rev)	Pin Profile							
	Normal Threaded Pin				Coarse Threaded Pin			
	Thread Only	3 Flats	3 Co-flow Flutes	3 Counter-flow Flutes	Thread Only	3 Flats	3 Co-flow Flutes	3 Counter-flow Flutes
400/ 203/2	√	AR	√	AR	√	√	√	√
320/ 203/1.6	√	AR	√	AR	√	√	√	√
240/ 203/1.2	√	AR	√	MM	√	√	√	AR
240/102/2.4	√	√	√	MM	√	√	AC	√
200/102/2	√	√	AC	MM	√	√	√	√
160/102/1.6	AM	AM	√	MM	√	√	√	√

\* Defect location codes: AM- Advancing side near **M**id plane (6.4 mm depth of weld), AR-Advancing- side near **R**oot of the weld, AC- Advancing-side near **C**rown of the weld, MM- **M**id of the nugget near **M**id plane.

Investigations have been made to study the effect of the pin features on the nugget geometries after friction stir welding. The total heights of recrystallized weld nugget zone were measured from the weld top surface. As seen in Figure 4.21, the nugget geometry generally follows that of the pin outline, however, there are some subtle variations related to pin features.

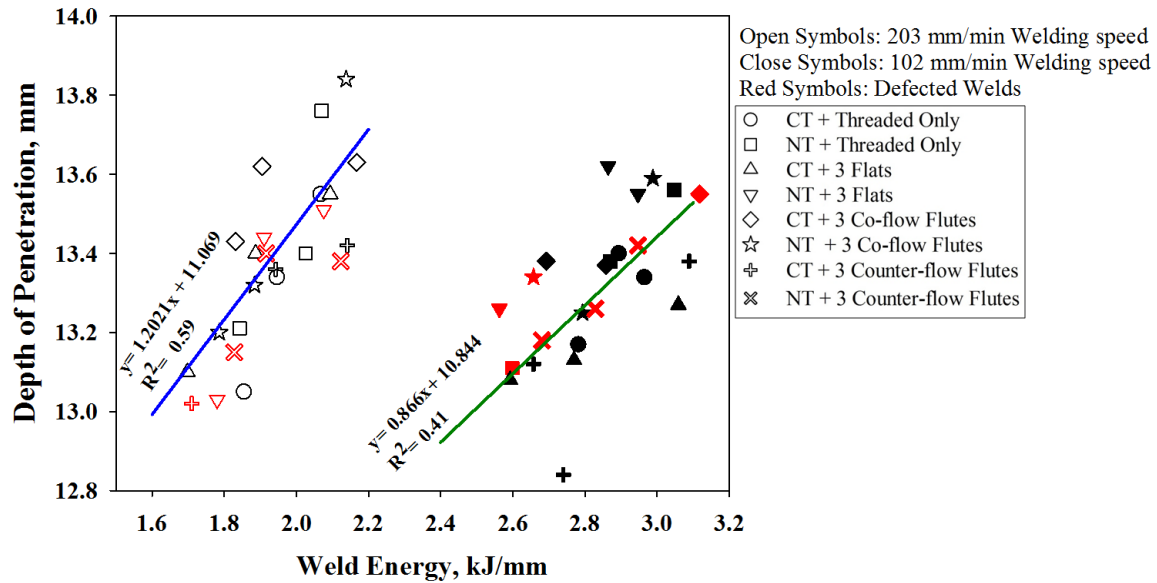


Figure 4.23 Geometric shape (depth) of the nugget zones as a function of weld energy for FSW with various pin features at different welding parameters

Figure 4.23 presents the depth of penetration as a function of weld energy input for different tool pin features and weld parameters. In general, the depth of penetration (DOP) as seen in Figure 4.23 is linearly proportional to weld energy. Two separate linear least square fit lines have been drawn through the data for defect free welds at 203 mm/min and 102 mm/min welding speed. Red symbols in Figure 4.23 indicate the defected welds. Excluding the defective welds, nominally linear relationships were observed between depth of penetration and weld energy with correlation coefficient 0.59 and 0.41 for 203 mm/min and 102 mm/min welding speed respectively. Welding with the same rotational speed and similar weld power, lower welding speed (102 mm/min) produces higher DOP than higher welding speed (203 mm/min). Welds performed with threaded only pin and pins with 3 co-flow flutes have higher depth of penetration compared to thread+ 3 flats and thread + 3 counter-flow flutes: this is consistent with ideas regarding the downward thrust of material. While a trend was observed for the

effect of thread interruptions, the difference in DOP for normal threaded and coarse threaded pins are insignificant.

#### 4.3.2 Effect of tool features on forge force

As discussed in previous section, FSW tool with right hand threaded pin is rotated in the counter-clock wise direction during the process. This causes the threads to drive material in the downward direction (toward the weld root) therefore resulting in an upward thrust applied to the tool. To maintain similar contact conditions between weld surfaces and the tool shoulder, the forge force is adjusted depending on pin features. Figure 4.24 shows the forge force requirement as a function of tool rotational speed for different tool pin features. The open symbols are for a welding speed of 203 mm/min and filled symbols are for 102 mm/min. In general, pins having thread only features and thread + 3 co-flow flutes require higher forge force than thread+ 3 flats and thread+ 3 counter-flow flutes for a given rotational speed. While threads and co-flow flutes provide continuous down thrust, flats are a nominally neutral features and counter flow flutes act opposite the threads. It is also observed from Figure 4.24 that NT pin require less forge force than CT pin. The difference in thread root depth of NT pin (0.76 mm) and CT pin (1.27 mm) may be the issue in this regard that will be described in greater detail in the Section 4.3.5. Overall it can be observed that the pin thread form and other features have significant effects on controlling the forge force during FSW.

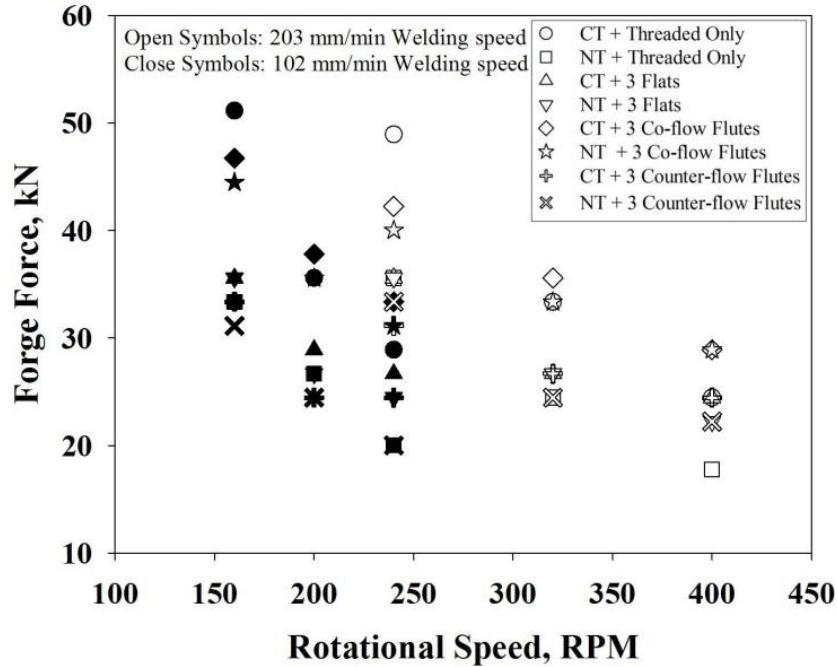


Figure 4.24 Required forge force for different tool pin features under different welding parameters

#### 4.3.3 Effect of tool features on in-plane reaction forces

Figure 4.25 (a-b) depicts the polar plots of average in-plane reaction forces (X-Y forces) on the tools for different pin features at 102 mm/min. (Figure 4.25-a) and 203 mm/min. (Figure 4.25-b) welding speed. The sign convention of these reaction forces is also shown in Figure 4.25: the positive X-axis force acts opposite the welding direction and positive Y-axis force acts perpendicular to the X force towards the advancing side. Essentially these polar plots are the vector sum of average X and Y forces, however, these forces are oscillatory and not necessarily in phase, therefore at any instance, the resultant force on the tool is not necessarily equal to the reported resultant force. The X and Y forces are averaged over 20 mm weld distance. This weld section selected for determination of the average was approximately where process temperature steadiness is obtained during friction stir welding and near the location from where the specimens

were cut for the macro and microscopic investigations. Different symbols in Figure 4.25 indicate pins with various features and relatively smaller symbols represent defective welds. The symbols with different color: green, blue, red, pink and grey are for welding at 160 RPM, 200 RPM, 240 RPM, 320 RPM and 400 RPM rotation rate respectively.

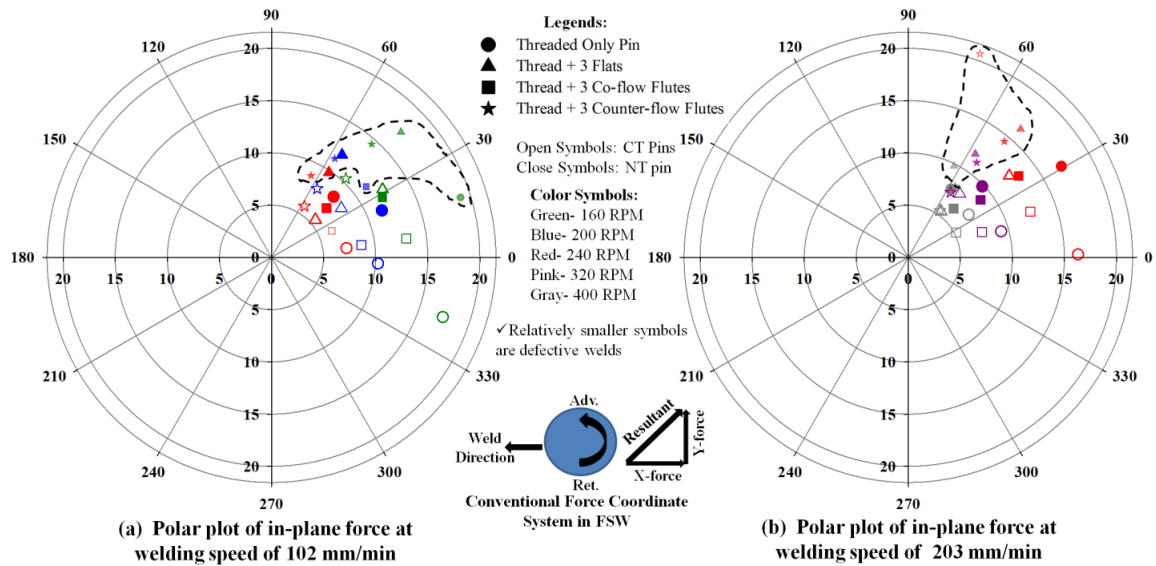


Figure 4.25 In-plane reaction force (avg. X-Y forces) in Polar plot for different pin features, weld parameters with the arrow marks showing conventional force co-ordinate system in FSW process

Figure 4.25 (a-b) shows the variation of magnitudes of in-plane forces as well as their orientation for welding with different pin features and control parameters. The variation in the orientation of resultant reaction with changing pin features can be seen in these polar plots. As observed from Figure 4.25, the angle which the resultant makes with the welding direction is greater for counter-flow fluted pins, least for co-flow fluted pins and intermediate for the flatted pins. However, the threaded only pins exhibit much greater scatter in resultant angle compared to pins with flats or flutes under the applied process control parameters. Table 4.3 summarizes the spread of orientation of the resultant reaction forces for different pin features in both thread forms (NT and CT)

under all welding conditions. As observed from Table 4.3, the counter-flow fluted pin has the greatest angle of resultant with the least spread. It is also interesting to note the similar trend of orientation and its range for threaded only and co-flow fluted pins.

Table 4.3 Spread of the orientation (angles are in degree) of resultant reaction with respect to the axis of zero X force

Pin thread features	Average Orientation ( $\theta$ ) with range
Threaded only	$20^\circ \pm 38^\circ$
Thread + 3 Flats	$47^\circ \pm 16^\circ$
Thread + 3 Co-flow Flutes	$27^\circ \pm 20^\circ$
Thread + 3 Counter-flow Flutes	$59^\circ \pm 12^\circ$

On the other hand, the magnitude of the in-plane resultant is a strong function of the welding parameters, however for similar welding conditions, NT pin with 3 flats has maximum resultant reaction in most of the welding conditions except for 160 RPM & 102 mm/min and 240 RPM & 203 mm/min. Coarse threaded pins have lower resultant reaction than normal threaded pin in all welding conditions except for 240 RPM and 203 mm/min with CT + counter-flow flutes which has the highest resultant reactions among all the applied welding conditions and pin feature variations. Excluding this exception, it is also interesting to note that differences in resultant reactions among the CT pins with flats/flutes are insignificant for similar welding conditions even though the orientation of the force is different. It should also be noted for higher welding speed (203 mm/min) that those pins which have relatively higher orientation of resultant (relatively smaller symbols separated by dashed curved boundary in Figure 4.25-b), are also prone to defect formation. However, at low welding speed this observation breaks down as defected welds were evident at both low and high values of resultant angles.

#### 4.3.4 Effect of tool pin features on Torque-Power-Temperature

Figure 4.26 shows the trends of torque for various tool pin geometries and features as a function of tool rotational speed. All pin features exhibit fairly tight grouping in the torque vs. rotational speed graph. The general trends include decreasing torque with increasing RPM and higher torque at higher welding speed for the same RPM. It is also interesting to compare the variation of torque with the applied forge forces for different pin features and welding parameters by combining Figure 4.23 and 4.26. Obviously there is distinct difference in forge force variation compared to torque variation due to the effect of pin features for corresponding welding parameter.

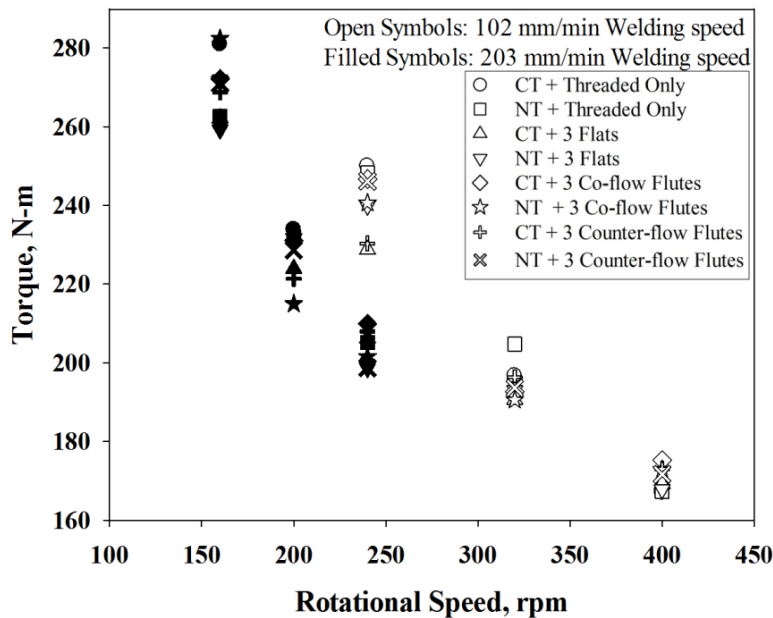


Figure 4.26 FSW torque as a function of tool rotational speed and forge force for various pin features

Figure 4.27 is the plot of average torque vs. forge force variation with double axes range (error bars) for different welding parameters due to variation of the pin features in each controlling parameter. The qualitative trend of thread form effects on forging force is presented symbolically in the ascending order from left to right on the horizontal error

bars. Alongside the vertical error bar, the effect of torque on thread features with extreme limit (minimum to maximum) for corresponding pin features in each welding parameters is also demonstrated in Figure 4.27. In general, it can be observed that for a given welding parameter/advance per revolution, torque variation is less than 10%, whereas substantial variations in applied forge forces (45%-67%) in order to produce comparable levels of tool plunge due the pin geometric features. The insignificant variation in torque for each welding parameter is presumably due to the fact that the actual pressure under the shoulder is not varying with the z-force: variation in z-force is required to counteract varying levels of pin thrust.

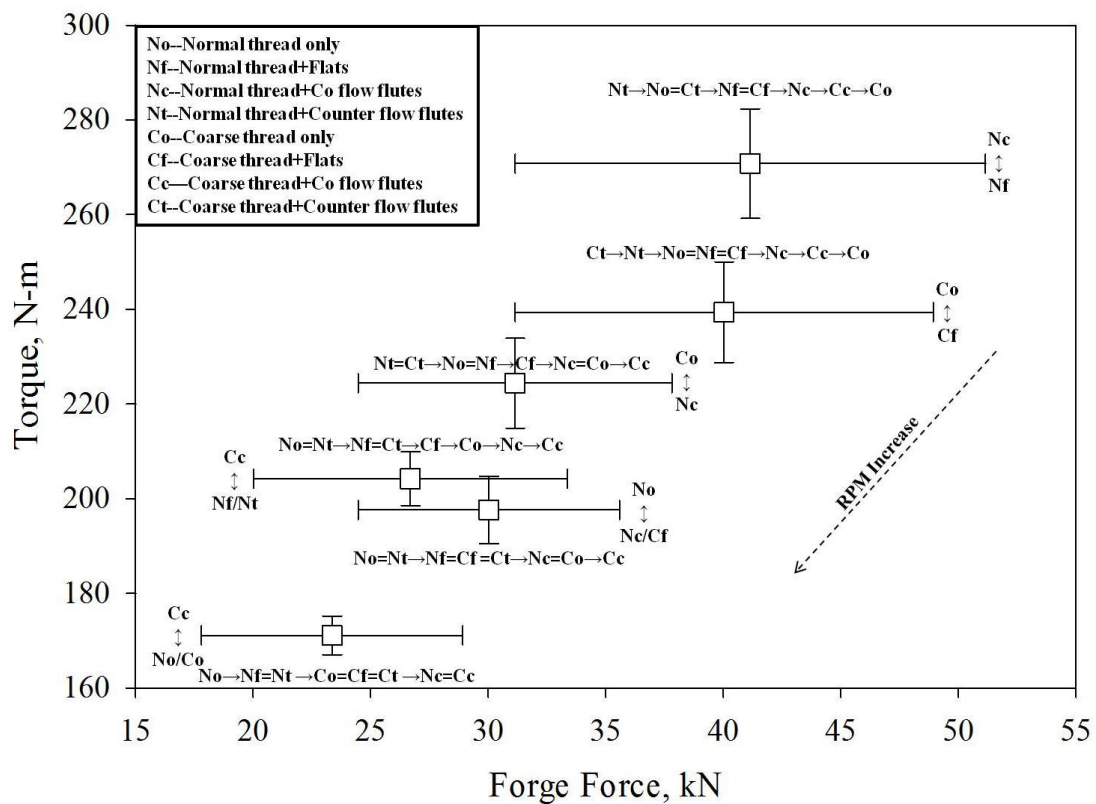


Figure 4.27 Average torque as a function of average required forge force for different welding parameters

It is also interesting to note from Figure 4.27 that, lower torque is not necessarily associated with the lower applied forge force, since in each case the pin feature that requires lower forge force did not involve with lower torque. Similarly, the above statement is also true for maximum limit for forge force and torque, however, for three welding conditions (400RPM\_ 203mm/min., 240RPM\_ 203mm/min. and 240RPM\_ 102mm/min.), highest torque is correlated with maximum forge force for a particular pin feature (coarse threaded pin with three counter flow flutes). Nevertheless the correlation of torque and forge force is more complex since flow stress properties of the weld material also play a significant role that predominantly governed by the weld power. However, it can be concluded at this point that torque is less sensitive to pin features compared to that in forge force dependence on pin geometry.

Temperature as a function of weld power is presented in Figure 4.28 for different rotational and traverse speed with various pin features. Temperature was found to increase with increasing weld power which is a commonly observed phenomenon.<sup>36, 114, 140</sup> Two linear least square fit lines have been drawn though data corresponds to higher and lower welding speed showing a nominally linear relationship between pin temperature and weld power. The correlation coefficient ( $R^2$ ) for both lines is 0.86 regardless of the quality of welds. The data for both welding speeds and 240 RPM are boxed in the graph showing that increased welding speed at constant RPM results in lower or similar pin temperature even though the power requirement is higher. Temperature, like torque, appears to be relatively insensitive to pin features, hence the major contribution for temperature change is due to change in rotational speed and welding speed.

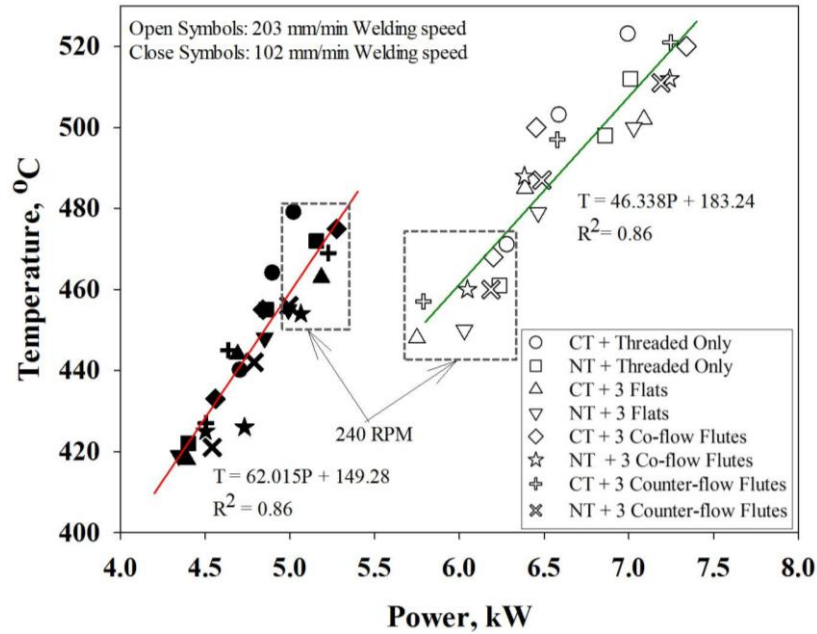


Figure 4.28 Pin peak temperature as a function of weld power

#### 4.3.5 Interrelationship among the parameters

##### *Thread form effects*

The CT pin produces defect free welds and also requires higher forge forces compared to the NT pin. The thread form geometric dimensions might have a key role in this respect. As mentioned earlier, CT pins have deeper thread root depth than NT pin and it was calculated that the CT pin has 1.6 times higher cutting volume in the threaded channels than NT pin even though the surface area in the threaded part of both pins are similar. This may facilitate engagement of a larger volume of weld material in the threaded channel of the CT pin than the NT pin and consequently CT pins require larger forge force due to greater pin up thrust. It was also revealed from Figure 4.25 that, the magnitudes of the in-plane resultant reactions are higher for NT pins compared to CT pins for defect free welds and Y forces were also higher for defected welds with NT pins. It should be noted here that, wormhole defects indicate that material is being expelled

from the stir zone as flash in order to satisfy the mass balance around the tool. Since, the pressure created by the weld material from the retreating side on the FSW tool is considered as positive Y-axis force, these Y forces in friction stir welding are in some aspect considered to be correlated with material flow around tool.<sup>141</sup> Higher, positive, Y force indicates higher pressure on the pin from the retreating side that may arise from resistance to these material movements from advancing side to retreating side. This reluctance in material transportation may be associated with the irregularity in material movement during stirring of pin and defect formation in the nugget zone during friction stir welding. It is interesting to note negative Y force for two welding conditions (160 RPM & 200 RPM) for CT only pin. However the genesis of this phenomenon of negative Y force is uncertain.

#### *Thread interruption (flats/flutes) effects*

It was mentioned earlier that, for similar welding conditions, required forge force varies by 45%-67%, while torque variation is only 5%-9% due to variation in pin features only. This indicates that, variation in the upward thrust due to pin features leads to an essentially constant pressure under the shoulder even though the Z-force is varied. This is of course the goal of varying the z-force to obtain similar penetration depths.

The threaded only pin and co-flow fluted pin produce higher depth of penetration and reach slightly higher pin peak temperature than flatted and counter-flow fluted pin. This might be influenced by contact conditions of work piece and tool pin due to presence of features on the tool pin. These contact conditions as well as the threaded channel in the pins dictate the volume of weld material to be transported due to pin rotation and traverse. That peak temperature for similar welding condition are consistently higher for

threaded only pin, may be due to the higher surface area of the pin, contributing to high heat generation compared to pin having thread interruptions. An alternative, and perhaps complementary, explanation is that the thread interruption features act as cutting surfaces which enable material to be transported around the tool as a rigid body, rather than via shear flow.

It is noticeable that coarse threaded pins with 3 counter-flow flutes produce defect free welds in most welding conditions except one with 240 RPM & 203 mm/min, whereas defects were obvious for welding with normal threaded pin with 3 counter-flow flutes. This is an interesting result where the effect of flow of material in the tool rotational direction as well as in the direction of helix angle of pin features can be distinguished due the presence of thread forms/flats/flutes. In the first case with CT + 3 counter-flow flutes pin, the threaded part governs the vertical downward movement to eliminate wormhole defects. On the contrary, for NT + 3 counter flow flute pin, flutes governed the upward material movement (pin is rotating in counter-clockwise direction as viewed from above and the flute is left hand helix that causes upward material movement) that leads to wormhole defects. In a nutshell, it can be said that, the action of entrapped material in the counter-flow flutes are surmounted by the pin grip volume in the coarse threaded pin during welding to cause proper consolidation of materials near the weld root while using CT + 3 counter-flow flutes pin.

Comparing the effect of pin feature on process forces, it can be noted that, three flatted or counter flow fluted pins requiring lower forge force (see Figure 4.23) also exhibited lower X-axis force (X components in Figure 4.25) and threaded only or three co-fluted pins requiring higher forge force experienced higher X force under the same

welding condition. Moreover, with these two types of pin features (threaded only and Thread+3 co-flow flutes), it is possible to minimize wormhole defects (see Figure 4.21, a-b) using either coarse/normal thread forms. This phenomenon indicates that, the more material is involved in the stir zone to be consolidated near the thread root; the more force is required, resulting in increased reaction force (X-axis force) on the pin.

#### *Welding parameters effects*

It was observed that, for the one RPM level used at both welding speeds (240 RPM: shown dotted box in Figure 4.28), the measured temperature is lower at the higher welding speed, although the measured power is also higher. It is noted that for a given rotational speed, increase in welding speed increases tool advance per revolution (APR) and higher APR requires a greater volume of material to be deformed and transported per revolution which will require higher weld power. However, the reduction in pin peak temperature at faster welding speed may be ascribed to higher rates of convection from the tool by a greater influx of “cool” material. Figure 4.24 and 4.28 also show that depth of nugget as well as pin peak temperature decrease at faster welding speed for the same rotational speed even though the measured weld power was observed higher.

#### **4.3.6 Summary observations**

The following observations are drawn from current study:

1. Coarse threaded pins (2.12 mm/rev) exhibit significantly less defect formation compared to Normal threaded pins (1.41 mm/rev) for similar welding conditions in 6061 welds.
2. Complex geometric features such as flats/flutes alter the flow of materials and may improve the weldability in FSW.

3. Forge force required to produce defect free welds can be reduced by introducing counter-flow flutes with an insignificant change in required torque. Moreover, the required forge force is higher for CT pins than NT pins.
4. The magnitudes and orientations of in-plane forces are less for CT pins compared to NT pins while producing good quality welds.

#### **4.4 Effect of Tool Pin Features on Process Response Variables during FSW of Dissimilar Aluminum Alloys**

It has been established the effectiveness of complex geometric features of tool pins during FSW of similar material in the preceding sections. Also, it is apparent that the coarse threaded (CT) pin that is, pin with 2.12 mm thread pitch exhibit good performance in the previous studies. Therefore, henceforward this thread form is considered for further studies. The scope of the present study has been extended to investigate the effect of the pin features (flats/flutes) and orientation/placement of the materials on advancing side for friction stir welding (FSW) of dissimilar aluminum alloys. In this section, CT pins having three flats/flutes were employed to join dissimilar alloy AA2050 and AA6061. Three sets of rotational speed/welding speed were used to perform a series of welds in a butt joint arrangement. The results show that, joint quality, process response variables and welding temperature are highly affected by pin features and material orientation in FSW. Defect free joints with effective material transportation in the weld nugget zone were obtained when welding was performed with AA2050 on the advancing side. The tool also encounters less in-plane reaction force for welding with 2050 on the advancing side. Pin with thread+3 flats produces quality welds at low rotational and travel speed regardless of the location of alloys on advancing or retreating side.

#### 4.4.1 Macro-scale cross sections of bi-material welds

Figure 4.29 (a-d) shows the macrographs of the cross sections for dissimilar metal welds for threaded only pin (Figure 4.29-a), thread+3 flats pin (Figure 4.29-b), thread+3 co-flow flutes pin (Fig. 4.29-c) and thread+3 counter-flow flutes pin (Fig. 4.29-d) respectively. The 6061 appears dark and 2050 appears light in these macro-scale cross sections. Figure 4.29 clearly indicates that bi-material weldability is strongly dependent on alloy placement and pin profile as macroscopic defects were observed only when 6061 was placed on the advancing side. No macro size defects were observed in FSW joints when 2050 was placed on the advancing side, regardless of the variation in pin features or weld parameters.

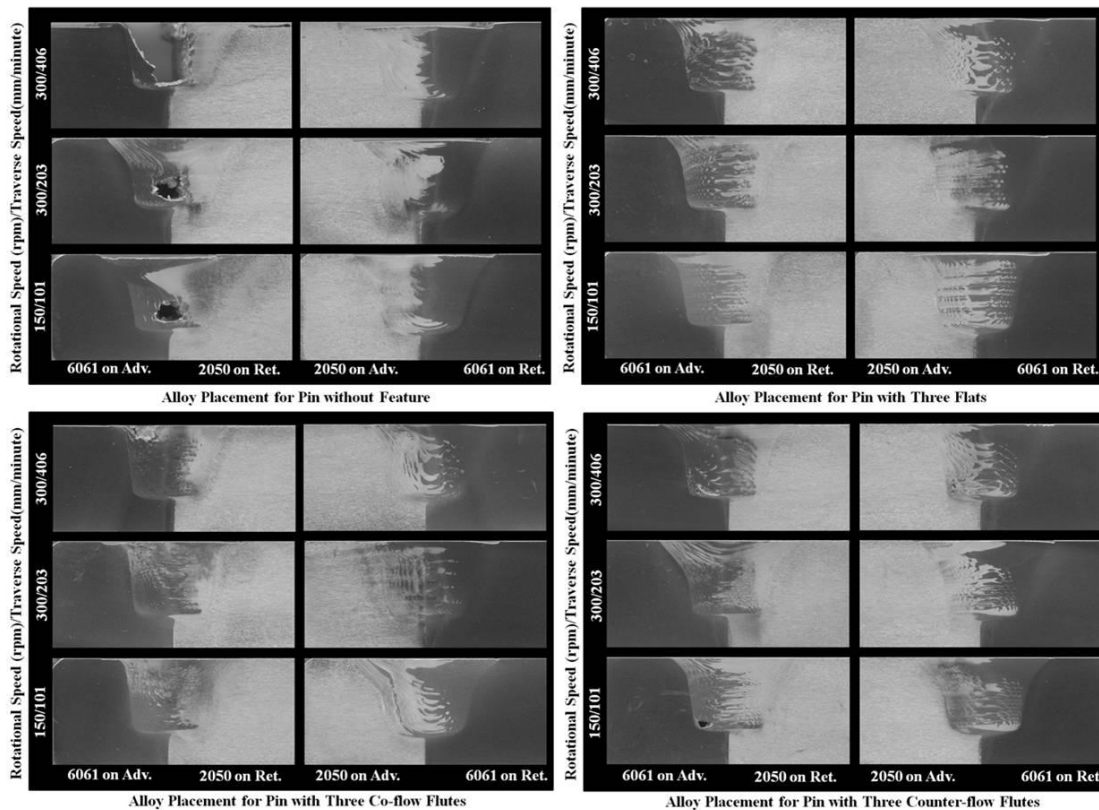


Figure 4.29 Macro Cross sections of bi-material FSW of AA2050 and AA6061 using different pin features and weld parameters with alloy placement

Table 4.4 summarizes the defect content in all of the welds. The types of defects have been characterized as (1) large or macroscopic wormhole defects (surface breaking for one case), (2) microscopic, near the root, advancing side defects, (3) small surface breaking defects (advancing side).

Table 4.4 Defect content and position in welds

<b>Tool</b>	<b>Alloy on Adv. Side</b>	<b>150 RPM, 101 mm/min</b>	<b>300 RPM, 203 mm/min</b>	<b>300 RPM, 406 mm/min</b>
<b>Threaded only</b>	<b>2050</b>	Defect free	Defect free	Defect free
	<b>6061</b>	Large surface breaking	Large , central wormhole	Large , central wormhole
<b>Thread+3-flats</b>	<b>2050</b>	Defect free	Defect free	Defect free
	<b>6061</b>	Defect free	Defect free	Micro, near root, adv. side wormhole
<b>Thread+ 3 co-flow flutes</b>	<b>2050</b>	Small Surface breaking	Defect free	Defect free
	<b>6061</b>	Small Surface breaking	Small Surface breaking	Surface breaking
<b>Thread+3 counter flow flutes</b>	<b>2050</b>	Micro, near root, adv. Side wormhole	Micro, near root, adv. Side wormhole	Micro, near root, adv. side wormhole
	<b>6061</b>	Macro, near root, adv. Side wormhole	Micro, near root, adv. Side wormhole	Macro, near root, adv. side wormhole

Figure 4.30 shows examples of micro scale defects. It is apparent that the pin features definitely affect FSW joint quality, including existence, severity, and position of defects. Defects produced using the threaded only pin with various welding parameters were large and almost centrally located in the weld nugget. The threaded only pin did not produce defects when 2050 was placed on the advancing side. The thread + flats pin produced micro-scale near the root advancing side defects for only one condition: 6061 on the advancing side and 300 RPM, 406 mm/min welding. The thread + co-flow flute pin resulted in small, crown surface breaking defects on the advancing side for all 6061

on the advancing side welds and for one condition with 2050 on the advancing side. The thread + counter flow flute pin produced small, near root, advancing side defects under all six conditions. The defect locations produced by the co- and counter-flow flute pins are consistent with expectation: it is anticipated that the counter flow flutes will pull the material away from the root region resulting (under some circumstances) in near root defects. Conversely, the co-flow flutes will push additional material downward potentially starving the crown region of material and leading to the surface breaking defects that were observed.

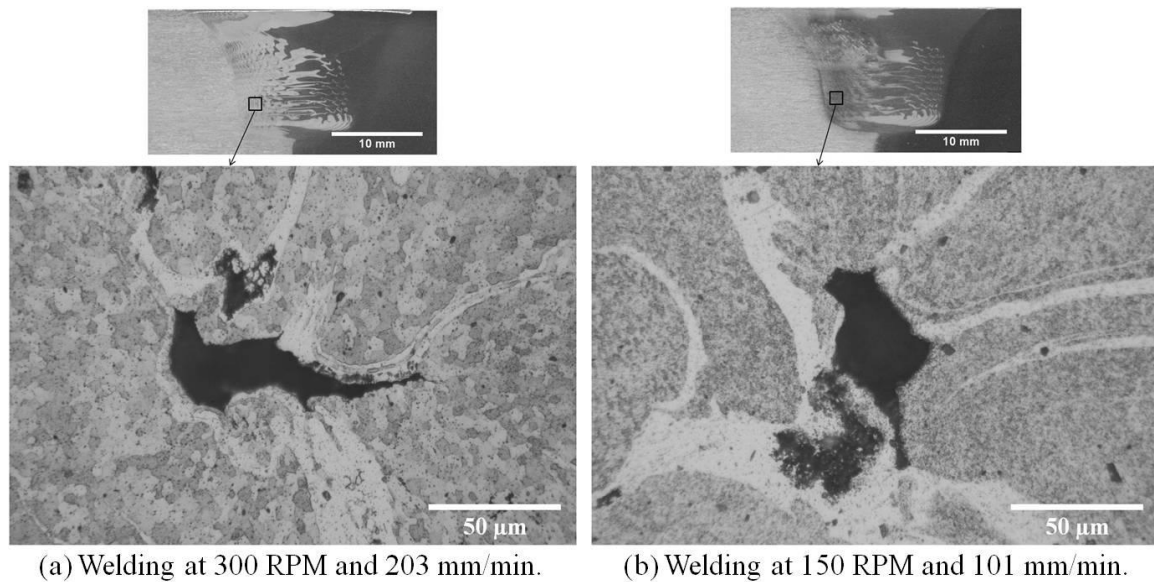


Figure 4.30 Microscopic defects in weld cross sections at the advancing side of nugget zone during friction stir welding with pin having thread+3 counter-flow flutes for different welding parameters

Figure 4.29 suggests that movement of material across the weld centerline and intermixing of the two alloys occurred with all tool types, but the amount of such movement and the level of intermixing was noticeably less for the threaded only tool. Alloy 6061/2050 interface lengths for each weld were determined by image analysis on scanned cross sections by detecting the change in etching characteristics. The results are

shown in Figure 4.31. The results for each pin type are normalized by the result for the pin with the largest interface length, all welding parameters and alloy positions are lumped together and only pin type is considered as a variable. Obviously, flats and counter-flow flutes produce the highest level of intermixing while the thread only pins produce the least.

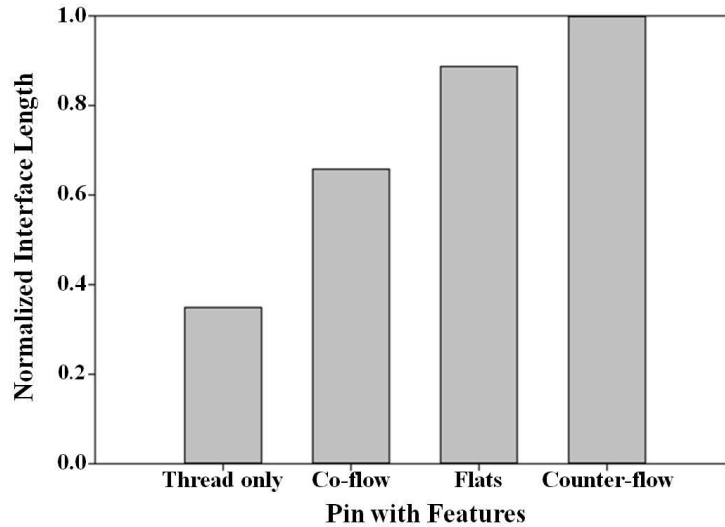


Figure 4.31 Normalized interface length between 6061 and 2050 depending on pin type

It was also noticed from the weld macrostructural observation that the region of recrystallized material under all of the pins was higher when AA2050 was placed on the advancing side compared to AA6061 on the advancing side. The measured average depth of recrystallization beneath the pin was  $(0.46 \pm 0.22)$  mm in the case of AA6061 on the advancing side, whereas with AA2050 on the advancing side the average deformation zone depth was measured as  $(1.36 \pm 0.2)$  mm. Finally the flow patterns in the welds made with different parameters, but same weld pitch or APR (150 RPM/101 mm per min. and 300 RPM/ 203 mm per min.) are not identical for a given tool and alloy combination. This indicates that the flow is not kinematically determined by the tool geometry and

advance per revolution (APR) even when the defects are absent: welding power input and its effect on temperature and hence the flow stresses of materials must also be factors.

Based on the differences in weldability observed depending on the placement of the two alloys relative to the weld centerline, the material flow and high temperature deformation behavior must somewhat different between AA2050 and AA6061 during friction stir welding. Arbegast<sup>133</sup> developed a thermal-mechanistic flow model of FSW using thermo-mechanical simulator (Gleeble) data to establish constitutive relationships for flow stress and extrusion pressure for different aluminum alloys. In that work it was found that at relevant temperatures, extrusion pressure and flow stresses of AA6061 are lower than those of AA2195. Because the chemical compositions and properties of AA2195 and AA2050 are similar, the flow stress characteristics of these two alloys can be considered similar. The ideas set forth by Arbegast<sup>133</sup> were utilized to understand the flow behavior of these two alloys in bi-material FSW. During welding, advancing side material AA6061 is required to flow around the retreating side and must displace AA2050 in order to make the trip. However, retreating side material, AA2050, requires higher extrusion pressure than AA6061. The difference in required optimum extrusion pressure in bi-material welds might inhibit mass balance in the nugget zone during material transportation. Consequently flash and/or wormhole defects were evident in some of the welds with 6061 on the advancing side with higher reaction forces encountered by the pins (see next section). On the other hand, with AA2050 on the advancing side, extrusion pressure is initially high enough to extrude the 2050 material from the advancing side and move that material around the pin: it is possible for the high flow stress 2050 to displace the retreating side material (6061) which has relatively low

flow stress and low required extrusion pressure. Therefore, mass balance in the nugget zone was satisfied and consequently effective material transportation with appropriate consolidation was achieved while 2050 was placed on the advancing side. Other studies have also found that defect free welds were more readily produced when stronger materials were placed on the advancing side during dissimilar material welds.<sup>85, 94-96</sup>

#### 4.4.2 In-plane reactions on pin

Figure 4.32 is a polar plot of average in-plane reaction forces on the tools for different pin features with different alloy placements. The conventional direction of the positive X-axis force, positive Y axis force and resultant force orientation with respect to tool rotational and travel direction during FSW are also presented schematically in Figure 4.32. The force exerted by the work piece that impedes the forward motion of the tool is defined as the positive X axis force. The positive Y-axis force acts perpendicular to the X direction towards the advancing side from the retreating side. It is evident from Figure 4.32 that the in-plane resultant reaction forces are much lower when AA2050 is placed on the advancing side (open symbols) compared to having AA6061 on the advancing side (filled symbols). This is true in every case regardless of the quality of welds in terms of defect content. It can also be observed from Figure 4.32 that, for some of the welds with 2050 on the advancing side the Y-axis reaction force is very small compared to the X axis force. Interestingly, two welds have negative Y-force value as seen in the polar plot. The graph also shows that in almost all cases, the highest welding speed welds have the highest in-plane resultant force.

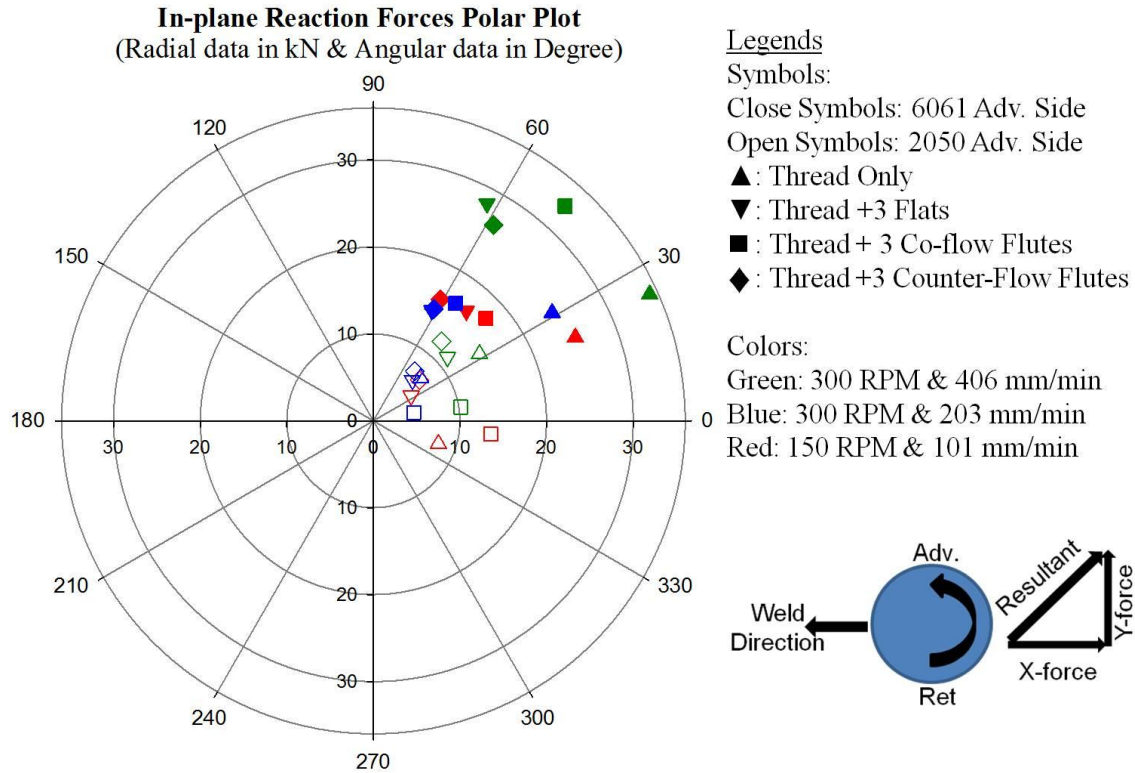


Figure 4.32 Average In-plane reaction force in Polar plot for different pin features, weld parameters and alloy placement with the arrow marks showing conventional force coordinate system in FSW process

#### 4.4.3 Forge Force-Torque-Power-Temperature relationships

Forge force in the Z direction was adjusted for welding with different pin features to maintain a similar contact condition of the tool shoulder and weld top surface. The right hand threaded pins rotated in the counterclockwise direction tend to push the material down and hence, the tool up. However, additional features on the pins will alter the upward thrust necessitating different levels of applied Z-force in order to maintain the desired shoulder contact. For welding with 2050 on the advancing side, the pin with thread+ 3 co-flow flutes required the highest forge force (Z-force) and the pin with thread+ 3 counter flow flutes required the lowest forge force to maintain similar plunge depth: this seems intuitively correct because it is anticipated that the counter flow flutes

will reduce the upward thrust on the pin and the co-flow will increase it: the first by intensifying the downward material flow induced by the threads and the second by performing the opposite function. The threaded only pin and thread+3 flats required intermediate forge force when 2050 was placed on the advancing side. When welding with 6061 on the advancing side, threaded only pin and pin with thread + 3 co-flow flutes required higher forge force than the pin with thread+ 3 flats and thread + 3 counter-flow flutes. It should be noted that the co-flow flute pin requires the highest forge force in every case except when large defects are observed in the threaded only pin welds (6061 on advancing side). Figure 4.33 is a plot of torque vs. forge force for various tools, alloy arrangements and welding parameters. By examining the variation of required Z-force for a given parameter set, one can see the effect of tool features on required forge force (same color legend for same welding parameters) on the horizontal axis. The torque vs. forge force, graphed in Figure 4.33, indicates that for all of the 300 RPM welds, at a given combination of alloy placement and welding speed, the torque is relatively insensitive to the applied forge force. It was observed in these welds that, regardless of alloy placement, variation of measured torque was insignificant (less than 5%) while considerable variations in forge forces (15%-33% for different pins) were required. It may be that this is due to variation in the upward thrust due to pin features leading to an essentially constant pressure under the shoulder even though the Z-force is varied. With lower rotational (150 RPM) and welding speed (101 mm/min) a greater change in torque with respect to forge force was observed for different pin features. For instance, in the defect free welds (with 2050 on advancing side and 150 RPM), a forge force increase from 28.9 kN (pin with counter flow flutes) to 44.5 kN (pin with co-flow flutes), the

required torque is increased from 258 N-m to 296 N-m. While this torque increase is significant it is still substantially less, percentage wise, than the increase in forge force (15% vs. 54%).

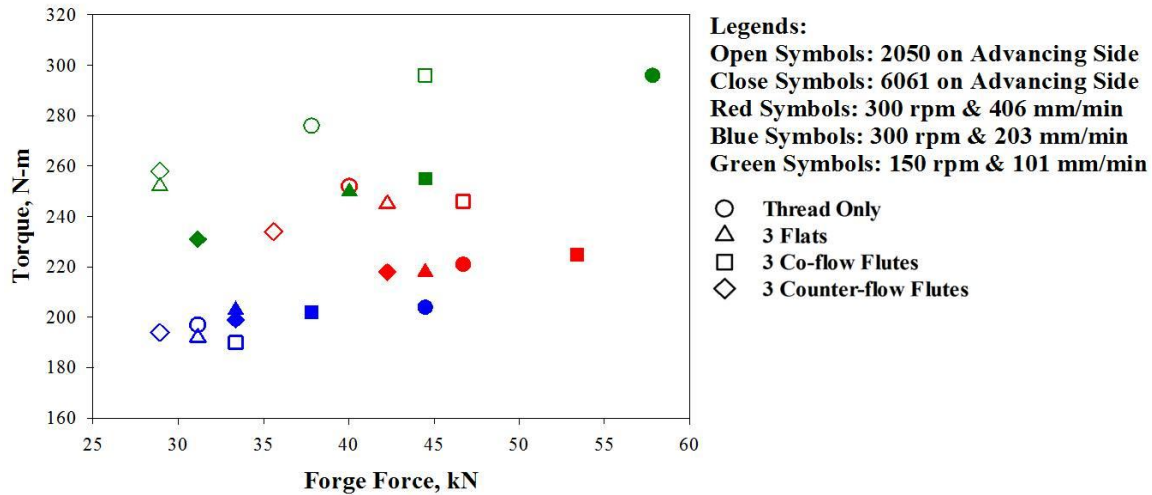


Figure 4.33 Torque as a function of Forge force for different tool and weld parameter

The observation of higher torque at lower RPM (green symbols vs. red and blue symbols in Figure 4.33) is consistent with generally observed trends and can be explained by the measured pin temperature as a function of weld power shown in Figure 4.34. Higher rotational speed results in higher temperature and reduced torque, presumably due to the reduced flow stress of the material in contact with the tool.<sup>140</sup> The temperature increased significantly (increased by 55°-80°C) when the weld parameters were changed from 150 RPM and 101mm/min. to 300 RPM and 203 mm/min. (Figure 4.33). However, at the same rotational speed, 300 RPM, when welding speed is increased from 203 mm/min to 406 mm/min, the welding power increases, but temperature decreases, due to reduced heat input per unit volume of processed material.

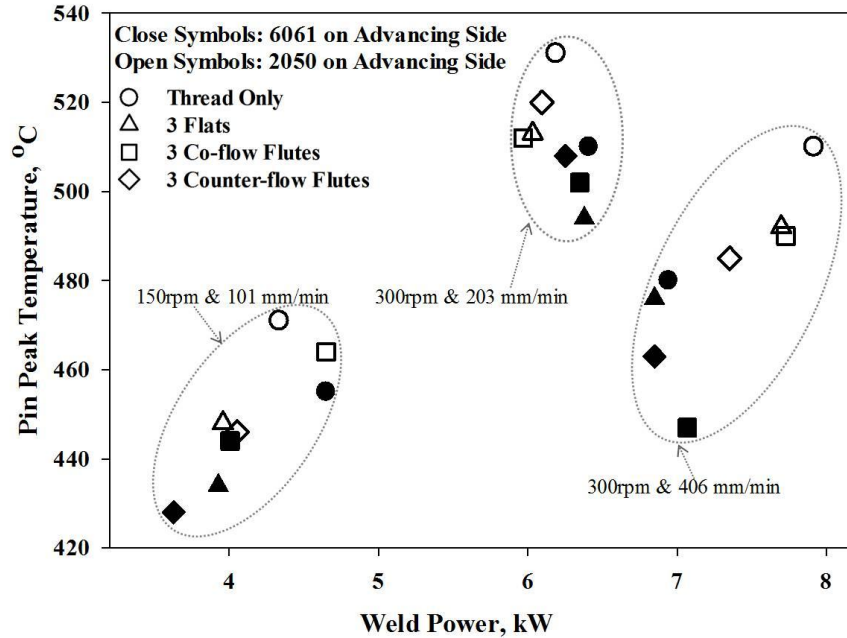


Figure 4.34 Pin Peak Temperature as a function of weld power for different tools and weld parameters

Based on the data in Figure 4.34, it is generally seen that, all other things being equal, the welds made with 2050 on the advancing side have higher temperatures than corresponding welds made with 6061 on the advancing side. This is true even when the measured weld power is lower for the 2050 advancing side welds (300 RPM, 203 mm/min.). It is not clear why this should be the case, however, it may be related to differences in amount of tool to specific alloy contact and the differing thermal conductivities of 6061 and 2050 (6061 is higher). From Figure 4.34 it can also be seen that for every combination of alloy placement and welding parameters, the highest pin temperature is measured in the thread only pin. In several, but not all cases, the power required when welding with the thread only pin is greater and this can certainly explain the higher temperature. However, it is more interesting to consider why might the power be generally higher with the threaded only pin? Higher power consumption for production of defect free welds implies a less efficient tool design. Examination of the

cross sections in Figure 4.29 indicates a quite significant difference in the level of mixing between the pins with and without thread interruptions as does the data in Figure 4.31. The differences in intermixing obviously result from some fundamental differences in the flow patterns due to the different tools. It seems likely that the thread interruptions, and in particular, those which are not complimentary to the flow produced by the threads, may act as cutting edges and promote the movement of materials around the tool as rigid body motions rather than solely as a shear flow. The typical shear zone model of FSW material flow in other studies <sup>75, 142, 143</sup> also implies that all of the material making up the weld goes through a severe shearing process (with greater strain on the advancing than retreating side) and that the maximum temperature of the deforming material will be at the tool surface. However, if some of the material transport occurs via rigid body motion, then some regions of high deformation could be remote from the tool surface, leading to reduced tool temperature and, possibly, lower total deformation required to maintain the material balance between the leading and trailing sides of the tool.

#### 4.4.4 Nugget microstructures and grain sizes

Figure 4.35 (a-d) presents typical microstructure of AA2050 and AA6061 for welds performed at 300 RPM and 203 mm/min using different pin features with 2050 on advancing side. Two different fine, equiaxed, fully recrystallized, grain structures resulting from deformation of two different base materials were evident for welding with different pin features. Black spots in the microstructures, mostly in 6061 sides may be due to the galvanic corrosion due to the contact with AA2050. <sup>58, 144</sup> The variations of grain structures in the center of the nugget zone for different tool features as observed in Figure 4.35 are the indicative of increase in temperature. Grain size is highest for welding

with threaded only pins: 8.3 $\mu\text{m}$  on AA6061 and 11.8 $\mu\text{m}$  on AA2050. However, lowest grain sizes were measured for welding with pin having threaded+ 3 counter-flow flutes: 5.6  $\mu\text{m}$  on AA6061 and 7.3  $\mu\text{m}$  on AA2050.

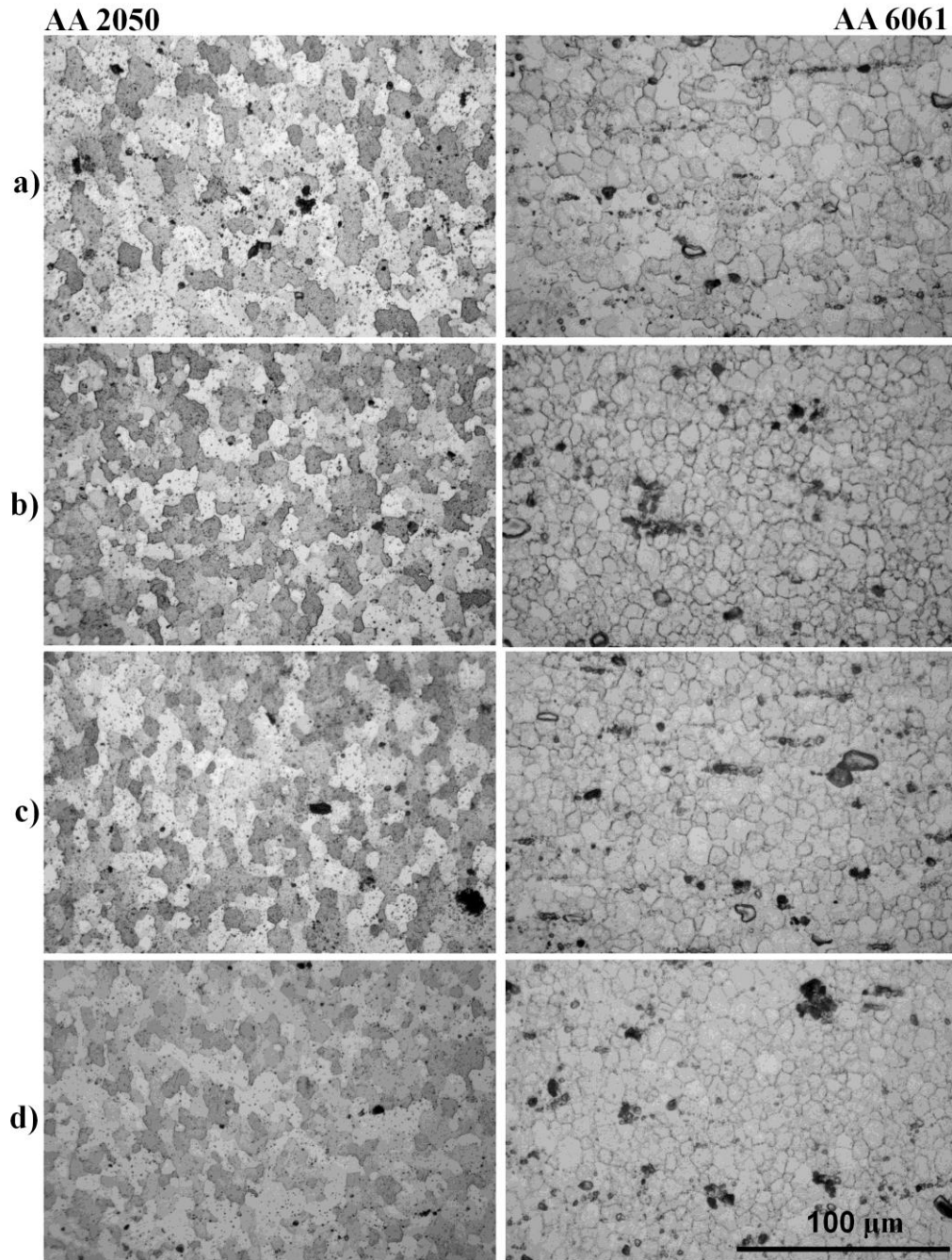


Figure 4.35 Grain structure of center of nugget for friction stir welding with pins: a) threaded only, b) thread+3 flats, c) thread+ 3 co-flow flutes & d) thread+ 3 counter-flow flutes under welding parameters: 300 RPM & 406 mm/min with 2050 on advancing side

Grain sizes of AA2050 and AA6061 near the center of nugget are plotted against the pin peak temperature after welding with different tool features (corresponding symbols) and welding parameters (corresponding colors) indicated in Figure 4.36 (a-d). The grain size measurement from the microstructures for 6061 (both advancing and retreating sides) was beyond the limit of optical microscope when welds performed at 150 RPM, i.e. the pin peak temperatures are below 450° and the resulting grains are not resolvable. Therefore grain sizes of those welds were not reported here. In the first set of Figure 4.36 a-b, 'X' marks on the left side of symbols indicate defected welds. In the second set (Figure 4.36, c-d), the defective weld data are removed to clarify the observed trend.

As mentioned in experimental procedure in Chapter 2, the grain size measurements were done at the center of the nugget, however, selecting the center of nugget to measure grain sizes are limited depending upon the position of defects and also the effects of zigzag features of lamellae of one alloy into another (2050 into 6061 and vice versa). The position of nugget center for measuring grain size of both alloys was considered accurate for the defect free welds. Excluding the defected welds indicated by black 'X' marks in Figure 4.36, grain size varies proportionally with the pin peak temperature: smaller grain size at a lower spindle rotation rate (low temperature) and larger grain at higher rotation rate (higher temperature). It can also be mentioned here that, in each condition threaded only pin generated high temperature that resulted larger grain size in the nugget than other pins with same FSW control parameters. This observation indicates that the relative temperature measurements for the various pins are likely to be indicative of real temperature difference and not merely artifacts of

thermocouple placement. However, the relationship between grain size and pin features is less critical than that between grain size/temperature and welding parameters. It is apparent that the grain size is mainly governed by temperature, which is consistent with prior experiences and can be explained by grain growth process concepts: including static recrystallization, continuous dynamic recrystallization<sup>47</sup> and geometric dynamic recrystallization<sup>51</sup>. Interestingly, the effect of temperature on the grain size is greater for the 2050 than for the 6061 and the 2050 grain size is larger for a given peak T. This is somewhat surprising given the relatively higher recrystallization resistance of 2050 compared to 6061.

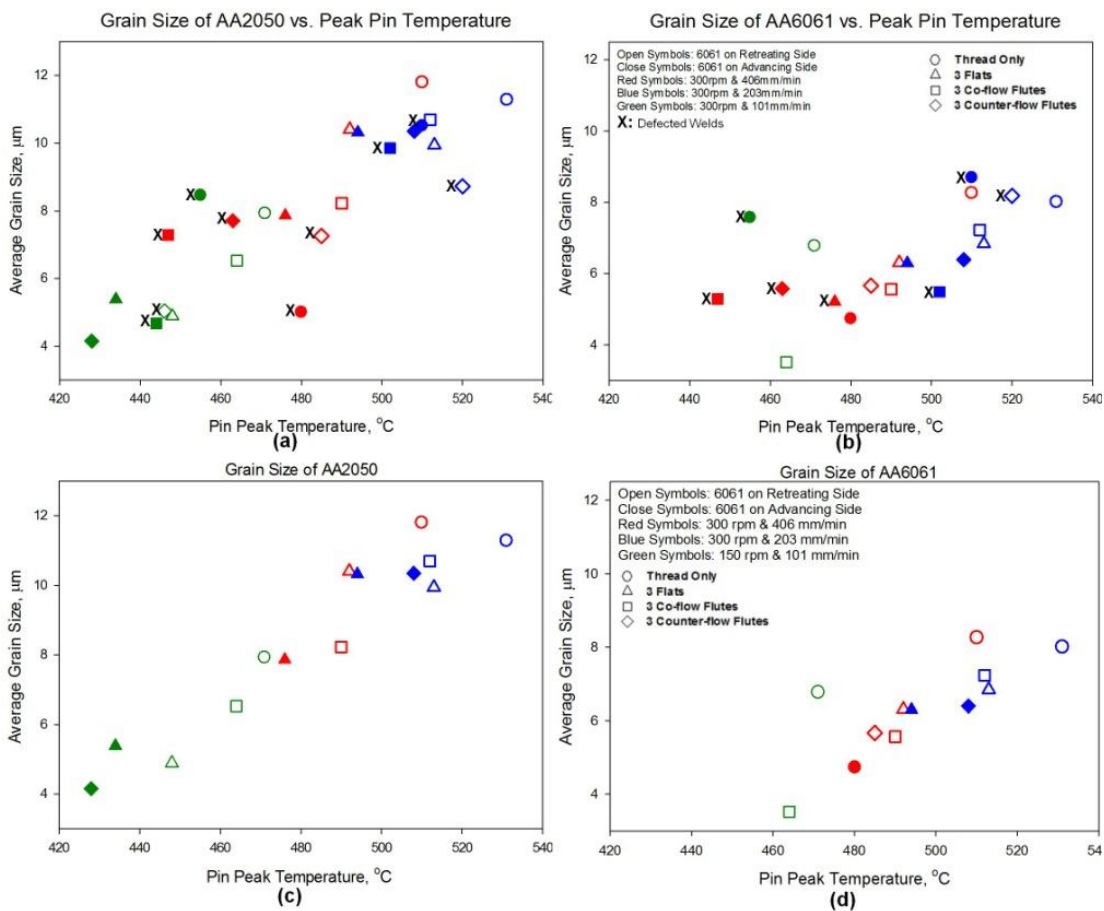


Figure 4.36 Average grain size a function of peak temperature for different pin features and welds parameters: (a) AA2050, (b) AA6061, (c) AA2050 excluding defected welds & (d) AA6061 excluding defected welds

#### 4.4.5 Summary observations on dissimilar aluminum alloy FSW

In this section, the effect of alloy placement and pin features (thread/flats/flutes) along with changing the process control parameters were examined in dissimilar material FSW of AA2050 and AA6061. The following concluding remarks are drawn based on observed trends:

- (1) Alloy placement has a significant effect on weldability of bi-material FSW. Placing stronger material, i.e. AA2050 on advancing side resulted in reduced defect content.
- (2) In plane reaction forces on the tool were reduced for welding with 2050 on the advancing side.
- (3) The presence or absence of thread interruptions had significant effects on weldability and material flow.
  - a. Thread resulted in large macroscopic defects in all cases where 6061 was on the advancing side.
  - b. Flats produced defect free welds in all but one case (at the highest welding speed, 6061 on the advancing side).
  - c. Counter flow flutes tended to produce near root defects: this is intuitively reasonable as the counter flow flutes would tend to move material away from the root.
  - d. Co-flow flutes produced surface breaking defects in some cases: this is intuitively reasonable as the co-flow flutes will tend to move more material away from the crown than will the threads alone.

e. Thread interruptions, especially those which did not reinforce the pin flow, resulted in substantially greater intermixing of the two alloys: it is suggested that this is due to increased levels of material transport via rigid body motion.

(4) Thread interruptions which are neutral (flats) or oppose the thread flow (counter flow flutes) reduce the needed forge force relative to the thread only or thread + co-flow flutes: this is intuitively reasonable and is compatible with conclusions 3-d and 3-e.

(5) The temperature was uniformly higher for welds made using the threaded only tool: it is supposed that this is related to conclusion 3.e. Also nugget grain size was increased proportionally with pin peak temperature and highest grain size was observed for threaded only pin for similar welding condition.

It is important to note that while some of these conclusions may be quite general, subtle variations in tool geometry might create substantial changes. Also, parameter ranges of different welds and selected alloys could lead to different conclusions. Regardless, the results presented here tend to be self consistent and it seems reasonable to expect that they can be used to guide process development and tool selection in similar cases.

#### **4.5 Understanding the effect of tool eccentricity and placement of alloy in dissimilar material friction stir welding**

In this section, misaligned friction stir welding was investigated in order to identify the flowability and tool reaction during stirring dissimilar material while the tool is eccentric from the abutting interface. Friction stir welding was performed between two

different combinations of aluminum alloys: (i) AA2050 to AA6061 and (ii) AA7050 to AA6061 with placement of both alloys on advancing side with other on retreating side. Welds were made with a misalignment of the FSW tool and plate interface using a conical shape coarse threaded (2.12mm pitch) pin having 3 flats. Figure 4.37 schematically shows the set up for misaligned friction stir welding with tool eccentricity. The interface of the two alloys was set misaligned with welding trail in such a way that tool travel from starting point while completely immersed in one material (starting in advancing side material) and exits from other material (ended in retreating side material). Therefore, with a 406 mm weld length, each point on weld seam represent different tool offset except at 203 mm distance, where tool centerline coincides with abutting interface. The examined rotational speed was 150 RPM and welding speed was 101 mm/min.

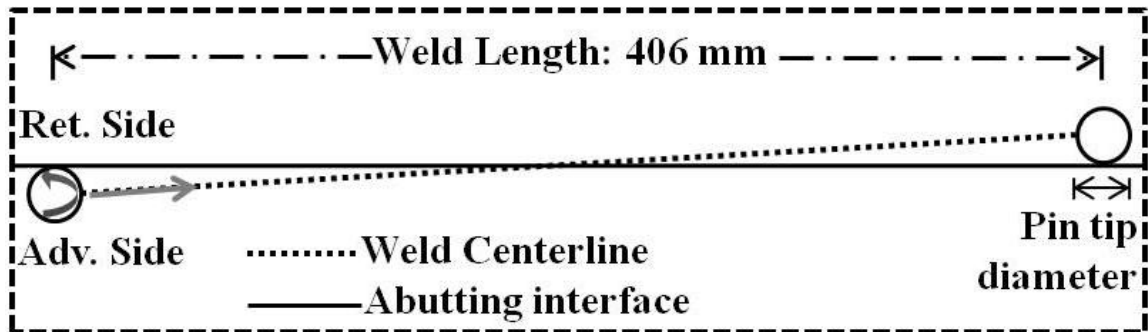


Figure 4.37 Misaligned friction stir welding set up

#### 4.5.1. Misaligned friction stir welding between AA2050 and AA6061

Figure 4.38 shows the transverse macro-sections of weld nuggets relating to different pin eccentricity (corresponding columns) with reference to the abutting interface while placing both 2050 and 6061 on advancing sides (corresponding rows). Completely defect free welds were produced irrespective of the placement of alloys or tool eccentricity, which have also been observed with centered weld in Figure 4.29 (b) under the similar welding condition and tool configuration. Similar to the centered welds as

described in the previous section, deformation region (thermo-mechanically affected zone) underneath the pin was higher when 2050 was placed on the advancing side compared to 6061 on the advancing side. These depths deformation zones were quantitatively determined using macro and micro images. The measured deformation zone depth was 1.1 mm - 1.6 mm when AA2050 was on advancing sides with the maximum of 1.6 mm with no pin eccentricity (tool axis coincide with abutting interface). However the range of a deformation zone depth beneath pin was measured as 0.33 mm to 0.47 mm when 6061 was placed on the advancing side during welding. Interestingly, the resultant reaction forces on the pin are higher when 6061 was placed on advancing side compared to 2050 on advancing side which is a similar phenomenon as observed in previously centered welds. Figure 4.39 depicts the polar plot to present the average X and Y axis forces for misaligned and centered welds. The arrow in the Figure 4.39 indicates the direction how the magnitude and orientation of the resultant force move during pin eccentricity varies from the advancing side to the retreating side. It should be noted here that, the average resultant forces for 0 mm pin eccentricity in these two misaligned welds are closely matched with previously shown average resultant forces in centered welds under similar welding conditions and tool configuration. Since, the deformation of material underneath the pin is less for 6061 on advancing side compared to 2050 on the advancing side, resistance to the rigid material under pin might impose excessive reactions on tool corresponding to the weld with 6061 on advancing side.

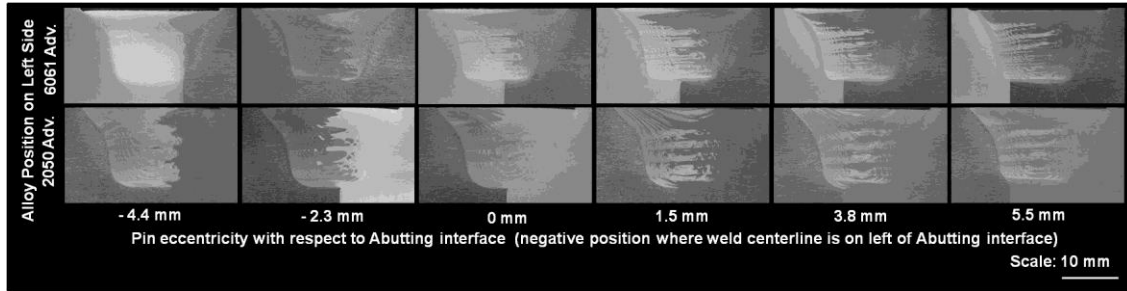


Figure 4.38 Weld transverse macrostructures of misaligned welds

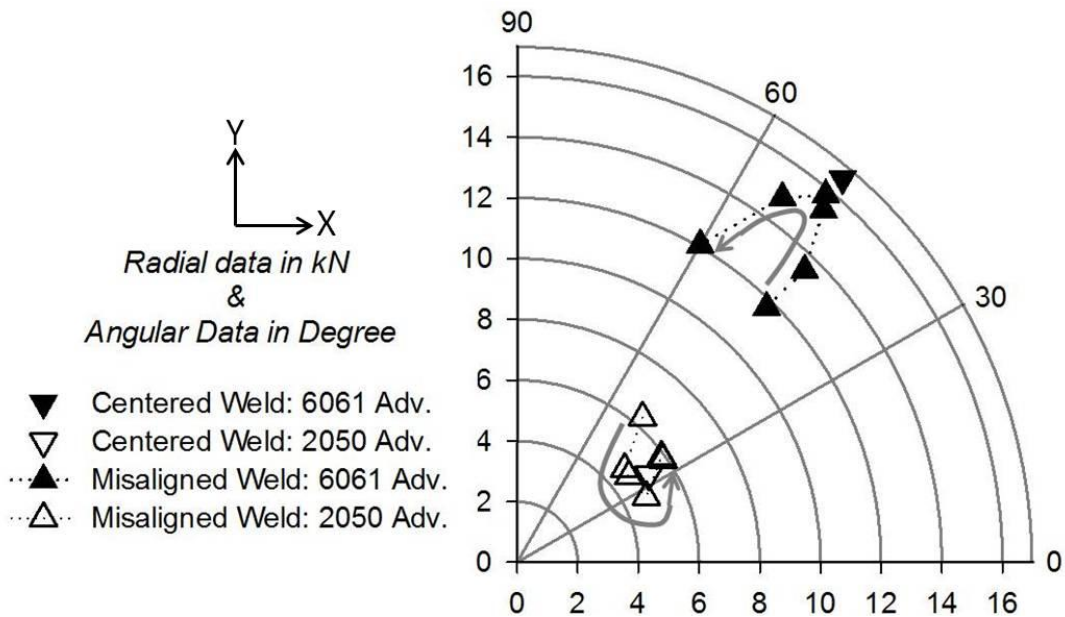


Figure 4.39 Polar plot of in-plane reaction forces while pin eccentricity move from advancing side material to retreating side material as indicated by the arrow mark

Investigations were made to establish the correlations among the response variables with the intermixing state of the bi-materials under tool eccentric conditions. Figure 4.40 (i-viii) shows all the response variables, including the fractional area of the dissimilar materials, deformation depth underneath pin and forge force (Z-force) when the tool eccentricity moves from advancing side materials towards retreating side materials.

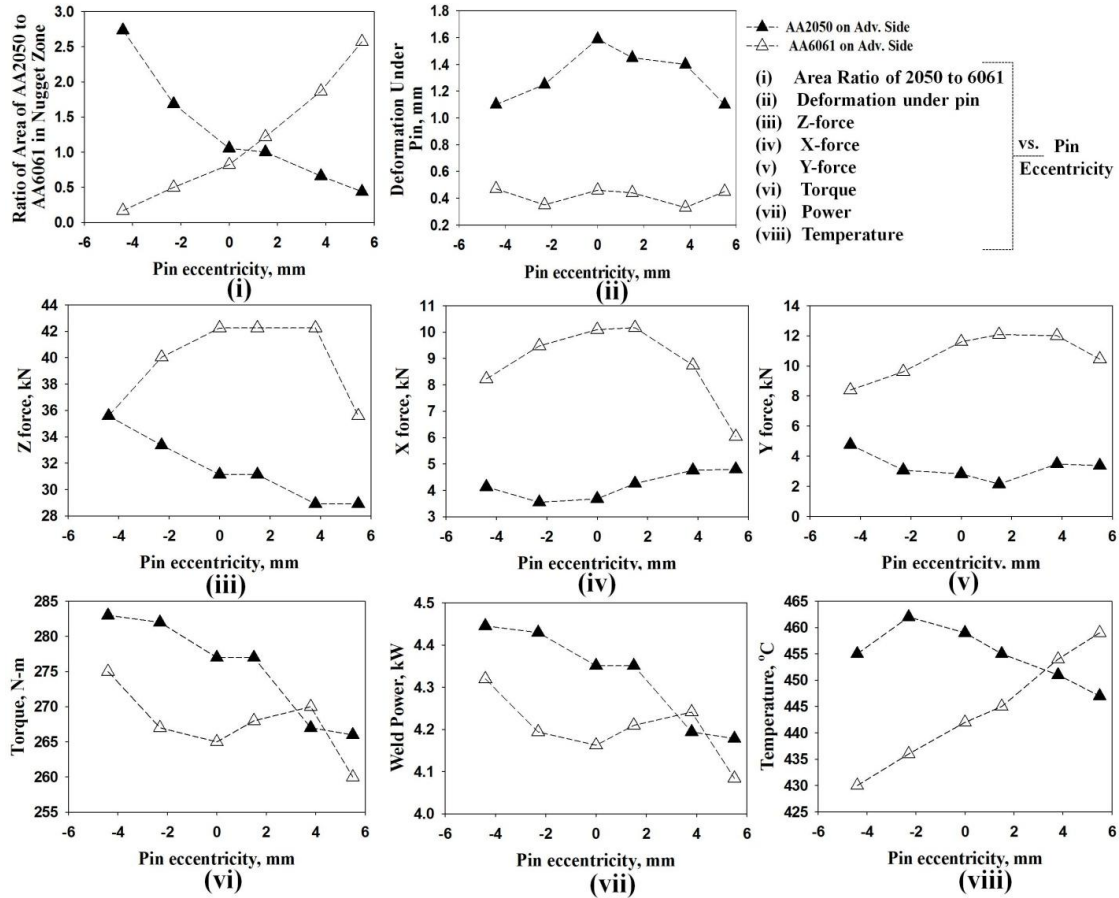


Figure 4.40 Response variables as a function of tool pin eccentricity

The inter-correlation derived from the observation of the response variables in Figure 4.40 are stated below:

- Obviously the pin eccentricities with respect to the abutting interfaces reflect on the fractional area of nugget zone. The ratio of the partial area of AA2050 to AA6061 was plotted against pin eccentricity as shown in Figure 4.40 (i) with the positioning of both alloys in advancing/retreating sides. It is obvious that, the fractional area decreases when eccentricities of pin move from 2050 to 6061 in both alloy placement conditions. These partial areas were obtained from the recrystallized zone of weld macrosections (Figure 4.37) using image processing software: ImageJ.

- b. It was mentioned earlier in this section that the deformation under the pin was higher when relatively stronger AA2050 was placed on the advancing side compared to AA6061 on advancing side. It is also interesting to note from Figure 4.40 (ii) that deformation underneath the pin is the highest when there is no pin eccentricity compared to either extreme in case of 2050 advancing side welds. Extrusion of stronger materials (AA2050) from advancing side might lead relatively low strength material (AA6061) to deform more rapidly by the stirring pin than the extrusion of low strength materials from advancing side. Moreover, this phenomenon can be explained in terms of process forces (forge force and in-plane reactions).
- c. Forge forces along Z direction were constantly required to adjust to maintain similar depth of penetration during misaligned welding processes. Weld with 6061 on advancing side require more forge force than that of 2050 on advancing side as seen in Figure 4.40 (iii). It is also interesting to note that, for 2050 on advancing side welds, forge force requirement decreases continuously while the pin eccentricity move from 2050 to 6061 and maximum 19% reduction in Z force was observed when the pin is immersed mostly in 6061 as shown in Figure 4.40 (iii). On the other hand, in 6061 advancing side weld, required Z force was observed maximum within the region of minimum pin eccentricity compared to both extreme eccentricity and Z force is reduced by 19% in case of maximum pin eccentricity on both advancing and retreating side. As mentioned earlier the rigid substrate underneath the pin might cause maximum Z-force in case of 6061 advancing side weld, whereas higher deformation zone under the pin might cause

- relatively less forge force requirement in case of 2050 advancing side weld. The variation of forging force eventually affects the response variables such as in-plane reaction on tool, torque, power and temperature.
- d. From figure 4.40 (iv) it is seen that, the average X axis force has minimum value (3.68 kN) in case of AA2050 on advancing side weld with minimum tool eccentricity. However, this X force is increased by 12% and 30% when pin eccentricity is 4.4 mm in advancing side material (2050) and 5.5 mm in retreating side material (6061) respectively. On the other hand, for AA6061 advancing side welds, X forces are relatively higher compared to 2050 advancing side weld as observed in Figure 4.40 (iv). This may be due to high forge force for 6061 welds. Moreover, X force has a maximum value of 10.2 kN at 0 mm pin eccentricity and reduced by 20% and 40% for farthest pin eccentricity in advancing side (6061) material and retreating side (2050) material respectively. The overall X force trend is opposite in two alloy placement conditions.
- e. It is also seen in Figure 4.40 (v) that, the average Y axis force has similar trend as of X axis force in case of AA2050 advancing side weld. The minimum Y force (2.15 kN) was observed at 1.5 mm pin eccentricity in retreating side materials (AA6061) and increased by 120% and 57% for pin eccentricity of 4.4 mm in advancing side material (2050) and 5.5 mm in retreating side material (6061) respectively. On the contrary, with 6061 advancing side weld, average Y force has the minimum value (8.4 kN) at 4.4 mm pin eccentricity in the advancing side material (AA6061), however, when pin approaches near and into the retreating side material (AA2050) Y force gradually increase and reaches to a maximum of

- 12 kN at 3.8 mm pin eccentricity into retreating side material. Stronger material (AA2050) in retreating side might impose higher Y forces in case of dissimilar material friction stir welding. However, this phenomenon might also be influenced by a complex interaction of applied forge force with the placement of alloys in advancing side and temperature dependent material flow stress.
- f. Torque (Figure 4.40-vi) and weld power (Figure 4.40-vii) have similar decreasing trend while pin eccentricity is moving from advancing side to retreating side, regardless of the position of alloy in advancing or retreating side. Moreover, for 2050 on the advancing side weld has higher torque and power compared to 6061 weld in most of the tool eccentric cases. However, variation of torque with pin eccentricity in each welding condition is not significant (less than 7%). These insignificant differences in torque and power might be because of contributing effect from constant shoulder geometry that primarily preside over the torque and weld power in conventional FSW with rotating pin and shoulder.
- g. It was noticed from Figure 4.40 (viii) that, in case of 2050 advancing side weld, the pin peak temperature was initially higher when the pin was immersed into AA2050 and decreased by 20°C while the pin eccentricity move towards retreating side AA6061. However, this decrease in temperature might be due to that, previously generated higher temperature which was required for softening advancing side material (AA2050) did not reach the steady condition within the temperature transient while the pin eccentricity move towards AA6061 on retreating side. Interestingly, temperature transient recorded for welding with AA6061 on advancing side was observed opposite to that of AA2050 advancing

side weld. The recorded temperature increased by 30°C while pin eccentricity move from advancing side (pin immersion into 6061) to retreating side (pin immersion into 2050). Higher the amount of AA2050 involved in the recrystallization process in nugget zone greater the peak temperature recorded in the pin. This highest temperature at 5.5 mm tool eccentricity towards retreating side material (AA2050) may also be the reason of a sudden reduction of required forge force as well as in-plane forces associated with that tool eccentricity.

#### 4.5.2. Aligned and misaligned friction stir welding between AA7050 and AA6061

After intensive examination on dissimilar materials friction stir welding between AA2050 and AA6061, the scope of the study was extended to bi-materials weld between AA7050 and AA6061 in both centered and misaligned FSW. The material selection in this study was based on the higher strength difference of alloys in abutting interface. Therefore similar study was performed as of Section 4.5.1 except that AA2050 was replaced by AA7050 in the current study since strength of 7xxx series aluminum alloys are much higher than that of 2xxx series.

Figure 4.41 is the macro cross sections of weld nuggets for corresponding alloy placement (same row) and welding parameters (same column) for 7050 and 6061 dissimilar materials FSW in the butt joint arrangement. Similar 2050-6061 welds; stronger material (AA7050) on advancing side produces good quality welds as evident from Figure 4.41, whereas large wormhole defects at low welding/rotational speed and thinning of cross section (deep undercut) at high welding/rotational speed were observed with 6061 on advancing side welds.

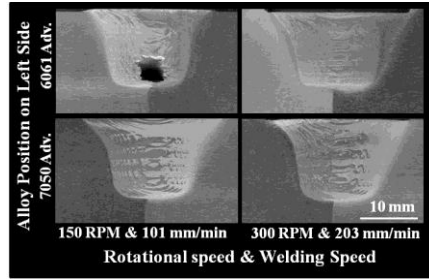


Figure 4.41 Weld transverse macrostructures of AA7050 to AA6061 centered welds

Figure 4.42 also presents the transverse macrosections of weld nuggets relating to different pin eccentricity (corresponding columns) with reference to the abutting interface while placing both 7050 and 6061 on the advancing sides (corresponding rows). Macro cross sectional evident reestablish the statement that the positioning of stronger alloy on advancing side demonstrates effective welds during dissimilar materials FSW in butt joint configuration.

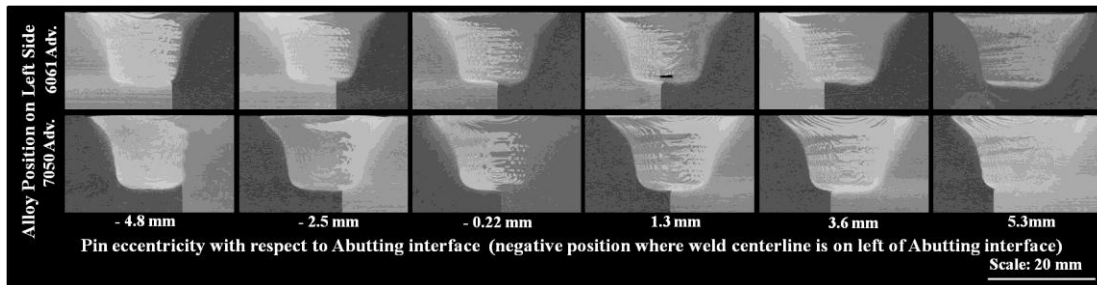


Figure 4.42 Weld transverse macrostructures of AA7050 and AA6061 welds with different tool eccentricity

Figure 4.43 also illustrates the polar plot of the average in-plane reactions on pin (X and Y axis forces) for aligned and misaligned welds. The arrow in the Figure 4.43 indicates the direction how the magnitude and orientation of the resultant force move during pin eccentricity varies from the advancing side to the retreating side. The resultant forces for misaligned welds are grouped whereas centered welds are offset from the group, although the trend for eccentric weld is close to that of centered weld. The most plausible explanation for this misfit of the resultant magnitude and orientation of centered

weld is because of continuous variation of tool eccentricity lead to frequent adjustment of forging force to maintain contact condition between the tool shoulder and the weld crown. Interestingly, welding with AA7050 on advancing side resulted negative Y force at low welding/rotational speed. This phenomenon is frequently observed for this particular threaded pin with 2.12 mm pitch in previous similar and dissimilar material welds. The stronger AA7050 on advancing side imparts dominating pressure on the tool than pressure from retreating side AA6061, therefore the negative Y force is experienced by the pin. However, Y force was observed lower only with low tool eccentricity in 7050 advancing side misaligned weld that is, when there is a balanced ratio of AA7050 and 6061 in the stir zone. Figure 4.44 elaborately describes the process forces, torque, power, temperature as a function of tool eccentricity.

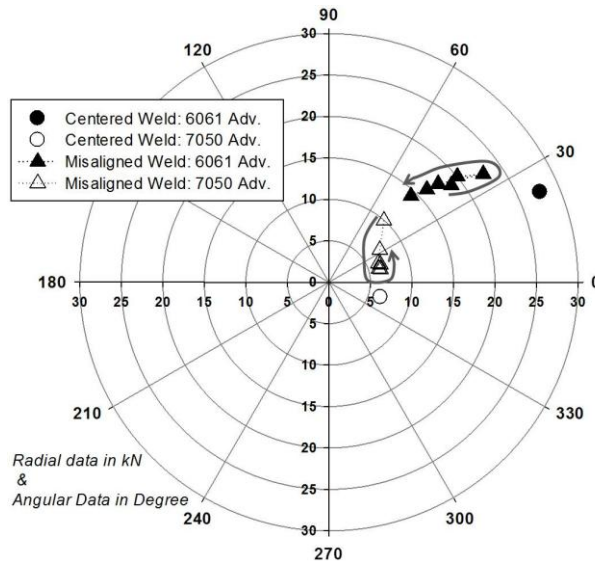


Figure 4.43 Polar plot of in-plane reaction forces while pin eccentricity move from advancing side material to retreating side material as indicated by the arrow mark

Figure 4.44 (i-viii) presents similar plots as in Figure 4.40 except that AA7050 was chosen instead of AA2050 as one of the weld materials beside AA6061 during dissimilar material FSW. The following statements can be drawn from the figures:

- a. The ratio of the partial area of AA7050 to AA6061 was plotted against pin eccentricity as shown in Figure 4.44 (i) with the positioning of both alloys in advancing/retreating sides. It is understandable that, the fractional area decreases when eccentricities of the pin travel from 7050 to 6061 in both alloy placement conditions.
- b. Similar to AA2050-AA6061 misaligned welds, stronger alloy AA7050 on advancing side cause deformation zone underneath the pin to be higher compared to AA6061 advancing side welds. This was evident from Figure 4.44 (ii), however the trend of the deformation depth under the pin with respect to the tool eccentricity was observed opposite while comparing 7050 and 6061 advancing side welds. In case of 7050 advancing side welds, the depth of the deformation beneath the pin increases during the pin eccentricity shift from 7050 (advancing side) towards the 6061 (retreating side). Moreover, at the highest eccentricity in the retreating side when only 6061 is involved in the stir zone, although this deformation is much higher than 6061 advancing side welds any instance of the tool eccentricity.
- c. Figure 4.44 (iii) presents the forge force as a function of tool eccentricity. It is interesting to note for the 6061 advancing side weld that, forge force increases continuously while the pin eccentricity move from 6061 to 7050 and maximum 35% increment in Z force was observed when the pin is immersed mostly in 7050 as shown in Figure 4.44 (iii). On the other hand, in 7050 advancing side weld, applied forge force continuously decreased with increasing pin eccentricity towards retreating 6061 side and reduced by 16% when the pin is completely

- immersed into 6061. As explained in the previous section that the rigid (less deformed) substrate under the pin might provide up thrust that maximizes the Z-force in case of 6061 advancing side. In contrast, a higher deformation zone under the pin might cause relatively less up thrust on tool therefore forge force requirement is less in case of 7050 advancing side weld.
- d. It is interesting to note the unvarying X force with respect to tool eccentricity in case of 7050 advancing side weld (see Figure 4.44-iv). However, for 6061 advancing side weld, X force reaches its maximum value near the region of minimum tool eccentricity (1.3 mm towards 7050) and minimum X-force was observed at maximum eccentricity in either direction. It should be noted here the maximum X force of 25.4 kN for centered weld are corresponding to wormhole defected weld as seen in Figure 4.41.
- e. While observing unvarying X force in 7050 advancing side weld, Y force decreases with the tool eccentricity move towards retreating 6061 side and reaches a plateau until the pin is completely immersed into AA6061 in the retreating side (see Figure 4.44-v). On the other hand, a minute variation in Y force was evident in the case of 6061 advancing side weld with maximum near the region of minimum tool eccentricity. It is also interesting to note that Y force is much higher when 7050 is on retreating side compared to 6061 on retreating side. One of the most plausible reasons for the higher Y force is might be associated with larger reaction on the tool by stronger AA7050 from the retreating side towards advancing side. Another important phenomenon of observing negative Y force in the case of centered weld with 7050 on the advancing side

- (open circle in Figure 4.44-v). This might also be associated with pressure induced by advancing side 7050 on the tool pin.
- f. Torque (Figure 4.44-vi) and weld power (Figure 4.44-vii) does not vary much (less than 4%) with tool eccentricity in case of 7050 advancing side weld. However, average torque or power for 7050 advancing side weld is higher than that of 6061 advancing side weld. It is also interesting to note that with the translation of tool eccentricity from 6061 towards 7050, torque and weld power was increased. This might be because of the involvement of stronger materials (7050) in the stir zone during the shifting of tool towards 7050 rich regions. Overall the variation of torque or power with pin eccentricity in each welding condition is not significant (less than 10%) regardless of alloy placement. This is likely due to the dominance of shoulder effects in torque.
- g. Figure 4.44 (viii) shows the pin peak temperature as a function of tool eccentricity with both welding conditions and alloy placement. Minute variation of temperature was observed for 7050 advancing side weld. This might be because the heat input that require to stir stronger 7050 resulted an increased temperature and does not drop while stirring AA6061 singly near the end of the weld within the temperature transient. However, recorded temperature increased by 40°C while pin eccentricity move from advancing side (pin immersion into 6061) to retreating side (pin immersion into 7050). Higher the amount of AA7050 involved in the recrystallization process in nugget zone greater the peak temperature recorded in the pin.

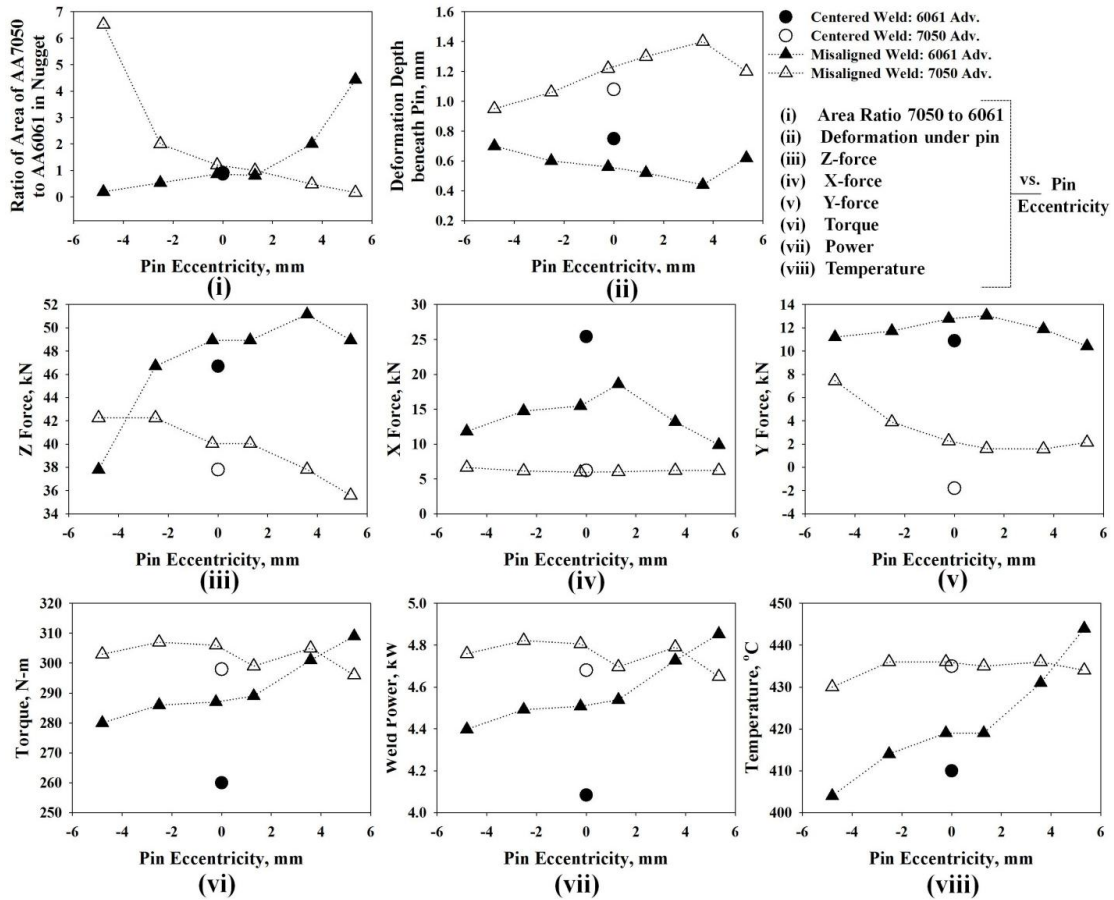


Figure 4.44 Response variables as a function of tool pin eccentricity

#### 4.5.3 Summary Observations from misaligned dissimilar alloy FSW

Following observation can be drawn from misaligned bi-materials welds

1. Deformation zone underneath pin is higher while stronger materials are placed on advancing side.
2. The lower deformation region under the pin lead to higher in-plane forces during welding.
3. Temperature variation is higher while the tool eccentricity shift from a low strength to high strength materials compared to opposite shifting of tool eccentricity.

## **4.6 Tool Features Effect on Material Flow during FSW of Lap Joints**

Friction stir welding of aluminum alloy was performed in the lap joint arrangement in order to explore the material transport phenomena due to the effect of different features (flats/flutes) on a threaded pin. Investigations were made to join AA6056-T4 in lap weld arrangement, using a threaded pin having various features (flats/co-flow flutes/counter-flow flutes). The results discussed in the previous section (Section 4.3) pursued the author to select the coarse thread form (2.12 mm pitch or 12 threads per inch) to pursue the lap weld investigations. The thickness of the base material AA6056 was 4.2 mm. Therefore, a pin having depth of 12.7 mm required stacking of four plates together to form a partial penetration lap joint on a steel backing anvil. The tracking of interface material movement in a lap joint provided quantitative information regarding the vertical motion that is distinctly affected by variation in pin features during FSW. Material flow, interface characteristics and process response variables of the lap welds were evaluated to compare the effect of different pin features

### **4.6.1 Weld cross sectional evaluation**

Figure 4.45 presents the weld transverse macro sections of friction stir lap welds with coarse threaded pin having various features under different rotational speed at constant welding speed (203 mm/min). In each image, the advancing side is on the left and retreating side is on the right. Each row of images shows the cross sections for a particular tool rotational speed while each column is for a particular pin features (flats/co-flow flutes/ counter-flow flutes). Macrostructures show wormhole defects for welding with 3 flatted pin at 240 RPM and 320 RPM, while completely defect free welds were obtained at 400 RPM rotational speed. Therefore, with the formation of wormhole defect

near weld mid plane on the advancing side, it can be said that, vertical material movement was not found effective at lower rotational speed for 3 flatted pin welds. In case of welding with CT + 3 co-flow flutes pin, this wormhole defect was eliminated; however surface breaking defects were evident in all applied rotational speed. These surface breaking defect formation may be due to the action of the right hand thread with co-flow fluted pin rotating in the counterclockwise direction (as viewed from above) thereby pushing material downward toward the weld root. This down thrust helps to eliminate near root wormhole defects, but, if too much material escapes as flash, a surface breaking defect may be created. Unlike butt joints or bead on plate welds as studied previously, a pin with counter-flow flutes was found to be effective in promoting the vertical material movement as well as producing quality welds compared to pin with flats and co-flow flutes at higher rotational speeds (320 RPM and 400 RPM). However, at 240 RPM micro defects near the weld root on the advancing side were evident for welding with counter-flow flutes. Figure 4.46 shows the microscopic defects in weld cross section for 240 RPM welding with counter-flow fluted pin. It is revealed from macro and micro structural evaluation wormhole, weld surface defect and porous defects (micro voids) were present in most of the welding conditions except for flats at 400 RPM and counter-flow flutes at 400 RPM and 320 RPM.

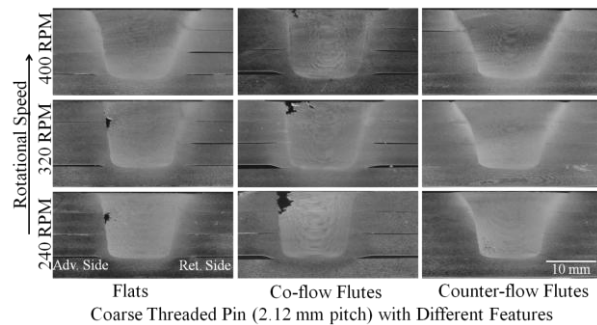


Figure 4.45 Macro cross sections of lap joint FSW of AA6056 with various pin

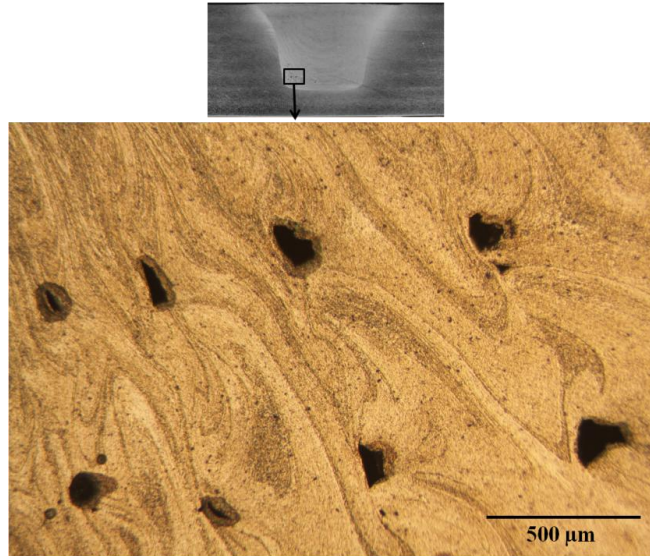


Figure 4.46 Microscopic defect at advancing side in the nugget zone for welding with counter-flow fluted pin at 240 RPM rotational speed

Overall, pin with thread + 3 counter-flow flutes effectively eliminate the surface breaking defects in the weld (that occur for thread + 3 co-flow flutes pin) by the action of counter-flow flutes to move material up at the same time remove wormhole defects (that happened to flatted pin) by promotion of downward material movement by threaded part.

#### 4.6.2 Evaluation of vertical material movement in lap welds

To elucidate the effect of the pin features on vertical motion a microscopic investigation was carried out at the interfaces of overlapping materials. Tracing of the interfacial movement provides quantitative information regarding material displacement by various pin features. Figure 4.47 illustrates the procedure to measure the maximum vertical displacement along the interfaces. From the Figure 4.47, the maximum vertical displacement of the interface was measured as 1.2 mm during FSW by a threaded + 3counter-flow flute pin at a rotational speed of 320 RPM and welding speed of 203 mm/min.

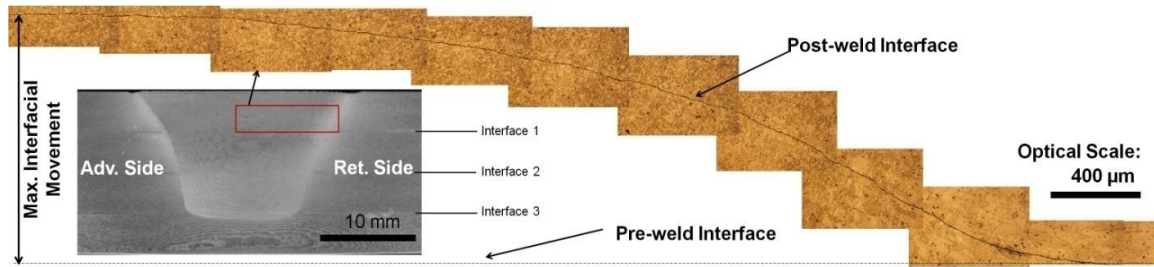


Figure 4.47 Tracing of interfacial movement in lap joint arrangement and method of measuring maximum interfacial displacement

Figure 4.48 also presents the comparison of maximum movement of the interface due to FSW with various pin features. Since four AA6056 plates (each plate is 4.2 mm thick) were stacked for this weld arrangement, movements along the three interfaces were measured on each weld sections. It should be noted here that, the maximum displacements in the interface were measured between the pre-weld interface and post weld interfaces at maximum vertical displacement. Moreover, interface 3 is the position where pin (12.7 mm depth) penetrates 0.1 mm into the bottom plate, therefore, all displacements of interface 3 was measured vertically downward, whereas interface 1 and 2 are measured vertically upward from the pre-weld interface. Considering interface 1 it is interesting to note that, pin with thread+3 flats have highest interfacial movement at 400 RPM followed by thread+3 co-flow flute and thread +3 counter-flow flute pins. However, at a rotational speed of 320 RPM, the descending orders of interfacial displacement are: flats, counter-flow flutes and co-flow flutes. On the other hand, at lowest rotational speed (240 RPM), this displacement is highest for counter-flow flutes. Pins having co-flow flutes always produce lowest displacement at 320 and 240 RPM. It was evident from the above observation that, the interfaces 1 and 2 have a tendency of moving vertically upward near weld centerline. However, right hand threaded pin with

co-flow flutes rotating counter clockwise direction cause the material to move downward that reduce the upward interfacial movement.

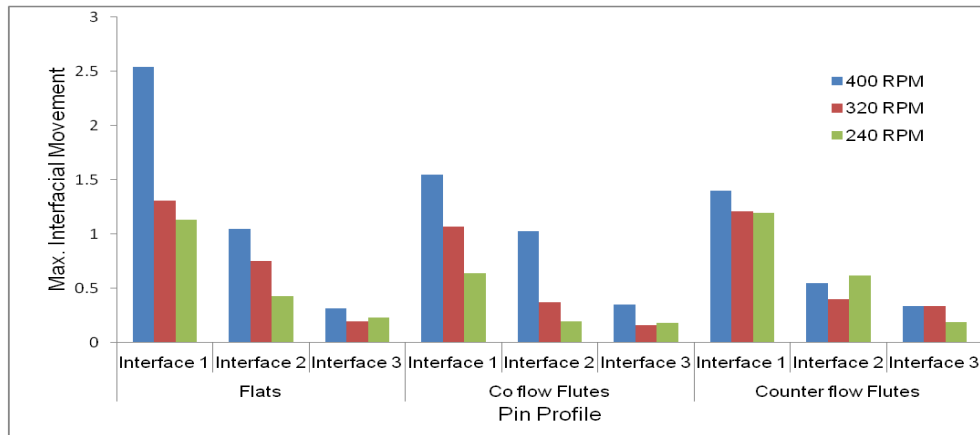


Figure 4.48 Maximum vertical displacement of interfaces for friction stir welding with different pin features

#### 4.6.3 Relationship among Process Variables in Friction Stir Lap welds

Figure 4.49 (a-f) presents several process variables (applied forge force, X-Y forces, torque, power and temperature) as a function of tool rotational speed for friction stir lap welding of AA6056-T4 with different pin features. Overall, the forge force, in-plane reaction forces (Avg. X-Y force) and torque generally decreased with increasing tool rotation as revealed from Figure 4.49 (a-d) while weld power and temperature are generally increases with increasing rotational speed also observed in Figure 4.49 (e-f) which are expected.

All the welds were performed with the force control mode in the conventional Z direction. However, forge force along Z direction was adjusted for welding with different pin features to maintain a similar contact condition of tool shoulder and weld top surface. Therefore, pin with various features experiences different amount of upward thrust due to variation in flow mechanism by features. It was observed in Figure 4.49 (a) that pin with thread + 3 co-flow flutes required the highest forge force compared to pin with thread + 3

flats or thread + 3 counter-flow flutes. This may be because of the continuity of downward material movement in the ‘shear zone’ adjacent to pin with thread + 3 co-flow flutes, therefore flowing material exert upward thrust to pin and to maintain pin shoulder at the level of the weld surface excessive Z force is required. On the contrary downward material movement was disrupted and/or opposed by flat or counter flow flutes resulting in lower applied forge force. Interestingly, with the lower forge force, counter-flow flutes produces defect free welds.

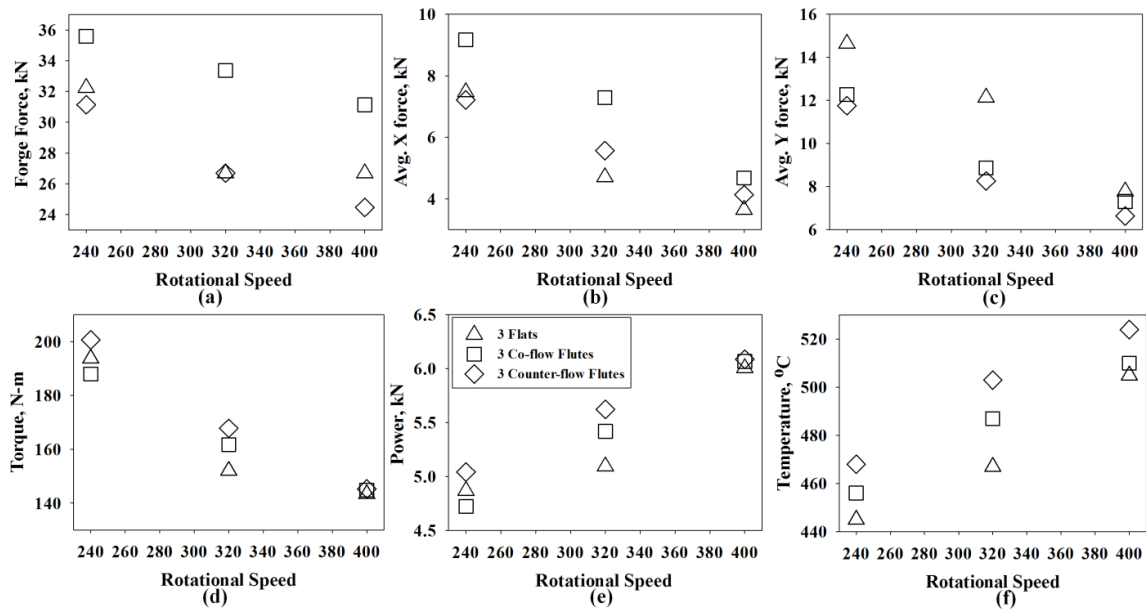


Figure 4.49 Process variables as a function of tool rotation rate: (a) Forge force, (b) Avg. X force, (c) Avg. Y force, (d) Torque, (e) Power & (f) Temperature vs. Rotational Speed

Average X forces were observed highest for pin with thread + 3 co-flow flutes for each welding condition as shown in Figure 4.49-b. This indicates that resistance offered to tool forward movement is significantly influenced by co-flow flute features compared to flats or counter-flow flutes in pin under such weld arrangement for this specific alloy. The average Y force trend (Figure 4.49-c) is different than X force in terms of pin feature effect, in which pin with thread +3 flats has always experiences higher Y force in each

rotational speed compared to co/counter-flow fluted pins. This may be due to action of flats that disrupt material upward (cause by counter-flow flute) or downward (caused by co-flow flute feature) movement by imposing more resistance to material flow. Albeit the mechanisms of material flow around tool in FSW process is complex and still not fully understood. It is also interesting to note from Figure 4.49 (b,c) that, both X force and Y force converges at 400 RPM rotational speed implies that the effect of tool features become insensitive on in-plane reaction forces at higher rotational speed.

Torque and weld power (product of tool rotational speed and torque) as a function of tool rotational speed (Figure 4.49-(d, e)) revealed that pin with thread + 3 counter-flow flutes required higher torque and weld power than flatted and co-flow fluted pin at 240 RPM and 320 RPM, however the variation is less than 10%. It is also interesting to note that, both torque and power converge at 400 RPM at which, the effect of features becomes completely insignificant, although the applied forge force was significantly higher for co-flow fluted pin. This may be due to effects of downward material movement that impose excessive upward thrust on pin due to the effect of co-flow flutes without altering the pressure underneath the shoulder. Pin peak temperature for counter flow fluted pin is highest in each rotational speed followed by co-flow fluted pin and flatted pin. However, as mentioned earlier the concern in temperature graph is that, thermocouple placement may have substantial effects on measured temperature, therefore it is probably best to use probe temperature to judge the effects of changing control parameters on the temperature for a single pin.

#### 4.6.4 Summary Observations from the study of lap welds

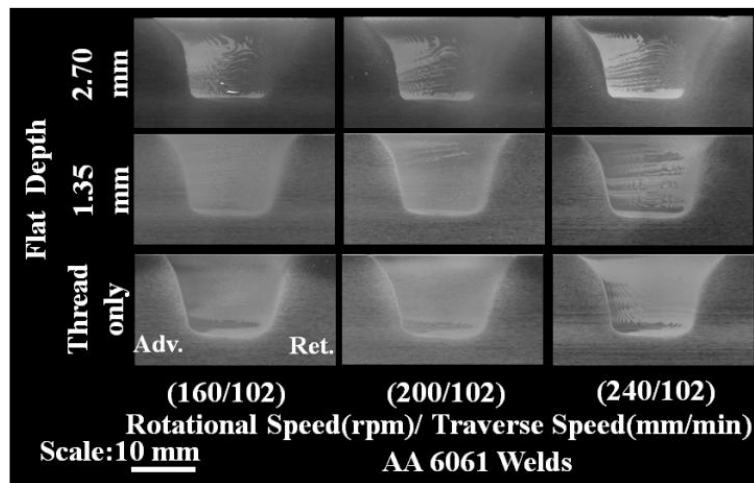
In this lap joint arrangement, vertical material movement was induced with the counter-flow flutes in a threaded pin, which was not previously observed in this dissertation in case of bead on plate welds or butt joints. This counter-flow flute also reduced the amount of forging force requirement during the FSW process. Therefore, this pin modification can be implemented in case of dissimilar material lap welds or in designing stationary shoulder friction stir welding tool.

#### **4.7 Effects of Pin Flat Depth on Process Responses Variables during FSW of Different Aluminum Alloys**

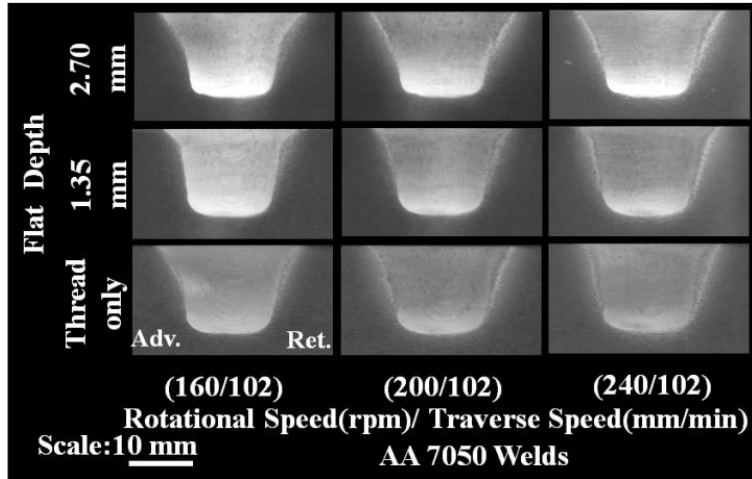
In this section, friction stir welding was made in order to investigate the variation in flat depths on process response variables and weldability of different aluminum alloys. Partial penetration bead on plate welds were performed on AA6061, AA7050 and AA7099 using conical pins ( $8^\circ$  tapered angle) machined with coarse thread (12 TPI or 2.12 mm/thread) along with 3 flats having different depths. All the welds were performed at a constant welding speed of 102 mm/min and three different rotational speeds: 160 RPM, 200 RPM and 240 RPM. Weld transverse macro and micro-structures were evaluated to identify defect contents. Process response variables (in-plane reaction force, torque, power, temperature) were also compared in order to obtain the most favorable flat dimension that is capable of reducing the forces on pin without compromising weld quality. In-plane forces obtained in this section will be considered for the stress analysis of pin in subsequent analysis (Section 4.8).

#### 4.7.1 Weld macro and micro-cross sectional evaluation

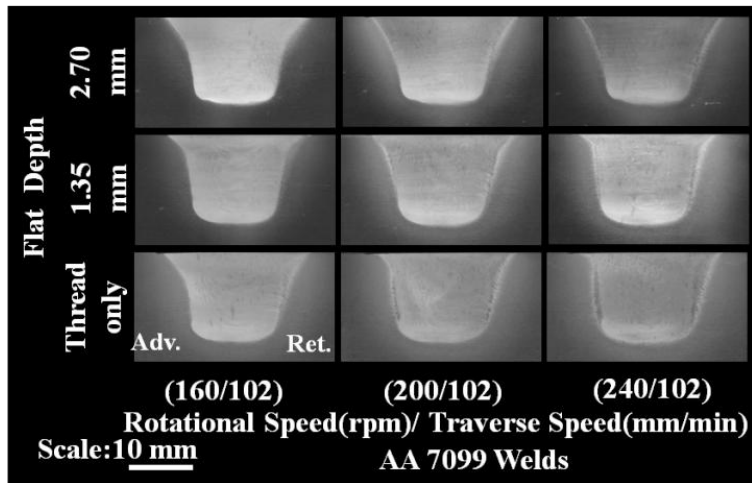
Figure 4.50 (a-c) shows the transverse macro sections for all welds performed on AA6061, AA7050 and AA7099 respectively, with pins having various flat depths (no flat, 1.35 mm flat depth and 2.7 mm flat depth). In each macro image, the advancing side is on the left and the retreating side is on the right. Each row of images shows the cross sections for a particular pin thread feature with flat depth variation (no flat, 1.35 mm flat depth and 2.7 mm flat depth) while each column is for a particular tool rotational speed. Macroscopically defect free welds were produced in all welding cases except for 6061 with the 2.7 mm deep flats at 160 RPM rotational speed where wormhole defects were observed in near nugget root at the center of the weld. This seems to indicate insufficient pressure at weld root with the deepest flat at lowest rotational speed. Further investigations were made to detect tiny wormhole defects or micro-porous defects in weld traverse sections. Figure 4.51 (a-h) illustrates all the micro defects in the weld nuggets under several welding conditions and variations in flat depth.



(a) AA 6061 weld macrosections



(b) AA 7050 weld macrosections



(c) AA 7099 weld macrosections

Figure 4.50 Weld Transverse macro structural images for welding of different aluminum alloys with variation of pin flat depth (corresponding rows) and tool rotational speed (corresponding column)

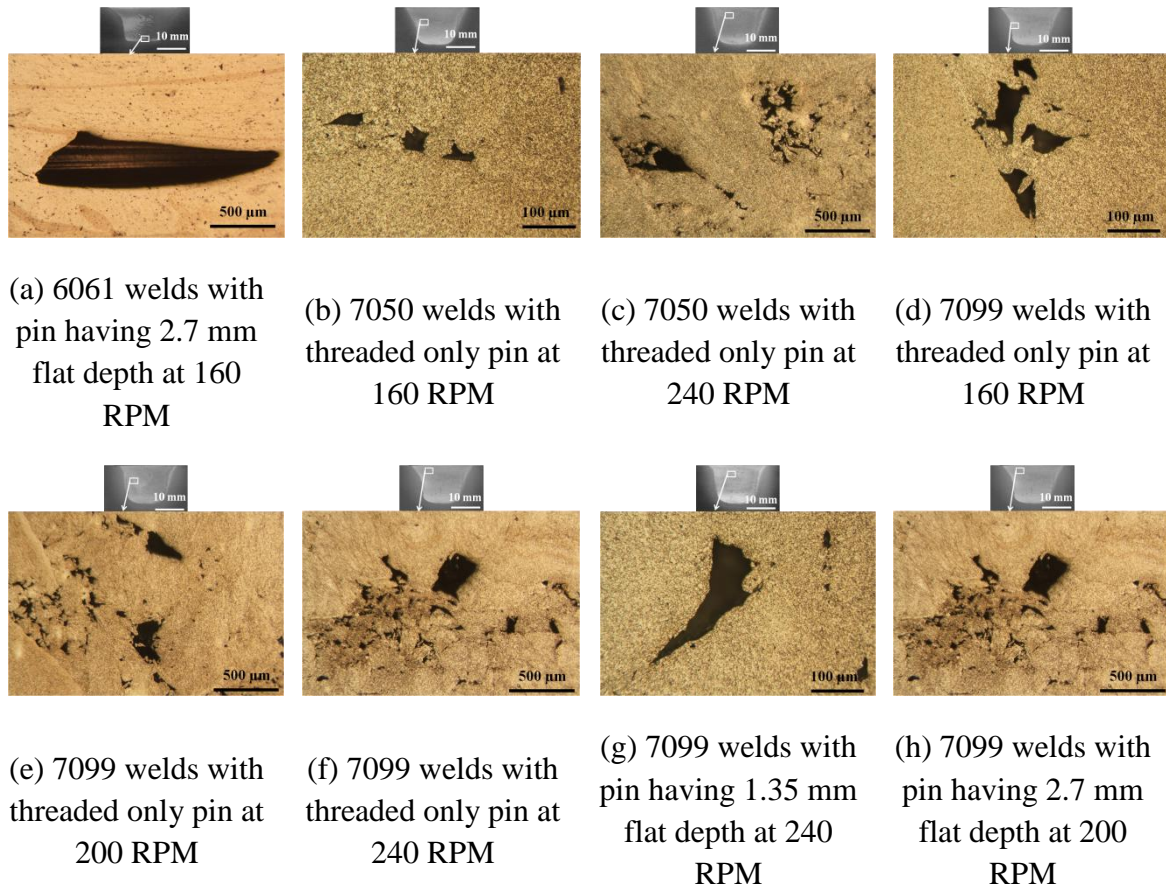


Figure 4.51 Microstructural defects in the nugget zone for welding different aluminum alloys at different welding conditions with various pin flat depths

Microscopic defects consisted of a region of micro pores in different selected weld nugget were revealed in Figure 4.51. The coarse threaded only pin produced microscopic defect in most of the welding conditions while welding AA7050 and AA7099 (relatively stronger alloys than AA6061). Interestingly these defects are located on weld mid depth near the weld center except one for AA7099 welds with threaded only pin at 160 RPM rotational speed in which microscopic defect is located on the advancing side. It can be said that, effective flow materials near root was obtained by coarse threaded only pin, however mechanism of surface breaking might lead to the mid depth defect formation in the pattern of discrete pores. This study re-establishes that machining of flats on a conical shape pin drastically improves weld quality of different aluminum

alloys. However, some distinct defects were evident for the flatted pin in AA6061 (Figure 4.51-a) and AA7099 (Figure 4.51 g-h) welds. Overall, good quality welds were produced while welding with coarse threaded pins having different flat depth with the exception of the above mentioned three defective welds.

#### 4.7.2 Comparison of Process Forces during Friction Stir Welding

The forge forces were controlled in all welds in order to produce flash-free weld without depressed crown (deep undercut): the primary goal is to maintain similar depth for all welding conditions. Therefore, the required forge forces were varied depending upon alloy properties, pin features as well as process parameters. Figure 4.52 presents the forge forces as a function of rotation rate for different aluminum alloys with the variation of pin flat depth in the form of a histogram.

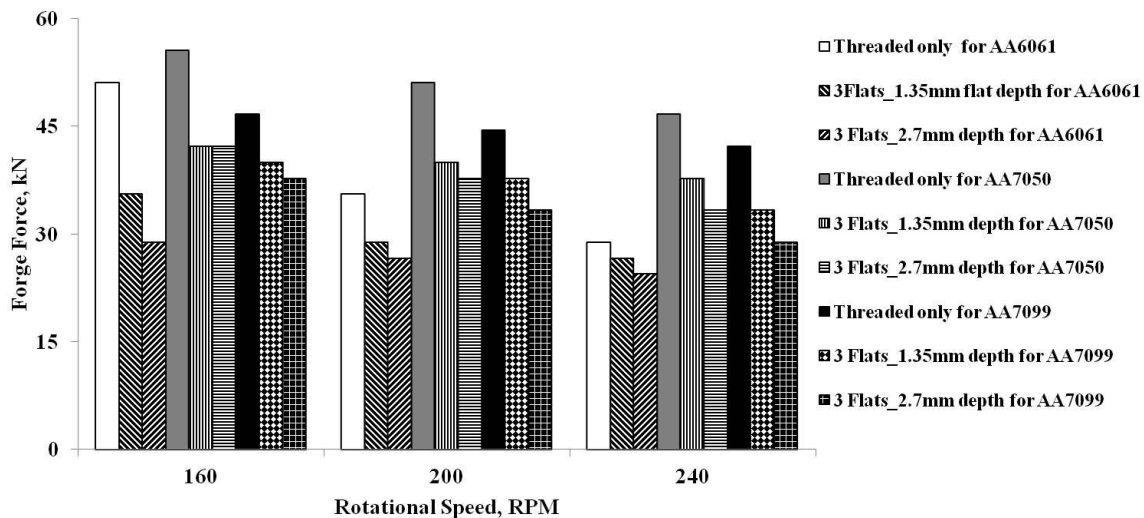
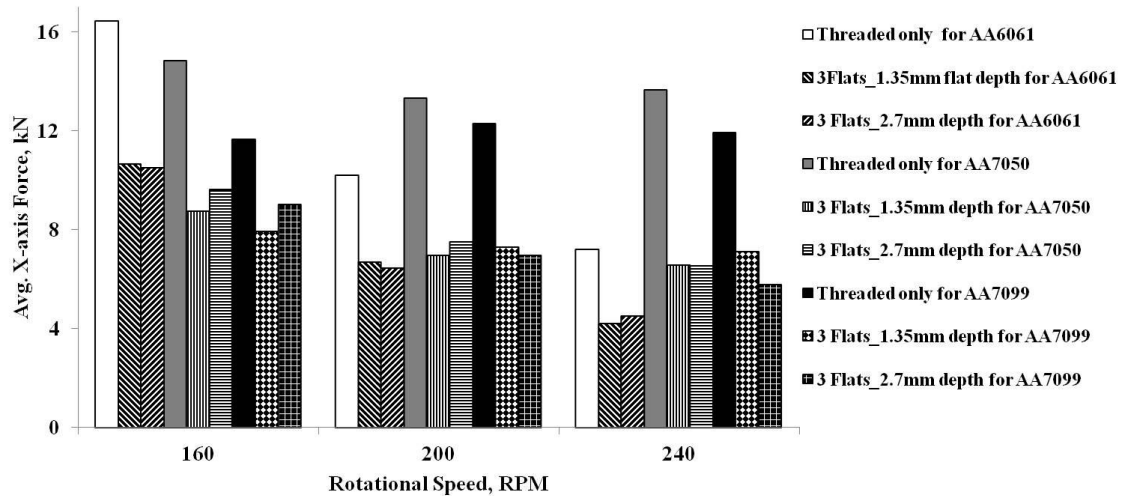


Figure 4.52 Required forge force as a function of tool rotational speed for friction stir welding of different aluminum alloys with pin having various flat depths

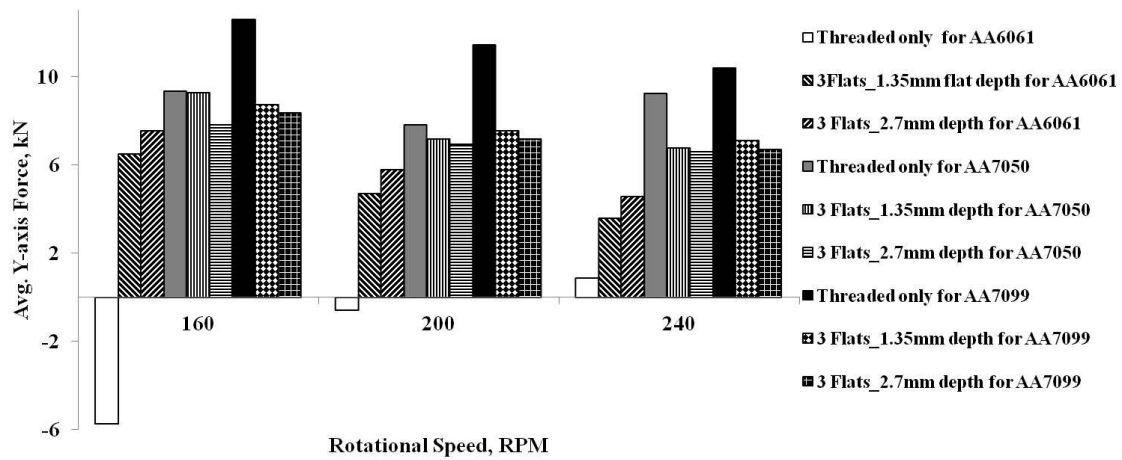
It was observed from Figure 4.52 that, the required forge forces were least for 6061 except one condition (threaded only pin at 160 RPM rotational speed) compared to AA7050 and AA7099 welds. Interestingly in all welding conditions, AA7050 required

higher forge force than AA7099 while latter material has higher hardness and strength. The threaded only pin always requires highest forge forces followed by shallower flats. Pin with deeper flat require lower forge force except one condition of AA7050 welds at 160 RPM. Therefore, use of deeper flat noticeably reduce the forge force requirement during FSW.

Figure 4.53 (a-b) shows the average X and Y axes forces for welding three different aluminum alloys at welding speed of 102 mm/min with different tool rotational speed using pin having various flat depth. For this range of welding parameters, the threaded only pin has always experienced highest X forces as evident in Figure 4.53-a. Moreover, at 160 RPM, X forces on threaded only pin are the highest for 6061 welds followed by 7050 and then 7099 welds. However, for rotation rate of 200 RPM and 240 RPM, the highest X forces experienced by threaded only pin was occurred during welding 7050 followed by 7099 welds and then 6061 welds. In case of welding with flatted pins, a mix of lower and higher X forces were evident on shallower and deeper flats, however, these values were significantly lower than that of threaded only pin. The Y-axis forces trend is opposite to X-axis forces as observed in Figure 4.53-b. The threaded only pin has the highest Y force while welding AA7099 and then 7050. Interestingly negative Y force was evident on threaded only pins for 6061 welds at 160 RPM and 200 RPM, this phenomenon of producing negative Y force is still unrevealed.



(a) Avg. X force vs. Tool rotational speed



(b) Avg. Y force vs. Tool rotational speed

Figure 4.53 Average X and Y –axes forces as a function of tool rotational speed for friction stir welding of different aluminum alloys with pin having various flat depths

In 7099 and 7050 welds, deeper flats generally lead to slightly lower Y axis force. In contrast the Y-axis forces are large for deeper flatted pin for 6061 welds. It is sometimes worthy to combine these X-Y forces and characterize by the in-plane resultant to estimate forces on the pins. A histogram in Figure 4.54 illustrates the resultant forces on different pins under different welding parameters. The maximum resultant force was

always experienced by the threaded only pin regardless of the alloy properties. Surprisingly, the differences in resultant reactions are insignificant for welding different alloy with the same pin at 160 RPM rotation rate, while at higher rotational speeds, pins experience lesser resultant for 6061 welds compared to 7050 and 7099 welds. Like the X-Y force plot shown in Figure 4.53, shallow and deep flatted pin has mix of lower and higher in-plane resultant, hence significantly lower than those of threaded only pin.

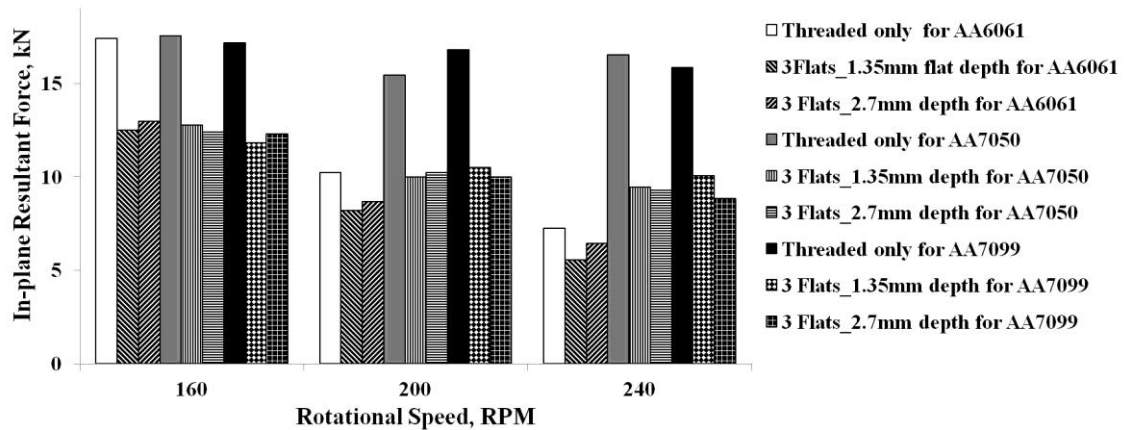
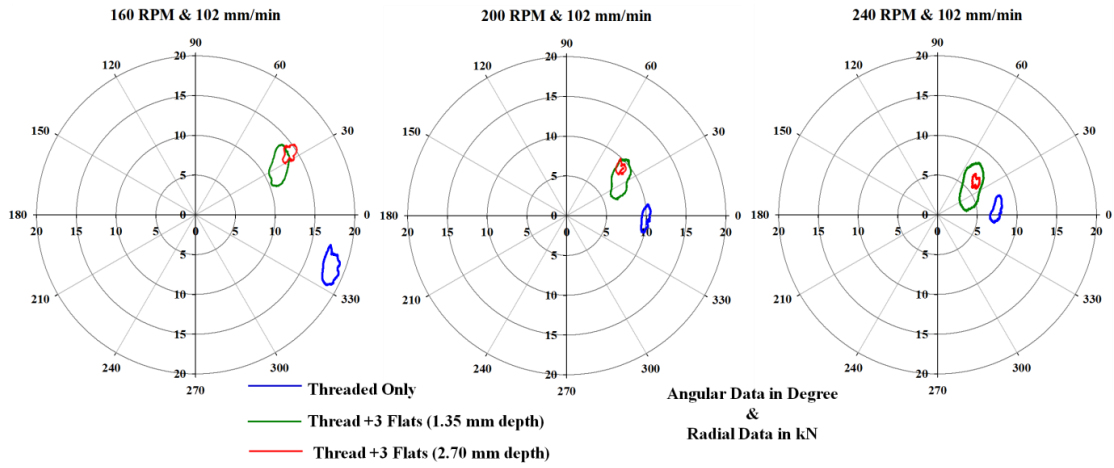
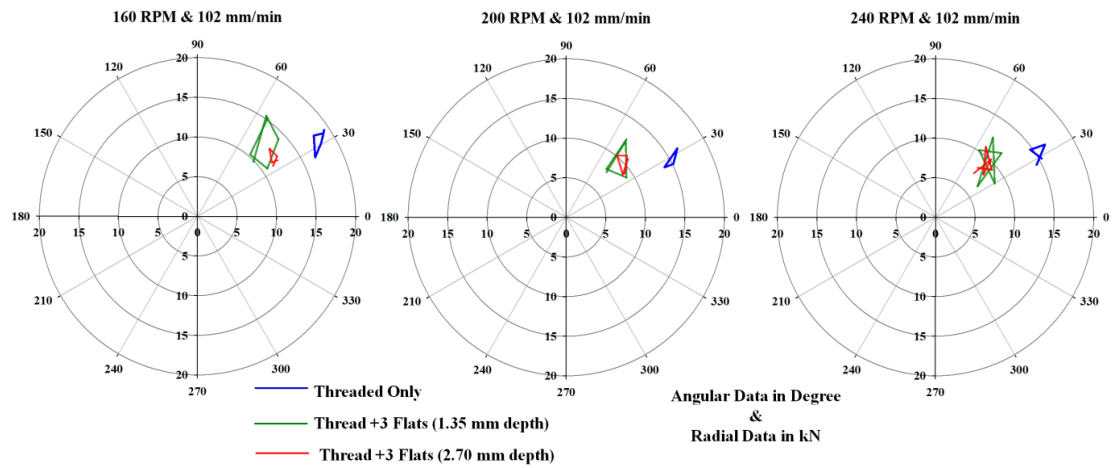


Figure 4.54 In-plane resultant forces as a function of tool rotational speed for friction stir welding of different aluminum alloys with pin having various flat depths

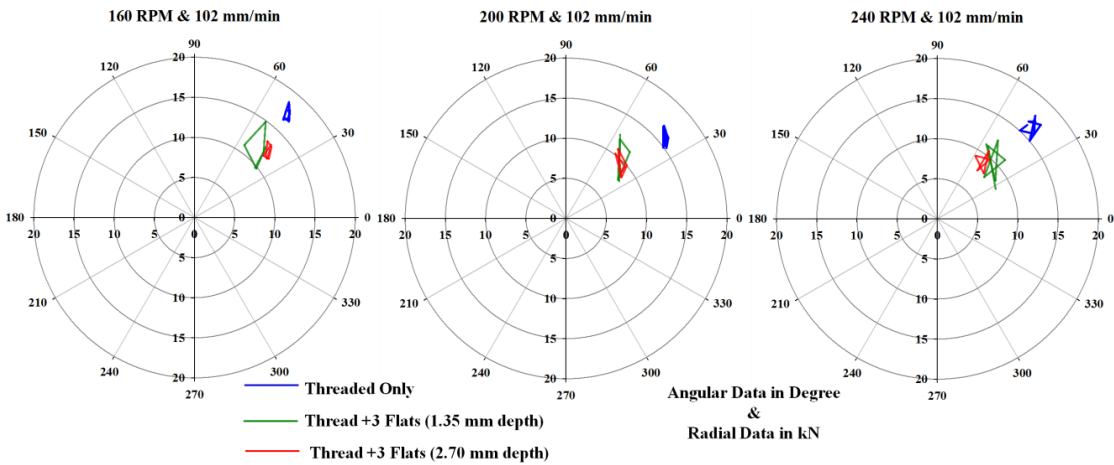
Figure 4.55 (a-c) shows another interesting effects that illustrates polar plots of the “force footprints” for all the AA6061, AA7050 and AA7099 welds with threaded only pin (blue lines), thread + 3 flats with 1.35 mm flat depth (shallow flat pin: green lines) and thread + 3 flats with 2.7 mm flat depth (deep flat pin: red lines) for all three sets of welding parameters. These force footprints are the locus of in-plane force resultants plotted for one complete revolution. It can be seen in the figures that the deep flat pin has nearly same average force as a shallow flat pin, but significantly lower variation in force, perhaps leading to better fatigue life under this condition. In all cases, the magnitudes of the forces are greater for threaded only pin, however, the oscillatory ranges are greater for shallow flat pins.



(a) 6061 welds



(b) 7050 welds



(c) 7099 welds

Figure 4.55 Polar plot of force footprints on three different pins for welding aluminum alloys

#### 4.7.3 Effect of pin flat depth on torque-power-temperature during FSW

The average tool torque was graphed against rotational speed shown in Figure 4.56. The measured tool torque at a lower rotation rate (160 RPM) was substantially higher for threaded only pin while the deeper flatted pin has the lowest torque. This might be because the threaded only pin would require more torque to grip, deform and transport weld material adjacent to pin interface. On the other hand, materials are being released near the leading region of flats and impulsive forces are being experienced by pin while materials are encountered on the trailing region of flats. Torque values are reduced with increasing rotation rate; however difference in these measured torque due to pin profile variation is subtle at 240 RPM.

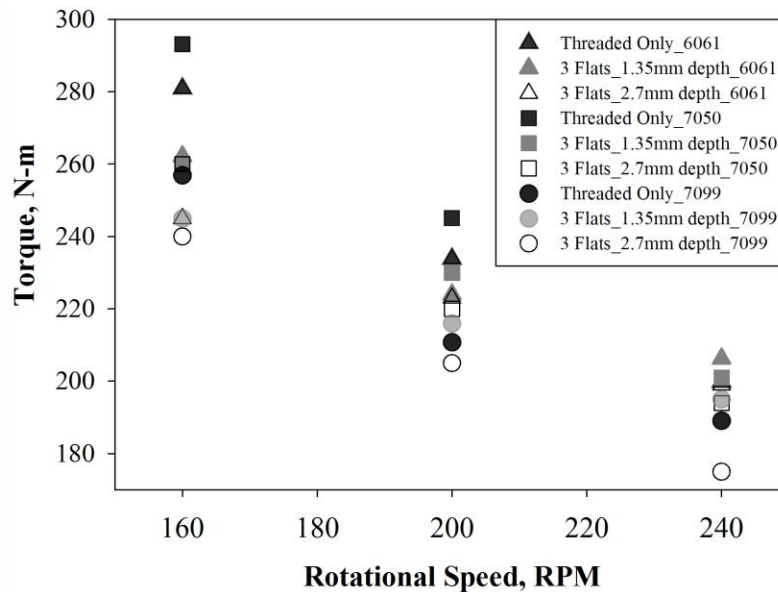


Figure 4.56 Torque as a function of rotational speed for FSW different aluminum alloys using threaded pin having different depth

Weld power (see Figure 4.57) on the other hand has the opposite trend as of torque with respect to rotational speed, however with respect to pin flat variation the trend are similar as of measured torque shown in Figure 4.56. The effect of weld power input variation is clearly seen with changing flat depth in which weld power for deeper

flat was lesser than threaded only pin. Interestingly 7099 require least weld power compared to 7050 and 6061 for similar welding condition with particular pin profile. For welding with same pin profile, 7050 require a higher weld power than 6061 at 160 RPM and 200 RPM rotation rate.

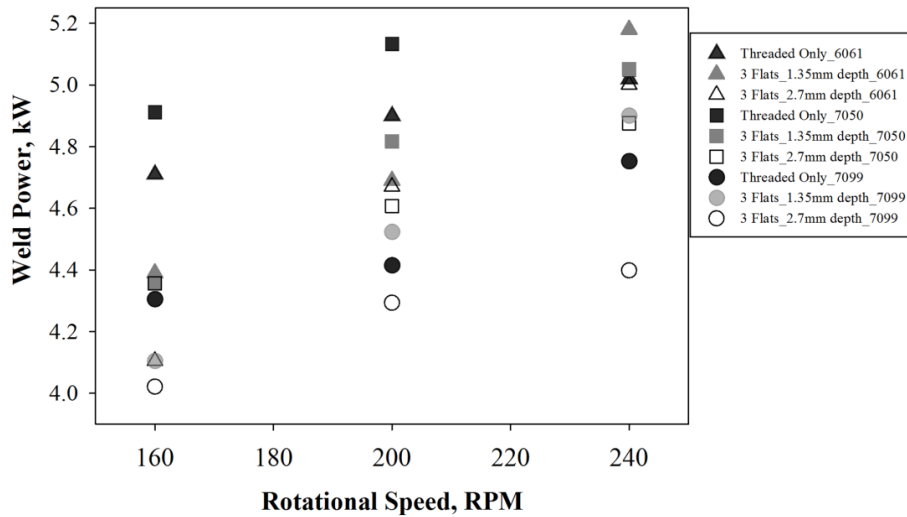


Figure 4.57 Weld power as a function of rotational speed for FSW different aluminum alloys using threaded pin having different depth

It was observed from Figure 4.58 that, pin peak temperature (measured near mid depth on the pin axis of rotation) has a similar relationship to that of weld power so increases with increasing RPM. The threaded only pin exhibits the highest temperature while welding AA7050 and the threaded pin with shallow flat has the lowest in case of 6061 welding. It is sometimes worthy to compare pin peak temperature for a particular pin and not compare between pins, because the placement of thermocouple might provide deviated results. Another important issue in temperature measurement is the flat depth variation: deeper flat has the shortest distance between thermocouple location and pin surface might lead to greater temperature recording during FSW. Therefore, for welding different alloys at each rotation rate, threaded only pin recorded highest peak temperature followed by deeper flatted pin and then shallower flatted pin. One effect which is

interesting is that the spread of temperature between the various pins is less for the higher rotational speed (240 RPM) than for the lower rotation rate (160 RPM and 200 RPM).

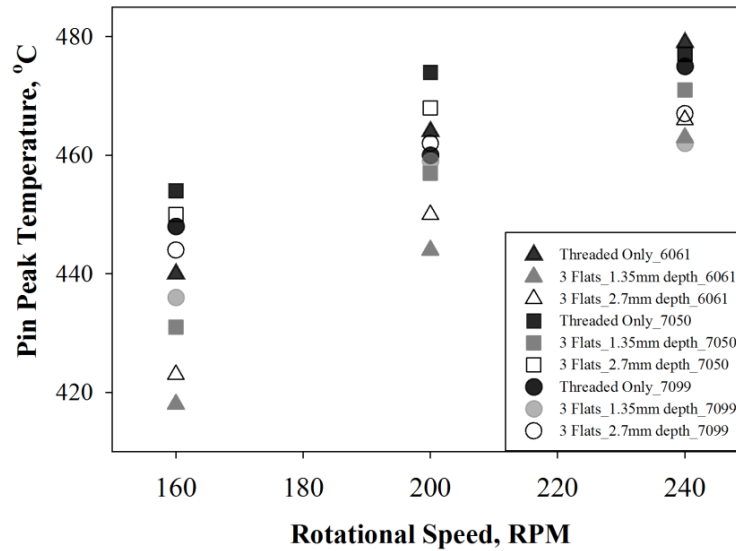


Figure 4.58 Temperature as a function of rotational speed for FSW different aluminum alloys using threaded pin having different depth

#### 4.7.4 Summary Observations on flat depth study

1. At high advance per revolution, deeper flats may result in lack of consolidation in the root for welding AA6061 and also the trend of surface breaking for threaded only pin while welding 7xxx series aluminum alloys: these not a typical advancing side defect, rather the formation of discrete pores around weld centerlines.
2. Flats at the levels examined do result in reduced in plane forces and more uniform direction of the in-plane force resultant than do similar pins with threads only.
3. The variation in in-plane forces are greatest for the shallow flat tool while the deeper flat tool exhibits less oscillation than either the thread only tool or the shallow flat: this may have implications for fatigue life of the tool.
4. For the conditions examined, weldability of 7050 is similar to that of 7099.

5. It appears that, based on weld quality and weld forces that a plot of in-plane force vs. RPM for 6061 would be shifted toward higher RPM relative to the 7XXX alloys. This is consistent with general “rules of thumb” for welding these alloy classes.

#### **4.8 Analyses of FSW Pin Stresses due to In-plane Reactions using Finite Element Method (FEM)**

##### 4.8.1 Methodology

It is required to understand the stress state of the pin in order to avoid potential failure of FSW tool by overloading. Experimental results of flat depth studies in the previous section (Section 4.7) have already shown that the reaction forces experiencing by pin are obviously different due to the variation in pin features and their dimensions. Consequently, the stress distribution and location of stress concentration in pins would be different due to these variations of threads/flats in pin. To predict the stresses and detect the area of stress concentration in FSW pins, three dimension finite element models of pins were generated using commercially available ABAQUS (version 6.12) finite element software package. To perform FEM analyses three distinct areas were investigated:

- a. Identify critical orientation of loading
- b. Provision of cutting of flats on pin with respect to thread termination
- c. Optimize flat dimensions

The application of force on the pin is attributed to geometrical argue since actual load distribution on the pin is unknown. The premises of arguments on this issue have been discussed in Section 2.5.2 in Chapter 2. Currently, the in-plane reaction forces on

the FSW pin as obtained from experimental feedback were considered in the static loading condition. To simulate the in-plane reaction forces on the threaded part of a pin, a general traction force projected on complex geometric surface of the pins was applied uniformly, which is analogous to that of wind force on a curved surface. Figure 4.59 (a) illustrates the procedure of applying force along with the boundary conditions. Figure 4.59 (b) also shows the snapshot of the ABAQUS graphical user interface (GUI) with the representative pin geometry along with the application of loading and the boundary conditions. The general traction force was applied on the threaded surface of pin to a specific vector direction, perpendicular to pin mid sections. The shank of the pin was fixed with no displacement and rotation allowed above the threaded part of the pins ( $U1=U2=U3=UR1=UR2=UR3=0$ ).

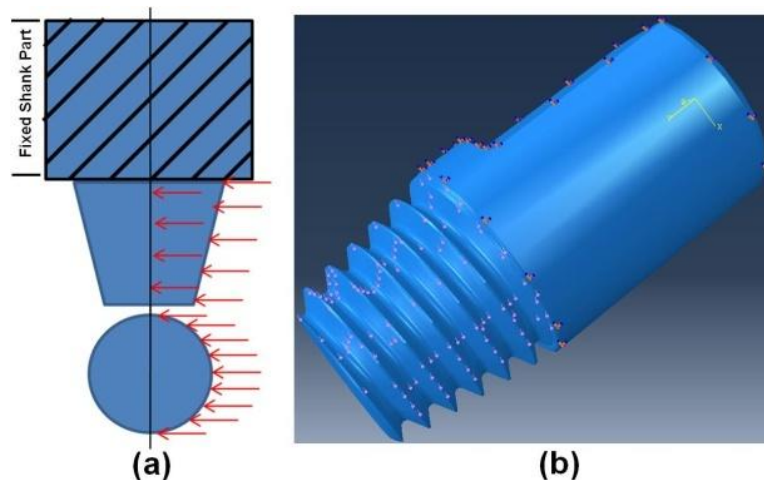


Figure 4.59 Schematically showing loading and boundary conditions for structural analysis of pin: (a) applied load with is analogous to wind load on curved surface and (b) snap shot of ABAQUS GUI with a FSW pin geometry including loading pattern and boundary conditions

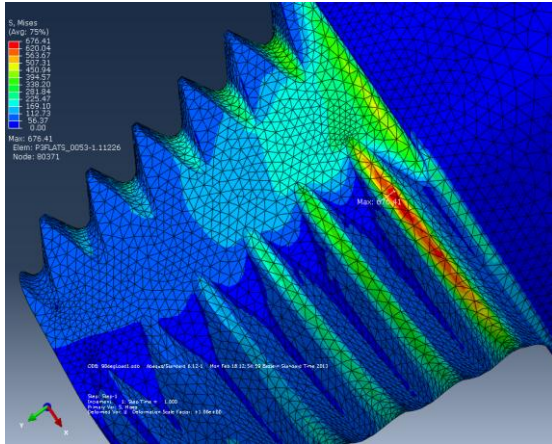
All the pins in this dissertation are manufactured from H13 steel. The material properties (H13 steel) used in this analysis with consistent units are tabulated in Table 4.5.

Table 4.5 Material properties of H13 steel with consistent unit for ABAQUS environment

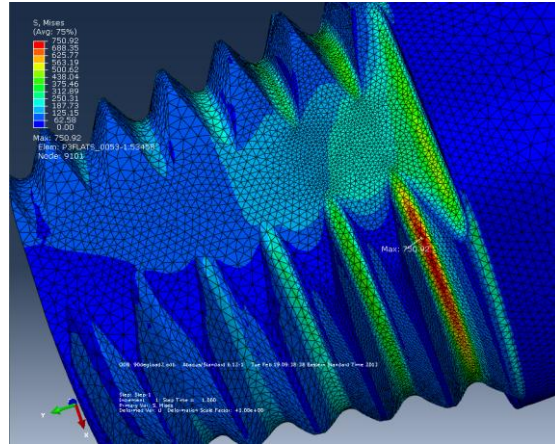
Density	$7.8 \times 10^{-9}$ Ton/mm <sup>3</sup>
Young's Modulus	210000 MPa
Poisson's Ratio	0.3
Yield Strength	1650 MPa

When the analysis is run, ABAQUS calculates the stress fields by solving the Von Mises yield criteria (Equation 2.5) in each element until satisfactory convergence is reached. Due to the complexity in geometric shape in threaded parts of the pin, the 3D geometry is meshed within ABAQUS with 10-node quadratic tetrahedron (C3D10). The finite element analysis in this study was a linear elastic event simulation.

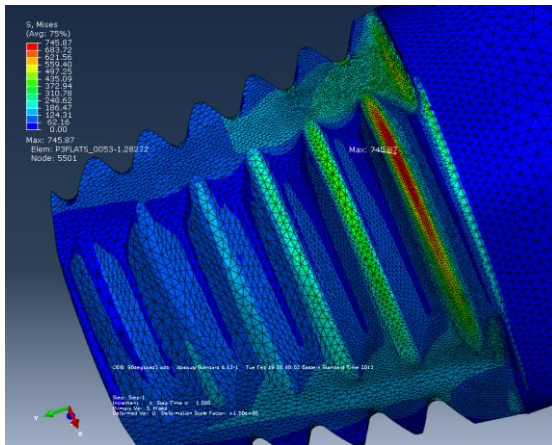
In order to provide guidance for the development of accurate mesh density in the region of high stress, a mesh convergence study was performed using local re-meshing near the area of stress concentration (around the area of maximum Von Mises equivalent stress). Figure 4.60 (a-d) shows some snapshot of stress contour with meshed geometry of 3 flatted pin with high mesh density near the maximum stress and coarse mesh elsewhere. The total force applied in all cases was 12.5 kN. It was observed from Figure 4.60 (a-d) that in each case the maximum stress was observed in the thread root near the pin shank and the maximum stress varies with the variation in local mesh size. Figure 4.61 is a plot of maximum von Mises stress for various level of mesh density. It was observed that the maximum stress with increasing mesh density and mesh size of 0.2 mm near stress concentration was considered optimal. With the consideration of CPU time, subsequent FEM analyses were performed using average mesh size of 0.2 mm near the area of stress concentration.



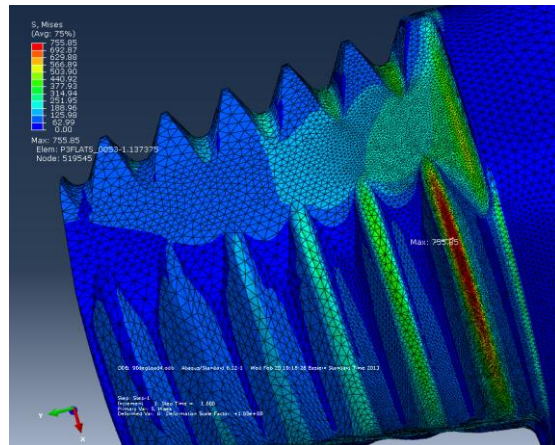
(a) Average mesh size near stress concentration: 0.4 mm and maximum stress (Von Mises): 676 MPa



(b) Average mesh size near stress concentration: 0.2 mm and maximum stress (Von Mises): 751 MPa



(c) Average mesh size near stress concentration: 0.1 mm and maximum stress (Von Mises): 746 MPa



(d) Average mesh size near stress concentration: 0.025 mm and maximum stress (Von Mises): 756 MPa

Figure 4.60 Snap shot of meshed geometry inside ABAQUS with manual re-meshing rule applied near stress concentration area

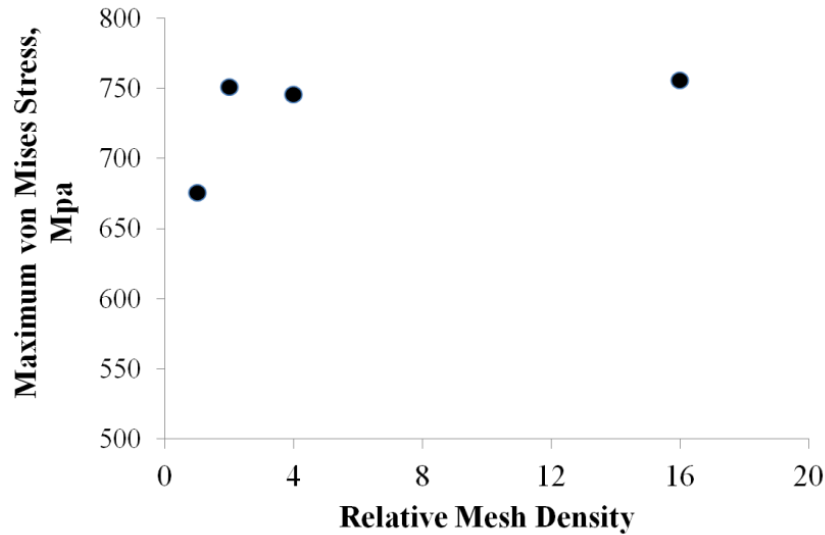


Figure 4.61 Mesh convergence study: von Mises maximum stress vs. relative mesh density

#### 4.8.2 Identify critical orientation of Loading

The pins and, consequently, the models, do not exhibit radial symmetry due to the helical nature of the thread leading to a variation in the minor diameter as a function of height in the critical region (near the shank). The termination of threads near the pin shank is another critical issue for this radially asymmetric model of the pin. Hence, it was necessary to load the pin from different directions in order to find the critical loading direction. Investigations were made to identify critical orientation of tool reaction by applying the same amount of static load on threaded only pin, but different directions. The loading orientation that provides the maximum stress on the pin is considered as critical orientation. Eight different orientations were chosen as shown in Figure 4.62 with the maximum von Mises stress used as a discriminator in this FEM analysis. It should be noted here that in current pin design, thread termination was modeled in such a way that run out of thread is tangential near the shank with respect to pin axis of rotation. For each case, the maximum von Mises stress is observed at a point where there is full thread

depth closest to the pin shank for the pin reaction force of 12.5 kN. It should also be noted from Figure 4.62 that the most critical orientation was observed in the ‘H’ direction of the pin where the thread is at full depth.

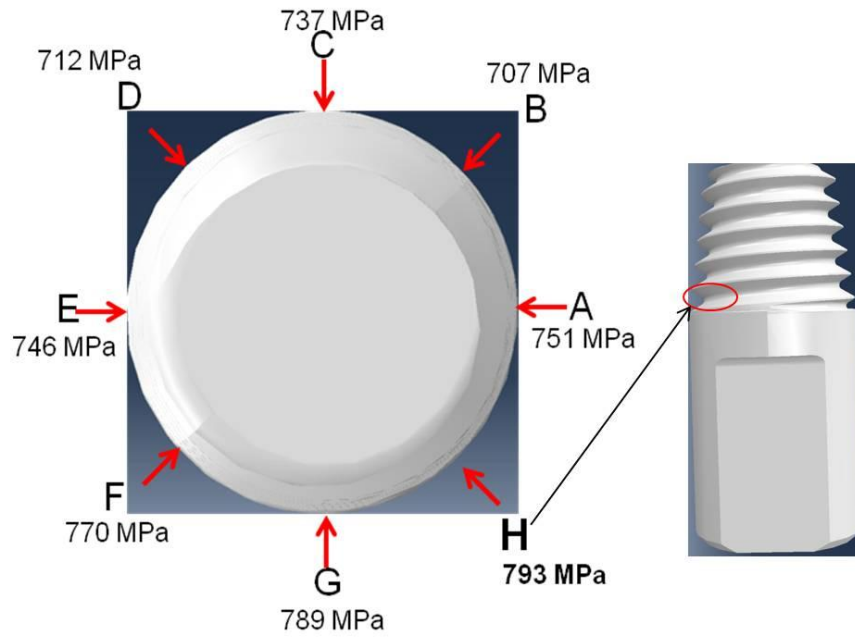


Figure 4.62 Orientation of forces and corresponding maximum stress (von Mises)

#### 4.8.3 Provision of cutting flats on pin with respect to thread termination

It is also required to identify the suitable orientation of cutting features (in this study: flats) with respect to thread termination during pin manufacturing process. The stress analysis using FEM provide important information to predict peak stress in pin and accordingly suggest the favorable orientation of cutting features. Figure 4.63 shows several pin models with different orientation of first flat cuts with respect to a reference plane (drive flat on pin that enter into shank). It is noted here that, subsequent flats are to cut at 120° and 240° angle with respect to the first flat for three flatted tool pins. It should also be noted here that the critical loading direction for maximum stress will be varied in each orientation of flat cut due to presence of flats in threads. Therefore, like previous analysis shown in Figure 4.62, the forces on pin were applied in eight selected direction

at 45° each to evaluate critical orientation of loading and estimate maximum stress on the pin.

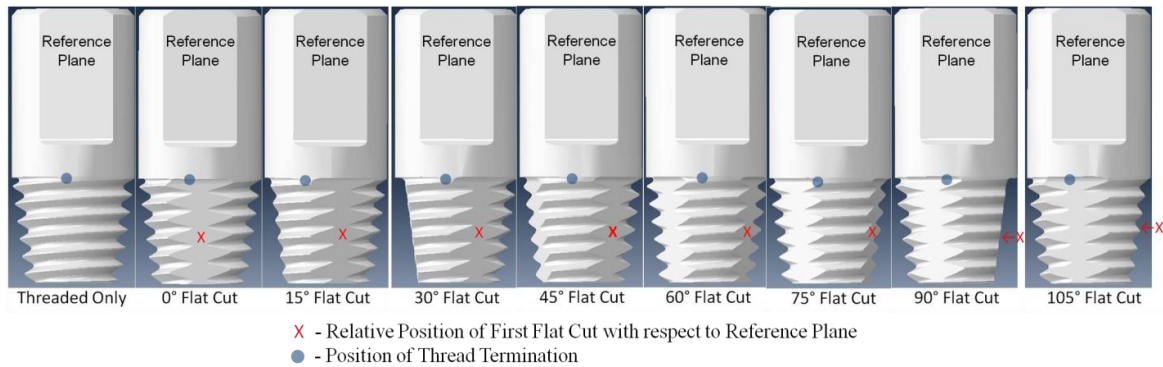


Figure 4.63 Orientation of first flat cut in models with respect to thread termination

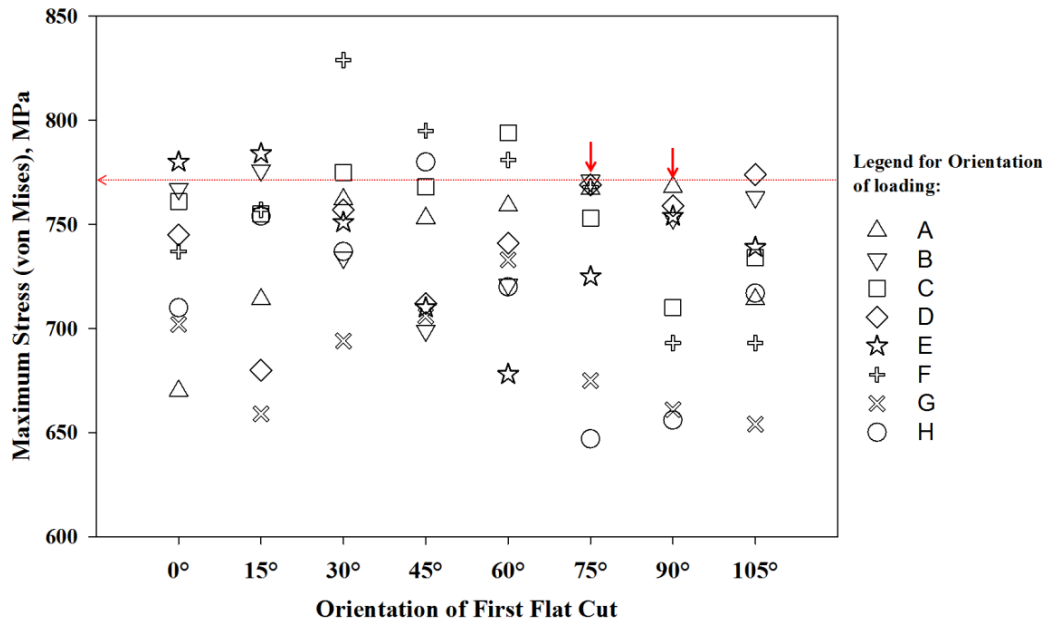


Figure 4.64 Maximum stresses on FSW tool pin having different flat cut orientation under different orientation of loading

Figure 4.64 illustrates the predicted maximum stress on the tool pin due to in-plane reaction force (12.5kN) under different orientations of flat cut, the analysis of which is similar to that shown in Figure 4.62. Based on stress distribution and peak maximum stress, the lowest maximum stress among all orientations of loading was observed in 90° flat cuts (see Figure 4.64). However, difference in maximum stress for other orientations

of flat cuts were subtle compared to 90° flat cut except 30° flat cut in which maximum stress (829 MPa) was observed for loading orientation in the ‘F’ direction. Therefore, it is recommended to avoid flat cut position at 30° with respect to the thread termination and drive flat on pin that enter into shank in this pin model. Moreover, the provision of flat cut with respect to thread run out as are illustrated and described in more detail according to Figure 4.65.

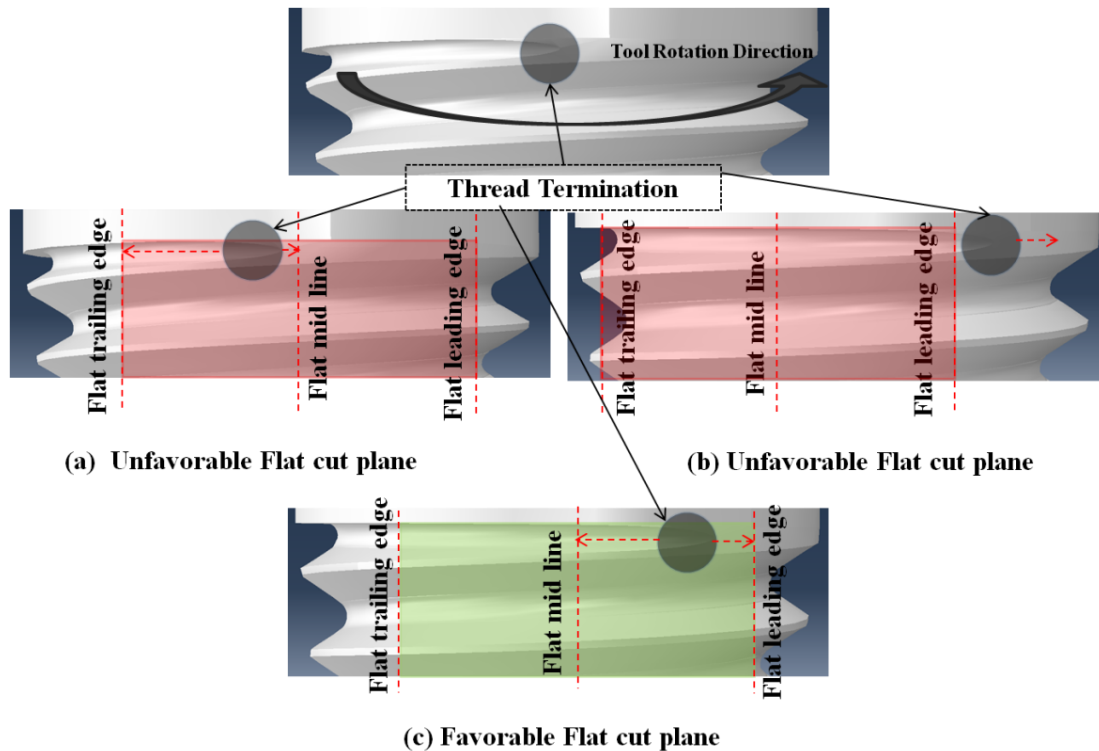


Figure 4.65 Proposed flat cut orientations to minimize maximum stress on tool pin, flat trailing edge is defined as the edge which lag behind the tool rotational direction and flat leading edge is the front of flat

With the consideration of maximum stress on the pin under different orientation of loading for different flat cut orientation, the unfavorable flat cut is shown in Figure 4.65 (a-b) where the point of thread termination (grey circular shaded area) is in between the flat trailing edge and flat mid line (red shaded area). However, the most favorable position of the first flat cut in pin should be placed in such a way that point of termination

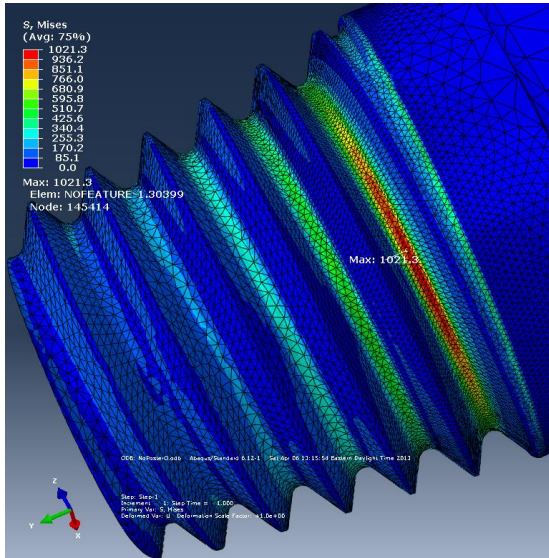
of the thread (grey circular shaded area) immerses into the flat near its leading edge (green shaded area Figure 4.65-c). Moreover, the range of the position of the first flat cut near thread run out is also preferred in between mid line and leading edge of flat for having lessened the maximum stress on the tool pin (for example 75° flat cut shown in Figure 4.64).

#### 4.8.4 Optimum Dimensions of Flat Depth

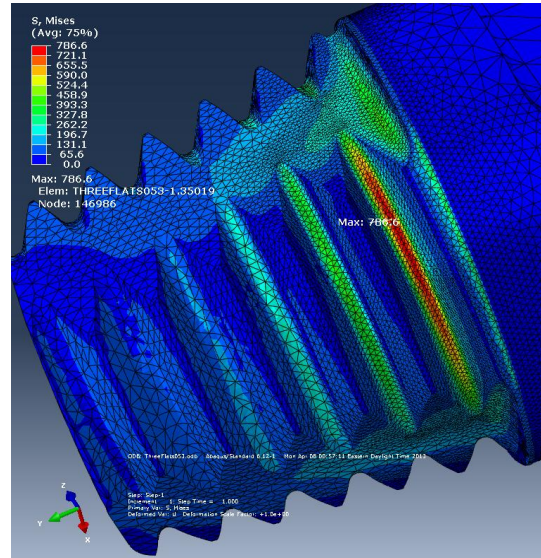
To optimize the pin flat dimensions on the basis of stress analysis, it is required to obtain the experimental feedback forces experienced by different pin features during FSW. It was previously observed from experimental investigation (see Figure 4.54) that, threaded only pin always encounter highest resultant reactions in all welding conditions, whereas pin having flat depth of 1.35 mm and 2.7 mm experience lower resultant forces. Therefore, the load applied to each pin model (threaded only/thread+ flats with various depths) were proportional to the actual average in-plane forces that each pin experienced while making a 6061 welds at 160 RPM and 102 mm/min (see Figure 4.54) in order to estimate stress on pin having various features and dimensions.

Figure 4.66 (a-c) presents the stress distribution (contour plot) of the pins having various features (threaded only, thread + 3 flats of 1.35 mm depth and thread + 3 flats of 2.7 mm depth). For the geometries and loading chosen, the lowest maximum stress was observed on the pin having 1.35 mm flat depth. The maximum stresses were: (a) thread only tool: 1021 MPa, (b) 1.35 mm depth flat tool: 787 MPa and (c) 2.7 mm depth flat tool: 1072 MPa. Shallow and deep flatted pin experience same in-plane forces, however maximum stress was higher on deeper flatted pin is due to the less moment of inertia for that pin model. It is to note that the magnitudes of the reported stresses are arbitrary;

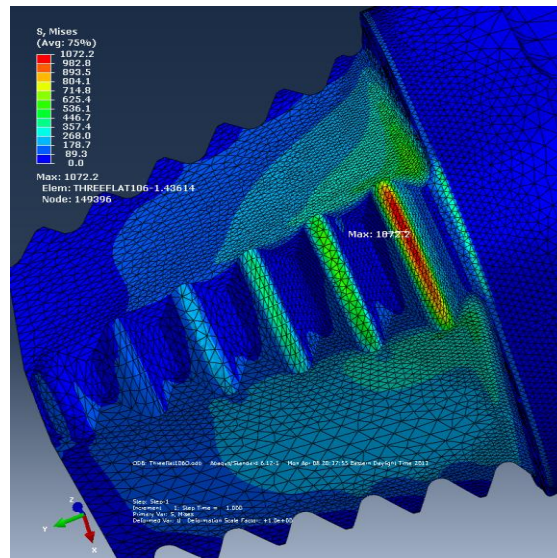
however, the ratios between them are expected to be meaningful. The results of FEA studies such as this one are potentially useful but, due lack of symmetry in the model geometries, a large number of calculations are required to find critical orientations. Also, real pin loads are certainly more complex (including torsion) and potentially distributed quite differently than those used in this study.



(a) Threaded only pin



(b) Thread + 3 Flats (1.35 mm flat depth)



Thread + 3 Flats (2.7 mm flat depth)

Figure 4.66 Stress distributions with stress concentration on pin due to corresponding In-plane resultant reactions

#### 4.8.5 Summary Observations from structural analysis of pin

Few observations made from this current section are as follows:

1. The maximum stress on the FSW pin was observed in the thread root where there is full thread depth closest to the pin shank.
2. Maximum stress on the pin can be minimized by changing the orientation of flat cut with respect to thread termination.
3. Flats at the levels examined do result in reduced in plane forces and hence reduction of maximum stress was observed for 1.35 mm flat depth.

### **4.9 Comparing Response Variables between Stationary Shoulder and Conventional Shoulder FSW**

#### 4.9.1 Stationary shoulder friction stir welding (SS FSW)

With the increasing interest of friction stir welding process for its robustness in various applications, SSFSW is a relatively new concept in which a pin is allowed to rotate with a non-rotating shoulder. This approach is expected to provide a potential benefit over conventional rotating shoulder friction stir welding because of: (i) generating uniform heat through the weld thickness, (ii) reducing the weld nugget and HAZ area and (iii) minimizing distortion of welded parts, since the shoulder does not contribute in generating heat during welding.<sup>21, 145</sup> Therefore, the heat generation as well as the effectiveness in material flow for producing good quality welds is exclusively governed by the pin under this stationary shoulder configuration. The scope of this present study is to investigate and compare the weld quality and process response variables of friction stir welding with an identical pin, but with different shoulder configurations: one with a single scrolled shoulder (conventional shoulder employed in this investigation, discussed

previously) and the other with a stationary shoulder. Since a coarse threaded conical shape ( $8^\circ$  taper) pin with 3 flats (1.35 mm flat depth with the orientation of  $120^\circ$  angle each) was found to be an optimum pin feature for welding different aluminum alloys studied in an earlier section of this dissertation, therefore a pin with same dimensions was employed to study SS FSW on aluminum alloy AA6061.

#### 4.9.2 Weldability and process response variables

Figure 4.67 presents the comparison of the surface appearance of CSFSW and SSFSW. The crescent shape tool mark with weld seam roughness (ripple) was observed while welding was being performed using a conventional shoulder during FSW (see Figure 4.67-a). Many times, post-weld-machining might require obtaining the smooth surface in CSFSW. On the other hand, in Figure 4.67-b very smooth weld surface was obtained by sliding the non-rotating shoulder over the stir zone during SSFSW.

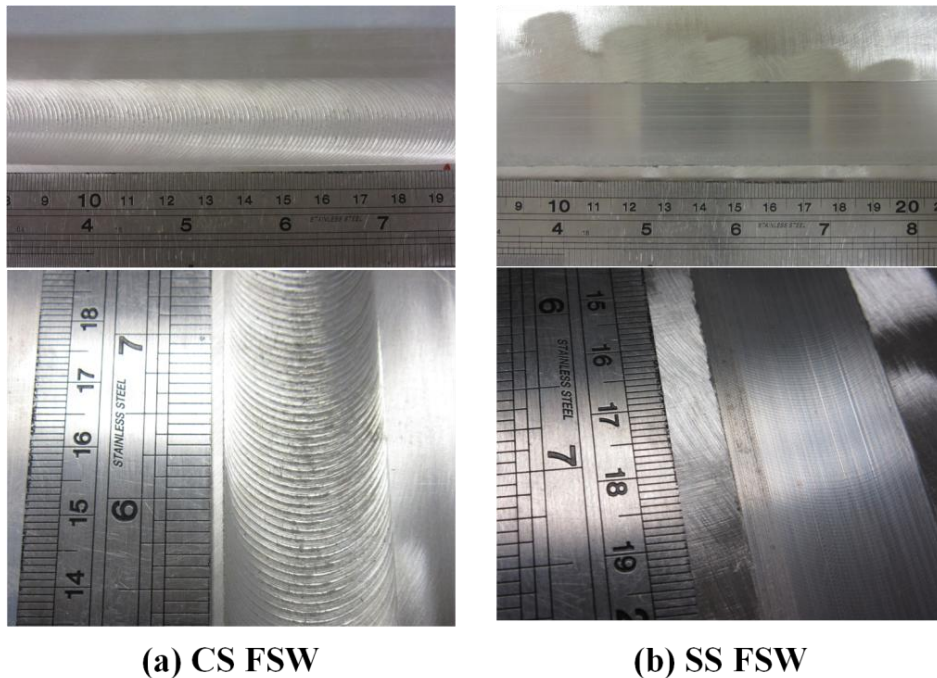


Figure 4.67 Weld surface comparison between conventional shoulder (CS) and stationary shoulder (SS) FSW

Figure 4.68 illustrates the comparisons of the weld transverse macro sections of partial penetration bead on plate welds on AA6061 using CS FSW and SS FSW. A distinct difference in the nugget shape was evident from welding with two different tools. A regular basin-shaped nugget with widen regions near the crown were observed for CS FSW due to deformation imposed by the rotating shoulder. However, widen regions near the crown was not evident in case of SS FSW. Interestingly, it appears that shape of the pin is superimposed on nugget zone considering a subtle increment in recrystallized zone.<sup>62</sup>

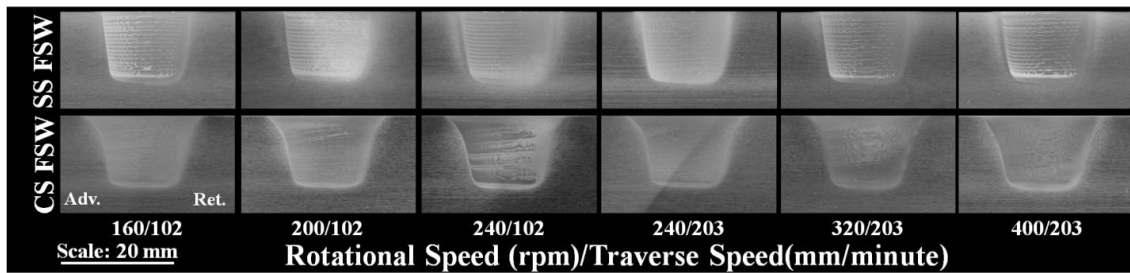


Figure 4.68 Weld transverse macro sections for conventional and stationary shoulder FSW for different welding parameters

Completely defect free welds were obtained using both SS and CS tool under the examined welding parameters. The nugget geometries of the welds using two different tools have been evaluated to compare and distinguish the effect of the shoulder dominated region. Figure 4.69 schematically shows the superposition of the weld cross sections, in which the green outline is the boundary of a nugget area for welding with conventional shoulder and the red outline is the boundary to that of stationary shoulder. For all welding conditions, it was measured that the nugget area for CSFSW is only 2-9% greater than that of corresponding SSFSW. Moreover, the shoulder dominated region for CSFSW was found to be one-fourth to three-tenths of the nugget depth as measured from these superimposed macrographs.

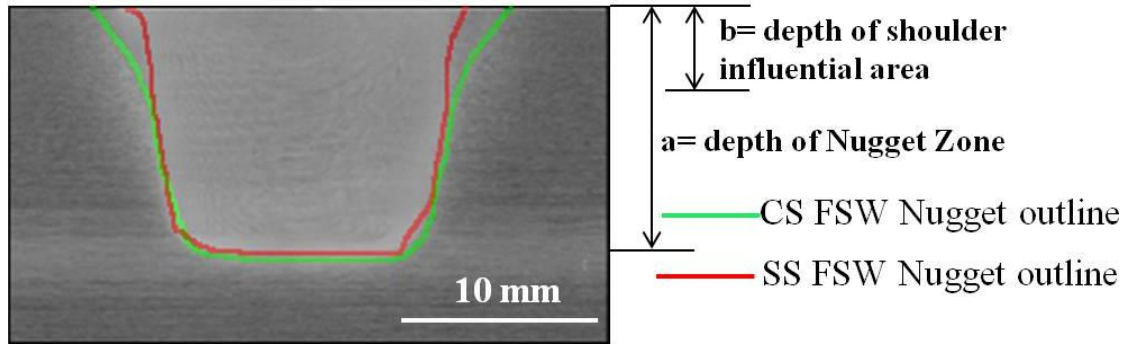


Figure 4.69 Superposition of deformation zone using CSFSW and SSFSW

Figure 4.70 (a-f) shows the comparisons of all the response variables of CSFSW and SSFSW including forge force as a function to tool rotational speed. It was observed in Figure 4.70 (a) that the applied forge force along the Z direction is higher for SSFSW compared to CSFSW. This might be due to the contribution of a rotating shoulder to balance the pressure exerted by the extruded materials in CSFSW. However, in case of SSFSW, additional pressure is required by the SS tool to encounter the uplift thrust of the extruded materials, which eventually leads to high forge force requirement. Figure 4.70-b shows the torque as a function of tool rotational speed for CSFSW and SSFSW. It is interesting to note here that the torque for SSFSW is less than that of CSFSW. However, the difference in torque is 7-13% at low welding speed and 0-9% at high welding speed. These insignificant differences in torque/power in CS and SS FSW might be associated with the deformation/displacement volume of the extruded materials by the tool. It was previously observed that the shoulder dominated deformation region is approximately less than 10% of the total nugget area of CSFSW. This might cause subtle increase in required torque.

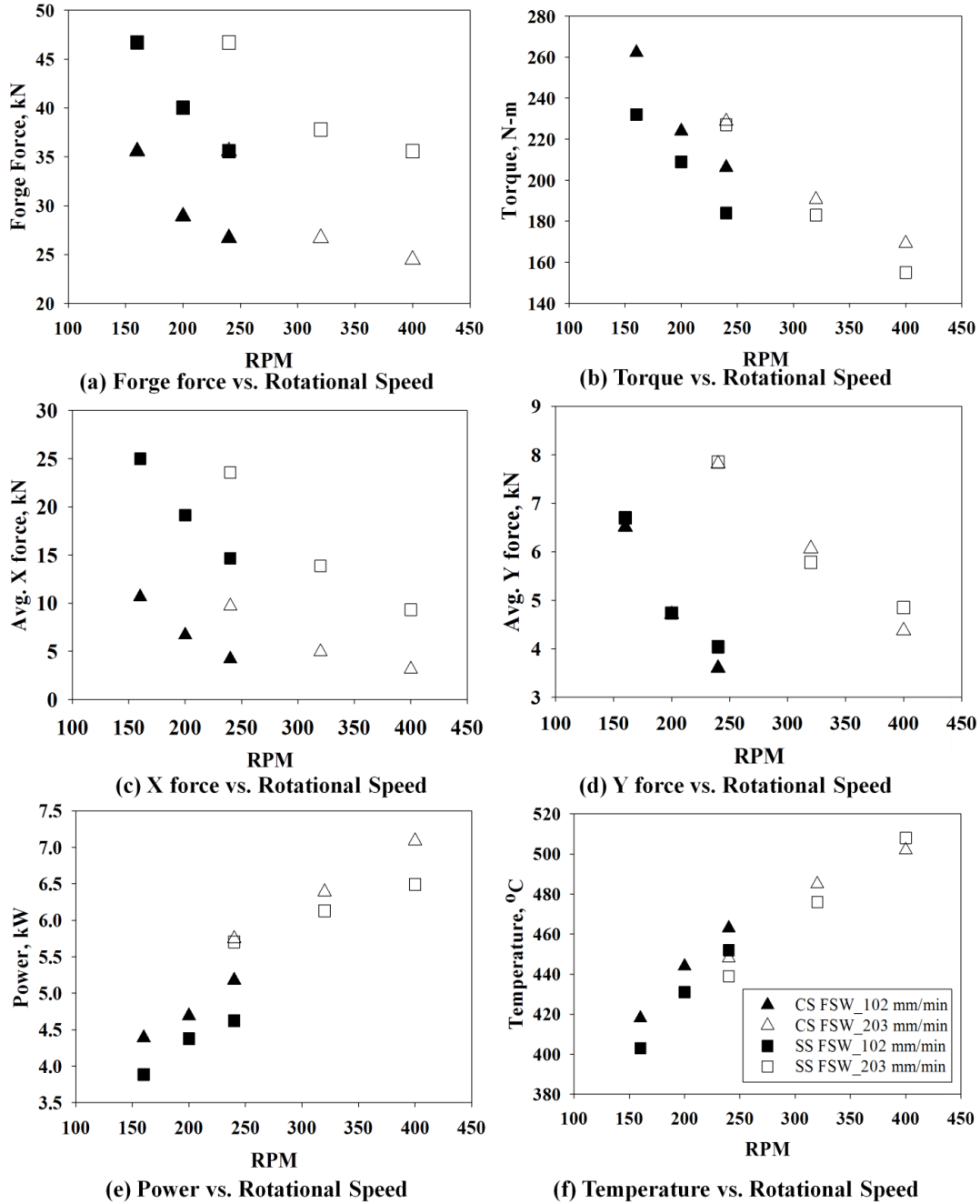


Figure 4.70 Comparison of process response variables for CSFSW and SSFSW

The X-axis force is mainly affected by the applied force force in this case, since SSFSW exhibits higher X force compared to CSFSW (Figure 4.70-c). The main reasons attributed to the variation of X force in CSFSW and SSFSW are: (i) resistance to rigid materials under the non-rotating shoulder impose excessive X force in SSFSW, (ii) the

rotating shoulder in CSFSW increases heat input and causes the tool to encounter lesser flow stress material, which might reduce X force. A minute difference in Y axis force was evident while comparing CS and SS FSW (Figure 4.70-d). The power required for CSFSW is always greater than the power required for SSFSW (see Figure 4.70-e) which caused the temperature to be higher for CSFSW than SSFSW (Figure 4.70-f). The pin peak temperature for CSFSW is 9°-15°C higher than SSFSW with the exception of welding with the highest rotational speed as seen in Figure 4.70-f. It has been mentioned earlier that the shoulder dominated deformation region is less than 10% of the nugget zone as determined from the differences in nugget areas between CSFSW and SSFSW. However, the ability of the pin to stir the material during SSFSW is superseding the combined action of rotating shoulder and pin in CSFSW at high rotational speed.

#### 4.9.3 Summary Observation

This section compares the process response variable for conventional shoulder friction stir welding to stationary. The highlighted observations from this study are given below:

- a. Defect free welds can be produced using both conventional shoulder (CS) and stationary shoulder (SS) FSW. Moreover, good weld surface finish was obtained only by using SSFSW.
- b. The shoulder dominated region in the nugget area can be distinguished by comparing the nugget geometry between CSFSW and SSFSW.
- c. The forge force and the X-axis force are higher for SSFSW compared to CSFSW and X-force is primarily governed by the applied forge force.
- d. Torque, power and temperature for CSFSW are higher than SSFSW

## CHAPTER 5

### CONCLUSIONS AND FUTURE WORK

#### 5.1 Concluding Remarks

The major objectives of this dissertation were to understand the effect of friction stir welding tool geometries and features on different aspects of the FSW process, including weld quality and process response variables. A systematic variation of pin profile and features was employed in order to perform friction stir welding of several precipitation hardened aluminum alloys. The effects of pin profile (shape/thread forms/flats/flutes) on the material flow, in-plane forces, weld power and process temperature were investigated within the range of examined welding parameters. The following conclusions can be drawn out of this work:

1. Helical features such as thread forms on the tool pin are beneficial to eliminate/minimize wormhole defects during FSW. Cylindrical pins with intermediate thread form (coarse thread) effectually perform welding of different aluminum alloys. However, excessive downward material movement by thread only resulted in surface breaking defects in welds, which justified the research trend towards the study of interrupting thread in pin.
2. Interrupting pin threads with flats significantly improved material movement and eliminated/minimized defect contents in welds as well as reduced in-plane forces on the tool. A coarse threaded cylindrical pin having three flats drastically enhance weld

quality by producing completely defect free welds. The pin reaction force and amplitude of the force oscillation were also reduced in defect free welds.

3. Changing pin shape from cylindrical to frustum resulted in a reduction of in-plane reaction forces for similar welding conditions. A coarse threaded conical pin having three shallow flats produced the best quality welds in 6XXX and 7XXX series aluminum alloys with reduced pin reaction forces.

4. The threaded pins were also incorporated with counter-flow or co-flow flutes that greatly alter the flow of materials and improve weld quality in different welding conditions. The forge force requirement was reduced while using pin with thread + 3 counter-flow flutes. The counter-flow flutes were implemented in lap joints in order to improve vertical intermixing. While guiding materials in the stir zone, wormhole defects might be produced if the counter-flow feature dominates over the thread feature. Several examples of wormhole defected welds were evident in the case of 6061 bead on plate welding with normal threaded pin having 3 counter-flow flutes or in AA2050-AA6061 dissimilar material welding with pin having coarse thread + 3 counter-flow flutes. In contrast, a co-flow fluted pin is favorable in eliminating wormhole defect. However, potential surface breaking defects in welds are often caused by a co-flow fluted pin.

5. Apart from the pin features (thread/flats/flutes), positioning of alloy on the advancing side also plays a significant role in dissimilar material friction stir butt welds. The placement of relatively stronger alloy on the advancing side resulted in defect free welds and caused less in-plane reaction forces on pin. However, a coarse conical pin having three flats or three counter-flow flutes produced the highest intensity of intermixing of bi-materials in the nugget zone. A significant effect of peak temperature

with respect to tool eccentricity was observed in case of dissimilar material friction stir butt welding. Increasing tool eccentricity towards stronger material resulted in the peak temperature increased by 30°- 40°C. A higher volumetric percentage of the stronger alloy in the nugget zone caused the process temperature to be increased.

6. The location of full thread depth near the shank was detected as the area of stress concentration in pin as estimated from the structural analysis of pin using FEM. It was also revealed that the maximum stress on pin can also be altered by shifting the orientation of the flats in pin with respect to thread termination. Experiments have shown that a threaded conical pin with shallow flat depth (1.35 mm) experiences less in-plane reaction during welding compared to threaded pin without flat. The FEM analysis also estimated less stress on such a pin (threaded + 3 shallow flats) compared to no flat or even a deeper (2.7 mm flat depth) flatted pin which is exposed to similar reaction force as that of a shallower flatted pin.

7. This study also demonstrated the effectiveness of the pin features in friction stir welding by comparing different shoulder configurations: one with conventional and the other with a stationary shoulder. Both shoulder configurations with the same pin (a coarse threaded conical pin with three shallow flats) produced defect free welds. However a smooth surface finish can only be obtained using the stationary shoulder as compared to rough surface due to the shoulder mark in conventional shoulder FSW. The forge force and the X-axis force were higher for stationary shoulder (SS) FSW compared to those of conventional shoulder (CS) FSW. However, torque, weld power and temperature were in practice, close while comparing CSFSW and SSFSW. This comparison of weld power and torque challenges the general proclamation of heat generation during FSW in the

literature-“shoulder predominantly generate frictional heat”, which is not necessarily true in all case. This phenomenon mostly depends on the applied forge force and present practice of producing good quality welds by the FSW process.

In essence, FSW pin design selection criteria for appropriate pin geometries and features can be adopted based on different aspects of the FSW process such as, defect formation, tool forces, etc. To eliminate wormhole defects in the weld, an intermediate thread with flats (three or four flats, depending on the weld material dimensions) is recommended. The relative depth of the flat corresponding to the thread root has to be within a reasonable limit to minimize the stress concentration on the pin. Meanwhile, oscillation of in-plane force spectra can be reduced by flat induced thread interruptions which might lead to a longer fatigue life of the tool. For a thick section weld, a conical shape pin is preferred over cylindrical pin having similar features due to lower in-plane reaction forces on the tool. The weld surface breaking defects occur because of excessive downward material movement by the pin having thread only or while the thread is combined with co-flow flutes. Hence, interrupted thread with flats or counter-flow flutes can eliminate such surface breaking defect by promoting the upward material movement. The apposite combination of thread pitch (preferably coarse thread) and counter-flow flute is capable of eradicating any kind of defects (wormhole/surface breaking) as well as reducing the forge force requirement during the FSW process. Similar pin features coupled with stationary shoulder is also effective in case of thick section lap joint or butt joints.

## 5.2 Future Works

### *Study on the pin taper angle*

This dissertation dealt with a cylindrical and a frustum shape pin having a mildly tapered conical angle ( $\theta = 8^\circ$ ) with the variety of pin features (threads/flats/flutes). It has been revealed from the results obtained in this research that the weld quality was improved and process forces were reduced due to the change in pin shape as well as insertion of geometric features in the pin. Reducing in-plane reaction forces on the pin is very desirable in order to increase the welding speed which will be advantageous in terms of manufacturing rapidity. It is therefore recommended to extend the study to the variable conical angles ( $\theta$ ) of the frustum shape of the pin. Intensive parametric experimentation with structural analysis can be performed in order to minimize stress on the pin at a faster welding speed without compromising the weld quality and properties.

### *Study on flute to replace thread as helical features*

The defect formation using unthreaded pin with different flat numbers in this research revealed an interesting trend in which, defects are minimized and localized with increasing flat numbers. This result indicates the effectiveness/importance of helical features in pin for assisting downward movement during the FSW process. The thread forms in the pin were considered to be the primary governing parameters in this dissertation, given that these thread forms could be easily introduced on the studied tool materials: H13 steel. Many times, FSW of high temperature alloys (nickel, cobalt, steel and titanium) requires sophisticated tool materials (poly crystalline boron nitride, tungsten-carbide, tungsten-rhenium or tungsten-lanthanum). Introduction of pin features is sometimes challenging on these tool materials. Moreover, thread roots are the potential

site of stress concentration due to small minor diameter in pin. Therefore, experiments can be performed using pin having wider flutes/tilt flats with shallow cutting depth as a replacement of the thread.

#### *Study on life prediction of FSW tool*

There are several factors that limit the life of the FSW tool in terms of total length of welds that a single tool performs before it breaks or erodes: (a) geometric dimension of weld materials and tool pin, (b) in-plane reaction force, (c) tool wear or chemical erosion, (d) fatigue life and (e) microstructural change due to thermal cycle during FSW. This research focused on the reduction of in-plane reaction force to eliminate premature failure of the pin due to overloading. Undoubtedly, the complex interaction among all the above five factors need to be addressed in order to have an appropriate estimation of tool life. The future effort would be to obtain a systematic body of knowledge that accumulate and consider all the affecting factors for predicting the life of a FSW tool.

#### *Study on stationary shoulder friction stir welding*

This dissertation provides a first glimpse of the potential benefits of using the stationary shoulder FSW. An extensive parametric investigation should be made to establish the interrelationship among pin geometric parameters, process control parameters and response variables in case of stationary shoulder FSW. The complex geometric features (thread/flat/flute) can also be evaluated under stationary shoulder configuration in both lab and butt joint arrangements.

## REFERENCES

1. Environmental Protection Agency & the National Highway Traffic Safety Administration, 'Regulatory Announcement: EPA and NHTSA Set Standards to Reduce Greenhouse Gases and Improve Fuel Economy for Model Years 2017-2025 Cars and Light Trucks', Office of Transportation and Air Quality, Report EPA-420-F-12-051, August 2012.
2. W. Thomas, E. Nicholas, J. Needham, M. Murch, P. Templesmith, and C. Dawes: 'GB Patent Application no. 9125978-9', 1991.
3. B. Irving: 'Interest in welded aluminum automobiles gathers momentum worldwide: Aluminium welding', *Welding journal*, 1998, **77**(6), 31-35.
4. M. R. Johnsen: 'Friction stir welding takes off at Boeing', *Welding journal*, 1999, **78**(2), 35-39.
5. Y. Kusuda: 'Honda develops robotized FSW technology to weld steel and aluminum and applied it to a mass-production vehicle', *Industrial Robot: An International Journal*, 2013, **40**(3), 208-212.
6. C. Andersson and R. Andrews: 'Fabrication of containment canisters for nuclear waste by friction stir welding', Proc. of the 1st Int. Symposium on Friction Stir Welding, 1999, 14-16.
7. B. Christner: 'Enabling technology for an aircraft alternative', *Mech Eng Mag*, 2003, **125**(3), D14.
8. D. J. Davis and J. C. McArthur: 'NASA Ares I Crew Launch Vehicle Upper Stage Overview', 44th AIAA/ASME/SAE/ASEE Joint Propulsion Conference & Exhibit, American Institute of Aeronautics and Astronautics - AIAA, Connecticut, CT, USA, July 21-23, 2008.
9. B. Gibson, D. Lammlein, T. Prater, W. Longhurst, C. Cox, M. Ballun, K. Dharmaraj, G. Cook, and A. Strauss: 'Friction stir welding: process, automation, and control', *Journal of manufacturing processes*, 2014, **16**(1), 56-73.
10. S. Kallee: 'Application of friction stir welding in the shipbuilding industry', *Lightweight Construction-Latest Developments*, The Royal Institution of Naval Architects. London, 2000, 24-25.

11. S. Kallee, E. Nicholas, and W. Thomas: 'Friction Stir Welding- Invention, Innovations and Applications', *Kei Kinzoku Yosetsu(Journal of Light Metal Welding and Construction)*, 2005, **43**(11), 34-35.
12. S. W. Kallee, J. Davenport, and E. D. NICHOLAS: 'Railway manufacturers implement friction stir welding', *Welding journal*, 2002, **81**(10), 47-50.
13. W. Thomas and E. Nicholas: 'Friction stir welding for the transportation industries', *Materials & Design*, 1997, **18**(4), 269-273.
14. R. S. Mishra and Z. Ma: 'Friction stir welding and processing', *Materials Science and Engineering: R: Reports*, 2005, **50**(1), 1-78.
15. C. B. Fuller: 'Friction Stir Tooling: Tool Materials and Designs', in 'Friction stir welding and processing', (eds. R. S. Mishra, et al.), 7-35; 2007, ASM International.
16. D. Burford, B. Tweedy, and C. Widener: 'Influence of shoulder configuration and geometric features on FSW track properties', Proceedings of the Sixth International Symposium on Friction Stir Welding, 2006, 10-13.
17. C. Dawes and W. Thomas: 'Development of improved tool designs for friction stir welding of aluminium', Proceedings of the First International Conference on Friction Stir Welding, Oaks, CA, USA, 1999, June 14–16, 1999.
18. R. Fonda, J. Bingert, and K. Colligan: 'Development of grain structure during friction stir welding', *Scripta materialia*, 2004, **51**(3), 243-248.
19. R. Leal, C. Leitao, A. Loureiro, D. Rodrigues, and P. Vilaça: 'Material flow in heterogeneous friction stir welding of thin aluminium sheets: effect of shoulder geometry', *Materials Science and Engineering: A*, 2008, **498**(1), 384-391.
20. R. Zettler, S. Lomolino, J. Dos Santos, T. Donath, F. Beckmann, T. Lippman, and D. Lohwasser: 'A study on material flow in FSW of AA 2024-T351 and AA 6056-T4 alloys', 5th International FSW Symposium-Metz, France, 2004, 14-16.
21. M. Russell, C. Blignault, N. Horrex, and C. Wiesner: 'Recent developments in the friction stir welding of titanium alloys', *Welding in the World*, 2008, **52**(9-10), 12-15.
22. P. Davies, B. Wynne, W. Rainforth, M. Thomas, and P. Threadgill: 'Development of microstructure and crystallographic texture during stationary shoulder friction stir welding of Ti-6Al-4V', *Metallurgical and Materials Transactions A*, 2011, **42**(8), 2278-2289.

23. M. Ahmed, B. Wynne, W. Rainforth, and P. Threadgill: 'Through-thickness crystallographic texture of stationary shoulder friction stir welded aluminium', *Scripta materialia*, 2011, **64**(1), 45-48.
24. M. Boz and A. Kurt: 'The influence of stirrer geometry on bonding and mechanical properties in friction stir welding process', *Materials & Design*, 2004, **25**(4), 343-347.
25. Y. Zhao, S. Lin, L. Wu, and F. Qu: 'The influence of pin geometry on bonding and mechanical properties in friction stir weld 2014 Al alloy', *Materials Letters*, 2005, **59**(23), 2948-2952.
26. H. Fujii, L. Cui, M. Maeda, and K. Nogi: 'Effect of tool shape on mechanical properties and microstructure of friction stir welded aluminum alloys', *Materials Science and Engineering: A*, 2006, **419**(1), 25-31.
27. K. Elangovan and V. Balasubramanian: 'Influences of pin profile and rotational speed of the tool on the formation of friction stir processing zone in AA2219 aluminium alloy', *Materials Science and Engineering: A*, 2007, **459**(1), 7-18.
28. O. Lorrain, V. Favier, H. Zahrouni, and D. Lawrjaniec: 'Understanding the material flow path of friction stir welding process using unthreaded tools', *Journal of materials processing technology*, 2010, **210**(4), 603-609.
29. P. Threadgill: 'Terminology in friction stir welding', *Science and Technology of Welding & Joining*, 2007, **12**(4), 357-360.
30. J. Hinrichs, J. Noruk, W. McDonald, and R. Heideman: 'Challenges of Welding Aluminium Alloys for Automotive Structures', *Svetsaren*, 1995, **50**(3), 7-9.
31. M. Sutton, A. Reynolds, D. Wang, and C. Hubbard: 'A study of residual stresses and microstructure in 2024-T3 aluminum friction stir butt welds', *Journal of Engineering Materials and Technology*, 2002, **124**(2), 215-221.
32. P. Upadhyay and A. Reynolds: 'Effects of thermal boundary conditions in friction stir welded AA7050-T7 sheets', *Materials Science and Engineering: A*, 2010, **527**(6), 1537-1543.
33. P. Upadhyay and A. Reynolds: 'Effects of forge axis force and backing plate thermal diffusivity on FSW of AA6056', *Materials Science and Engineering: A*, 2012, **558**, 394-402.
34. Y. S. Sato, H. Kokawa, M. Enomoto, S. Jogan, and T. Hashimoto: 'Precipitation sequence in friction stir weld of 6063 aluminum during aging', *Metallurgical and Materials Transactions A*, 1999, **30**(12), 3125-3130.

35. A. Reynolds, W. Tang, Z. Khandkar, J. Khan, and K. Lindner: 'Relationships between weld parameters, hardness distribution and temperature history in alloy 7050 friction stir welds', *Science and Technology of Welding & Joining*, 2005, **10**(2), 190-199.
36. Y. S. Sato, M. Urata, and H. Kokawa: 'Parameters controlling microstructure and hardness during friction-stir welding of precipitation-hardenable aluminum alloy 6063', *Metallurgical and Materials Transactions A*, 2002, **33**(3), 625-635.
37. K. J. Colligan and R. S. Mishra: 'A conceptual model for the process variables related to heat generation in friction stir welding of aluminum', *Scripta materialia*, 2008, **58**(5), 327-331.
38. M. Reza-E-Rabby, W. Tang, and A. Reynolds: 'EFFECT OF TOOL PIN FEATURES AND GEOMETRIES ON QUALITY OF WELD DURING FRICTION STIR WELDING', *Friction Stir Welding and Processing VII*, 2013, 163.
39. G. Buffa, J. Hua, R. Shivpuri, and L. Fratini: 'Design of the friction stir welding tool using the continuum based FEM model', *Materials Science and Engineering: A*, 2006, **419**(1), 381-388.
40. P. Colegrove and H. Shercliff: 'CFD modelling of friction stir welding of thick plate 7449 aluminium alloy', *Science and Technology of Welding & Joining*, 2006, **11**(4), 429-441.
41. S. Sayer and Q. Yeni: 'Influence of Tool Geometry on Microstructure and Mechanical Properties of a Friction Stir Welded 7075 Aluminum Alloy', *Materials Testing*, 2009, **51**(11-12), 788-793.
42. H. Mohanty, M. M. Mahapatra, P. Kumar, P. Biswas, and N. R. Mandal: 'Study on the effect of tool profiles on temperature distribution and material flow characteristics in friction stir welding', *Proceedings of the Institution of Mechanical Engineers, Part B: Journal of Engineering Manufacture*, 2012, **226**(9), 1527-1535.
43. P. Colegrove and H. Shercliff: 'Development of Trivex friction stir welding tool Part 2—three-dimensional flow modelling', *Science and Technology of Welding & Joining*, 2004, **9**(4), 352-361.
44. D. Trimble, J. Monaghan, and G. O'Donnell: 'Force generation during friction stir welding of AA2024-T3', *CIRP Annals-Manufacturing Technology*, 2012, **61**(1), 9-12.

45. A. Astarita, A. Squillace, and L. Carrino: 'Experimental Study of the Forces Acting on the Tool in the Friction-Stir Welding of AA 2024 T3 Sheets', *Journal of Materials Engineering and Performance*, 2014, **23**(10), 3754-3761.
46. D. Hattingh, C. Blignault, T. Van Niekerk, and M. James: 'Characterization of the influences of FSW tool geometry on welding forces and weld tensile strength using an instrumented tool', *Journal of materials processing technology*, 2008, **203**(1), 46-57.
47. K. Jata and S. Semiatin: 'Continuous dynamic recrystallization during friction stir welding of high strength aluminum alloys', *Scripta materialia*, 2000, **43**(8), 743-749.
48. J.-Q. Su, T. Nelson, R. Mishra, and M. Mahoney: 'Microstructural investigation of friction stir welded 7050-T651 aluminium', *Acta Materialia*, 2003, **51**(3), 713-729.
49. B. Heinz and B. Skrotzki: 'Characterization of a friction-stir-welded aluminum alloy 6013', *Metallurgical and Materials Transactions B*, 2002, **33**(3), 489-498.
50. Y. S. Sato, H. Kokawa, M. Enomoto, and S. Jogan: 'Microstructural evolution of 6063 aluminum during friction-stir welding', *Metallurgical and Materials Transactions A*, 1999, **30**(9), 2429-2437.
51. K. A. Hassan, P. Prangnell, A. Norman, D. Price, and S. Williams: 'Effect of welding parameters on nugget zone microstructure and properties in high strength aluminium alloy friction stir welds', *Science and Technology of Welding & Joining*, 2003, **8**(4), 257-268.
52. H. J. Aval, S. Serajzadeh, and A. Kokabi: 'The influence of tool geometry on the thermo-mechanical and microstructural behaviour in friction stir welding of AA5086', *Proceedings of the institution of mechanical engineers, part c: journal of mechanical engineering science*, 2011, **225**(1), 1-16.
53. K. Elangovan, V. Balasubramanian, and M. Valliappan: 'Influences of tool pin profile and axial force on the formation of friction stir processing zone in AA6061 aluminium alloy', *The International Journal of Advanced Manufacturing Technology*, 2008, **38**(3-4), 285-295.
54. Ø. Frigaard, Ø. Grong, and O. Midling: 'A process model for friction stir welding of age hardening aluminum alloys', *Metallurgical and Materials Transactions A*, 2001, **32**(5), 1189-1200.
55. C. Genevois, A. Deschamps, A. Denquin, and B. Doisneau-Cottignies: 'Quantitative investigation of precipitation and mechanical behaviour for AA2024 friction stir welds', *Acta Materialia*, 2005, **53**(8), 2447-2458.

56. M. Mahoney, C. Rhodes, J. Flintoff, W. Bingel, and R. Spurling: 'Properties of friction-stir-welded 7075 T651 aluminum', *Metallurgical and Materials Transactions A*, 1998, **29**(7), 1955-1964.
57. L. Murr, G. Liu, and J. McClure: 'A TEM study of precipitation and related microstructures in friction-stir-welded 6061 aluminium', *Journal of materials science*, 1998, **33**(5), 1243-1251.
58. P. Threadgill, A. Leonard, H. Shercliff, and P. Withers: 'Friction stir welding of aluminium alloys', *International Materials Reviews*, 2009, **54**(2), 49-93.
59. K. Colligan: 'Material flow behavior during friction welding of aluminum', *Weld J*, 1999, **75**(7), 229s-237s.
60. R. Fonda, A. Reynolds, C. Feng, K. Knipling, and D. Rowenhorst: 'Material flow in friction stir welds', *Metallurgical and Materials Transactions A*, 2013, **44**(1), 337-344.
61. M. Guerra, C. Schmidt, J. McClure, L. Murr, and A. Nunes: 'Flow patterns during friction stir welding', *Materials characterization*, 2002, **49**(2), 95-101.
62. A. Reynolds: 'Visualisation of material flow in autogenous friction stir welds', *Science and Technology of Welding & Joining*, 2000, **5**(2), 120-124.
63. H. N. B. Schmidt, T. Dickerson, and J. H. Hattel: 'Material flow in butt friction stir welds in AA2024-T3', *Acta Materialia*, 2006, **54**(4), 1199-1209.
64. T. Seidel and A. Reynolds: 'Visualization of the material flow in AA2195 friction-stir welds using a marker insert technique', *Metallurgical and Materials Transactions A*, 2001, **32**(11), 2879-2884.
65. C. R. Tolle, T. A. White, K. S. Miller, D. E. Clark, and H. B. Smartt: 'Investigation of material flows within FSWs using 3D tomography', Proceedings of the 8<sup>th</sup> International Conference on Trends in Welding Research, 2008, 126-132.
66. W. Xu, J. Liu, and D. Chen: 'Material flow and core/multi-shell structures in a friction stir welded aluminum alloy with embedded copper markers', *Journal of Alloys and Compounds*, 2011, **509**(33), 8449-8454.
67. Y.-H. Zhao, S.-B. Lin, F.-X. Qu, and L. Wu: 'Influence of pin geometry on material flow in friction stir welding process', *Materials science and technology*, 2006, **22**(1), 45-50.

68. A. Bastier, M. Maitournam, K. Dang Van, and F. Roger: 'Steady state thermomechanical modelling of friction stir welding', *Science and Technology of Welding & Joining*, 2006, **11**(3), 278-288.
69. G. Bendzsak, T. North, and C. Smith: 'An experimentally validated 3D model for friction stir welding', Proceedings of the Second International Symposium on Friction Stir Welding, Gothenburg, Sweden, 2000.
70. P. A. Colegrove and H. R. Shercliff: '3-Dimensional CFD modelling of flow round a threaded friction stir welding tool profile', *Journal of materials processing technology*, 2005, **169**(2), 320-327.
71. X. Deng and S. Xu: 'Two-dimensional finite element simulation of material flow in the friction stir welding process', *Journal of manufacturing processes*, 2004, **6**(2), 125-133.
72. M. Grujicic, G. Arakere, B. Pandurangan, J. Ochterbeck, C. Yen, B. Cheeseman, A. Reynolds, and M. Sutton: 'Computational analysis of material flow during friction stir welding of AA5059 aluminum alloys', *Journal of Materials Engineering and Performance*, 2012, **21**(9), 1824-1840.
73. H. Schmidt and J. H. Hattel: 'Thermal and material flow modelling of friction stir welding using Comsol', Proceedings of the COMSOL Conference 2008 Hannover, 2008.
74. P. Prangnell and C. Heason: 'Grain structure formation during friction stir welding observed by the 'stop action technique'', *Acta Materialia*, 2005, **53**(11), 3179-3192.
75. A. Reynolds: 'Flow visualization and simulation in FSW', *Scripta materialia*, 2008, **58**(5), 338-342.
76. B. London, M. Mahoney, W. Bingel, M. Calabrese, R. Bossi, and D. Waldron: 'Material flow in friction stir welding monitored with Al-SiC and Al-W composite markers', TMS Annual Meeting 2003, 3-12.
77. L. Fratini, G. Buffa, D. Palmeri, J. Hua, and R. Shivpuri: 'Material flow in FSW of AA7075-T6 butt joints: numerical simulations and experimental verifications', *Science and Technology of Welding & Joining*, 2006, **11**(4), 412-421.
78. M. Aissani, S. Gachi, F. Boubenider, and Y. Benkedda: 'Design and optimization of friction stir welding tool', *Materials and Manufacturing Processes*, 2010, **25**(11), 1199-1205.
79. W. M. Thomas, D. Staines, I. Norris, and R. De Frias: 'Friction stir welding tools and developments', *Welding in the World*, 2003, **47**(11-12), 10-17.

80. P. Alvarez, G. Janeiro, A. Da Silva, E. Aldanondo, and A. Echeverría: 'Material flow and mixing patterns during dissimilar FSW', *Science and Technology of Welding & Joining*, 2010, **15**(8), 648-653.
81. S. Amancio-Filho, S. Sheikhi, J. Dos Santos, and C. Bolfarini: 'Preliminary study on the microstructure and mechanical properties of dissimilar friction stir welds in aircraft aluminium alloys 2024-T351 and 6056-T4', *Journal of materials processing technology*, 2008, **206**(1), 132-142.
82. P. Bahemmat, M. Haghpanahi, M. K. B. Givi, and K. R. Seighalani: 'Study on dissimilar friction stir butt welding of AA7075-O and AA2024-T4 considering the manufacturing limitation', *The International Journal of Advanced Manufacturing Technology*, 2012, **59**(9-12), 939-953.
83. P. Cavaliere, A. De Santis, F. Panella, and A. Squillace: 'Effect of welding parameters on mechanical and microstructural properties of dissimilar AA6082-AA2024 joints produced by friction stir welding', *Materials & Design*, 2009, **30**(3), 609-616.
84. A. Da Silva, E. Arruti, G. Janeiro, E. Aldanondo, P. Alvarez, and A. Echeverria: 'Material flow and mechanical behaviour of dissimilar AA2024-T3 and AA7075-T6 aluminium alloys friction stir welds', *Materials & Design*, 2011, **32**(4), 2021-2027.
85. H. Izadi, J. Fallu, A. Abdel-Gwad, T. Liyanage, and A. Gerlich: 'Analysis of tool geometry in dissimilar Al alloy friction stir welds using optical microscopy and serial sectioning', *Science and Technology of Welding and Joining*, 2013, **18**(4), 307-313.
86. H. Jamshidi Aval, S. Serajzadeh, A. Kokabi, and A. Loureiro: 'Effect of tool geometry on mechanical and microstructural behaviours in dissimilar friction stir welding of AA 5086-AA 6061', *Science and Technology of Welding and Joining*, 2011, **16**(7), 597-604.
87. C. Jonckheere, B. de Meester, A. Denquin, and A. Simar: 'Torque, temperature and hardening precipitation evolution in dissimilar friction stir welds between 6061-T6 and 2014-T6 aluminum alloys', *Journal of materials processing technology*, 2013, **213**(6), 826-837.
88. S. A. Khodir and T. Shibayanagi: 'Friction stir welding of dissimilar AA2024 and AA7075 aluminum alloys', *Materials Science and Engineering: B*, 2008, **148**(1), 82-87.

89. H. Larsson, L. Karlsson, S. Stoltz, and E. Bergqvist: 'Joining of dissimilar Al-alloys by friction stir welding', 2nd International Symposium on Friction Stir Welding, Gothenburg, Sweden, TWI, June 2000, 26-28.
90. W.-B. Lee, Y.-M. Yeon, and S.-B. Jung: 'The joint properties of dissimilar formed Al alloys by friction stir welding according to the fixed location of materials', *Scripta materialia*, 2003, **49**(5), 423-428.
91. Y. Li, L. Murr, and J. McClure: 'Solid-state flow visualization in the friction-stir welding of 2024 Al to 6061 Al', *Scripta materialia*, 1999, **40**(9), 1041-1046.
92. J. Ouyang and R. Kovacevic: 'Material flow and microstructure in the friction stir butt welds of the same and dissimilar aluminum alloys', *Journal of Materials Engineering and Performance*, 2002, **11**(1), 51-63.
93. R. Palanivel, P. K. Mathews, N. Murugan, and I. Dinaharan: 'Effect of tool rotational speed and pin profile on microstructure and tensile strength of dissimilar friction stir welded AA5083-H111 and AA6351-T6 aluminum alloys', *Materials & Design*, 2012, **40**, 7-16.
94. S.-K. Park, S.-T. Hong, J.-H. Park, K.-Y. Park, Y.-J. Kwon, and H.-J. Son: 'Effect of material locations on properties of friction stir welding joints of dissimilar aluminium alloys', *Science and Technology of Welding & Joining*, 2010, **15**(4), 331-336.
95. M. Peel, A. Steuwer, P. Withers, T. Dickerson, Q. Shi, and H. Shercliff: 'Dissimilar friction stir welds in AA5083-AA6082. Part I: Process parameter effects on thermal history and weld properties', *Metallurgical and Materials Transactions A*, 2006, **37**(7), 2183-2193.
96. A. Simar, C. Jonckheere, K. Deplus, T. Pardoen, and B. De Meester: 'Comparing similar and dissimilar friction stir welds of 2017-6005A aluminium alloys', *Science and Technology of Welding & Joining*, 2010, **15**(3), 254-259.
97. K. Kumar and S. Kailas: 'Positional dependence of material flow in friction stir welding: analysis of joint line remnant and its relevance to dissimilar metal welding', *Science and Technology of Welding & Joining*, 2010, **15**(4), 305-311.
98. J. Guo, H. Chen, C. Sun, G. Bi, Z. Sun, and J. Wei: 'Friction stir welding of dissimilar materials between AA6061 and AA7075 Al alloys effects of process parameters', *Materials & Design*, 2014, **56**, 185-192.
99. Y. Zhang, X. Cao, S. Larose, and P. Wanjara: 'Review of tools for friction stir welding and processing', *Canadian Metallurgical Quarterly*, 2012, **51**(3), 250-261.

100. C. Dawes, P. Threadgill, S. EJR, and S. DG: 'Development of the New Friction Stir Technique for Welding Aluminum-Phase II', The Welding Institute, 1995.
101. W. Thomas: 'Friction stir welding-recent developments', *Materials Science Forum*, 2003, Trans Tech Publ, 229-236.
102. W. M. Thomas, E. D. Nicholas, and S. D. Smith: 'Friction stir welding - tool developments', *Aluminum Joining Symposium 2001*, TMS Annual Meeting, New Orleans, Louisiana, USA, 11-15 February 2001, 2001.
103. W. M. Thomas: 'Friction stir welding and related friction process characteristics', *Proc. 7th Int. Conf. on 'Joints in aluminium-INALCO*, 1999, 157-174.
104. W. M. Thomas, K. I. Johnson, and C. S. Wiesner: 'Friction stir welding—recent developments in tool and process technologies', *Advanced Engineering Materials*, 2003, **5**(7), 485-490.
105. J. Schneider and A. Nunes Jr: 'Characterization of plastic flow and resulting microtextures in a friction stir weld', *Metallurgical and Materials Transactions B*, 2004, **35**(4), 777-783.
106. E. Mahmoud, M. Takahashi, T. Shibayanagi, and K. Ikeuchi: 'Effect of friction stir processing tool probe on fabrication of SiC particle reinforced composite on aluminium surface', *Science and Technology of Welding & Joining*, 2009, **14**(5), 413-425.
107. K. Wang, J. Liu, K. W. Xu, and Y. Shen: 'The influence of the stirrer's shape and process parameter on friction stir welded MB3 magnesium joining', *Materials Science Forum*, 2005, Trans Tech Publ, 485-488.
108. S. Chowdhury, D. Chen, S. Bhole, and X. Cao: 'Tensile properties of a friction stir welded magnesium alloy: Effect of pin tool thread orientation and weld pitch', *Materials Science and Engineering: A*, 2010, **527**(21), 6064-6075.
109. G. Buffa, J. Hua, R. Shivpuri, and L. Fratini: 'A continuum based fem model for friction stir welding—model development', *Materials Science and Engineering: A*, 2006, **419**(1), 389-396.
110. N. Balasubramanian, B. Gattu, and R. S. Mishra: 'Process forces during friction stir welding of aluminium alloys', *Science and Technology of Welding & Joining*, 2009, **14**(2), 141-145.
111. E. Boldsaikhan: 'The use of feedback forces for nondestructive evaluation of friction stir welding', *South Dakota School of Mines and Technology*, Rapid City, 2008.

112. E. Boldsaikhan, D. A. Burford, and P. Gimenez: 'Effect of plasticized material flow on the tool feedback forces during friction stir welding', Proc. Conf. On 'Friction stir welding and processing VI', San Francisco, CA, USA, 2011, 335-343.
113. T. Long and A. Reynolds: 'Parametric studies of friction stir welding by commercial fluid dynamics simulation', *Science and Technology of Welding & Joining*, 2006, **11**(2), 200-208.
114. T. Long, W. Tang, and A. Reynolds: 'Process response parameter relationships in aluminium alloy friction stir welds', *Science and Technology of Welding & Joining*, 2007, **12**(4), 311-317.
115. A. Arora, M. Mehta, A. De, and T. DebRoy: 'Load bearing capacity of tool pin during friction stir welding', *The International Journal of Advanced Manufacturing Technology*, 2012, **61**(9-12), 911-920.
116. W.-B. L. Jeong-Luh Lin, Yang I-Horng, Dai Jian-Ting: 'Stress Analysis of FSW Tools under Torsional and Bearing loads', *WHAMPOA-An Interdisciplinary Journal*, 2007, **52**, 33-45.
117. C. D. Sorensen and A. L. Stahl: 'Experimental measurements of load distributions on friction stir weld pin tools', *Metallurgical and Materials Transactions B*, 2007, **38**(3), 451-459.
118. K. S. K. Rajesh guptha, N. Jeevan kumar: 'Analysis Of Friction Stir Welding Tools With Various Threaded Pin Profiles', *International Journal of Engineering Research and Applications (IJERA)*, 2013, **3**(1), 758-761.
119. R. Dif, B. Bes, T. Warner, P. Lequeu, H. Ribes, and P. Lassince: 'Recent developments in AA 6056 aluminum alloy used for aerospace', *ASM International, Advances in the Metallurgy of Aluminum Alloys(USA)*, 2001, 390-397.
120. J. Scheuring, F. Baldwin, Z. Long, R. Nash, and P. Lassince: 'Kaisersselect® 7099 Aerospace Plate Products', 25th Advanced Aerospace Materials and Processes (AeroMat 2014) Conference and Expositio, Orlando, FL, USA, June 16-19, 2014, 2014.
121. P. Lequeu, K. Smith, and A. Daniélou: 'Aluminum-Copper-Lithium Alloy 2050 developed For medium to thick plate', *Journal of Materials Engineering and Performance*, 2010, **19**(6), 841-847.
122. 'Properties of Wrought Aluminum and Aluminum Alloys', in 'Properties and Selection: Nonferrous Alloys and Special-Purpose Materials', (eds. L. A. Abel, et al.), 62-122; 1991, Materials Park, OH, ASM International.

123. N. A. Belov, D. G. Eskin, and A. A. Aksenov: 'Multicomponent Phase Diagrams: Applications for Commercial Aluminum Alloys: Applications for Commercial Aluminum Alloys', 2005, Elsevier.
124. M. Tiryakioglu and J. T. Staley: 'Physical metallurgy and the effect of alloying additions in aluminum alloys', *Handbook of Aluminum: Physical Metallurgy and Processes*, 2003, **1**, 81-209.
125. J. C. Williams and E. A. Starke: 'Progress in structural materials for aerospace systems', *Acta Materialia*, 2003, **51**(19), 5775-5799.
126. I. Dutta and S. Allen: 'A calorimetric study of precipitation in commercial aluminium alloy 6061', *Journal of Materials Science Letters*, 1991, **10**(6), 323-326.
127. G. Edwards, K. Stiller, G. Dunlop, and M. Couper: 'The precipitation sequence in Al–Mg–Si alloys', *Acta Materialia*, 1998, **46**(11), 3893-3904.
128. D. Chakrabarti and D. E. Laughlin: 'Phase relations and precipitation in Al–Mg–Si alloys with Cu additions', *Progress in Materials Science*, 2004, **49**(3), 389-410.
129. S. Esmaeili, X. Wang, D. Lloyd, and W. Poole: 'On the precipitation-hardening behavior of the Al-Mg-Si-Cu alloy AA6111', *Metallurgical and Materials Transactions A*, 2003, **34**(3), 751-763.
130. C. Gallais, A. Denquin, Y. Bréchet, and G. Lapasset: 'Precipitation microstructures in an AA6056 aluminium alloy after friction stir welding: characterisation and modelling', *Materials Science and Engineering: A*, 2008, **496**(1), 77-89.
131. W. Miao and D. Laughlin: 'Effects of Cu content and preaging on precipitation characteristics in aluminum alloy 6022', *Metallurgical and Materials Transactions A*, 2000, **31**(2), 361-371.
132. L. Backerud, G. Chai, and J. Tamminen: 'Solidification Characteristics of Aluminum Alloys. Vol. 2. Foundry Alloys', *American Foundrymen's Society, Inc.*, 1990, 1990, 266.
133. W. Arbegast: 'Using Gleeble flow stress data to establish optimum FSW processing parameters in aluminum alloys', Presentation for the 13th AeroMat Conference & Exposition, Orlando, Florida USA, 2002, 1-39.
134. ASTM: 'Standard Test Method for Determining Average Grain Size', in 'Annual Book of ASTM Standard Section 3: Metals Test Method and Analytical Procedure', 313-338; 2007, PA, USA, ASTM International.

135. R. Brown, W. Tang, and A. Reynolds: 'Multi-pass friction stir welding in alloy 7050-T7451: Effects on weld response variables and on weld properties', *Materials Science and Engineering: A*, 2009, **513**, 115-121.
136. D. Burford, P. G. Britos, E. Boldsaikhan, and J. Brown: 'Evaluation of friction stir weld process and properties for aerospace application: e-NDE for friction stir processes', 6th annual technical review meeting, FAA Joint Advanced Materials & Structures (JAMS), 2010.
137. R. Crawford, G. Cook, A. Strauss, D. Hartman, and M. Stremmer: 'Experimental defect analysis and force prediction simulation of high weld pitch friction stir welding', *Science and Technology of Welding & Joining*, 2006, **11**(6), 657-665.
138. J. Yan, M. Sutton, and A. Reynolds: 'Processing and banding in AA2524 and AA2024 friction stir welding', *Science and Technology of Welding & Joining*, 2007, **12**(5), 390-401.
139. H. R. Doude, J. A. Schneider, and A. C. Nunes Jr: 'Influence of the Tool Shoulder Contact Conditions on the Material Flow During Friction Stir Welding', *Metallurgical and Materials Transactions A*, 2014, **45**(10), 4411-4422.
140. W. Tang, X. Guo, J. McClure, L. Murr, and A. Nunes: 'Heat input and temperature distribution in friction stir welding', *Journal of Materials Processing and Manufacturing Science*, 1998, **7**, 163-172.
141. E. Boldsaikhan and M. McCoy: 'Analysis of Tool Feedback Forces and Material Flow during Friction Stir Welding', *Friction Stir Welding and Processing VII*, 2013, 311-320.
142. M. Khandkar, J. Khan, and A. Reynolds: 'Prediction of temperature distribution and thermal history during friction stir welding: input torque based model', *Science and Technology of Welding & Joining*, 2003, **8**(3), 165-174.
143. A. P. Reynolds, Z. Khandkar, T. Long, W. X. Tang, and J. Khan: 'Utility of relatively simple models for understanding process parameter effects on FSW', *Materials Science Forum*, 2003, Trans Tech Publ, 2959-2964.
144. A. M. Rahman, S. Kumar, and A. R. Gerson: 'Galvanic corrosion of laser weldments of AA6061 aluminium alloy', *Corrosion Science*, 2007, **49**(12), 4339-4351.
145. H. Wu, Y. C. Chen, D. Strong, and P. Prangnell: 'Assessment of the Advantages of Static Shoulder FSW for Joining Aluminium Aerospace Alloys', *Materials Science Forum*, 2014, Trans Tech Publ, 1770-1775.

APPENDIX A  
DETAILING OF FSW TOOL



## APPENDIX B

### LIST OF ALL WELDING PROCESS CONTROL PARAMETERS

**1. AA7050 Friction Stir Welding**  
**a. Cylindrical pin with different thread forms**

<i>Pin Profile</i>	<i>Weld #</i>	<i>Rotational Speed</i>	<i>Welding Speed</i>	<i>Z-Force</i>
		<i>RPM</i>	<i>mm/min. (IPM)</i>	<i>kN (lbf)</i>
Unthreaded	3561-A	180	51 (2)	44.5 (10000)
	3561-B	150	51 (2)	44.5 (10000)
	3561-C	120	51 (2)	44.5 (10000)
	3560-A	240	102 (4)	62.3 (14000)
	3560-B	200	102 (4)	62.3 (14000)
	3560-C	160	102 (4)	62.3 (14000)
Fine Threaded, 1.02 mm pitch (25 thread/inch)	3571-A	180	51 (2)	37.8 (8500)
	3571-B	150	51 (2)	37.8 (8500)
	3571-C	120	51 (2)	37.8 (8500)
	3572-A	240	102 (4)	51.2 (11500)
	3572-B	200	102 (4)	44.5 (10000)
	3572-C	160	102 (4)	44.5 (10000)
Normal Threaded, 1.41 mm pitch (18 thread/inch)	3595-A	180	51 (2)	40 (9000)
	3595-B	150	51 (2)	40 (9000)
	3595-C	120	51 (2)	40 (9000)
	3596-A	240	102 (4)	46.7(10500)
	3596-B	200	102 (4)	48.9 (11000)
	3596-C	160	102 (4)	46.7 (10500)
Coarse Threaded 1,2.12 mm pitch (12 thread/inch)	3598-A	180	51 (2)	51.2 (11500)
	3598-B	150	51 (2)	48.9 (11000)
	3598-C	120	51 (2)	46.7 (10500)
	3599-A	240	102 (4)	66.7 (15000)
	3599-B	200	102 (4)	60.1 (13500)
	3599-C	160	102 (4)	57.8 (13000)
Coarse Threaded, 3.18 mm (8 thread/inch)	3600-A	180	51 (2)	53.4 (12000)
	3600-B	150	51 (2)	51.2 (11500)
	3600-C	120	51 (2)	48.9 (11000)
	3601-A	240	102 (4)	66.7 (15000)
	3601-B	200	102 (4)	64.5 (14500)
	3601-C	160	102 (4)	60.1 (13500)

**b. Conical coarse threaded pin with various flat depth**

<i>Pin Profile</i>	<i>Weld #</i>	<i>Rotational Speed</i>	<i>Welding Speed</i>	<i>Z-Force</i>
		<i>RPM</i>	<i>mm/min. (IPM)</i>	<i>kN (lbf)</i>
Coarse Threaded 1,2.12 mm pitch (12 thread/inch) Threaded only	4287-A	240	102 (4)	46.7 (10500)
	4287-B	200	102 (4)	51.2 (11500)
	4287-C	160	102 (4)	55.6 (12500)
Coarse Threaded 1,2.12 mm pitch (12 thread/inch) + 3 Flats of 1.35 mm(0.053 inch) depth	4093-A	240	102 (4)	37.81 (8500)
	4093-B	200	102 (4)	40 (9000)
	4093-C	160	102 (4)	42.3 (9500)
Coarse Threaded 1,2.12 mm pitch (12 thread/inch) + 3 Flats of 2.7 mm(0.106 inch) depth	4097-A	240	102 (4)	33.36 (7500)
	4097-B	200	102 (4)	37.81 (8500)
	4097-C	160	102 (4)	42.26 (9500)

**2. AA 6061 Friction Stir Welding**

**a. Cylindrical pin with different thread forms**

<i>Pin Profile</i>	<i>Weld #</i>	<i>Rotational Speed</i>	<i>Welding Speed</i>	<i>Z-Force</i>
		<i>RPM</i>	<i>mm/min. (IPM)</i>	<i>kN (lbf)</i>
Unthreaded	3652 A	240	102 (4)	20.9 (4700)
	3652 B	200	102 (4)	18.7 (4200)
	3652 C	160	102 (4)	24.5 (5500)
	3653 A	400	203 (8)	26.7 (6000)
	3653 B	320	203 (8)	26.7 (6000)
	3653 C	240	203 (8)	28.9 (6500)
Fine Threaded, 1.02 mm pitch (25 thread/inch)	3654 A	240	102 (4)	20 (4500)
	3654 B	200	102 (4)	22.2 (5000)
	3654 C	160	102 (4)	24.5 (5500)
	3655 A	400	203 (8)	22.2 (5000)
	3655 B	320	203 (8)	22.2 (5000)
	3655 C	240	203 (8)	26.7 (6000)
Normal Threaded, 1.41 mm pitch (18 thread/inch)	3656 A	240	102 (4)	24.5 (5500)
	3656 B	200	102 (4)	26.7 (6000)
	3656 C	160	102 (4)	31.1 (7000)
	3658 A	400	203 (8)	24.5 (5500)
	3658 B	320	203 (8)	26.7 (6000)
	3658 C	240	203 (8)	31.1 (7000)
Coarse Threaded 1,2.12 mm pitch (12 thread/inch)	3659 A	240	102 (4)	28.9 (6500)
	3659 B	200	102 (4)	37.8 (8500)
	3659 C	160	102 (4)	46.7 (10500)
	3660 A	400	203 (8)	33.4 (7500)
	3660 B	320	203 (8)	35.6 (8000)

<i>Pin Profile</i>	<i>Weld #</i>	<i>Rotational Speed</i>	<i>Welding Speed</i>	<i>Z-Force</i>
		<i>RPM</i>	<i>mm/min. (IPM)</i>	<i>kN (lbf)</i>
	3660 C	240	203 (8)	46.7 (10500)
Coarse Threaded, 3.18 mm (8 thread/inch)	3661 A	240	102 (4)	31.1 (7000)
	3661 B	200	102 (4)	37.8 (8500)
	3661 C	160	102 (4)	42.3 (9500)
	3662 A	400	203 (8)	35.6 (8000)
	3662 B	320	203 (8)	35.6 (8000)
	3662 C	240	203 (8)	46.7 (10500)

**b. Cylindrical pins with different flat numbers**

<i>Pin Profile</i>	<i>Weld #</i>	<i>Rotational Speed</i>	<i>Welding Speed</i>	<i>Z-Force</i>
		<i>RPM</i>	<i>mm/min. (IPM)</i>	<i>kN</i>
<b>1 Flat</b>				
Unthreaded 1 Flat	3685A	240	102 (4)	20
	3685B	200	102 (4)	22.2
	3685C	160	102 (4)	26.7
	3686A	400	203 (8)	26.7
	3686B	320	203 (8)	26.7
	3686C	240	203 (8)	31.1
Coarse Threaded 1,2.12 mm pitch (12 thread/inch) 1 Flat	3689A	240	102 (4)	33.36
	3689B	200	102 (4)	28.91
	3689C	160	102 (4)	31.14
	3691A	400	203 (8)	40.03
	3691B	320	203 (8)	28.91
	3691C	240	203 (8)	31.14
<b>2 Flats</b>				
<i>Pin Profile</i>	<i>Weld Number</i>	<i>Rotational Speed</i>	<i>Welding Speed</i>	<i>Z-Force</i>
		<i>RPM</i>	<i>mm/min. (IPM)</i>	<i>kN</i>
Unthreaded 2 Flats	3692A	240	102 (4)	24.47
	3692B	200	102 (4)	26.69
	3692C	160	102 (4)	33.36
	3693A	400	203 (8)	26.69
	3693B	320	203 (8)	26.69
	3693C	240	203 (8)	35.59
Coarse Threaded 1,2.12 mm pitch (12 thread/inch) 2 Flats	3696A	240	102 (4)	24.47
	3696B	200	102 (4)	28.91
	3696C	160	102 (4)	35.59
	3697A	400	203 (8)	28.91
	3697B	320	203 (8)	31.14
	3697C	240	203 (8)	37.81

<b>3 Flats</b>				
<i>Pin Profile</i>	<i>Weld #</i>	<i>Rotational Speed</i>	<i>Welding Speed</i>	<i>Z-Force</i>
		<i>RPM</i>	<i>mm/min. (IPM)</i>	<i>kN</i>
Coarse Threaded 1,2.12 mm pitch (12 thread/inch) 3 Flats	3731 A	240	102 (4)	26.69
	3731 B	200	102 (4)	28.91
	3731 C	160	102 (4)	33.36
	3732 A	400	203 (8)	22.24
	3732 B	320	203 (8)	28.91
	3732 C	240	203 (8)	33.36
<b>4 Flats</b>				
<i>Pin Profile</i>	<i>Weld #</i>	<i>Rotational Speed</i>	<i>Welding Speed</i>	<i>Z-Force</i>
		<i>RPM</i>	<i>mm/min. (IPM)</i>	<i>kN</i>
Unthreaded 4 Flats	3698A	240	102 (4)	26.69
	3698B	200	102 (4)	31.14
	3698C	160	102 (4)	37.81
	3699A	400	203 (8)	24.47
	3699B	320	203 (8)	31.14
	3699C	240	203 (8)	40.03
Coarse Threaded 1,2.12 mm pitch (12 thread/inch) 4 Flats	3702A	240	102 (4)	24.47
	3702B	200	102 (4)	24.47
	3702C	160	102 (4)	31.14
	3703A	400	203 (8)	22.24
	3703B	320	203 (8)	26.69
	3703C	240	203 (8)	31.14

**c. Cylindrical pins with different flat numbers**

<i>Pin Profile</i>	<i>Weld #</i>	<i>Rotational Speed</i>	<i>Welding Speed</i>	<i>Z-Force</i>
		<i>RPM</i>	<i>mm/min. (IPM)</i>	<i>kN</i>
8° taper Normal Threaded, 1.41 mm pitch (18 thread/inch) Threaded only	3739 A	240	102 (4)	20.02
	3739 B	200	102 (4)	26.69
	3739 C	160	102 (4)	33.36
	3740 A	400	203 (8)	17.79
	3740 B	320	203 (8)	24.47
	3740 C	240	203 (8)	35.59
8° taper Coarse Threaded 1,2.12 mm pitch (12 thread/inch) Threaded only	3737 A	240	102 (4)	28.91
	3737 B	200	102 (4)	35.59
	3737 C	160	102 (4)	51.15
	3738 A	400	203 (8)	24.47
	3738 B	320	203 (8)	33.36
	3738 C	240	203 (8)	48.93

<i>Pin Profile</i>	<i>Weld #</i>	<i>Rotational Speed</i>	<i>Welding Speed</i>	<i>Z-Force</i>
		<i>RPM</i>	<i>mm/min. (IPM)</i>	<i>kN</i>
8° taper Normal Threaded, 1.41 mm pitch (18 thread/inch) 3 Flats	3743 A	240	102 (4)	24.47
	3743 B	200	102 (4)	26.69
	3743 C	160	102 (4)	35.59
	3744 A	400	203 (8)	22.24
	3744 B	320	203 (8)	26.69
	3744 C	240	203 (8)	35.59
8° taper Coarse Threaded 1,2.12 mm pitch (12 thread/inch) 3 Flats	3741 A	240	102 (4)	26.69
	3741 B	200	102 (4)	28.91
	3741 C	160	102 (4)	35.59
	3742 A	400	203 (8)	24.47
	3742 B	320	203 (8)	26.69
	3742 C	240	203 (8)	35.59
8° taper Normal Threaded, 1.41 mm pitch (18 thread/inch) 3 Co-flow Flutes	3748 A	240	102 (4)	31.14
	3748 B	200	102 (4)	35.59
	3748 C	160	102 (4)	44.48
	3749 A	400	203 (8)	28.91
	3749 B	320	203 (8)	33.36
	3749 C	240	203 (8)	40.03
8° taper Coarse Threaded 1,2.12 mm pitch (12 thread/inch) 3 Co-flow Flutes	3747 A	240	102 (4)	33.36
	3747 B	200	102 (4)	37.81
	3747 C	160	102 (4)	46.71
	3746 A	400	203 (8)	28.91
	3746 B	320	203 (8)	35.59
	3746 C	240	203 (8)	42.26
8° taper Normal Threaded, 1.41 mm pitch (18 thread/inch) 3 Counter-flow Flutes	3750 A	240	102 (4)	20.02
	3750 B	200	102 (4)	24.47
	3750 C	160	102 (4)	31.14
	3751 A	400	203 (8)	22.24
	3751 B	320	203 (8)	24.47
	3751 C	240	203 (8)	33.36
8° taper Coarse Threaded 1,2.12 mm pitch (12 thread/inch) 3 Counter-flow Flutes	3752 A	240	102 (4)	24.47
	3752 B	200	102 (4)	24.47
	3752 C	160	102 (4)	33.36
	3753 A	400	203 (8)	24.47
	3753 B	320	203 (8)	26.69
	3753 C	240	203 (8)	31.14

**d. Conical Coarse Threaded pin with deeper flat depth (2.7 mm)**

<i>Pin Profile</i>	<i>Weld #</i>	<i>Rotational Speed</i>	<i>Welding Speed</i>	<i>Z-Force</i>
		<i>RPM</i>	<i>mm/min. (IPM)</i>	<i>kN (lbf)</i>
Coarse Threaded 1,2.12 mm pitch (12 thread/inch) + 3 Flats of 2.7 mm(0.106 inch) depth	4095-A	240	102 (4)	24.47 (5500)
	4095-B	200	102 (4)	26.69 (6000)
	4095-C	160	102 (4)	28.91 (6500)

**e. Stationary shoulder FSW with coarse threaded pin having 3 flats**

<i>Pin Profile</i>	<i>Weld #</i>	<i>Rotational Speed</i>	<i>Welding Speed</i>	<i>Z-Force</i>
		<i>RPM</i>	<i>mm/min. (IPM)</i>	<i>kN</i>
Coarse Threaded 1,2.12 mm pitch (12 thread/inch) + 3 Flats of 1.35 mm(0.053 inch) depth 1degree head	4284 A	240	102 (4)	35.59
	4284 B	200	102 (4)	40
	4284 C	160	102 (4)	46.7
	4285 A	400	203 (8)	35.59
	4285 B	320	203 (8)	37.81
	4285 C	240	203 (8)	46.71

**3. AA7099 Friction Stir Welding**

<i>Pin Profile</i>	<i>Weld #</i>	<i>Rotational Speed</i>	<i>Welding Speed</i>	<i>Z-Force</i>
		<i>RPM</i>	<i>mm/min. (IPM)</i>	<i>kN (lbf)</i>
Coarse Threaded 1,2.12 mm pitch (12 thread/inch) Threaded only	4288-A	240	102 (4)	42.26 (9500)
	4288-B	200	102 (4)	44.48 (10000)
	4288-C	160	102 (4)	46.71 (10500)
Coarse Threaded 1,2.12 mm pitch (12 thread/inch) + 3 Flats of 1.35 mm(0.053 inch) depth	4094-A	240	102 (4)	33.36 (7500)
	4094-B	200	102 (4)	37.81 (8500)
	4094-C	160	102 (4)	40.03 (9000)
Coarse Threaded 1,2.12 mm pitch (12 thread/inch) + 3 Flats of 2.7 mm(0.106 inch) depth	4098-A	240	102 (4)	28.9 (6500)
	4098-B	200	102 (4)	33.36 (7500)
	4098-C	160	102 (4)	37.81 8500)

#### 4. AA 6056 Friction Stir Welding

Pin Profile	Weld #	Rotational Speed	Welding Speed	Z-Force
		RPM	mm/min. (IPM)	kN
8° taper Coarse Threaded 1,2.12 mm pitch (12 thread/inch) 3 Flats	3821 A	400	203 (8)	26.69
	3821 B	320	203 (8)	26.69
	3825 C	240	203 (8)	32.25
8° taper Coarse Threaded 1,2.12 mm pitch (12 thread/inch) 3 Co-flow Flutes	3822 A	400	203 (8)	31.14
	3822 B	320	203 (8)	33.36
	3822 C	240	203 (8)	35.59
8° taper Coarse Threaded 1,2.12 mm pitch (12 thread/inch) 3 Counter-flow Flutes	3823 A	400	203 (8)	24.47
	3823 B	320	203 (8)	26.69
	3823 C	240	203 (8)	31.14

#### 5. AA2050 & AA6061 Dissimilar material Friction stir welding

Pin Profile	Adv. side	Weld #	Rotational Speed	Welding Speed	Z-Force
			RPM	mm/min. (IPM)	kN
8° taper Coarse Threaded 1,2.12 mm pitch (12 thread/inch) Threaded only	6061	3857 A	300	406 (16)	46.7
	6061	3858 B	300	203 (8)	44.5
	6061	3858 C	150	102 (4)	57.8
	2050	3859 A	300	406 (16)	40
	2050	3859 B	300	203 (8)	31.1
	2050	3859 C	150	102 (4)	37.8
8° taper Coarse Threaded 1,2.12 mm pitch (12 thread/inch) 3 Flats	6061	3851	300	406 (16)	44.5
	6061	3850 A	300	203 (8)	33.4
	6061	3850 C	150	102 (4)	40.0
	2050	3852 A	300	406 (16)	42.3
	2050	3852 B	300	203 (8)	31.1
	2050	4286	150	102 (4)	28.9
8° taper Coarse Threaded 1,2.12 mm pitch (12 thread/inch) 3 Co-flow Flutes	6061	3855 A	300	406 (16)	53.4
	6061	3855 B	300	203 (8)	37.8
	6061	3855 C	150	102 (4)	44.5
	2050	3856 A	300	406 (16)	46.7
	2050	3856 B	300	203 (8)	33.4
	2050	3856 C	150	102 (4)	44.5
8° taper Coarse Threaded 1,2.12 mm pitch (12 thread/inch) 3 Counter-flow Flutes	6061	3853 A	300	406 (16)	42.3
	6061	3853 B	300	203 (8)	33.4
	6061	3853 C	150	102 (4)	31.1
	2050	3854 A	300	406 (16)	35.6
	2050	3854 B	300	203 (8)	28.9
	2050	3854 C	150	102 (4)	28.9

**6. AA7050 & AA6061 Dissimilar material Friction stir welding**

<i>Pin Profile</i>	<i>Adv. side</i>	<i>Weld #</i>	<i>Rotational Speed</i>	<i>Welding Speed</i>	<i>Z-Force</i>
			<i>RPM</i>	<i>mm/min. (IPM)</i>	<i>kN</i>
8° taper Coarse Threaded 1,2.12 mm pitch (12 thread/inch) 3 Flats	7050	4275 A	150	102 (4)	37.8
	7050	4275 B	300	203 (8)	37.8
	6061	4276 A	150	102 (4)	46.7
	6061	4276 B	300	203 (8)	44.5

**7. Misaligned Dissimilar Material Friction Stir Butt Weld**

**a. Between AA2050 and AA6061**

<i>Pin Profile</i>	<i>Adv. Side</i>	<i>Tool Eccentricity</i>	<i>Weld #</i>	<i>Rotational Speed</i>	<i>Welding Speed</i>	<i>Z-Force</i>
		<i>mm</i>		<i>RPM</i>	<i>mm/min. (IPM)</i>	<i>kN</i>
8° taper Coarse Threaded 1,2.12 mm pitch (12 thread/inch) 3 Flats	2050	4.4	4273-A	150	102 (4)	35.59
	2050	2.3	4273-B	150	102 (4)	33.36
	2050	0	4273-C	150	102 (4)	31.14
	2050	-1.5	4273-D	150	102 (4)	31.14
	2050	-3.8	4273-E	150	102 (4)	28.9
	2050	-5.5	4273-F	150	102 (4)	28.9
	6061	4.4	4279-A	150	102 (4)	35.59
	6061	2.3	4279-B	150	102 (4)	40.04
	6061	0	4279-C	150	102 (4)	42.26
	6061	-1.5	4279-D	150	102 (4)	42.26
	6061	-3.8	4279-E	150	102 (4)	42.26
	6061	-5.5	4279-F	150	102 (4)	35.59

**b. Between AA7050 and AA6061**

8° taper Coarse Threaded 1,2.12 mm pitch (12 thread/inch) 3 Flats	7050	4.8	4277-A	150	102 (4)	42.26
	7050	2.5	4277-B	150	102 (4)	42.26
	7050	0.22	4277-C	150	102 (4)	40
	7050	-1.3	4277-D	150	102 (4)	40
	7050	-3.6	4277-E	150	102 (4)	37.8
	7050	-5.3	4277-F	150	102 (4)	35.6
	6061	4.8	4278-A	150	102 (4)	37.8
	6061	2.5	4278-B	150	102 (4)	46.7
	6061	0.22	4278-C	150	102 (4)	48.9
	6061	-1.3	4278-D	150	102 (4)	48.9
	6061	-3.6	4278-E	150	102 (4)	51.2
	6061	-5.3	4278-F	150	102 (4)	48.9

## APPENDIX C

### DESIGN OF EXERIMENT-STATGRAPHICS RESULTS

#### Analysis of Variance for Area of Defect for AA7050

<i>Source</i>	<i>Sum of Squares</i>	<i>Df</i>	<i>Mean Square</i>	<i>F-Ratio</i>	<i>P-Value</i>
A:Thread Form Level	1760.32	1	1760.32	9.24	0.0058
B:Welding Speed	60.5707	1	60.5707	0.32	0.5783
C:Rotational Speed	4288.44	1	4288.44	22.51	0.0001
AA	4305.24	1	4305.24	22.60	0.0001
AB	3616.98	1	3616.98	18.98	0.0002
CC	810.89	1	810.89	4.26	0.0506
Total error	4382.35	23	190.537		
Total (corr.)	23951.5	29			

R-squared = 81.7032 percent  
 R-squared (adjusted for d.f.) = 76.9302 percent  
 Standard Error of Est. = 13.8035  
 Mean absolute error = 10.2972  
 Durbin-Watson statistic = 1.72165 (P=0.0856)  
 Lag 1 residual autocorrelation = 0.126959

#### **The StatAdvisor**

The ANOVA table partitions the variability in Area of Defect into separate pieces for each of the effects. It then tests the statistical significance of each effect by comparing the mean square against an estimate of the experimental error. In this case, 4 effects have P-values less than 0.05, indicating that they are significantly different from zero at the 95.0% confidence level.

The R-Squared statistic indicates that the model as fitted explains 81.7032% of the variability in Area of Defect. The adjusted R-squared statistic, which is more suitable for comparing models with different numbers of independent variables, is 76.9302%. The standard error of the estimate shows the standard deviation of the residuals to be 13.8035. The mean absolute error (MAE) of 10.2972 is the average value of the residuals. The Durbin-Watson (DW) statistic tests the residuals to determine if there is any significant correlation based on the order in which they occur in your data file. Since the P-value is greater than 5.0%, there is no indication of serial autocorrelation in the residuals at the 5.0% significance level.

**Analysis of Variance for Area of Defect for AA6061**

<i>Source</i>	<i>Sum of Squares</i>	<i>Df</i>	<i>Mean Square</i>	<i>F-Ratio</i>	<i>P-Value</i>
A:Thread Form Level	85.4426	1	85.4426	3.51	0.0751
B:Welding Speed	0.0291275	1	0.0291275	0.00	0.9727
C:Rotational Speed	72.4661	1	72.4661	2.97	0.0993
AA	270.258	1	270.258	11.09	0.0032
AB	24.5859	1	24.5859	1.01	0.3266
AC	7.24128	1	7.24128	0.30	0.5914
BC	0.650719	1	0.650719	0.03	0.8718
CC	4.21443	1	4.21443	0.17	0.6817
Total error	511.816	21	24.3722		
Total (corr.)	1433.57	29			

R-squared = 64.2977 percent  
R-squared (adjusted for d.f.) = 50.6968 percent  
Standard Error of Est. = 4.93682  
Mean absolute error = 3.29421  
Durbin-Watson statistic = 1.24025 (P=0.0069)  
Lag 1 residual autocorrelation = 0.371288

**The StatAdvisor**

The ANOVA table partitions the variability in Area of Defect into separate pieces for each of the effects. It then tests the statistical significance of each effect by comparing the mean square against an estimate of the experimental error. In this case, 1 effect have P-values less than 0.05, indicating that they are significantly different from zero at the 95.0% confidence level.

The R-Squared statistic indicates that the model as fitted explains 64.2977% of the variability in Area of Defect. The adjusted R-squared statistic, which is more suitable for comparing models with different numbers of independent variables, is 50.6968%. The standard error of the estimate shows the standard deviation of the residuals to be 4.93682. The mean absolute error (MAE) of 3.29421 is the average value of the residuals. The Durbin-Watson (DW) statistic tests the residuals to determine if there is any significant correlation based on the order in which they occur in your data file. Since the P-value is less than 5.0%, there is an indication of possible serial correlation at the 5.0% significance level. Plot the residuals versus row order to see if there is any pattern that can be seen.